

# DIVERSE SECRETED BACTERIAL PROTEINS MANIPULATE EUKARYOTIC MEMBRANE DYNAMICS

by

EMILY MARIE CARPINONE

(Under the Direction of Vincent Starai)

## ABSTRACT

Bacterial pathogens have evolved innumerable tactics to enhance their survival in eukaryotic hosts by evading host cell defenses. Notably, the secretion of proteins to modulate host cell membrane dynamics through unique means is one broad method that aids in bacterial survival, as seen in the case of each of the bacteria presented in this work: *Wolbachia pipientis*, *Rhodococcus equi*, and *Vibrio parahaemolyticus*. Through the use of the model eukaryotic host, *Saccharomyces cerevisiae*, the unique means by which a protein from each of the aforementioned bacteria manipulates host membrane dynamics for survival have been analyzed and include the modulation of actin dynamics (*wBm0076*), endosomal maturation and membrane trafficking (*wBm0152*, VapA, VopQ), and autophagic processes (VopQ). *wBm0076* is an actin modulator that causes cell bloating and lysis in *S. cerevisiae* while *wBm0152* modulates the vacuole protein sorting trafficking pathway. A ligand for VapA binding at the macrophage membrane has been identified and explored in greater detail through mutations in specific regions of VapA, however its activity as a modulator of endosome maturation remains unknown. Finally, VopQ is shown to bind specifically  $V_o$  containing membranes through its interaction with Vma3p and block vacuole:vacuole fusion. The unique inhibitory behavior of VopQ has led to its utilization as a model protein inhibitor in fusion reactions and means to evaluate historically debated roles of the V-ATPase in

yeast fusion events, specifically in regards to vacuolar acidification. Collectively, the function of each protein described presents the well-conserved target for bacterial invaders or symbionts of eukaryotic hosts as membrane dynamics. Through modulation of membrane dynamics in *S. cerevisiae* as a model host, such proteins demonstrate features necessary for successful bacterial invasion and/or intracellular survival and provide continued evidence for the effectivity of using *S. cerevisiae* to identify bacterial effector or virulence associated proteins.

INDEX WORDS: *Saccharomyces cerevisiae*, membrane dynamics, *Wolbachia pipientis*  
endosymbiont of *Brugia malayi*, *Rhodococcus equi*, *Vibrio parahaemolyticus*,  
wBm0076, wBm0152, VopQ, VapA

DIVERSE BACTERIAL SECRETED PROTEINS MANIPULATE EUKARYOTIC MEMBRANE DYNAMICS

by

EMILY MARIE CARPINONE

B.S., University of Florida, 2013

A Dissertation Submitted to the Graduate Faculty of The University of Georgia in Partial Fulfillment of  
the Requirements for the Degree

DOCTOR OF PHILOSOPHY

ATHENS, GEORGIA

2018

© 2018

Emily Marie Carpinone

All Rights Reserved

DIVERSE BACTERIAL SECRETED PROTEINS MANIPULATE EUKARYOTIC MEMBRANE DYNAMICS

by

EMILY MARIE CARPINONE

Major Professor:

Vincent Starai

Committee:

Jorge Escalante-Semerena

Eileen Kennedy

Zachary Lewis

Electronic Version Approved:

Suzanne Barbour  
Dean of the Graduate School  
The University of Georgia  
December 2018

## ACKNOWLEDGEMENTS

This work would not have been possible without the help and support of many people. Vinny Starai, thank you for being an understanding and supportive mentor, for letting me take the reins and learn through my own successes and failures, for always being open to new and exciting ideas, and for the entertainment. You are one of the few mentors that support their students being human and for that I am truly grateful. I'd like to thank my committee members - Zack Lewis, Eileen Kennedy, and Jorge Escalante-Semerena – for your support of my projects and depth of knowledge to guide my journey through graduate school.

I've been very lucky to have amazing labmates that have truly become my family over the years. To those who have moved on to other things, Terry, Kevin, and Shannon, thank you for your patience, training, and companionship. To Nathan and Michael, thank you for always being a source of encouragement, ideas, and entertainment to keep lab the enjoyable place it has been.

Finally, I'd like to thank my family, my friends, and Nathan. Mom and Dad, you've always supported my education and I owe you my endless appreciation for helping me make it this far. I would be lost without my friends that have kept me sane during graduate school - oh the rants and game nights we have had - you're truly my dearest friends. Nathan, there will never be enough words to thank you for everything you've done and helped me to do, but suffice it to say thank you for everything always.

## TABLE OF CONTENTS

	Page
ACKNOWLEDGEMENTS.....	iv
CHAPTER	
1 Introduction.....	1
2 Literature Review .....	2
Bacterial effectors manipulate host trafficking for survival .....	2
<i>Wolbachia pipientis</i> .....	2
<i>Rhodococcus equi</i> .....	10
<i>Vibrio parahaemolyticus</i> .....	17
<i>Saccharomyces cerevisiae</i> as a model organism .....	24
Membrane trafficking in yeast.....	25
The yeast vacuole .....	44
Actin .....	53
3 Identification of putative effectors of the Type IV secretion system from the <i>Wolbachia</i> endosymbiont of <i>Brugia malayi</i> .....	58
4 Mutations in the conserved domain of VapA of <i>Rhodococcus equi</i> alter its binding affinity for phosphatidic acid .....	99
5 The <i>Vibrio</i> effector protein, VopQ, inhibits fusion of V-ATPase containing membrane .....	111
6 Conclusions.....	147
REFERENCES .....	155

## APPENDICES

I	wBm0152 associates with Sna3-GFP containing compartments .....	192
II	VapA of <i>Rhodococcus equi</i> binds phosphatidic acid .....	194
III	Analysis of the interplay between VopQ and V <sub>O</sub> -containing membranes .....	227

## CHAPTER 1

### INTRODUCTION

*Saccharomyces cerevisiae*, or baker's yeast, is a well-studied model eukaryotic organism that is highly tractable to standard laboratory manipulations. Historically, *S. cerevisiae* has been used not only to expand the understanding of higher eukaryotic cellular processes due to high conservation of such processes between yeast and higher eukaryotes, but also as a model host to characterize proteins secreted by organisms that are unamenable to traditional laboratory techniques. It is the goal of this study to use *S. cerevisiae* as a model organism to demonstrate how distinct proteins, secreted by three phylogenetically distinct bacterium that survive in unique environments, can manipulate eukaryotic trafficking pathways to aid in survival. The proteins analyzed in this work are secreted by the following bacteria: *Wolbachia pipientis* (wBm), a Gram-negative intracellular symbiont of the filarial nematode, *Brugia malayi*; *Rhodococcus equi*, a Gram-positive soil-dwelling pathogen of humans and animals; and *Vibrio parahaemolyticus*, a Gram-negative marine-dwelling opportunistic pathogen. wBm poses a particularly difficult challenge to standard laboratory techniques as it cannot be cultured without its nematode host, lending most molecular techniques inapplicable and limiting current knowledge regarding the relationship between nematode and bacterium. In the case of both *R. equi* and *V. parahaemolyticus*, specific secreted proteins prevent cells from phagocytosis and are required for successful invasion of the bacteria into host cells, yet the mechanism of action for such proteins remains unknown. The following work provides insight into the role and activity of bacterial secreted proteins in the context of their eukaryotic hosts using the model eukaryote, *S. cerevisiae*.

## CHAPTER 2

### LITERATURE REVIEW

#### BACTERIAL EFFECTORS MANIPULATE HOST TRAFFICKING FOR SURVIVAL

As means for survival, bacteria have evolved intricate methods to evade host cell defenses that induce a range of toxic effects. Manipulating host membrane trafficking through the secretion of proteins is one method that many bacteria, such as *Mycobacterium tuberculosis*, *Salmonella enterica* serovar Typhimurium, and *Legionella pneumophila* (to name only a few), rely on to evade degradation in the lysosome by altering the flux of vesicles or alter the host cytoskeletal arrangement. Inhibition of phagosome maturation, manipulation of autophagic processes, hijacking of membrane trafficking pathways, and alteration of host cytoskeleton are four such tactics that the bacteria *Wolbachia pipientis*, *Rhodococcus equi*, and *Vibrio parahaemolyticus* utilize for survival upon delivery of secreted proteins. Specific proteins secreted by these organisms are the focus of this work as their role in invasion continues to be elucidated.

#### **WOLBACHIA PIPIENTIS**

##### **Taxonomy and Distribution**

Found in a staggering two-thirds of the world's population of arthropods [1], *Wolbachia pipientis* (*Wolbachia*) is a maternally transmitted Gram-negative intracellular  $\alpha$ -proteobacterium of the Rickettsiales order that was first formally identified in the cells of the mosquito, *Culex pipiens*, in 1936 [2]. *Wolbachia* is classified into sixteen supergroups (A-Q, excluding G) (Figure 2.1) based on the 16S rRNA gene [3], *Wolbachia* surface protein gene (WSP) [4], and multilocus sequence typing loci across different host organisms [5], and yet despite being classified into separate supergroups, all isolates of *Wolbachia* are considered *Wolbachia pipientis* without further speciation due to an overwhelming

amount of strain diversity, the ability of identical *Wolbachia* strains to infect different hosts across supergroups while maintaining varied relationships with each host, and the ability to undergo horizontal gene transfer with other *Wolbachia* strains within the same host [6]. With ~90% 16S rRNA sequence identity (corrected), the closest relatives to *Wolbachia* are *Ehrlichia*, *Anaplasma*, and *Rickettsia*, all of which are pathogenic intracellular bacteria transmitted by arthropod vectors to mammalian hosts [7, 8]. Unlike its relatives however, *Wolbachia* is not transmitted to vertebrate hosts and rather maintains its lifecycle within an arthropod or nematode, minimizing the parallels regarding host:bacterium relationship that can be drawn across these intracellular bacteria.

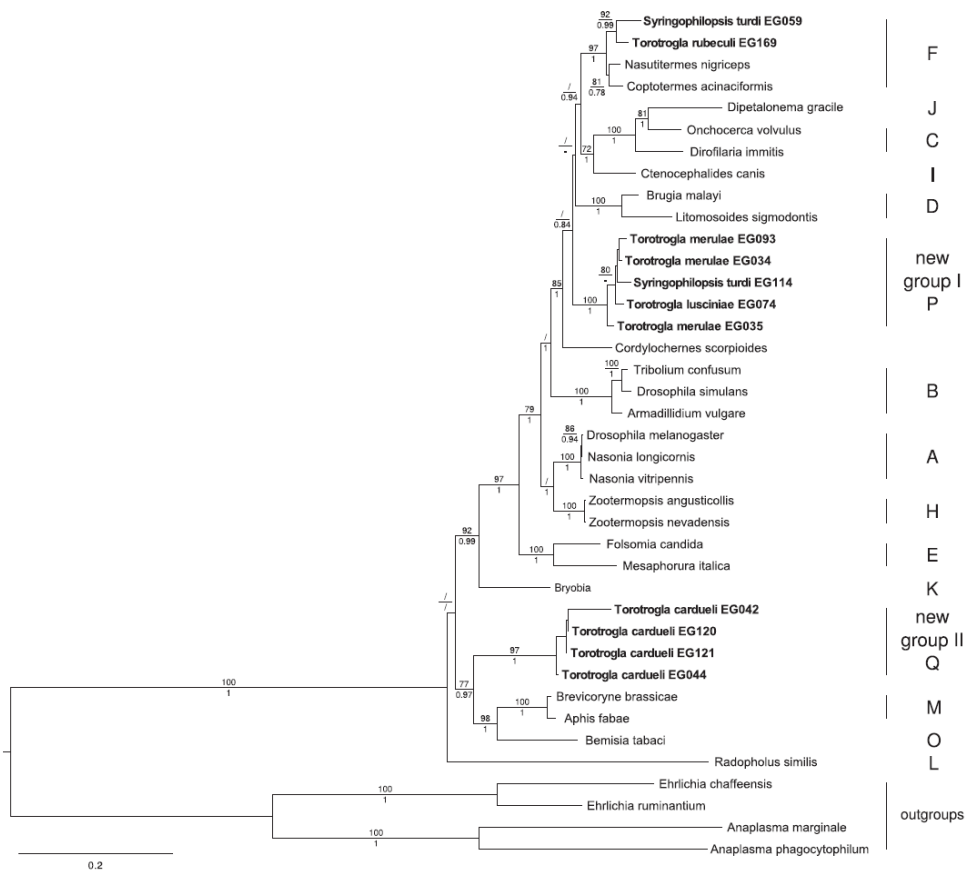


**Figure 2.1. *Wolbachia* supergroups.** Supergroups are designated A-Q by host organism. [3]

## ***Wolbachia* as a manipulator of host biology**

Though not independently pathogenic to vertebrates, *Wolbachia* plays a significant role as an intracellular organism of arthropods and nematodes, maintaining different relationships (mutualistic or parasitic) with each host species and manipulating host cell biology (i.e. male killing, feminization, parthenogenesis, and cytoplasmic incompatibility) to select for females, and thus their progeny, that carry *Wolbachia*.

The most commonly observed form of host cell manipulation is cytoplasmic incompatibility (CI) [9], which is an incompatible cross that occurs between an infected male and uninfected female. CI is lethal to the progeny of such an incompatible cross as the eggs eliminate the infected-male chromosomes causing haploid, and thus inviable, eggs. CI ultimately results in a male bias in the population or population mortality as only those females carrying *Wolbachia* produce viable eggs with infected males [9].

Other forms of significant host population manipulations are less common but are observed in different hosts. Parthenogenesis inducing (PI) *Wolbachia* alter early mitotic division to produce diploid female-only eggs from unfertilized eggs. This is a process known as thelytoky and it results in a predominantly feminized population of *Wolbachia* carrying wasps. Feminization occurs in crustaceans and some insects when *Wolbachia* manipulates the normal sex determination, causing males to develop as females. Finally, male killing occurs when male progeny are killed during embryogenesis, again swaying the population of many insects towards a *Wolbachia*-infected female bias. Collectively, these methods enable *Wolbachia* to enhance its replicative niche among populations and show a significant ability as symbionts to severely manipulate host cell biology.

The presence or absence of *Wolbachia* in the host germline is paramount to many alterations in population biology described here, particularly to cytoplasmic incompatibility. More specifically, the ability of *Wolbachia* to localize to the female germline in a range of hosts is pivotal for its transmission

and involves significant manipulation of host cell biology. The method by which *Wolbachia* mobilizes to oocytes is undefined though the use of proteins secreted by its Type IV Secretion System (T4SS) is likely the key factor in its mobility and localization [10, 11].

### ***Brugia malayi* and *Wolbachia pipientis* endosymbiont of *Brugia malayi* (wBm)**

*Brugia malayi* (Figure 2.2) is a filarial nematode that causes lymphatic filariasis, evinced by severe swelling of appendages and genitalia in humans. According to the Center for Disease Control, over 120 million people suffer with lymphatic filariasis, with approximately 10% of those people infected specifically with *B. malayi* (*Wuchereria bancrofti* and *Brugia timori* are the two other causative nematode species of lymphatic filariasis, with *W. bancrofti* the dominant agent of lymphatic filariasis). *B. malayi* is transmitted via mosquito from the *Mansonia* and *Aedes* genera distributed primarily across Southeast Asia. Microfilaria are ingested by mosquitoes during blood meals and upon maturation in the mosquito to third larval stage (L3), the nematodes are transmitted to humans as the mosquitoes continue to take blood meals. L3 nematodes are deposited on the surface of the skin where they penetrate the bite wound and enter the bloodstream for maturation into adult nematode and reproduction. Nematodes then reside and reproduce in the lymphatic system, causing a distinct swelling of appendages. Currently, chemotherapy treatments containing a combination of antihelmintics (i.e. ivermectin and diethylcarbamazine) and antibiotics (i.e. doxycycline) are used to fight infection, however drug-resistant nematodes in endemic areas with different nematode infections have increased the difficulty of fighting *B. malayi* and other filarial nematode infections with antihelmintics [12]. Studies show that targeting the *Wolbachia* endosymbiont of filarial nematodes in treatment effectively kills and aids in clearance of the nematode infection [13-16]. These findings have called for further research to untangle the relationship between nematode and endosymbiont as a means to provide effective treatment, particularly in endemic areas.

wBm, classified as a member of *Wolbachia pipientis* supergroup D, maintains an obligate mutualistic relationship with its nematode host, *B. malayi*. Within the nematode, wBm is found within presumably host-originated vesicles that are likely derived from the Golgi apparatus [17, 18]. These wBm laden vesicles are found within the lateral chord of the male and female nematode and within the ovaries and embryos of mature female worms, allowing for the transmission of wBm via the female germline [19]. wBm is considered nonmotile as it lacks genes encoding flagellum or pilus, however it may utilize the WASP (Wiskott-Aldrich syndrome protein) family protein, wBm0076, to manipulate host cytoskeletal arrangements, thus allowing it to move to the germline in female worms [20]. In adult female worms, wBm vesicles are densely accumulated in the lateral chord and are often associated with glycogen granules though the reason for this association is unknown as wBm does not possess all required enzymes for the glycolytic pathway [18].

Though the dynamics of the relationship between the host and bacterium are still largely unknown, current research suggests that *Wolbachia* provides essential nutrients to its host, such as riboflavin, heme, flavin adenine dinucleotide (FAD), and nucleotides while the host provides a protective replicative niche and essential vitamins and cofactors for wBm [20]. wBm is required for *B. malayi* to complete its full life cycle and for its survival as treatment of *B. malayi* with antibiotics results in nematode sterility and eventual death [13, 14]. As an intracellular organism, wBm requires its nematode host for replication and survival and may also scavenge amino acids, vitamins, and cofactors (biotin, coenzyme A, folate, NAD, and ubiquinone) from its host as wBm does not maintain complete synthesis pathways for many essential molecules [20, 21].

wBm possesses the entire pathway for the synthesis of riboflavin (vitamin B2), a pathway which *B. malayi* lacks completely, and actively expresses *ribA*, which encodes an enzyme that catalyzes two steps of the riboflavin synthesis pathway throughout all stages of the nematode lifecycle [22]. Furthermore, in nematodes cleared of wBm and treated with the antibiotic doxycycline, the addition of

riboflavin (10  $\mu\text{g/ml}$ ) to nematode growth medium aids in the survival rate of the nematode in comparison to nematodes treated either without riboflavin or with low levels ( $<2\mu\text{g/ml}$ ) of riboflavin [22]. In addition to riboflavin, *wBm* likely provides nucleotides, FAD, and heme to the nematode as *B. malayi* lacks the genes required for their synthesis de novo [20]. It is likely that riboflavin, FAD, and heme play an important role in the molting and reproduction of *B. malayi* while nucleotides are important for oogenesis and embryogenesis, suggesting that in *wBm* cleared nematodes, the observed reduction in *B. malayi* reproduction and eventual death is due to the lack of access to these necessary components [20, 23, 24]. Although it is likely that *wBm* provides riboflavin, heme, FAD, and nucleotides to the nematode throughout its lifecycle, the degree to which each of these is important in the *wBm*:nematode relationship and in nematode survival is uncertain as other *Wolbachia* do not possess genes for such synthesis pathways and other filarial nematodes, such as *Loa loa*, exist without either a *Wolbachia* endosymbiont or the genes required to synthesize several cofactors [22].

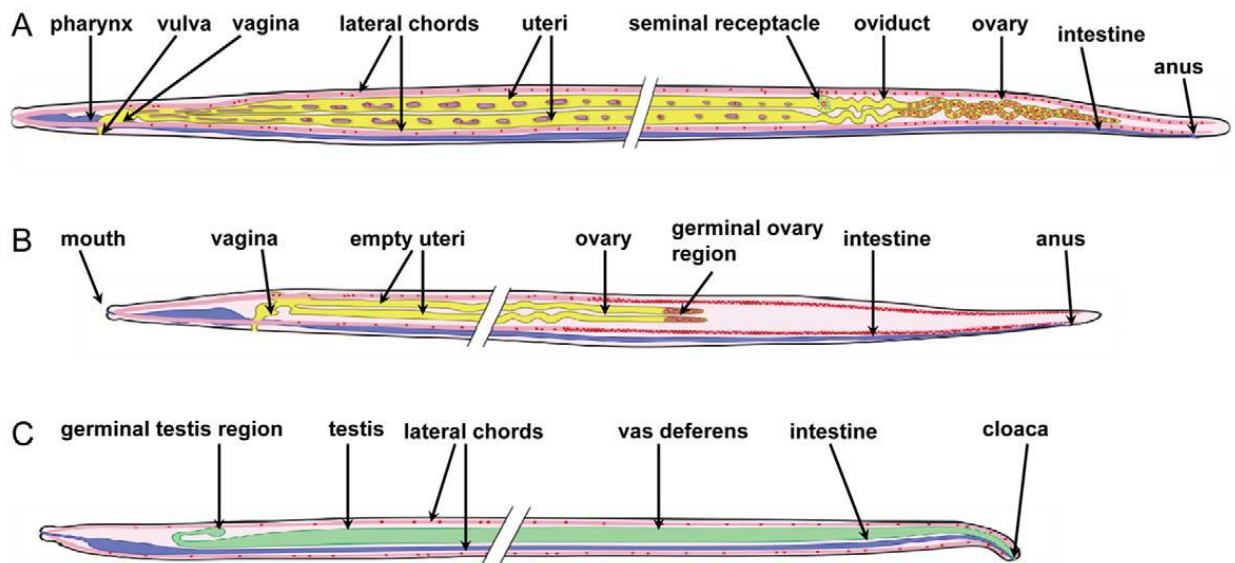


**Figure 2.2. Schematic of *B. malayi* anatomy of an (A) adult female (B) immature female and (C) adult male. [19]**

## Type IV Secretion System (T4SS) of wBm

The T4SS is found in a multitude of pathogenic bacteria, both Gram-negative and Gram-positive, and can function as either a conjugation system to transfer DNA to a donor, a translocator of proteins and other molecules into the cytoplasm of eukaryotic organisms, or a contact-independent system for DNA uptake or release from the surrounding environment [25, 26]. The T4SS consists of at least the VirB proteins (VirB1-11) and the VirD4 protein which collectively form the cytoplasmic inner membrane (consisting of ATPases), the core complex (scaffolding complex), and the outer membrane pilus (contacts recipient cell) [27] (Figure 2.3). Through genetic screening and later genome sequencing of *Wolbachia*, and specifically of wBm, homologues of *virB* and *virD4* genes were identified in a split operon organization, showing the presence of a T4SS in the *Wolbachia* genome [20, 28]. A split *virB-virD4* operon has also been identified in other intracellular bacteria of the Rickettsiales order [25] though the role of the T4SS and its secreted proteins in most members of the Rickettsiales order, including *Wolbachia*, is at times limited.

Identified in *Ehrlichia chaffeensis*, EcxR is a transcription factor that binds to promoter regions of the T4SS *virBD* genes as well as its own promoter, playing a pivotal role in the regulation of T4SS genes during intracellular development of *E. chaffeensis* [29]. Since *Wolbachia* is related to Rickettsiales order organisms, the protein sequence of EcxR was used to search for homologue transcription factors in the wBm genome, leading to the identification of two proteins - wBmxR1 (wBm0386) and wBmxR2 (wBm0498)– that have 50% and 42% identity (respectively) to EcxR [22]. wBmxR1 and wBmxR2 each bind to different promoter regions of the wBm T4SS, with wBmxR1 binding regions upstream of wBmxR2, *virB9-2*, *ribA*, and *sodA* (encodes a superoxide dismutase located outside of T4SS operon 2) and wBmxR2 binding wBmxR1, *virB4-2*, and *ribA* promoter regions [22]. EcxR binds to five different promoter regions and of those, shares *virB9-2*, *virB4-2*, and *sodB* (encodes a superoxide dismutase located within operon 2 with 52% identity to wBm *sodA*) with wBmxR1 and wBmxR2 [22]. It was

determined that both *wBmxR1* and *wBmxR2* are expressed during all life stages of the nematode (microfilaria, L3, L4, and adult) [22]. Additionally, *virB8*, a key component of the T4SS, is also expressed during all life stages of the nematode, revealing that the T4SS of *wBm* is likely active during the nematode life cycle and may play an important role in *wBm* intracellular development [22]. There are many genes co-transcribed with the T4SS and efforts are underway to characterize their translated proteins, however no proteins have formally been labeled as secreted effector proteins as no evidence shows the secretion of such proteins in the host nematode to date.

Despite the current lack of data to show the secretion of proteins into the nematode, the *Wolbachia* surface protein (WSP) *wBm0432*, the predicted outer membrane peptidoglycan associated lipoprotein (PAL)-like protein *wBm0152*, and the T4SS components *wBm0794* (*VirB6*), are present on the surface of *wBm* throughout the lifecycle of the nematode [30]. Of these, *wBm0152* and *wBm0432* have been studied with unremarkable results. Melnikow et al. describe *wBm0152* as a WSP that binds host actin and tubulin while *wBm0432* binds host glycolytic enzymes [31], however they fail to show that the interaction is distinct as some of the presented data are inconclusive and contradictory. More specifically, Melnikow et al. present *wBm0152* as binding actin though data only shows this as an indirect interaction in the context of one assay while in other assays that require a direct interaction, no interaction is observed [31]. Furthermore, actin is one of the most abundant proteins as well as a “sticky” protein in *B. malayi* extract, perhaps resulting in the inconclusive data.

Candidate effectors have been identified in *Wolbachia* endosymbiont of *Drosophila melanogaster* (*wMel*), classified as supergroup A, in Rice et al. This study uses *S. cerevisiae* as a eukaryotic model to identify toxic candidate effectors that are likely secreted by *wMel* into its arthropod host. *wBm* has 696 proteins that have an orthologous protein in *wMel*, however *wMel* genome is larger and contains more repeats than does the genome of *wBm*. *wMel* is more similar to other *Wolbachia* in supergroups A and B (*Wolbachia* of arthropods) than it is to *wBm* or *Wolbachia* of other nematodes [20,

32]. Nonetheless, the use of *S. cerevisiae* as a tool to identify candidate effectors of *Wolbachia* was effective as fourteen candidate effector proteins secreted by wMel were described in the context of their toxicity in *S. cerevisiae* [32]. These proteins have some identity to wBm proteins however it is uncertain if the proteins behave similarly in their respective host because *Wolbachia* proteins often evolve in a host-dependent manner and wBm maintains a mutualistic relationship while wMel maintains a parasitic relationship with its host [33].

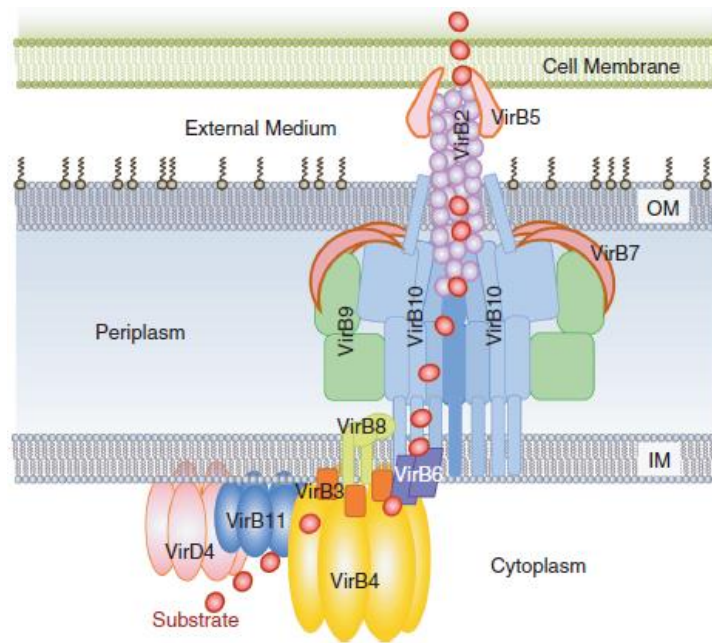


**Figure 2.3. Generic schematic of a T4SS. [27]**

## ***RHODOCOCCUS EQUI***

### **Taxonomy and Disease Presentation**

*Rhodococcus equi* is a ubiquitous Gram-positive soil-dwelling bacterium that was first identified as *Corynebacterium equi* in 1923 in pulmonary lesions of foals [34]. *R. equi* is a member of the Actinomycetales order which besides *Rhodococcus*, notably houses *Corynebacterium*, *Mycobacterium*, and *Streptomyces*, and has significant similarity phylogenetically and pathogenically to *Mycobacterium tuberculosis* [35]. Though *R. equi* has historically been classified in a number of genera by several different names within the Actinomycetales order, the *Rhodococcus* genus and *R. equi* classification was

established in 2013 in an attempt to resolve constant reclassification and naming unrest and *R. equi* currently appears to be the informally accepted classification of the organism [36-38].

Since its isolation from foals nearly one-hundred years ago, *R. equi* has been identified as the causative agent of pyogranulomatous infections in foals, pigs, cattle, sheep, and immunocompromised humans (reviewed in [35]). Of these mammals, foals, but not horses older than six months of age, are particularly susceptible to *R. equi* infection that presents as subacute or chronic purulent bronchopneumonia, manifested by coughing, fever, pneumonia, and abscesses in the lungs [35, 39, 40]. Pigs and cattle infected with *R. equi* most often appear healthy however may have lesions in the submaxillary lymph nodes that they colonize but significantly less is understood about *R. equi* infection in cattle and pigs [41]. Presentation in humans typically mimics tuberculosis though in some cancer patients *R. equi* can also form biofilms in venous catheters (reviewed in [35]). Currently, there are no vaccines available but the disease is treatable in most cases with antibiotics, though antibiotic-resistant infections have occurred [42]. Transmission of *R. equi* occurs through inhalation of aerosolized particles carrying *R. equi* or through ingestion as it is found in abundance in herbivore feces in farm settings [43-45]. Arid weather conditions as well as highly stocked or poorly maintained farms can increase the risk of transmission to mammalian hosts [46-48]. *R. equi* has shown the ability to adapt to different hosts and maintains species specific virulence variants, making its virulence factors the subject of much research.

### **Pathogenesis**

*R. equi* is a facultative intracellular bacterium that upon inhalation by a host is taken up by host alveolar macrophages in the lung where it replicates [49]. Replication of *R. equi* occurs in the *R. equi* containing vacuole (RCV) after modification of the macrophage phagocytic vacuole which prevents acidification and fusion of the phagosome with the lysosome [50-52], though how exactly *R. equi*

manipulates phagosome maturation and trafficking are unknown. *R. equi* replication in the RCV results in macrophage necrosis that results in abscess formation and tissue degradation [35, 53].

Typically, the phagosome, which contains bacteria that the macrophage phagocytosed, undergoes a process of maturation as it interacts and fuses with endocytic vesicles until the phagolysosome forms and eventually fuses with the lysosome [54]. Throughout maturation, the contents of the phagosome are exposed to a slew of hydrolytic enzymes for degradation [54]. Similar to trafficking of yeast endosomes from Golgi-to-vacuole (described in a later section), there are specific proteins associated with the phagosome as it matures such as the Rab GTPases, Rab5 and Rab7, associated with early and late endosomes respectively, early endosome antigen-1 (EEA1) associated with early endosomes, lysosome associated membrane proteins (LAMP)-1 and -2 associated with late endosomes, V-ATPase components associated with late or mature lysosome, and LAMPs and mature hydrolases associated with the lysosome (reviewed in [54]). Under standard conditions, the phagosome, which consists of macrophage plasma membrane and engulfed contents, acquires first the early endosome marker Rab5 which in turn brings the phospholipid phosphatidylinositol-3-phosphate [PI(3)P] to the membrane of the phagosome which then collectively recruit EEA1 and results in fusion with early endosomes. Early endosomes then transition to late endosomes through an unclear process that involves the replacement of Rab5 with Rab7 and the phosphorylation of PI(3)P to generate the late endosome lipid marker, phosphatidylinositol-3,5-bisphosphate [PI(3,5)P<sub>2</sub>]. Additionally, V-ATPase subunits, LAMP-1 and -2, other effectors, and hydrolases are recruited to the late endosome which will ultimately fuse with the lysosome, generating the phagolysosome (reviewed in [54, 55]). Interestingly, the RCV progresses through early maturation - which is unlike *M. tuberculosis* - and recruits the late endosome marker Rab7 but V-ATPase components cannot be detected and therefore it appears to be arrested in late endosome maturation and ultimately does not fuse with the mature lysosome [50], thereby evading degradation. *R. equi* maintains a virulence plasmid that is required for the manipulation

of phagosome maturation as plasmid-cured *R. equi* fails to evade degradation, is not as toxic to macrophages and does not result in disease manifestation in foals [49, 50, 52, 53, 56, 57].

### Virulence Plasmids

Both avirulent and virulent *R. equi* are ubiquitously present with the presence of a virulence plasmid family, designated pVap, being the basis for virulent *R. equi* [49, 56, 57]. *R. equi* can lose (likely because of environmental conditions) [58, 59] and gain its virulence plasmid back by conjugation easily [60]. There are three virulence plasmids that have been identified: pVapA (80.1kb), pVapB (80kb), and pVapN (119kb) typically associated with foals, swine, and cattle respectively, while humans can be infected with any of the three nonspecifically and crossover of plasmids in different hosts has been observed [35, 58, 61-63]. Each pVap maintains four distinct regions arranged in order as conjugation, unknown, replication, and variable/pathogenicity (CURV motif) with the conjugation, unknown, and replication components generating what is referred to as the backbone of the plasmid and maintaining housekeeping functions [63-65]. Though the backbone is quite similar at least between pVapA and pVapB, the variable regions are less similar in identity and have unique genes that comprise the pathogenicity island (PAI) of each pVap [64, 65]. A region that is similar within the variable region though is the regulatory operon, *virR*, which transcriptionally activates other PAI genes as well as chromosomal genes [66-68].

The PAI of pVapA (Figure 2.4) consists of nine genes, six of which (*vapA*, *-C*, *-D*, *-E*, *-G*, and *-H*) are full length genes while three (*vapF*, *-I*, and *-X*) are pseudogenes [64, 65]. Of these nine genes and pseudogenes, only *vapA* has been implicated in pathogenicity while all others are dispensable during infection and their functions are unknown [69, 70]. The PAI of pVapB (*vapB*, *-J*, *-K1*, *-K2*, *-L*, and *-M*) and pVapN (*vapO*, *-P*, *-N*, *-Q*, *-R* and *-S*) each have six full length genes that differ in amino acid sequence compared to pVapA or each other (pVapA:pVapB 41-99% *vap* identity; pVapN:pVapA/B 20-81% *vap* identity) but clearly arose from a common ancestor after gene duplication, diversification based on host,

and gene rearrangement [35, 63, 64]. *vapB* of pVapB, which has homology to *vapA*, is also a surface lipoprotein but results in a less toxic effect and is considered only an intermediately virulence plasmid when compared to pVapA [59]. In addition to the fact that pVapA is the most comprehensively studied virulence plasmid, the primary focus of this work is *vapA* of pVapA and therefore the details of each pVap PAI will not be described in further detail.

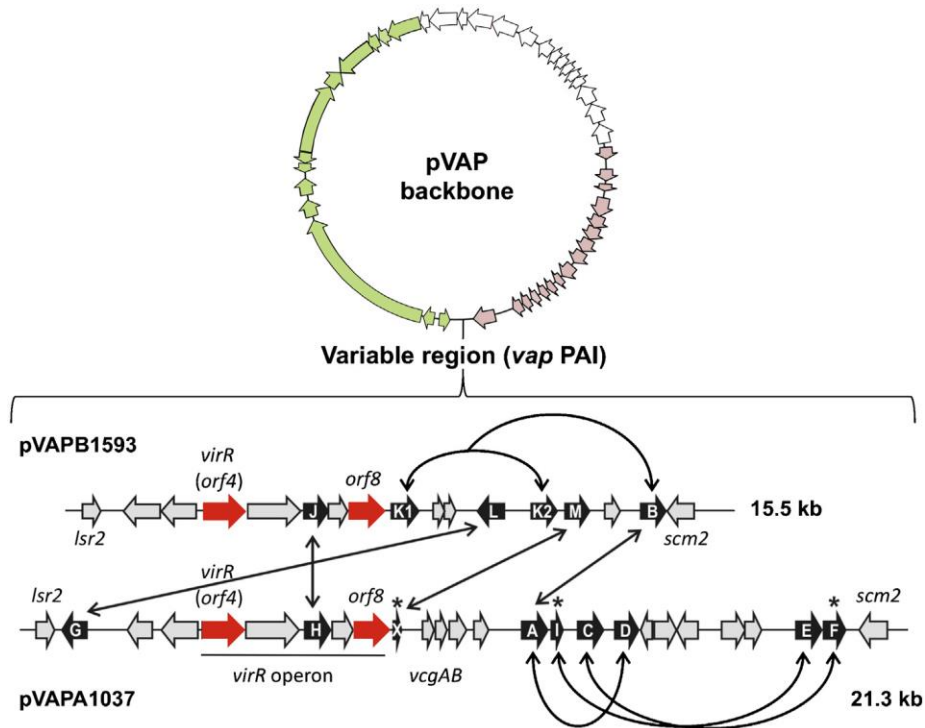


**Figure 2.4. Schematic of pVapA and pVapB variable regions.** Straight arrows show conserved genes, curved arrows show genes resulting from gene duplication. [35]

VapA is a 15-17kDa lipoprotein that is associated with the cell surface [71] and has been implicated in the characteristic defect in endosomal maturation [72] however beyond this, little is understood of its activity. Transcription of *vapA* as part of the *vapAICD* operon is regulated by temperature, pH, and the two transcriptional regulators of the *virR* operon, *virR* (*orf4*) and *virS* (*orf8*). Expression of *vapA* and other PAI genes is upregulated at 37°C and pH 6.5, which mimics macrophage conditions, while downregulated at 30°C and pH 8.0 [66, 71, 73-75]. The *virR* operon consists of five genes, two of which (*virR* and *virS*) encode regulatory proteins [68]. *virR* is a LysR-type regulator while

*virS* is an orphan two-component regulator that together control the expression of *vapA* and are required for its toxic effects as deletion of both *virR* and *virS* results in an attenuated mutant despite the presence of *vapA* [68, 76, 77]. *virR* negatively autoregulates its promoter however in acidic conditions and at 37°C an additional promoter within *virR* is activated which leads to the transcription of *virS*, collectively inducing expression of *vap* genes [77, 78].

To date, the structure of VapA is yet to be solved, however the crystal structure of VapB (76% sequence identity to VapA) [79], VapD (57% sequence identity to VapA) [80], and VapG (58% sequence identity to VapA) [81] have been solved. Each Vap structure is similar in structure but the following is specifically a description of VapB. The N-terminus was removed in order for successful crystallization and therefore is unresolved [79] but without the N-terminus, VapB forms an eight-stranded antiparallel  $\beta$ -barrel with a single helix and turn at the bottom and two loops between strands at the top [79]. The  $\beta$ -barrel consists of two Greek-key motifs which are common in five-stranded  $\beta$ -barrels, not eight-stranded, and follows strand organization of  $\beta$ -4, -1, -2, -3, -8, -5, -6, -7 rather than an organization of  $\beta$ -1-8 [79]. In general, the bottom of VapB contains more polar residues while the top is more hydrophobic [79]. VapB does not form a central pore but rather may be involved in yet unknown ligand binding [79]. Because of similarities in across all Vaps with crystal structures and high sequence identity, it is believed that VapA has a similar  $\beta$ -barrel structure with the first 20-50 amino acids considered the disordered domain and the remaining considered the conserved domain [79-81].

### **Chromosomal Virulence Factors**

Beyond the virulence plasmid, *R. equi* maintains several other chromosomal virulence factors that are similar to those of *M. tuberculosis*. *R. equi* maintains a type VII secretion system (T7SS) which can secrete proteins into the RCV [72] and may play a role in modulation of host immune response like *M. tuberculosis* [35] though there are no data to support that concept and its role in invasion is unknown. *R. equi* also has homologues to *M. tuberculosis* DosR regulon which encodes stress response

proteins and aids in the survival of *M. tuberculosis*, again however the role of these proteins in *R. equi* virulence is unknown (reviewed in [35]).

The outer membrane of *R. equi* consists largely of mycolic acids, which are necessary for *M. tuberculosis* survival, however deletion of an enzyme required to elongate side chains did not alter *R. equi* growth independently but did diminish its cytotoxicity in vivo, suggesting mycolic acids play a role in endosome maturation [82]. The cell envelope of *R. equi* contains lipoarabinomannan (LAM) which is a glycolipid that induces a host immune response in both *M. tuberculosis* and *R. equi*, and specifically for *R. equi* has been shown to play an important role in the initial equine macrophage cytokine response [83].

The primary carbon source for *R. equi* is short-chain organic and fatty acids and requires the activity of an isocitrate lyase for gluconeogenesis. Upon deletion of the isocitrate lyase, *R. equi* was less virulent in vivo and was not as capable replicating within macrophages, suggesting an important role in nutrient acquisition and intracellular survival [66, 84]. Consideration of nitrogen in the context of intramacrophage survival is important as well as the macrophage and phagosome have low nitrogen or nitrogen sources (nitric oxide) that cannot easily be utilized by *R. equi* [85]. Deletion of a nitrate reductase (*narG*), which is transcribed in the *narGHJ* operon of *R. equi* and responsible collectively for denitrification in anaerobic growth conditions, caused complete attenuation in vivo infections [86].

Iron is necessary for many metabolic pathways and thus, the growth of bacteria in many environments. The macrophage, specifically the phagosome, presents a particularly difficult environment for bacterial survival because in addition to hydrolytic enzymes, iron is depleted from the phagosome by an exporter, Nramp (natural resistance-associated macrophage protein), which plays a key role in macrophage survival in the presence of bacteria [87]. *R. equi* possess three different siderophores based on the iron ligation group to uptake iron from its environment. One siderophore (hydroxamate siderophore) was shown to play a role in the intracellular proliferation of *R. equi*, making it

an important factor for survival, while the other two were dispensable for virulence but were required for growth in non-intracellular conditions [88, 89].

Lastly, *R. equi* encodes for pili and maintains between two and five pili per cell that attach to epithelial cells and macrophages and are necessary for colonization of the lung in mouse models [35, 66]. *R. equi* also encodes for other surface-associated virulence factors such as its polysaccharide capsule that has led to the generation of over twenty serotypes of *R. equi* but does not play a distinct role in virulence [66, 90]. Both its pili and polysaccharide capsule are encoded within the horizontal gene transfer island of *R. equi* which is an area of continued interest in the context of the virulence of *R. equi* [66].

## **VIBRIO PARAHAEMOLYTICUS**

### **A Global Concern**

*Vibrio parahaemolyticus*, member of the Vibrionaceae family, is a halophilic Gram-negative opportunistic pathogen found globally in marine and estuarine waters and organisms [91]. *V. parahaemolyticus* is characteristically rod-shaped and maintains either a single polar flagellum for swimming or lateral flagella for swarming [92, 93]. *V. parahaemolyticus*, originally named *Pasteurella parahaemolytica*, was first identified as the cause of seafood borne illness in 1950 in Japan when an outbreak of *V. parahaemolyticus* in sardines resulted in the death of twenty people and gastroenteritis (symptoms include diarrhea, vomiting, and abdominal pain) in 272 people [94, 95]. Since its identification, *V. parahaemolyticus* has been identified as the cause of food borne illness outbreaks worldwide and remains the leading cause of gastroenteritis from food borne outbreaks in the United States and many southeastern Asian countries [96, 97]. Though better recognized as a food borne illness, infection with *V. parahaemolyticus* also occurs by its entry into open wounds or orifices while people are physically in marine waters and can result in wound infection (necrotic fasciitis) or septicemia [98]. Infections occur most frequently in summer months when waters are warmer and growth

conditions are optimal for *V. parahaemolyticus* [98]. In its most recent available report, the Centers for Disease Control and Prevention (CDC) describes that of all incidences of *Vibrio* infections (excluding *V. cholera*) in 2014, 48% (605 people)- which is the most abundant of all *Vibrio* reported - was caused by *V. parahaemolyticus*, with approximately 86 people hospitalized and 4 fatalities from *V. parahaemolyticus* infection in the U.S. alone [99]. Even as recent as this summer, the CDC reports outbreaks of *V. parahaemolyticus* from contaminated seafood [100]. Although these data are striking, many cases of *V. parahaemolyticus* infection go unreported and the actual number of *V. parahaemolyticus* infections may be higher [97, 98]. Typically for immunocompetent humans, the infection via ingestion is self-limiting however, in severe cases of wound infection or septicemia or in immunocompromised patients, antibiotics are used to treat *V. parahaemolyticus* infection often with limited success [98, 101, 102]. Multidrug antibiotic resistant *V. parahaemolyticus* has been isolated and is likely due to the excessive and improper use of antibiotics, particularly in aquaculture [97].

### **Virulence Determinants**

Though there are at least twelve different serotypes of *V. parahaemolyticus* that are pathogenic to humans, there are also many environmental strains that pose no threat to humans [97, 103]. Both clinical and environmental isolates have virulence determinants that play important roles in their survival.

#### *Toxins and Adhesins*

Nearly all clinical isolates of *V. parahaemolyticus* maintain thermostable direct hemolysin (TDH) and TDH-related hemolysin (TRH) genes which collectively result in hemolytic, cytotoxic, cardiotoxic, and enterotoxic effects to host intestinal cells [104]. TDH forms pores in erythrocyte membranes, allowing the passage of water and ions with low selectivity and in part, resulting in diarrhea that occurs during *V. parahaemolyticus* infection [104-107]. TRH is similar to TDH and additionally activates Cl<sup>-</sup> channels, exacerbating the ion flux from host cells [108, 109]. Though TDH and TRH aid in enterotoxic effects, they

alone are not responsible for the pathogenicity of *V. parahaemolyticus* as cytotoxic effects are observed in strains, clinical or environmental, that lack both TDH and TRH and suggests other cytotoxic components are present in all isolates (reviewed in [91]).

*V. parahaemolyticus* expresses the multivalent adhesion molecule, MAM7, which is an adhesin that attaches to eukaryotic cells during the onset of bacterial infection [110]. MAM7 interacts with PA at the plasma membrane as well as surface proteins [110, 111]. Without MAM7, it is possible *V. parahaemolyticus* cannot properly dock its target cell and therefore would fail to deliver its toxins necessary for pathogenesis [110].

### *Secretion Systems*

All isolates of *V. parahaemolyticus* contain the type III secretion system (T3SS), designated T3SS1, and the type VI secretion system (T6SS), designated T6SS2, while clinical isolates maintain an additional T3SS and T6SS designated T3SS2 and T6SS1 [112-117]. The T6SSs of *V. parahaemolyticus* have not been well studied and are beyond the scope of this work however studies show that each T6SS is activated in different conditions (marine water versus host cell) and are responsive to quorum sensing regulators [115, 118, 119]. The T3SSs are far better understood are described in more detail.

### T3SSs

T3SSs are common across Gram-negative bacteria and are known injectisomes that function to deliver effector proteins into target cells. Effector proteins are proteins that modulate host cell biology to counter host defenses and allow for the survival of the bacterium secreting such effectors [120].

Structurally, the T3SS consists of a needle complex and sorting platform where the needle complex is responsible for the translocation of effectors across the bacterial membrane and connected to the sorting platform which is a large cytoplasmic protein complex that sorts and prepares substrates for secretion (reviewed in [120]). Much of the protein secretion process is unknown however it has been implicated that the tip of the needle complex must be in contact with a target cell in order for protein

secretion and its preceding events that guide the proteins to and through the secretion complex to occur [120].

The T3SS1 present in all *V. parahaemolyticus* isolates is homologous to the T3SS of *Yersinia* in secretion system components however not in encoded effector proteins [121]. T3SS1 is regulated by three proteins, ExsC, D, and E which collectively control the transcriptional regulator, ExsA [122]. Typically, ExsA is inactive and bound to ExsD while ExsC, an anti-anti-activator, is bound to ExsE [122]. The system is activated in conditions of higher temperatures and lower  $\text{Ca}^{2+}$  concentration [121] which causes the secretion of ExsE and subsequent release of ExsC. ExsC then binds ExsD, releasing ExsA and allowing the transcription of T3SS1 genes [122].

To date, there are four secreted effectors that have been identified with T3SS1: Vibrio outer protein Q (VopQ), VopR, VopS, and VPA0450 [121]. Together, these effectors induce a series of events within the host cell beginning with autophagy, followed by cell rounding, and cell lysis within three hours of infection (Figure 2.5) [123]. VopQ is the focus of this project and will be described in more detail, briefly though, VopQ is a vacuole membrane specific pore-forming protein that induces autophagy upon injection into host cells and is necessary for *V. parahaemolyticus* cytotoxicity [124, 125]. VopS AMPylates Rho-family GTPases, targeting actin and causing cell rounding [126]. Rho GTPases are known to play an important role in actin dynamics, specifically in the assembly and organization of filamentous actin (F-actin) (reviewed in [127]). VopS contains a Fic domain (filamentation induced by cAMP) that allows for VopS to modify specifically Rho family GTPases at the switch I region with AMP and block downstream signaling of cell processes which results in cell rounding [126]. VPA0450 is an inositol polyphosphate-5-phosphatase that induces plasma membrane blebbing and cell lysis by hydrolyzing phosphate from  $\text{PI}(4,5)\text{P}_2$ , thereby disturbing actin anchoring sites at the host cell membrane [128]. VopR does not have a known function or target yet.

T3SS2 is considered responsible for the general enterotoxicity of *V. parahaemolyticus* infection (gastroenteritis symptoms) and is found only rarely in environmental isolates [112]. T3SS2 is induced in the presence of bile salts, which is present in the human gastrointestinal tract, and is regulated by VtrA, VtrB, and VtrC proteins [129, 130]. VtrA and VtrC are co-transcribed and form a  $\beta$ -barrel with a hydrophobic channel that specifically binds bile salts [129, 130]. Bile salts activate the cytoplasmic domain of VtrA which induces the transcription factor, VtrB, and results in the transcription of T3SS2 genes [129].

There are five characterized effectors associated with T3SS2: VopC, VopT, VopA, VopV, and VopL (Figure 2.5). VopC, through its deamidation activity, results in Rac GTPases and CDC42, which are involved in regulation and organization of F-actin that form phagocytic cups, being always active which subsequently causes cytoskeletal modulation and facilitates *V. parahaemolyticus* invasion into nonphagocytic cells [131]. VopT is an ADP-ribosyltransferase that modifies a Ras GTPase with NAD<sup>+</sup> and thereby alter its signaling capabilities, the precise activity caused by VopT is unclear however may involve further modification of the cytoskeleton as Ras GTPase typically play an important role in actin dynamics [132]. VopA is similar to Yersinia protein YopJ and inhibits MAPK (mitogen activated protein kinases) pathway signaling, which is necessary for communication from cell surface to nucleus, through the acetylation of a conserved catalytic loop present on kinases [133]. This acetylation mediated by VopA causes inhibition of the kinases by preventing their interaction with ATP and blocks future activation of kinases by preventing its ability to be phosphorylated and therefore, modulates eukaryotic signaling [133]. VopV binds specifically to and bundles F-actin [134]. VopL contains three Wiskott-Aldrich homology 2 (WH2) domains at its N-terminus that interact with and nucleate actin, resulting in the formation of long unbranched actin filaments instead of a network of branched actin which causes significant cytoskeletal stress for the host cell [135]. Ultimately, these effectors cooperate to modulate eukaryotic cell signaling and cell structure and results in cell lysis.

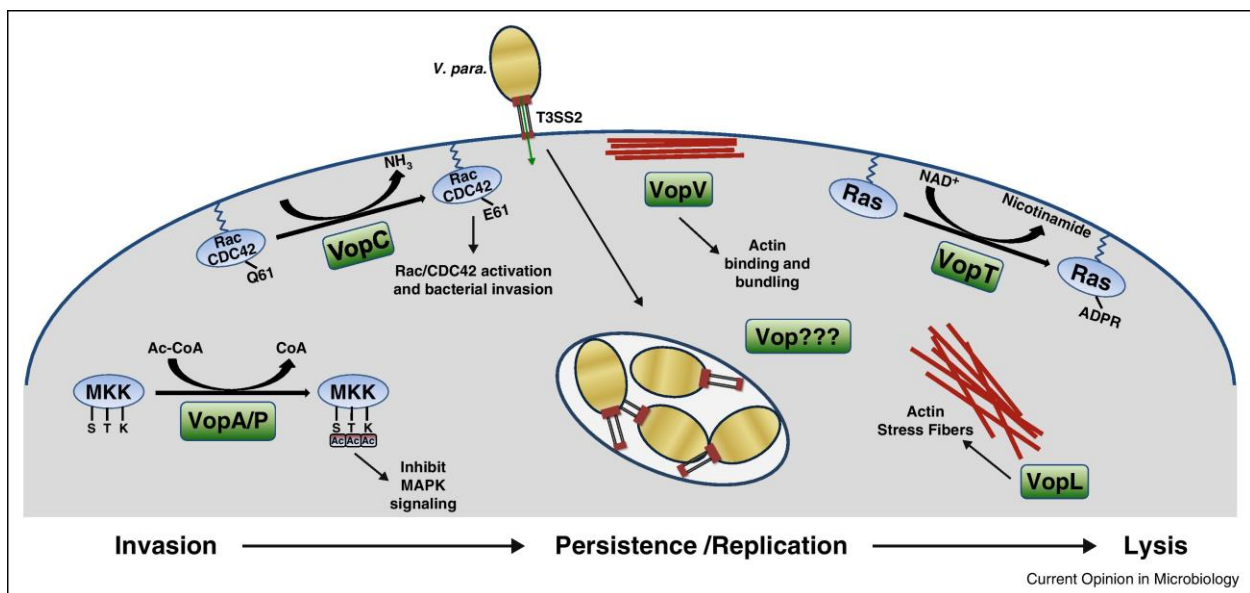
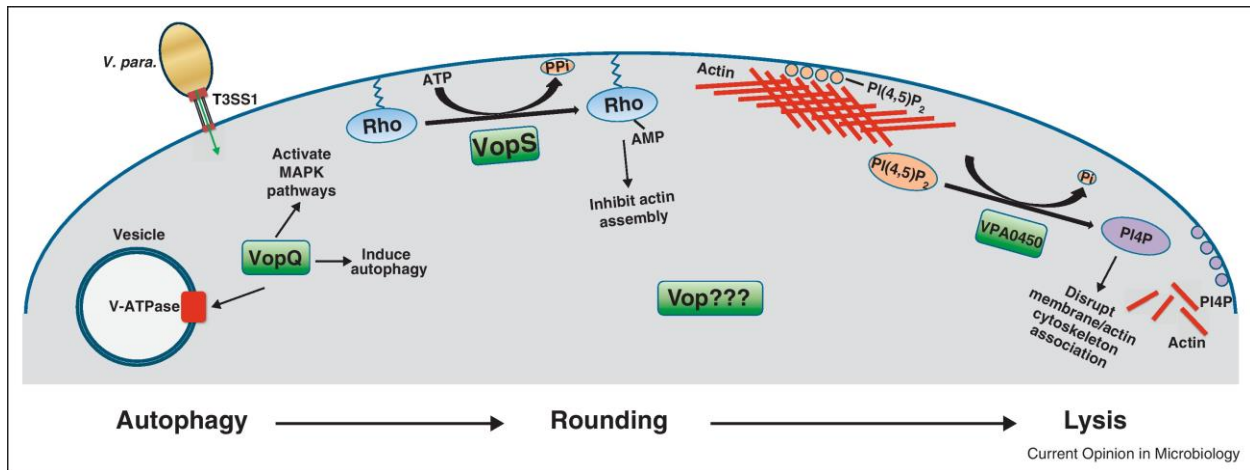


**Figure 2.5. Schematic of T3SS effector proteins and their role during invasion. Top) T3SS1 Bottom) T3SS2. [91]**

### VopQ

VopQ is a ~54kDa protein that shares little homology to other bacterial proteins outside of the *Vibrio* genus and is alone cytotoxic to cells through its multifaceted activity. In an analysis of the cytotoxicity of *V. parahaemolyticus* expressing only T3SS1, it was determined that VopQ alone is sufficient for the induction of autophagy and cell lysis as *vopQ* deletion strain is attenuated in tissue infections while *vopS* deletion strain is not [124]. Autophagy induced by VopQ occurs in a PI3-kinase

independent pathway which is unlike typical cellular processes in which the PI3-kinase (or kinase complex in higher eukaryotes) is necessary for the enrichment of PI(3)P at early endosomal membranes and subsequent processes that traffic the early endosome to the vacuole/lysosome (described previously) [136]. Though independent of PI3-kinase activity, VopQ induced autophagy does require the downstream autophagy proteins for activity [124]. Interestingly, in the presence of chemical autophagy inhibitors, VopQ can still induce autophagy [124]. Upon induction of autophagy by VopQ protein alone in eukaryotic cells, autophagic vesicles accumulate within an hour (which is rapid) of *V. parahaemolyticus* infection [124]. Because VopQ induces autophagy rapidly, it coincidentally causes the attenuation of phagocytosis as cellular machinery is hijacked for autophagic processes, thus preventing multiple or additional bacteria from phagocytosis following the activity of VopQ

In addition to its ability to induce autophagy, VopQ interacts with the V-ATPase and forms a gated 18Å pore in the vacuole membrane [125, 137]. Through biochemical analysis, it was determined that VopQ interacts in vitro with the assembled membrane embedded  $V_o$  domain of the V-ATPase but not with  $V_1$  in yeast and mammalian cells [125]. In a toxicity growth assay using V-ATPase subunit deletion strains, VopQ was no longer toxic to yeast upon its expression in a *VMA3Δ* strain and had only intermediate toxicity in *VMA21Δ* and *VMA9Δ* strain. Interestingly, deletion of any  $V_o$  subunit results in the failure of proper  $V_o$  formation or failure of  $V_o$  transport to the vacuole membrane so the need for Vma3p alone is interesting when essentially in most cases,  $V_o$  is not assembled or tagged to the vacuole membrane. The method with which VopQ targets  $V_o$  and how it precisely recognizes the  $V_o$  domain remains unknown. VopQ maintains a pI ~6 and is positively charged in acidic conditions and has been shown to embed itself in liposome membranes in the absence of the  $V_o$  at pH 5.5 if the liposomes consist of greater than 5% negatively charged lipid containing liposomes but not at pH 7.5 when VopQ is negatively charged [125]. Though this suggests an electrostatic role in the interaction of VopQ with

acidic membranes, the presence of  $V_o$  is necessary for the targeting of VopQ to acidic membranes at physiological pH and physiological lipid membrane compositions.

Upon VopQ recognizing the  $V_o$  domain, VopQ embeds itself into the membrane in a yet unknown manner and forms a pore in the vacuole membrane gated and facing outward (towards the cytoplasm) [125]. The pore formed allows the nonselective passage of ions, small molecules, and proteins less than 3kDa in size across the vacuole membrane, resulting in the abrogation of both the proton (pH) and electrochemical gradients but does not rupture the organelle [125]. VopQ both causes the deacidification of acid vacuoles and lysosomes and prevents acidification of vacuoles [125]. Nonetheless, VopQ does not interfere with V-ATPase pumping activity despite its contact with the V-ATPase [125]. The ability of VopQ to deacidify degradative compartments is comparable to chloroquine which perturbs the turnover of autophagosomes through its neutralization of acidic compartments [125]. Comparison of VopQ to chloroquine shows that VopQ similarly deacidifies acidic compartments, causing failed turnover of autophagosomes, and an accumulation of autophagic vesicles in the cell [125], showing that the autophagic and pore-forming activities of VopQ are interconnected. [124]. VopQ has also been implicated in the modulation of the MAPK signaling pathway and induction of IL-8 secretion (interleukin-8, cytokine that targets neutrophils and induces chemotaxis), which has been a feature identified among other pore forming proteins, and may be a direct result of its pore forming activity as its disruption of cytosolic ion concentrations can act as a stress signal to MAPK pathway which induces IL-8 secretion [125, 138-140]. Collectively, VopQ alone shows an impressive ability to modulate eukaryotic host cell processes for survival of *V. parahaemolyticus* upon its invasion.

### **SACCHAROMYCES CEREVISIAE AS A MODEL ORGANISM**

With the function of over 75% of yeast ORFs described and readily accessible in public databases [141], *S. cerevisiae* (yeast) remains a widely used and well-researched model eukaryotic organism that is tractable for standard genetic and biochemical laboratory procedures. Because eukaryotic cellular

processes are highly conserved from yeast to higher mammals, *S. cerevisiae* has been used as an effective tool to identify putative effector proteins secreted by bacterial pathogens of mammals, such as *Legionella pneumophila* [142], *Salmonella typhimurium* [143], *Shigella flexneri* [144], *Vibrio parahaemolyticus* [137], and *Yersinia* species [143]. Such bacterial effectors often target conserved eukaryotic processes and result in significant growth and trafficking defects in yeast, making specifically yeast lethality upon protein induction an identifier for bacterial modulation of eukaryotic processes [141]. *S. cerevisiae* as a mock eukaryotic host provides the means to study proteins secreted by organisms - rather than the organisms themselves - that live in broadly unique environments, including obligate or facultative intracellular organisms that would otherwise pose significant challenges to researchers using standard laboratory techniques. Further, *S. cerevisiae* provides an inexpensive way to pilot studies of pathogens that significantly impact human and animal health. Understanding how bacterial secreted proteins modulate yeast cellular processes allows researchers to draw valuable parallels to cellular processes in higher eukaryotes, including humans.

#### **MEMBRANE TRAFFICKING IN YEAST**

*S. cerevisiae* maintains several trafficking pathways necessary for the flux of highly specialized compartments around the cell containing material synthesized within the cell, endocytosed from the environment, or targeted for degradation or exocytosis. Trafficking plays a vital role in the overturn of material, allowing for the recycling of spent proteins, lipids, and other small molecules. Trafficking pathways in *S. cerevisiae* are highly conserved among eukaryotes and have provided a wealth of information regarding these processes in higher eukaryotes, such as humans, where defects in trafficking can result in disease [145] or defects are the result of a bacterial secreted protein manipulator that aids in bacterial pathogenesis in humans.

## The Secretory (SEC) Pathway

The secretory pathway (Figure 2.6) begins in the endoplasmic reticulum (ER) where newly synthesized proteins are prepared for transport via vesicles to the Golgi. Vesicles moving between ER and Golgi are laden with coat proteins – clathrin, COPI, or COPII – which shape budding membranes into spherical vesicles. COPII vesicles specifically move from the ER to the Golgi and contain ER sorting receptors that sort the protein cargo based on protein location (i.e. soluble luminal proteins would be sorted with a different ER receptor than would plasma membrane proteins) [146]. COPI-coated vesicles are specific for the retrograde pathway that moves cargo from the Golgi back to the ER or between Golgi cisternae, while clathrin-coated vesicles originate from the plasma membrane (PM) and trans-Golgi network (TGN) and fuse with endosomes or the vacuole depending on clathrin associated adaptor protein complexes (APs) present on the vesicle [147].

### *Vacuole Protein Sorting (VPS) Pathway*

Following COPII-coated vesicles that have been transported to the Golgi, proteins that are targeted to the vacuole and have been sorted by their interaction to the adaptor AP-1 complex (among other proteins), will follow the vacuole protein sorting (VPS) pathway that directs now clathrin-coated TGN-derived vesicles to fuse with the early endosome, late endosome [or multivesicular body (MVB)], and finally, to the vacuole [148, 149]. At each stage, the process of fusion requires a tethering complex to mediate contact between the donor and target compartment, a Rab GTPase to anchor the tethering complex to the target compartment, and a set of four SNAREs [soluble NSF(N-ethylmaleimide-sensitive factor) attachment protein receptor] to form a zippered complex that mediate the mixing of lipid bilayers and luminal content.

Within the VPS pathway, proteins targeted to the vacuole must be further sorted in accordance with their solubility. The sorting of soluble proteins follows the carboxypeptidase Y (CPY) pathway, so named because CPY is a highly studied soluble protease trafficked to the vacuole in this pathway [146].

In the ER, synthesized preproCPY (immature form of CPY) undergoes cleavage of its signal sequence to form p1 proCPY (p1CPY) and further oligosaccharide modification to form p2CPY [150]. p2CPY is bound to a transmembrane receptor protein, Vps10p, that facilitates its transport from the TGN to the endosome [151]. At the endosome, the CORVET (class C core vacuole/endosome tethering) complex interacts with the Rab GTPase, Vps21p, and the luminal contents, including soluble p2CPY, are released into the MVB while Vps10p is recycled for further sorting [150, 151]. Upon fusion of the MVB with the vacuole, p2CPY is cleaved by proteases to result in the active and mature form of CPY in the lumen of the vacuole.

Membrane proteins targeted to the vacuole necessitate an additional step and undergo MVB sorting which requires the five ESCRT (endosomal sorting complex required for transport) protein complexes (0-IV) for protein sorting, inward budding or scission of membranes, and degradation of membrane proteins [152]. Membrane proteins exiting the TGN are ubiquitinated which serves as a signal for entry to the ESCRT pathway [153]. Ubiquitin modified proteins are sorted into intraluminal vesicles (ILVs) which are vesicles within an endosomal compartment that empty into the vacuole after eventual MVB fusion with the vacuole [153]. Sna3p is one well-studied ligase adaptor protein that travels this pathway and is used commonly to following trafficking to the vacuole in yeast [154].

#### *Alkaline Phosphatase (ALP) Pathway*

Through analysis of the unique trafficking pattern of the vacuolar protease, alkaline phosphatase (Pho8p), a direct Golgi-to-vacuole pathway was identified [155]. Proteins targeted directly to the vacuole from the TGN are sorted into AP-3 clathrin coated vesicles that fuse with the vacuole without intermediary sorting or endosome fusion. Regardless of the pathway taken to reach the vacuole, which is the final destination for many trafficking pathways, fusion at the vacuole requires the HOPS (homotypic fusion and protein sorting) tethering complex, the Rab GTPase Ypt7, and the four vacuolar SNAREs (described in more detail below).

## Exocytic (EXO) Pathway

The exocytic pathway refers to the transport of newly synthesized proteins from the TGN to the plasma membrane for secretion outside of the yeast cell. The vesicles destined for the plasma membrane move along yeast actin filaments to the exocyst. The exocyst is a multimeric protein complex of eight subunits that is localized at the growing bud neck and is pivotal for polarized membrane growth [156, 157]. Some components of the exocyst are localized to the plasma membrane to recruit other components that are present on the membranes of secretory vesicles [158]. Once at the plasma membrane, docking and fusion occur to release the contents outside of the yeast cell.

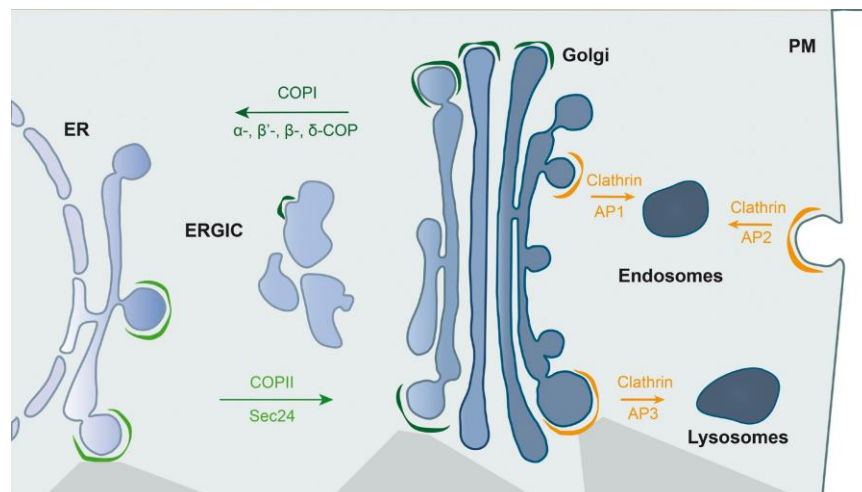


**Figure 2.6. Overview of secretory pathways and coat proteins required for each pathway.** Modified from [147].

## Endocytic (END) Pathway

The endocytic pathway involves the internalization of extracellular or surface-cellular matter that is either recycled or degraded in the vacuole. The influx of extracellular material (or fluid-phase endocytosis) is considered both nonspecific and constitutive while receptor mediated endocytosis at the surface of the cell requires the binding of a ligand to a receptor to initiate endocytosis. The endocytic pathway for either process (fluid-phase or receptor-mediated) require clathrin coat with AP-2 adaptors and are actin-dependent [reviewed in [146, 159]]. The recruitment of AP-2 to the endocytosis site

initiates endocytosis and results in the recruitment of other epsin coat proteins. Invagination and scission of the membrane occurs with the recruitment of the WASP (Wiscott-Aldrick Syndrome Protein) protein Las17p, myosin (Myo5p), actin, and Arp2/3 complex, which nucleates actin filaments [160-162]. With the activity of a few additional proteins, the vesicle is released from the plasma membrane and trafficked to endosomes for sorting that directs cargo to the vacuole or back to the Golgi.

## **Autophagy**

Autophagy is the process by which cellular material is shuttled to the vacuole for degradation and recycling, particularly during times of cellular damage and/or starvation. There are four overarching types of autophagy in yeast: Selective or nonselective macroautophagy and selective or nonselective microautophagy. The following is an overview of each of these processes that presents the highlights of each process as it pertains to the larger theme and goal of this work.

### *Nonselective Microautophagy*

Nonselective microautophagy is a poorly understood process, both in scope of the machinery needed for the process to occur and in physiological benefits for such a process. The process of nonselective microautophagy entails the invagination and inward budding of the vacuolar membrane, generating an intravacuolar vesicle(s) containing nonspecific cytoplasmic fluid. The intravacuolar vesicle must then be degraded by the vacuole however since it originates from the vacuolar membrane, it is unknown how the cell degrades the vesicle without perturbing or degrading the entirety of the vacuolar structure. [reviewed in [163]]

### *Selective Microautophagy*

Selective microautophagy targets mitochondria (micromitophagy), peroxisomes (micropexophagy), and the nuclear membrane (micronucleophagy) but much like nonselective microautophagy, the uptake of targeted cell structures involves the invagination of the vacuolar membrane to form ILVs and the mechanism by which this invagination is initiated remains unknown.

Micromitophagy is not well understood in this context, but it is suggested that the vacuole protrudes to sequester mitochondria at the vacuolar membrane where it is then undergoes inward blebbing to generate an ILV for degradation [164]. Micropexophagy involves the formation of a micropexophagic apparatus (MIPA) that acts as a scaffolding complex to sequester peroxisomes at the vacuolar membrane, which is then enclosed in ILV within the vacuole [165]. Much of this work however has been performed in methylotrophic yeast and has not been confirmed in *S. cerevisiae*. Finally, micronucleophagy occurs when small pieces of the nucleus protrude into the vacuole lumen and then undergoes scission to separate the small nuclear piece and generate an ILV [163, 166].

#### *Nonselective Macroautophagy*

Nonselective macroautophagy is the bulk sequestration of cytoplasmic cargo in a double membrane compartment that is targeted to the vacuole for degradation. The biogenesis of the initial compartment, termed the phagophore, is poorly understood but it is known that the phagophore nucleation site occurs near the vacuole where autophagy-related (Atg) proteins are concentrated and is therefore deemed the phagophore assembly site (PAS). The phagophore will expand and complete the sequestration of cargo, forming a sealed compartment called the autophagosome. The autophagosome then fuses with the vacuole, transferring the cargo to the lumen of the vacuole for degradation.

[reviewed in [163]]

#### *Selective Macroautophagy*

The process of selective macroautophagy follows the same general process as nonselective macroautophagy, the primary difference being that the cargo is specific and thus the sequestered compartments have unique names. Selective macroautophagy targets mitochondria (mitophagy), peroxisomes (pexophagy), ribosomes (ribophagy), endoplasmic reticulum (reticulophagy), and hydrolases (noncanonical autophagy process called the Cvt pathway) [163]. For each target of selective macroautophagy, recognition of cargo involves specific Atg receptors. The Cvt pathway is one of the

best characterized examples of selective macroautophagy and can be used as a general model for the understanding of other processes.

#### *Cytoplasm to Vacuole Trafficking (Cvt) Pathway*

Cvt trafficking is considered a noncanonical autophagy pathway that bundles hydrolases within the cytoplasm for delivery to the vacuole. This process relies on the aminopeptidase I (Ape1) which in its immature form, prApe1, maintains signaling information to target cargo to the vacuole [167, 168]. prApe1 binds Atg proteins (specifically Atg19p, which then binds Atg11p and Atg8p located at the PAS) and forms a complex, called the Cvt complex [169, 170], which is enveloped by a membrane to develop into an autophagosome that will then fuse with the vacuole for release of its contents [171, 172]. This process is used during vegetative periods or times of nutrient deprivation to recycle materials for biosynthetic processes [173].

#### *Vacuole Import and Degradation (Vid) Pathway*

The Vid pathway is responsible for the translocation of specific substrate proteins into vesicles that cluster with endosomes at actin patches prior to transport and fusion with the vacuole. The process requires the HOPS tethering complex and Ypt7p as well as the Vph1p subunit of the vacuolar-type H<sup>+</sup>-ATPase (V-ATPase). The Vid pathway is induced following significant glucose starvation. [163]

#### **Fusion Components and Stages of Fusion**

The final step of membrane trafficking is fusion of the donor and target compartments. Each pathway requires a unique set of fusion proteins and lipids to regulate the fusion process which moves through a series of stages (priming, tethering, docking, and fusion). Here, components of the fusion process and stages of fusion will be broadly presented.

#### *Rab GTPases*

Rab GTPases (Rabs) are members of the Ras superfamily of small GTPases and play a pivotal role in the organization of membrane trafficking in eukaryotes from yeast to humans by correctly

transporting vesicles, targeting cargo, and attaching proper donor and target membranes for fusion [174]. Across eukaryotes, the structure of Rabs is highly conserved with six-stranded  $\beta$ -sheet flanked by 5  $\alpha$ -helices and a variable cysteine motif for prenylation at the tail [174]. *S. cerevisiae* maintains eleven Rabs [175] that are present at different stages of membrane trafficking and fusion (Table 2.1), though how Rabs are targeted to specific membranes remains conjecture [176]. In order for Rabs to localize to membranes, they require prenylation at their C-terminal cysteines following their synthesis [177, 178]. Prenylation requires that the Rab is first bound by the Rab escort protein, Mrs6p, to allow the Rab geranylgeranyltransferase to perform the prenylation [179, 180]. The prenylated Rab is then transported to an appropriate target membrane where it is activated by a GEF (guanine nucleotide exchange factor) which catalyzes the exchange of bound GDP with GTP, thereby activating the Rab (reviewed in [176]). Rabs have two conformations, GTP-bound and GDP-bound, and are considered active in the GTP-bound conformation [181] in which Rabs are membrane bound and are additionally bound by effectors (i.e. tethering complexes) for targeted membrane fusion. The conformational changes that allow GTP or GDP to bind require significant change to variable regions, designated switch I and switch II, which have a more ordered form when GTP is bound than GDP [182]. Following their role in fusion events, Rabs are inactivated by GAPs (GTPase activating proteins), which catalyze the hydrolysis of GTP to GDP, and can be removed from target membranes through the activity of GDIs (GDP-dissociation inhibitor), which solubilizes the GDP-bound Rab [176]. Finally, a GDF (GDP-dissociation factor) can dissociate the GDI to allow solubilized and inactivated Rabs to become membrane bound once again [183].

**Table 2.1. Overview of *S. cerevisiae* Rab GTPases [184, 185]**

<b>Yeast Rab GTPase</b>	<b>Locale/Function</b>
Ypt1p	Localized to ER, early Golgi, early autophagosomal, and cytoplasmic vesicles; required for ER-to-Golgi, intra-Golgi trafficking, and ER-to-autophagosome transport
Ypt6p	Localized to the Golgi (GTP-bound) or cytosol (GDP-bound); required for retrograde traffic endosome-to-Golgi, intra-Golgi, and Golgi-to-ER as well as delivery of Atg9 to PAS during autophagy
Ypt7p	Localized to vacuole:mitochondrial contact sites; required for late endosome and vacuole fusion events
Ypt10p	Unknown localization; involved in vesicular transport
Ypt11p	Localized to the peripheral ER; involved in vesicular transport of cortical ER, late Golgi, and mitochondria from mother-to-daughter bud
Ypt31p	Localized to Golgi; involved in late Golgi-to-PM (exocytic pathway), intra-Golgi transport, and budding of trans-Golgi vesicles
Ypt32p	Paralog of Ypt31, functionally indistinct and interchangeable with Ypt31
Ypt52p	Localized to endosomes; required for localization of CORVET to endosomes, required for vacuolar protein and MVB sorting as well as endocytosis, involved in ionic stress tolerance and autophagy
Ypt53p	Paralog of Vps21, localized to endosomes; stress-induced but function is Vps21 redundant
Vps21p	Localized to early endosomes; required for localization of CORVET to endosomes, endocytic transport, and vacuole hydrolase sorting, required for MVB sorting with Ypt52, involved in ionic stress tolerance and autophagy
Sec4p	Localized to trans-Golgi vesicles (GTP bound), required for exocytic secretion and autophagy

### *Tethering Complexes - Overview*

There are two overarching categories of tethering complexes, multisubunit tethering complexes (MTCs) and coiled-coil proteins tethers that operate throughout different stages of trafficking and play a pivotal role in bridging donor to target vesicles. MTCs consist of multiple subunits (3-10) that can span distances between membranes of up to 30nm. Typically, MTCs are active in the endomembrane system and at the plasma membrane and maintain Rab recognition subunits for appropriate membrane tethering. MTCs are further divided into three groups – the endolysosomal complexes (HOPS and CORVET), the SEC pathway complexes (Complex Associated with Tethering Containing Helical Rods (CATCHR) family complexes), and the TRAPP (transport protein particle) complex. Conversely, coiled-coil

protein tethers are hydrophilic dimers with two globular heads that can span larger distances (more than 200nm) and are found primarily in the Golgi and a few at endosomes. Coiled-coil tethers can bind adaptors, such as the Arf GTPase, lipids, or maintain a carboxyterminal transmembrane domain. Coiled-coil protein tethers will not be discussed in further detail as it extends beyond the scope of this work. [Reviewed in [186, 187]]

### *Vps Class C Complexes*

The endolysosomal tethering complexes, collectively called the Vps Class C complexes, are involved in fusion at early endosomes (CORVET complex) and fusion at the late endosome and vacuole (HOPS complex). Performing a similar function, both the CORVET and HOPS complex are believed to have a similar “seahorse” structure (Figure 2.7) that consists of four shared core subunits and two (each) unique Rab-binding subunits located on either end of the complex [188]. The shared core subunits are Vps16p, Vps33p, Vps18p, and Vps11p and the Rab specific subunits are Vps3p and Vps8p for CORVET (specific to Vps21p/Rab5) [189] and Vps39p and Vps41p for HOPS (specific to Ypt7p/Rab7) [190]. Both the HOPS and CORVET complexes form a physical bridge between membranes, binding to Rab GTPases present on two distinct membranes with Rab specific subunits and bridging the two membranes with its core subunits [191].

Each of the four core subunits plays a unique role in the progression of membrane fusion. Vps16p interacts with the H<sub>abc</sub> domain of Vam3p, the vacuolar Qa-SNARE [192], and is required for the proper association of Vps33p with other core subunits, as without Vps16p, Vps33p does not associate with core subunits of tethering complexes [193]. Vps18p maintains a RING (really interesting new gene)-finger domain, a domain that is important for the function of the tethering complexes as mutations result in temperature-sensitive sorting defects [194, 195], and is required for Vps33p to interact Vam3p at the vacuole [193]. Vps11p also has a RING-finger protein domain and functions in membrane tethering and proofreading of SNAREs in conjunction with other subunits [196]. Finally, Vps33p is a

Sec1/Munc18 SNARE master (SM) protein that interacts with Vam3p and Nyv1p SNARE motifs on opposing membranes during vacuolar fusion, acting as a template to ensure appropriate *trans*-SNARE complex formation [197]. Vps33p also interacts with Vam7p, the vacuolar SNARE that lacks a transmembrane domain, via its PX (phox homology) domain to recruit it to the vacuole membrane [198-201]. Additionally, Vps33p, at least in the context of the HOPS complex, is known as a proofreader of proper SNARE complex formation at the 0-layer (3Q:1R) and will inhibit the fusion of membranes if mismatched or rotated SNARE assembly is detected [202]. Vps33p also binds to the assembled vacuolar Q-SNARE complex to prevent its disassembly by the chaperone protein, Sec18p [200, 203].

### HOPS

The two unique subunits of the HOPS complex, Vps39p and Vps41p, are known to interact with Ypt7p (homologue of mammalian Rab7). Although initially it was believed that Vps39p additionally served as the GEF for Ypt7p, it has since been determined that a separate complex, the Mon1-Ccz1 complex, acts as the GEF that modulates the conversion of GTP to GDP at Ypt7p [204]. Vps41p, the HOPS effector of Ypt7p, is essential for HOPS binding of Ypt7p and predominantly binds the GTP-bound (active) conformation while Vps39p binds either the GTP or GDP-bound (inactive) conformation of Ypt7p [205]. Vps41p plays a pivotal role in the modulation of HOPS-specific fusion events from different trafficking pathways at the vacuole as it is known to bind additional proteins associated with specific fusion events. Importantly, one form of HOPS regulation via Vps41p phosphorylation has been identified as a necessary component of the AP-3 clathrin coated vesicle/ALP fusion pathway. Yck3p is a casein kinase localized to the vacuolar membrane via the ALP pathway [206] that phosphorylates the ALPS (amphipathic lipid packaging sensor) helix of Vps41p, consequently weakening the interaction between Vps41p and its associated membrane [207, 208]. The ALPS motif is known to detect membrane curvature and is inserted into highly curved membranes (i.e. late endosomes), however when the ALPS motif of Vps41p is phosphorylated, it prevents Vps41p from reinserting its ALPS into the membrane

[207]. Once Vps41p is phosphorylated, it cannot shield Ypt7p and thus, makes Ypt7p more susceptible to known Ypt7p inhibitors, Gdi1p and Gyp7p, which collectively block the dissociation of GDP from Ypt7p and leave the pool of Ypt7p inactive and incapable of being bound by Vps41p [208, 209]. Finally, the phosphorylation of Vps41p and the weakening of its interaction with membranes allows for the presentation of an AP-3 complex protein (Apl5p) binding pocket in Vps41p which will then promotes the fusion of AP-3 vesicles with the vacuole [210]. In the absence of Yck3p, Vps41p accumulates at endosomes and the trafficking of AP-3 vesicles to the vacuole is defective, therefore making the phosphorylation of Vps41p necessary for successful trafficking of AP-3 vesicles [207].

### CORVET

The CORVET complex is not as well understood as the HOPS complex, however the general concept of structure and function is similar. The two unique CORVET complex subunits are Vps3p and Vps8p. Vps3p is in the same structural position as the HOPS subunit Vps39p while Vps8p and Vps41p mimic each other in complex position. As is the case in the HOPS complex, Vps8p binds to Vps21p (homologue of mammalian Rab5) preferentially in its GTP-bound conformation while Vps3p binds to Vps21p in any conformation [189]. Vps8p maintains a RING-finger domain that is suggested to play a role in the integrity of protein sorting [211].

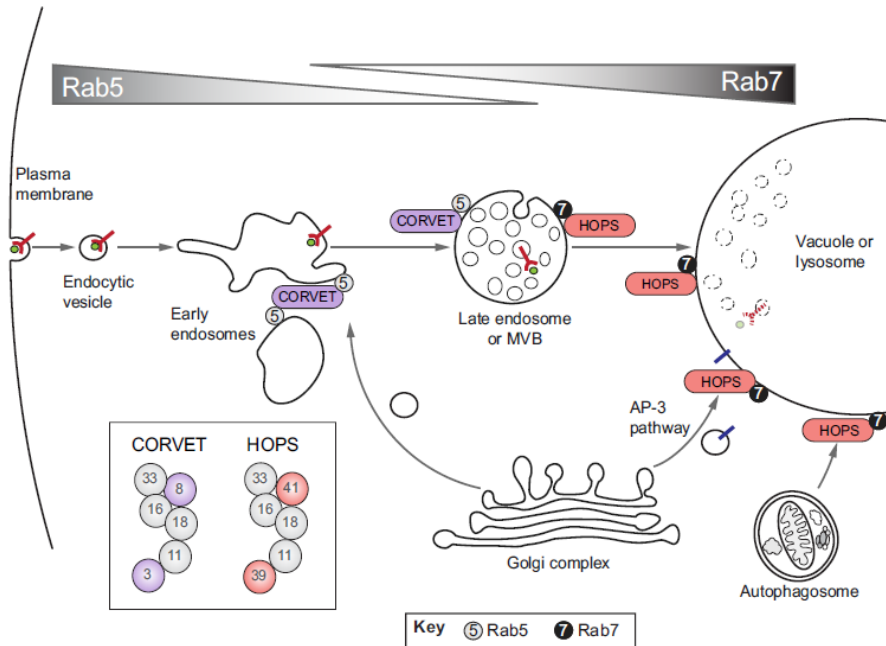


**Figure 2.7. HOPS and CORVET tethering complexes during progression of successive fusion events.** [188]

### *CATCHR Family*

The CATCHR family tethering complexes operate throughout the SEC pathway to tether vesicles and include the Dsl1 complex, the COG (conserved oligomeric Golgi) complex, the GARP (Golgi associated retrograde protein) complex, and the exocyst complex. The details of each complex are beyond the scope of this work, however the function of each complex is briefly noted. Dsl1 is present in the ER and binds COPI Golgi derived vesicles for delivery at the ER [212, 213]. The COG complex mediates retrograde transport of vesicles in between Golgi cisternae [214] while the GARP complex operates in retrograde traffic between the endosome and TGN [215]. Both the COG and GARP complexes directly bind an SM protein and SNAREs [186]. Finally, the exocyst is present at the plasma membrane where it mediates the fusion of vesicles with the plasma membrane and is known to interact with an SM protein and SNAREs [216, 217].

### *TRAPP Complexes*

Transport protein particle (TRAPP) family tethering complexes consist of the TRAPP I, II, and III complexes, each consisting of many subunits all building on the six core subunits that derive the TRAPP I complex [186, 218]. TRAPP I mediates ER to Golgi transport of COPII vesicles [218-220], TRAPP II is required at the TGN and binds COPI vesicles [221, 222], while TRAPP III is required for autophagy as it localizes at the PAS [223]. The TRAPP complexes act as GEFs to release GDP from bound GTPases (specifically TRAPP I for Ypt1p and TRAPP II for Ypt31p/Yt32p) [220, 222, 224]. It is believed that their function as GEFs allows TRAPP complexes to mediate tethering at different locations within the cell [186].

### *SNAREs*

SNAREs (souble NSF [N-ethylmaleimide sensitive factor] attachment protein receptors) are structurally conserved proteins that are required typically in sets of four (3Q:1R) for fusion between two membranes [225, 226]. SNAREs have heptad repeat domains which form a tetrameric  $\alpha$ -helical coil upon association with each other [227]. Each SNARE domain has layers with its centermost layer designated the 0-layer or ionic layer [227]. At the highly conserved 0-layer, SNAREs have either a glutamine residue, deemed Q-SNAREs, or an arginine residue, deemed R-SNAREs [225]. Q-SNAREs are then further classified based on sequence conservation of the N- and C- terminal regions into Qa, Qb, and Qc subfamilies [228]. Of note, the Qa subfamily contains the conserved N-terminal H<sub>abc</sub> domain which may bind tethering complexes and autoinhibit SNARE complex formation [192, 229-231]. Collectively, a typical SNARE complex must consist of one of each classification of SNARE - Qa, Qb, Qc, and R or 3Q:1R – to maintain its function [225, 227]. Beyond the 0-layer, SNAREs in complex interact at additional layers (-7 through +8) with hydrophobic amino acid residues that form leucine zipper-like layers [227]. SNAREs typically are anchored to membranes by a transmembrane domain however some SNAREs instead

contain a prenylation consensus motif that requires palmitoylation or farnesylation prior to becoming membrane anchored [232].

SNARE proteins at the same membrane that are in complex with each other are in *cis* (or *cis*-SNAREs) and fusion-inactive while SNAREs that interact with SNAREs on opposing membranes are in *trans* (or *trans*-SNAREs) and fusion-active [233]. Prior to membrane fusion occurring, inaccessible *cis*-SNARE complexes must be disassembled to allow the interaction and formation of *trans*-SNARE complexes between two membranes. This disassembly in the context of yeast vacuole fusion is performed by Sec17p and Sec18p which are an  $\alpha$ -SNAP (soluble NSF attachment protein) adapter and an AAA (ATPases associated with diverse cellular activities)-ATPase/NSF, respectively. Sec17p binds the *cis*-SNARE complex which results in the recruitment of Sec18p, Sec18p then couples the hydrolysis of ATP with the disassembly of the *cis*-SNARE complex and the dissociation of Sec17p from the complex with the aid of ergosterol [226, 234, 235]. The activity of Sec18p is dependent on  $Mg^{2+}$  which is shown to aid in coupling the hydrolysis of ATP and disassembly of *cis*-SNAREs [236, 237]. Tethering complexes can then aid in the formation of *trans*-SNARE complexes and, as is the case with the HOPS complex, may provide proofreading to ensure the *trans*-SNARE complex is correctly assembled prior to membrane fusion [197, 202, 238]. Following the fusion event, SNAREs return to *cis*-SNARE complexes as they now reside within the same membrane.

Different SNAREs are specific to different membranes for specific fusion events, though overlap does occur. SNAREs are depicted by trafficking pathway in Figure 2.8.

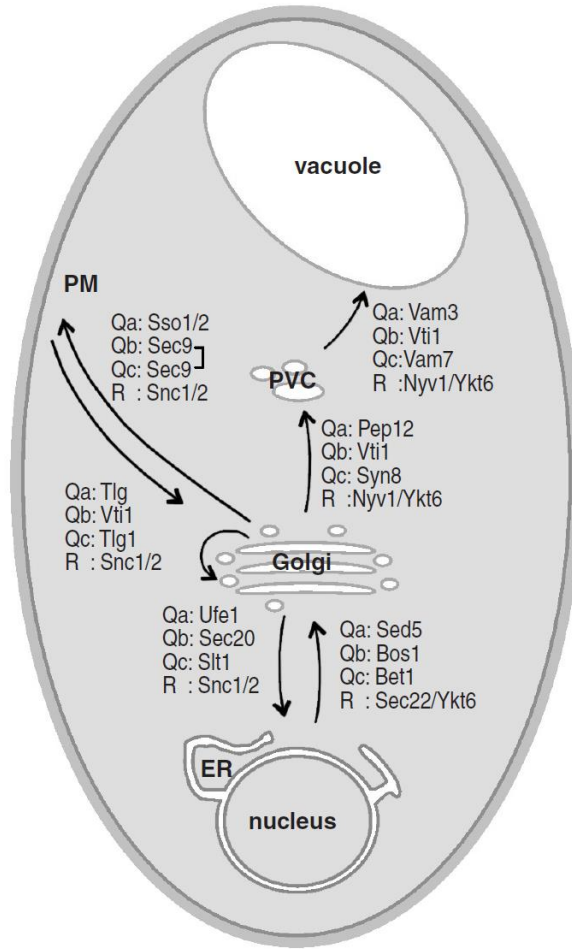


**Figure 2.8. Different SNAREs are required for different fusion events.** [239]

*Lipids in trafficking and fusion*

In addition to a host of proteins, membrane trafficking and fusion events often require the presence of certain lipids in a pathway/membrane-specific manner. Notably, phosphoinositides, which are phosphatidylinositols phosphorylated at position 3, 4, or 5 of the inositol group, are required throughout membrane trafficking and fusion [240, 241].

Phosphatidylinositol-3-phosphate [PI(3)P] is enriched at endosomes and required for vesicle traffic Golgi-to-endosomes and for fusion at endosomes [242]. PI(3)P is important to most aspects of endosomal membrane function, especially because many proteins have PI(3)P binding domains [243]. FYVE-domain (zinc finger containing domain) proteins, of which yeast expresses five, bind specifically to

PI(3)P [241, 244]. During early endosome fusion, Vps19p (or Vac1p; yeast homolog of mammalian EEA1) binds PI(3)P in early endosomes and then GTP-bound Vps21p (homolog of mammalian Rab5), which is required for fusion of early endosomes [245-247]. Vps27p, a subunit of the ESCRT complex, contains a FYVE domain and aids in protein sorting and transport to the late endosome and vacuole [248]. Additionally, Vps34p is a PI(3)-kinase (activated by the protein kinase Vps15p) required for traffic of proteins Golgi-to-vacuole as it in complex with Vps15p produces a viable pool of PI(3)P that allows for protein sorting [136]. Finally, the vacuolar Qc-SNARE Vam7p, which does not contain a transmembrane domain, binds PI(3)P with its PX domain which aids in targeting Vam7p to the vacuolar membrane to participate in SNARE complex formation during fusion [249]

Phosphatidylinositol 4,5-bisphosphate [PI(4,5)P<sub>2</sub>] is enriched at the PM of yeast cells and is known to play a role in binding proteins associated with the exocyst, namely, Sec3p and Exo70p [250, 251]. Sec3p specifically contains a pleckstrin homology (PH) domain which is a PI(4,5)P<sub>2</sub> binding domain [252, 253]. Mutant analyses in yeast that cause the depletion of PI(4,5)P<sub>2</sub> at the PM result in defective polarized secretion [254], a hallmark of the exocytic pathway. Though the precise purpose is unclear, PI(4,5)P<sub>2</sub> is required for and becomes enriched during the early stages of vacuolar fusion [255]. Additionally, mutant studies of the phosphatidylinositol 4-kinases, Stt4p and Pik1p, which phosphorylate phosphatidylinositols to produce PI(4)P and PI(4,5)P<sub>2</sub> reveal that their activity is necessary for proper vacuole morphology, actin polarization, and Golgi structure and protein secretion, suggesting a role of PI(4,5)P<sub>2</sub> in many membrane trafficking events [256].

Other phosphatidylinositols that play a role in trafficking include PI(4)P, which is enriched at Golgi and promotes ER-to-Golgi traffic [243] and may function as a receptor for the GTPase Arf1p, a regulator of AP-1 vesicle formation and vesicle traffic within the Golgi [257, 258], and PI(3,5)P<sub>2</sub> which functions in autophagy and the Cvt pathway (Atg18p binds PI(3,5)P<sub>2</sub>) [259] and may aid in the internalization of the MVB during MVB:vacuole fusion [241]. PI(3,5)P<sub>2</sub> is bound by the ENTH (epsin NH<sub>2</sub>-terminal homology)

domain of Ent3p and ANTH (AP180 NH<sub>2</sub>-terminal homology) domain of Ent5p [260-263]. Ent3p and Ent5p are localized to prevacuolar compartments and deletion of these genes result in defective MVB sorting [262, 263]. Ent3p and Ent5p also bind Vps27p and clathrin coated vesicles, suggesting an important role for both these proteins and PI(3,5)P<sub>2</sub> in the MVB sorting pathway [260-263].

Other known lipids that play a role in late endosome and vacuole fusion are described briefly: ergosterol (ERG) regulates the release of Sec17p from *cis*-SNARE complexes during the priming stage of fusion [235], diacylglycerol (DAG), generated by its PI(4,5)P<sub>2</sub> precursor, is important for membrane curvature and is enriched at fusing membranes [264], and phosphatidic acid (PA) promotes the membrane association of HOPS and Sec18p [265].

Lipids hold particular value as an experimental tool as they can be used to produce liposomes of a specific lipid content and membrane size. Simple liposomes can be used to examine protein:lipid interactions that can aid in understanding protein localization or charge requirement. Furthermore, the addition of SNARE proteins generates proteoliposomes that are fusogenic in the presence of other fusion components (Sec17p, Sec18p, HOPS, ATP) that provide a simplified avenue to examine other proteins involved in fusion [266] or the interaction between yeast fusion proteins and non-native proteins that manipulate fusion activity. Early work with reconstituted proteoliposomes was pivotal in determining different lipids and proteins that were required for in vitro membrane fusion events [265-269].

### *Stages of Fusion*

Vacuole fusion is a well-studied system and model of membrane fusion that can be used to describe the stages of membrane fusion, thus the following is based on the current understanding of fusion in the context of the yeast vacuole. Vacuole fusion progresses through several stages: priming, tethering, docking, and fusion (mixing of lipid and luminal content).

Priming is the first stage of vacuole fusion and involves the recruitment of Sec17p and Sec18p to disassemble *cis*-SNARE complexes, freeing them to participate in *trans*-SNARE complexes [234]. In ALP/AP-3 fusion, the HOPS complex is phosphorylated during priming to allow its interaction with AP-3 vesicles [209]. ERG and PI(4,5)P<sub>2</sub> promote priming [235, 255], in the case of ERG by regulating Sec17p release from *cis*-SNARE complexes to allow Sec18p to disable said complexes [235]. During tethering, the HOPS complex associates with the vacuole membrane by binding to Ypt7p [190], SNAREs [197, 198, 203], and phosphoinositides [198]. Formation and proofreading of *trans*-SNARE complexes occurs during the docking stage [202]. At this point, the membranes have assembled a microdomain vertex ring which is the area at which proteins and regulatory lipids have become enriched in preparation for fusion [270]. During the final stage of fusion, both lipid bilayers and luminal contents are mixed together at the vacuole membrane. Gathering evidence suggests that prior to vacuolar fusion, the membranes proceed through a hemifusion intermediate in which membranes are just beginning to mix in the form of a bilayer “stalk” without luminal content mixing (Figure 2.9). This intermediate concept is based on the increased length of time required for luminal mixing to occur compared to other fusion stages [271], the presence of vacuolar membrane proteins and cytoplasmic lipids at the opposing vertex ring membranes [272], the occasional presence of vacuolar ILVs [272, 273], and most recently, the capture of hemifusion intermediates with stalk formation via transmission electron microscopy [273]. The hemifusion intermediate may proceed through either a delayed or immediate fusion; delayed fusion resolves the hemifusion stalk without the formation of ILVs while immediate fusion events result in the formation of ILVs [273]. It is possible that the hemifusion model that proceeds through immediate fusion and produces ILVs is in part responsible for maintaining vacuolar organization of lipids and proteins present typically present at the vacuole membrane [273]. Hemifusion intermediates are observed in other fusion processes, such synaptic vesicle fusion [274-276], thus lending more credence to such intermediates in yeast membrane fusion.

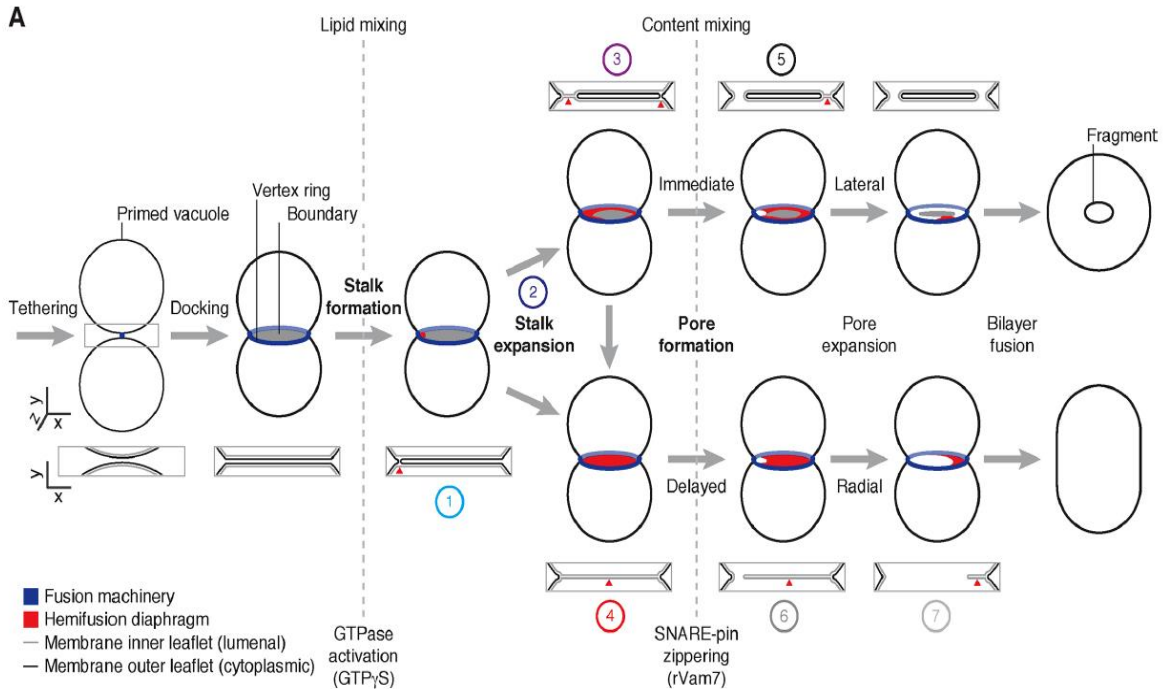


**Figure 2.9. Schematic of stages of vacuole fusion and hemifusion intermediates. [273]**

## THE YEAST VACUOLE

The yeast vacuole, often deemed the trash can of the cell, is a highly conserved eukaryotic organelle that functions much like the mammalian lysosome and is involved in a multitude of cellular processes and the regulation of cellular homeostasis [277]. The vacuole is a dynamic organelle that undergoes fusion and fission and maintains a specific lipid and protein content, important for many of its functions. The vacuole (under normal cell growth conditions) maintains a pH of approximately 6.2, only slightly more acidic than the cytosol of the cell at pH 7.2-7.4 [278], with the pH gradient maintained by the V-type H<sup>+</sup>-ATPase (V-ATPase) at the vacuolar membrane (described in more detail below). Wild-type yeast cells in standard growth conditions may contain between one and five vacuoles that occupy as much as 20% of the cell's volume. Importantly, yeast vacuoles can be isolated from yeast culture, allowing researchers to develop many assays to study vacuoles and vacuole fusion.

## Vacuolar Functions

Perhaps its most recognized function, the yeast vacuole is an acidic organelle that functions extensively in the degradation of cellular material from several pathways. Though its acidity assists in many vacuolar processes, specifically protease activation and proteolytic activity, the vacuole likely does not need to maintain an acidic pH for degradative processes as enzymatic activity still occurs at a more neutral pH, though significantly delayed [279]. There are many hydrolases present in the vacuole with vacuolar proteases the most studied and utilized in experimental techniques. Resident vacuolar proteases include both soluble proteases – Proteinase A (Pep4p) and B (Prb1p), Carboxypeptidase Y (Prc1p) and S (Cps1p), and Aminopeptidases I (Ape1p) and Y (Ape3p) – and the membrane bound protease - Dipeptidylaminopeptidase B (Dap2p) (reviewed in [280, 281]). Most vacuolar hydrolases are synthesized as zymogens which are inactive forms of enzyme. Upon proper trafficking to the vacuole, zymogens are activated by the proteases Pep4p and/or Prb1p, thereby ensuring that the activity of the vacuolar proteases is limited to the vacuole lumen so as to protect the integrity of other proteins along shared trafficking pathways (reviewed in [280, 281]). One additional vacuolar hydrolase worth noting is the alkaline phosphatase Pho8p, which is also modified by vacuolar protease Pep4p. Modulated in response to phosphate levels in the cell, Pho8p is a repressible enzyme that works in concert with other *PHO* genes to maintain cellular homeostasis (reviewed in [281]). *PHO8* and *PEP4* deletion strains have been exploited to measure homotypic vacuole fusion in vitro by first isolating two sets of vacuoles, one *pep4Δ* and one *pho8Δ*, allowing the vacuoles to fuse under standard fusion conditions, and then measuring total fusion by the addition of *p*-nitrophenyl phosphate, a substrate that is cleaved in the presence of alkaline phosphatase activity to produce a yellow reaction product that can be measured by its absorbance [282]. Increased levels of alkaline phosphatase activity result in more product and thus, increased absorbance values which in turn correspond to relative levels of fusion because Pho8p is only

active in the presence of Pep4p which in the context of this assay, would first require vacuolar fusion between the vacuoles from the two deletion strains [282].

The vacuole also functions as a storage organelle that can regulate cytosolic levels of nutrients during nutrient deprivation or starvation. There are amino acid transporters for both basic and neutral amino acids and ion (i.e.  $\text{Ca}^{2+}$ ,  $\text{Fe}^{3+}$ ,  $\text{K}^+$ ,  $\text{Na}^+$ ,  $\text{Zn}^{2+}$ ) transporters localized at the vacuole that function in both uptake and export of amino acids and ions from/to the cytosol (reviewed in [277]). The transport of amino acids and ions is often coupled with proton antiport or rely on the presence of the vacuole proton gradient for transport [277, 283]. The cytosolic levels of amino acids and many ions are held relatively constant however their levels fluctuate within the vacuole based on environmental availability [277]. Typically during times of abundance, amino acids or ions accumulate in the vacuole via transporters while during deprivation, stored amino acids and ions are released via transporters. Polyphosphate is also stored in the vacuole as a source of inorganic phosphate and to facilitate the uptake of amino acids and cations [277]. Much like amino acids and ions, polyphosphate release is regulated by the cellular levels of inorganic phosphate which is monitored by the *PHO* system potentially in conjunction with other genes [284-286].

Detoxification is another important function of the vacuole which involves the sequestration of toxins into the vacuole and away from other organelles to prevent them from damage. In addition to toxic compounds, nutrients present in excess can become toxic to the cell and are sequestered by vacuolar transporters to return the cell to appropriate homeostatic levels. (reviewed in [277])

Finally, the vacuole functions during different states of cellular stress to provide nutrients or attempt to return to homeostatic levels. Autophagy can function as a stress response to deliver cargo (proteins, organelles, etc.) to the vacuole for degradation to restore nutrients to the cell during deprivation [163]. In the case of ionic shock, the vacuolar and plasma membrane ion transporters operate to control the cytosolic levels of ions as well as the influx and efflux from the environment

[277]. Hyperosmotic stress can be mitigated by the vacuole through its release of calcium by Yvc1p (cation transporter), which in turn acts as a signaling molecule for other cellular osmotic shock responses and vacuolar ion transporters [277, 287]. Namely, calcineurin, a  $\text{Ca}^{2+}$ /calmodulin dependent phosphatase, activates the transcription factor Crz1, which increases the expression of many stress response genes including cell wall synthesis, vesicle transport, and lipid synthesis [288, 289]. During periods of osmotic stress, the vacuolar lipid  $\text{PI}(3,5)\text{P}_2$  rapidly enriches, resulting in vacuolar morphology defects and fragmentation, possibly to release contents from the vacuole lumen in order to restore osmotic pressure [287, 290, 291]. Additionally,  $\text{PI}(3,5)\text{P}_2$  enrichment acts as a signal that regulates the activation of ion transport channels to mediate osmotic stress [287, 290-293].

### **Vacuolar Lipids**

The vacuole has a distinct lipid composition that enables it to perform many of its functions. The regulatory fusion lipids present at the vacuole have been described on page 40 in “Lipids in trafficking and fusion.” In addition to these regulatory fusion lipids,  $\text{PI}(3,5)\text{P}_2$  is a phosphatidylinositol that is present at the vacuole membrane and plays an important role in signaling and vacuole morphology. The pool of  $\text{PI}(3,5)\text{P}_2$  at the vacuole is produced by the kinase Fab1p, which phosphorylates  $\text{PI}(3)\text{P}$  upon its activation by Vac14p and Vac7p [291, 294-296]. As described above,  $\text{PI}(3,5)\text{P}_2$  functions during periods of osmotic stress to modulate the release of vacuolar contents through its regulation of ion transporters. The absence or enrichment of  $\text{PI}(3,5)\text{P}_2$  at the vacuole results in morphology defects [297-299] and in the case of  $\text{PI}(3,5)\text{P}_2$  absence, the vacuole cannot undergo fission due to defective trafficking of proteins between the MVB and vacuole [300-302].

### **Vacuole Proteins - the V-ATPase**

The proteome of the vacuole is abundant with hydrolases, fusion proteins, sorting proteins, ion transporters, and proteins of yet unknown function [303, 304]. Many of the proteins present in the vacuole are responsible for degradation and recycling of other cellular components and nutrients as well

as the transport of amino acids and ions between the vacuole and the cytosol [303, 304]. Perhaps one of the most notable protein complexes present at the vacuole is the V-type H<sup>+</sup>-ATPase (V-ATPase), which is responsible for generating the proton gradient in the vacuole through its coupling of proton pumping with ATP hydrolysis and maintaining pH homeostasis in the vacuole [305]. The V-ATPase consists of fourteen subunits divided into two domains, V<sub>1</sub>, which is the cytoplasmic domain consisting of eight subunits (A-H) and responsible for the binding and hydrolysis of ATP, and V<sub>o</sub>, which is the membrane bound domain of six subunits (a, c, c', c'', d, and e) and responsible for the pumping of protons into the vacuole lumen [305] (Figure 2.10). The V<sub>1</sub> subunit stoichiometry is A<sub>3</sub>B<sub>3</sub>CDE<sub>3</sub>FG<sub>3</sub>H [306] and the V<sub>o</sub> domain stoichiometry is ac<sub>8</sub>c'c''de [307].

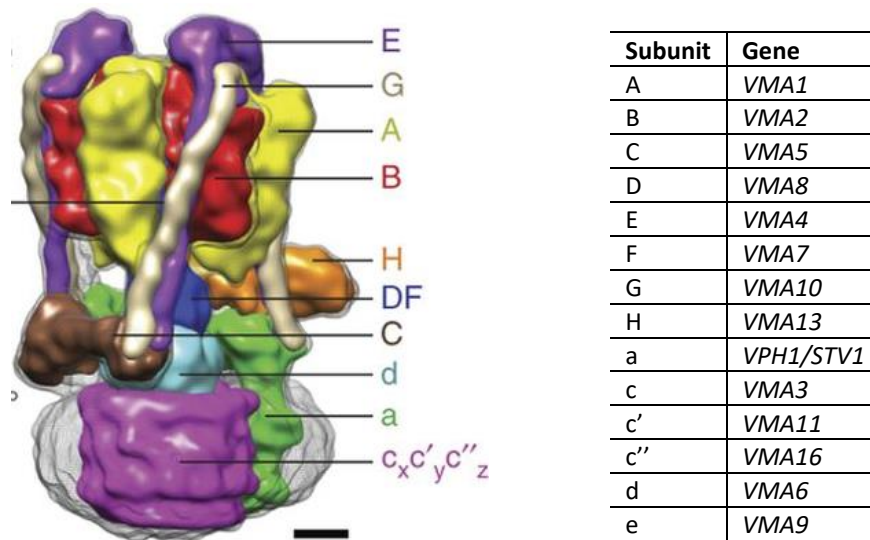


**Figure 2.10. Structure of the V-ATPase [308] and list of subunits and corresponding gene names.** Structure was determined by cryo-EM at 11Å resolution; scale bar 25Å.

The V<sub>1</sub> domain consists of the A<sub>3</sub>B<sub>3</sub> cylinder, the central stalk, and the peripheral stalks. The A<sub>3</sub>B<sub>3</sub> cylinder is a hexamer of alternating A and B subunits that performs ATP hydrolysis at three hydrolytic sites [309]. The hydrolytic sites are present at the A-B subunit interface at which the A subunit contributes the majority of the residues present while the non-hydrolytic sites are the interface at which the B subunit contributes the majority of the residues [310]. At the hydrolytic site, there is a cluster of hydrophobic residues that are necessary for the hydrolysis of ATP and may additionally function in

alternating the conformation of the cylinder [310]. The hydrolysis of ATP powers the alternation of the  $A_3B_3$  cylinder between an open (no nucleotide bound), loose (ADP and phosphate bound), and tight formation (ATP bound), which in turn drives the rotation of the center stalk of the V-ATPase, composed of subunits D, F, and d [311, 312]. The rotations of the center stalk occur in  $120^\circ$  increments and are associated with the complete cycle of the hydrolytic sites binding ATP, hydrolyzing ATP, and releasing ADP and  $P_i$  [311, 312]. The peripheral stalks consist of the subunits E and G that form three E-G heterodimers around  $V_1$ , two of which connect to subunit C and one of which connects to subunit H [308]. The subunits C and H consist of two globular domains connected by linkers and act as two of the connections between the  $V_1$  and  $V_0$  domains [313]. The C subunit connects to one E-G heterodimer through its head domain which has a strong affinity for the heterodimer, while its foot domain has a lower affinity for the second heterodimer but binds both this heterodimer and more strongly, the N-terminus of subunit a of the  $V_0$  domain [314-317]. The H subunit similarly binds both the a subunit and an E-G heterodimer [308, 317]. The peripheral stalks function to resist the torque generated by the rotation of the central stalk [317].

As the central stalk rotates, the proteolipid c-ring consisting of ten subunits ( $c_8c'c''$ ), also rotates and functions as the proton translocator. Each proteolipid contains one lipid exposed glutamate residue that becomes protonated [318, 319] at the cytosolic half-channel of the c-ring and then rotates  $360^\circ$  at which point the protons are released into the lumenal half-channel (Figure 2.11) [320]. The two aqueous half-channels are located at the interface of the c-ring and the C-terminus of the a subunit, which contains eight transmembrane helices embedded in the vacuole membrane and an essential arginine residue (Arg<sup>735</sup>) located directly across from proteolipid c-ring glutamate residues. Arg<sup>735</sup> is required for proton transport across the membrane as it stabilizes the glutamate residues of the c-ring while deprotonated between the two half-channels [311, 320, 321]. The a subunit of the  $V_0$  domain is crucial for the pumping of protons, tethering  $V_1$  to the membrane as it is in contact with both the cytosolic and

membranous domains of the complex, withstanding the torque of the rotor, and targeting the entire V-ATPase to the proper membrane [309]. The vacuolar a subunit (Vph1p) targets the V-ATPase to the vacuolar membrane while the other yeast isoform, Stv1p, targets its pump to the Golgi [322, 323]. The  $V_0$  domain also includes subunit d, which is shaped like and acts as a plug that blocks the c-ring pore during inhibitory periods when  $V_1$  dissociates from  $V_0$  [324]. The d subunit is an important component of the rotor as it serves as a connection between the c-ring and the  $V_1$  domain through its association with the D and F stalk components [305]. The e subunit of  $V_0$  is embedded in the membrane and interacts with  $V_0$  chaperones for assembly but its function remains unknown and recent studies suggest that it is not required for V-ATPase pumping activity [325].

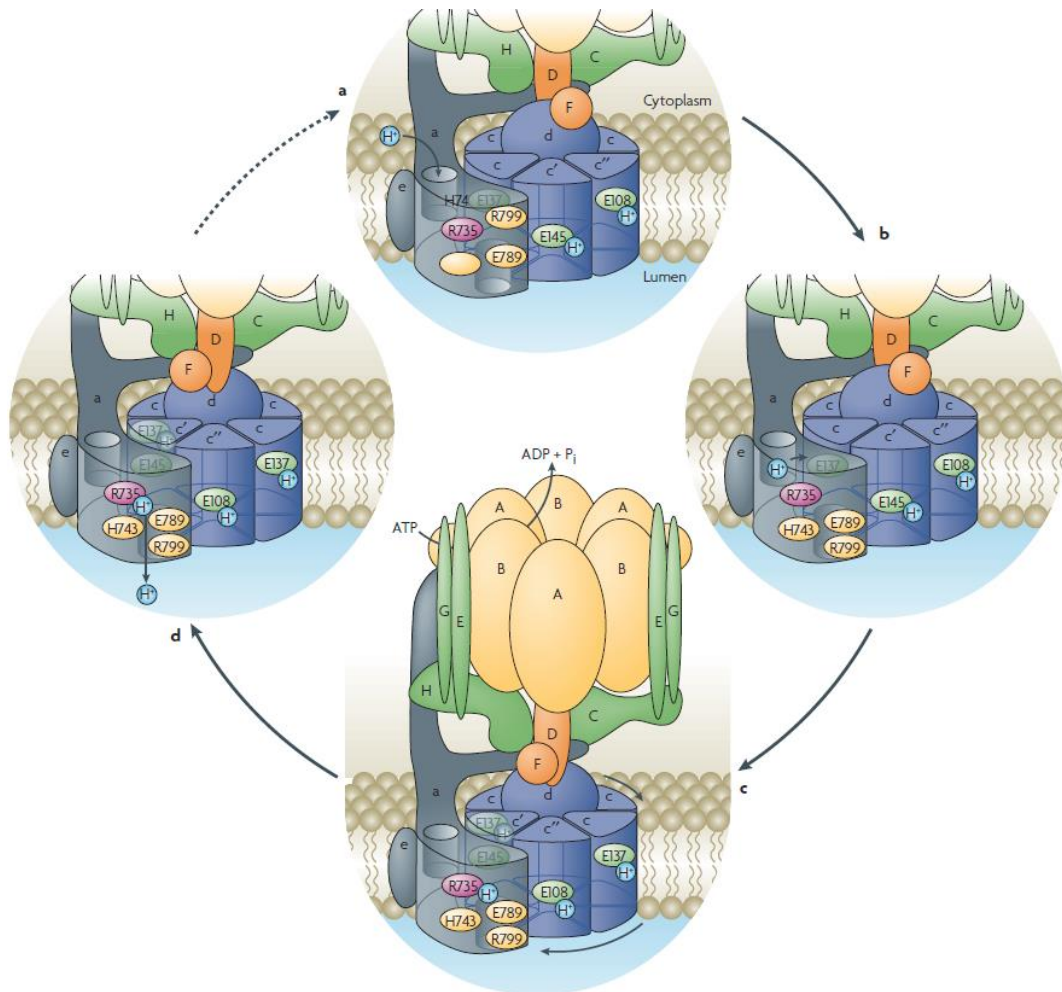


**Figure 2.11. Rotation of the c-ring and translocation of protons. [305]**

Outside of the V-ATPase, other chaperones contribute to the assembly and stability of the V-ATPase but are not formally considered components of the complex. Vma12p, Vma21p, Vma22p, and Voa1p are each associated with the assembly of the V-ATPase. Vma12p and Vma22p form a complex and each of the Vma proteins is localized to the ER and required for V-ATPase assembly [326-328]. Voa1p is present in the ER for assembly and is found at mature V<sub>O</sub> domains where it enhances the stability of the c-ring and its interactions with other subunits [320].

The activity of the V-ATPase is highly regulated by the reversible dissociation of the V<sub>1</sub> and V<sub>O</sub> domains [329, 330] which typically occurs in response to environmental conditions such as nutrient deprivation, osmotic stress, and extracellular pH (reviewed in [311]). V-ATPase dissociation results in a cytoplasmic pool of inactive V<sub>1</sub> [331, 332] and an inactive membrane embedded V<sub>O</sub> domain [333], each of which have unique conformations in an inhibited state [320, 334]. During disassembly, the C subunit of the V<sub>1</sub> domain dissociates from the complex entirely [335] and the H subunit undergoes significant conformational changes at its C-terminus that result in silencing of ATP hydrolytic activity [332, 334]. The H subunit C-terminus rotates from its assembled position where it bound to the a subunit N-terminus to the bottom of the A<sub>3</sub>B<sub>3</sub> cylinder where it contacts the B subunit with an open catalytic site and the central rotor D subunit [308, 334]. The c-ring of the V<sub>O</sub> is blocked by subunit d whose N-terminus interacts with the cytosolic loops of the c'', c', and adjacent c subunit [320]. Subunit d additionally interacts with the N-terminus of the a subunit, perhaps to ensure the d subunit does not dissociate upon V-ATPase disassembly, as it is not a membranous protein [320]. When the V-ATPase is disassembled, the glutamate residue of the c'' subunit is asymmetrical when compared to the spacing of other c-ring members and is observed in contact with the a subunit Arg<sup>735</sup> residue in its inhibitory conformation, suggesting that the c'' subunit cannot pass the Arg<sup>735</sup> residue in the reverse direction and thereby prevents the passive flux of protons during disassembly [336]. Reassembly of the V-ATPase requires a change in both V<sub>1</sub> and V<sub>O</sub> conformations as well as the chaperone RAVE (regulator of H<sup>+</sup>-

ATPase of vacuolar and endosomal membranes) which is known to bind  $V_1$ ,  $V_0$  and the C subunit to promote assembly, however the exact method by which RAVE promotes assembly is not known [311, 337]. Other factors that contribute to the reassembly of the V-ATPase include the activation of the Ras/cAMP/protein kinase A pathway [338], interaction with aldolase [339], and interaction with phosphofructokinase [340] which collectively occur in response to environmental levels of glucose and additionally to cytosolic pH in the case of Ras/cAMP/protein kinase A pathway [341] to enhance V-ATPase assembly.

Despite performing an important acidification function at the vacuole, subunits of the V-ATPase can be deleted without lethal effects to yeast, making it a viable model to examine the V-ATPase in detail. Deletion of individual V-ATPase subunits results in a characteristic *VMA*<sup>-</sup> mutant pH sensitivity (except for *VPH1* due to the *STV1* isoform) that results in growth defects at neutral pH but can be evaded by provided acidic growth media [342]. *VMA* mutants are also sensitive to elevated  $Ca^{2+}$  levels, heavy metals, oxidants, drugs, and nonfermentable carbon sources [342, 343]. Many of these sensitivities can be understood in the context of vacuolar functions as described previously, as many transporters rely on the proton gradient for their function. *VMA* mutants can also cause the missorting of proteins post-Golgi in the secretory pathway, likely due to the delayed or diminished activation of vacuolar proteases in the absence of an acidified vacuole [344], again a concept described in the context of the vacuolar function above. *VMA* mutants lack V-ATPase activity and nearly all *VMA* deletions result in failure of the V-ATPase to assemble properly at the vacuole membrane (reviewed in [277, 345]).

The role of the V-ATPase in membrane fusion has been debated historically and to date remains unresolved. The V-ATPase has been suggested to play a role in vacuole fusion in two ways: a) vacuole fusion requires an acidified vacuole [346] and b) the  $V_0$  domain acts as a pore that promotes lipid mixing across two membranes during fusion [347]. Early studies using the ALP homotypic vacuole fusion assay (described previously) suggested that the proton gradient or electrochemical gradient generated by the

V-ATPase were required for *trans*-SNARE pairing, however they did not directly assay whether the gradient requirement was specific to SNARE pairing or the fusion reaction in general [348]. More recently, *in vivo* work suggests that at least one acidic vacuole is required for vacuole fusion, however this study fails to establish whether the proton or electrochemical gradient generated by the V-ATPase is directly or indirectly required for fusion [349] and further, draws conclusions based on ill-designed assays and mutants that could inherently impair the results. This study was countered by work suggesting that acidified organelles negatively regulates fusion because inactivated V-ATPase enhanced membrane fusion [350]. *In vitro* studies utilizing fusogenic liposomes at physiological pH lack both an acidified compartment and structural components of the V-ATPase [266, 351], though there is question regarding the relevance of liposome membrane size and curvature as liposomes are much smaller than vacuoles as well as the overall simplicity of the assay. Research in our laboratory has utilized an effector protein, VopQ, to determine that an acidified vacuole is not required for membrane fusion and is described in Chapter 5.

There is a significant amount of work that maintains there is a physical requirement of the V-ATPase, specifically the  $V_o$  domain, during fusion. Initial conclusions for this requirement were drawn from analysis of a mutant hunt that showed  $Ca^{2+}$  bound V-ATPase subunits and later determined that  $Ca^{2+}$  acted as a signal for calmodulin which targets Vma3p proteolipids to trigger membrane fusion specifically after the docking stage of fusion [347, 352]. Since then, this mutant has been identified as an inappropriate method to evaluate calcium requirements and the necessity for calcium at the vacuole membrane has been disproven [353], though undoubtedly, *trans*-SNARE complexes do induce a luminal release of  $Ca^{2+}$  perhaps for downstream fusion interactions at the membrane or lipid bilayer remodeling [352-354]. Studies also used tagged  $V_o$  subunits (Vph1p and Vma3p) in fusion reactions and showed that the tags accumulated only during fusion, aimed at confirming the formation of a *trans*- $V_o$  complex through  $V_1$  dissociation and conformational changes brought upon by *trans*-SNARE complex formation

to facilitate lipid mixing [347], however controls are severely lacking in these data. Additional mutant analyses of the a subunit and c-ring proteolipids suggested that the a subunit was required for fusion and even point mutations in c-ring subunits reduced fusion activity [355, 356], but again these data fail to show a direct structural requirement for  $V_o$  as the compartments were still somewhat acidified and fusion still occurred with point mutants. Though there is an abundance of data to suggest a role (or lack thereof) of the V-ATPase in fusion, none of it can aptly separate proton or electrochemical gradients from structural requirements in a physiologically relevant or scientifically sound manner, thus leaving a gap in the understanding of the V-ATPase and in membrane fusion.

### **Vacuole Morphology and *VPS* mutants**

Early research regarding proteins involved in trafficking to the vacuole via the CPY pathway identified mutants known as vacuole protein sorting (VPS) mutants that upon deletion induced defects in protein sorting and trafficking to the vacuole [357, 358]. These mutants were later examined via microscopy to evaluate their vacuole structure for possible defects. These studies led to the current yeast vacuole morphology classifications, class A-F, each with unique appearance associated with known *vps* mutants [359]. The following is a summary of the work presented in Raymond et al [359]. Wild-type vacuoles are not fragmented and appear as smooth organelles (up to 5) in yeast. Class A *vps* mutants have wild-type vacuole morphology but still play a role in protein sorting as their deletion results in missorting. Class B vacuoles are highly fragmented vacuoles typically with over ten vacuole lobes present, giving the appearance of soap bubbles or grape clusters within the cell. Class B *vps* mutants include Ypt7p specific members of the HOPS tethering complex, Vam7p SNARE, and two other proteins that form a complex and play a role in retrograde transport of membrane proteins from endosome to Golgi. Class C vacuole morphology lacks vacuole structure and rather appears as small punctate structures haphazardly present within the cell. Class C mutants consist of deletions of the core subunits of the CORVET and HOPS tethering complex. Class D mutants appear as one enlarged vacuolar structure

(much larger than wild-type vacuoles) and cannot generate a pH gradient across the vacuole membrane or properly assemble the V-ATPase in some cases at the membrane. Additionally, class D mutants have defective vacuole inheritance mother to bud and result in daughter cells with class C morphology or a lack of evident vacuole structure. Class D mutants include early endosome trafficking proteins, including SNAREs, CORVET Rab specific subunit Vps3p, and Vps21p (Rab GTPase). Class E vacuoles have a prevacuolar structure distinct from but present at a somewhat enlarged vacuole and are include deletions of ESCRT complex genes which is necessary for the transport of integral membrane proteins to the vacuole. Finally, class F vacuole morphology appears as many smaller vacuole lobes within one larger vacuole structure and mutants are involved in Golgi-to-endosome transport (in either direction). The classification of *vps* mutants based on vacuole morphology has greatly assisted later studies of proteins native or nonnative to yeast that induce morphological defects in the vacuole as they provide direction to the “type” of protein sorting defect that they may be inducing or where in a pathway such proteins are inducing trafficking defects.

## **ACTIN**

A necessary component of cell structure, membrane trafficking, and an additional target of bacterial effectors is actin, one of the most abundant proteins in yeast [360]. Actin is a highly conserved eukaryotic protein that exists in two forms, F-actin and G-actin, where F-actin is the filamentous and polymeric form that incorporates ATP-bound G-actin, as the globular monomeric form, at its barbed end. The network of actin filaments in yeast generates the actin cytoskeletal arrangement and can undergo polymerization or disassembly to remodel the cytoskeleton or move vesicles within the cell [361]. Yeast actin structures exist in three forms: cortical actin patches, actin cables, and the actomyosin ring [362-364] and are reviewed here only briefly to highlight the importance and function of actin structures in eukaryotic processes.

Cortical actin patches are dense patches of branched actin filaments present at the periphery of the cell, particularly at areas of polarized growth (reviewed in [365]). The network of actin patches importantly participates in clathrin-mediated endocytosis and requires the recruitment of many proteins at the site of PM invagination (described previously, page 28 in “the endocytic pathway”). Of the proteins that participate in endocytosis, Arp2/3 is an important protein complex (consisting of subunits Arp2, Arp3, ARPC1-5) that nucleates branched actin filaments in response to cell signals [360, 366]. Arp2/3 activity is stimulated by nucleation promoting factors which in yeast include the WAS- family protein, Las17p, myosin 5 (Myo5p), Pan1p, and Abp1p [366]. Las17p is the strongest nucleation factor and contains a VCA (or WCA) domain [verprolin homology or WASP homology 2 (WH2), central acidic] at its C-terminus which is necessary to activate Arp2/3 actin nucleation [366]. Myo5p is localized to the plasma membrane and independently activates Arp2/3 while Pan1p forms a complex with other proteins (Sla1p and End3p) and again functions in the activation of Arp2/3 [260, 365]. Abp1p (actin binding protein) is important for the recruitment and activation of Arp2/3 at actin filaments and is particularly important in endocytosis as it aids in the localization of other endocytic factors [367]. Actin patches are internalized upon PM invagination and formation of the endocytic vesicle which signals for the disassembly of the actin patch network at that location [365]. Collectively, these proteins and a number of other regulatory proteins orchestrate actin branching at actin patches, actin turnover, and invagination of endocytic vesicles.

Actin cables are bundles of parallel actin filaments that extend along the long axis of the cell [362]. The primary role of actin cables is to maintain polarized cell growth and to direct intracellular transport, including secretory vesicles [368]. Nucleation of actin cable filaments occurs by the activity of Bni1p and Bnr1p, which are formins that, although redundant, localize to the bud cortex and bud neck respectively to nucleate filaments [369]. Formins are proteins that contain formin homology (FH) domains such as FH1, which are known to bind profilin and actin, and FH2, which is necessary for actin

nucleation and assembly, and cooperate to perform cable filament nucleation (reviewed in [365]).

Despite the important role of actin cables in cellular processes, many aspects of actin cables remain poorly understood.

Finally, the actomyosin ring is a ring structure that assembles at the site of cell division where it generates necessary force to divide the cell and targets cell wall assembly to the site of division. The location of the actomyosin ring requires septins which are proteins that form an hourglass and eventually a double-ringed shaped at the bud neck [370]. There is a myriad of proteins involved with the nucleation and organization of actin filaments into a ring structure and such detailed information extends beyond the scope of this work. Suffice it to say that actin is essential for at least yeast endocytic, secretory, and cytokinetic processes.

## CHAPTER 3

### IDENTIFICATION OF PUTATIVE EFFECTORS OF THE TYPE IV SECRETION SYSTEM FROM THE *WOLBACHIA* ENDOSYMBIONT OF *BRUGIA MALAYI*

Carpinone EM, Li Z, Mills MK, Foltz C, Brannon ER, Carlow CKS, Starai, VJ. Identification of putative effectors of the Type IV secretion system from the *Wolbachia* endosymbiont of *Brugia malayi*. PLoS ONE. 2018. Reprinted here with permission of publisher.

## Abstract

*Wolbachia* is an unculturable, intracellular bacterium that persists within an extremely broad range of arthropod and parasitic nematode hosts, where it is transmitted maternally to offspring via vertical transmission. In the filarial nematode *Brugia malayi*, a causative agent of human lymphatic filariasis, *Wolbachia* is an endosymbiont, and its presence is essential for proper nematode development, survival, and pathogenesis. While the elucidation of *Wolbachia*:nematode interactions that promote the bacterium's intracellular persistence is of great importance, research has been hampered due to the fact that *Wolbachia* cannot be cultured in the absence of host cells. The *Wolbachia* endosymbiont of *B. malayi* (*wBm*) has an active Type IV secretion system (T4SS). Here, we have screened 47 putative T4SS effector proteins of *wBm* for their ability to modulate growth or the cell biology of a typical eukaryotic cell, *Saccharomyces cerevisiae*. Five candidates strongly inhibited yeast growth upon expression, and six additional proteins showed toxicity in the presence of zinc and caffeine. Studies on the uptake of an endocytic vacuole-specific fluorescent marker, FM4-64, identified 4 proteins (*wBm0076*, *wBm00114*, *wBm0447* and *wBm0152*) involved in vacuole membrane dynamics. The WAS(p)-family protein, *wBm0076*, was found to colocalize with yeast cortical actin patches and disrupted actin cytoskeleton dynamics upon expression. Deletion of the Arp2/3-activating protein, Abp1p, provided resistance to *wBm0076* expression, suggesting a role for *wBm0076* in regulating eukaryotic actin dynamics and cortical actin patch formation. Furthermore, *wBm0152* was found to strongly disrupt endosome:vacuole cargo trafficking in yeast. This study provides molecular insight into the potential role of the T4SS in the *Wolbachia* endosymbiont:nematode relationship.

## Introduction

After leprosy, lymphatic filariasis is the leading cause of permanent disability, afflicting at least 150 million people worldwide [371, 372]. The World Health Organization reports that 1.23 billion people in 58 countries are at risk for developing the disease [371]. Lymphatic filariasis results from the

mosquito-borne transmission of three distinct pathogenic nematodes: *Wuchereria bancrofti*, *Brugia timori* and *Brugia malayi*. In the early stages of the infection, anti-parasitic agents such as diethylcarbamazine and ivermectin have proved to be effective in eliminating immature worms, and have been used in mass treatment programs [373]. Unfortunately, adult worms which are largely responsible for the pathology associated with infection cannot be easily treated by early-stage anti-parasitic drugs [13, 14]. With the discovery that these filarial nematodes require the presence of an obligate intracellular, Gram-negative bacterial endosymbiont of the *Wolbachia* genus to survive and reproduce, effective clearance of filarial infections has been achieved with antibiotic treatment [13-16, 374]. Accordingly, significant efforts to understand the interactions of *Wolbachia* with nematodes at the molecular level have been undertaken to identify additional potential drug targets [375].

In *B. malayi*, *Wolbachia* exists and replicates within membrane-bound vacuoles in the lateral hypodermal chord and female germline [11, 19, 376]. These bacteria-laden compartments are often seen in close association with the endoplasmic reticulum and Golgi compartments [18], suggesting that *Wolbachia* may directly interact with host organelles to support its survival and co-opt normal host pathways in order to obtain nutrients and to prevent autophagic degradation in the host [20, 22, 377]. Only recently, however, have researchers identified a small number of secreted proteins from *Wolbachia* that appear to directly interact with host nematode proteins [31, 378]. Identification and characterization of the full complement of *Wolbachia*:host interactions will likely provide important information regarding the ability of *Wolbachia*, and other endosymbionts, to be maintained in the host.

Many Gram-negative intracellular bacteria utilize type III or type IV secretion systems (T3SS; T4SS) to deliver bacterial proteins into host cells, ensuring their successful invasion, survival, and replication within the host [379, 380]. Recent genomic studies have shown that *Wolbachia* from the filarial nematode *B. malayi* (*wBm*) contain the necessary gene products to produce an active T4SS which is regulated by the *wBmxR1* and *wBmxR2* transcriptional regulators [22]. It is thought that *Wolbachia*

utilizes its T4SS to secrete a number of effector proteins to modulate bacteria:host interactions, much like the related human pathogenic bacteria from the order Rickettsiales, such as *Rickettsia conorii*, *Ehrlichia chaffeensis*, and *Anaplasma phagocytophilum* [381]. However, identifying and characterizing these putative effectors has proven difficult in the filarial system due to the fact that the full life cycle of neither *Wolbachia* nor *B. malayi* can be supported in culture for facile genetic or biochemical manipulation. With modern bioinformatics, molecular biology, and a surrogate eukaryotic host system capable of genetic manipulation, the activities of individual putative effector proteins from these bacteria can be evaluated.

The budding yeast *Saccharomyces cerevisiae* has routinely been used as a “host” organism to screen for T3SS/T4SS effectors, as many of its core physiological pathways, such as protein trafficking, endolysosomal membrane dynamics, and cytoskeletal dynamics, are conserved in higher eukaryotes [382-384]. By expressing individual genes encoding predicted effector proteins in yeast, researchers have successfully identified and characterized several secreted effectors from a diverse set of bacterial pathogens including *Shigella flexneri* [144, 385], *Legionella pneumophila* [386, 387], and *Chlamydia trachomatis* [388]. Oftentimes, these effector proteins contain eukaryotic-like motifs, such as ankyrin repeat and coiled-coil domains – known protein-protein interaction motifs – suggesting the ability of these effectors to directly interact with and modulate eukaryotic cell biology. Secreted bacterial effectors with activities on eukaryotic physiology are often inhibitory to yeast growth [144], and can therefore be rapidly screened to identify potential candidates for further study. Additionally, powerful biochemical assays to measure protein trafficking pathways and the visualization of intracellular organelle morphologies can be used to identify effectors that may modulate intracellular membrane or general organelle dynamics during infection or symbiosis [389, 390].

By using some of these classical eukaryotic protein motifs as an identifier, and combining this information with genes known to be associated with, or co-transcribed with, the components of the

wBm T4SS [22, 25], we have identified and cloned forty-seven potential effector proteins from wBm into yeast expression vectors. These putative effectors were then screened for the ability to inhibit yeast growth, alter normal vacuole protein sorting pathways, and to disrupt normal yeast vacuolar morphology. Five candidates strongly inhibit yeast growth upon expression, and six additional proteins show toxicity in the presence of zinc and caffeine. Studies on the uptake of an endocytic vacuole-specific fluorescent marker, FM4-64, identify 4 proteins (wBm0076, wBm00114, wBm0152, and wBm0447) capable of altering vacuole membrane dynamics. Additionally, we find that wBm0076 disrupts normal actin cytoskeleton dynamics by inducing the aberrant formation of cortical actin patches *in vivo*. wBm0152 expression strongly inhibits the delivery of representative endosomal protein cargo to the yeast vacuole, suggesting the ability of a *Wolbachia* protein to manipulate eukaryotic membrane traffic. These findings provide insight into the potential role of these proteins in the nematode:*Wolbachia* symbiotic relationship.

## Results

### Identification of a set of putative effectors from the wBm genome.

In a previous study [22], the existence of an active bacterial T4SS was confirmed in the *Wolbachia* endosymbiont of the filarial parasite *Brugia malayi*. Due to the probability that the T4SS acts as a major communication channel between *Wolbachia* and *B. malayi*, we set out to identify potential substrates/effectors of the wBm T4SS. Using a variety of bioinformatic approaches (Materials and Methods), we identified 47 candidate effectors (Table 3.1) that displayed one or more of the following characteristics: i) eukaryotic-like protein possessing domains which share higher levels of homology to eukaryotic proteins than bacterial ones. These regions of homology include ankyrin repeats, Ser/Thr kinase motifs and coiled-coil domains, which have been previously identified in the T4SS effector proteins from *Legionella pneumophila* [391], *Bartonella henselae* [392], and *Coxiella burnetii* [393], ii) protein sequences that are potentially related to T4SS machineries, based on sequence homology to

*Rickettsia sibirica* proteins shown to interact with components of its T4SS [394], or genes that are co-transcribed with components of the *wBm* T4SS [22], and **iii**) bacterial proteins identified in excretory-secretory products from *B. malayi* adult worms and microfilaria [395]. Each of the 47 open reading frames was cloned into the galactose-inducible yeast expression vector pYES2/NT A (see Materials and Methods), and further studied for their ability to modulate yeast physiology.

**Table 3.1. *Wolbachia* putative Type IV effector proteins screened in this study.**

<i>wBm</i> gene designation	Predicted function	Reason <sup>a</sup>	<i>wBm</i> gene designation	Predicted function	Reason <sup>a</sup>
<b>WBM0014</b>	<b>ABC transporter</b>	4	<i>WBM0430</i>	invasion associated protein B	S
<b>WBM0032</b>	<b>tRNA modification GTPase</b>	4	<i>WBM0432</i>	WSP family	S, <i>Bm</i>
<i>WBM0044</i>	amino acid transporter	<i>Bm</i>	<i>WBM0447</i>	ankyrin repeat protein	S, <i>Bm</i> , E
<i>WBM0057</i>	ZapA superfamily, hypothetical		<i>WBM0452</i>	SAM-dependent methyltransferase	E, 4
<i>WBM0064</i>	FAD-dependent oxidoreductase		<i>WBM0482</i>	hypothetical, tropomyosin-like	<i>Bm</i> , E
<i>WBM0070</i>	Mg <sup>2+</sup> /Co <sup>2+</sup> transporter	4	<b>WBM0484</b>	<b>hypothetical protein</b>	S
<b>WBM0076</b>	<b>WAS(p) family protein, proline-rich</b>	E	<i>WBM0491</i>	cytochrome C oxidase assembly protein	S
<b>WBM0100</b>	<b><i>Wolbachia</i> Surface Protein (WSP) family</b>	S	<i>WBM0506</i>	outer membrane protein	E
<b>WBM0114</b>	<b>peptide deformylase</b>	4	<i>WBM0582</i>	ankyrin repeat protein	S
<b>WBM0152</b>	<b>PAL-like</b>	S, E	<i>WBM0665</i>	ankyrin repeat protein	4
<b>WBM0164</b>	<b>hypothetical, tropomyosin-like</b>	E	<b>WBM0666</b>	<b>dihydrolipoamide acetyltransferase</b>	4
<b>WBM0165</b>	<b>hypothetical protein</b>	U	<i>WBM0671</i>	DNA uptake lipoprotein	
<b>WBM0181</b>	<b>ATP-binding chaperone</b>	<i>Bm</i> , 4	<b>WBM0672</b>	<b>hypothetical protein</b>	<i>Bm</i> , U
<b>WBM0193</b>	<b>hypothetical, tropomyosin-like</b>	<i>Bm</i> , E	<b>WBM0709</b>	<b>coproporphyrinogen III oxidase</b>	4
<b>WBM0209</b>	<b>pyruvate phosphate dikinase</b>	<i>Bm</i>	<i>WBM0711</i>	DNA recombination <i>rmuC</i> -like	S, <i>Bm</i> , 4
<i>WBM0213</i>	hypothetical protein	E, U	<i>WBM0736</i>	secreted FK506 binding protein-like	<i>Bm</i>
<b>WBM0222</b>	<b>preprotein translocase YajC</b>	4	<b>WBM0748</b>	<b>hypothetical protein</b>	4
<b>WBM0277</b>	<b>calcineurin-like phosphodiesterase</b>	4	<i>WBM0749</i>	hypothetical protein	<i>Bm</i> , 4
<b>WBM0284</b>	<b>WSP family</b>	4	<i>WBM0751</i>	hypothetical protein	4
<i>WBM0287</i>	ankyrin repeat protein	E	<b>WBM0752</b>	<b>hypothetical protein</b>	4
<b>WBM0290</b>	<b>D-alanyl D-alanine carboxypeptidase</b>	S	<i>WBM0772</i>	hypothetical protein	<i>Bm</i> , E
<i>WBM0307</i>	cytochrome C oxidase subunit	4	<b>WBM0791</b>	<b>N6-adenine methylase</b>	
<b>WBM0384</b>	<b>ankyrin repeat protein, metalloprotease</b>	E	<b>WBM0792</b>	<b>hypothetical protein</b>	E
<i>WBM0394</i>	ankyrin repeat protein	E			

<sup>a</sup>Characteristics of gene or protein product that supported selection: S, detected in *Wolbachia* secretome; *Bm*, detected in dissected *Brugia malayi*; E, predicted eukaryotic-like protein motifs; 4, co-regulated with *wBm* Type IV secretion apparatus or similar to predicted Type IV effectors from related organisms; U, unique to *Wolbachia*. ORFs noted in bold text were visualized to express in yeast via immunoblot (Fig S1)

### **Putative wBm effectors inhibit yeast growth.**

In an effort to identify those wBm proteins that manipulate eukaryotic physiology, we tested the ability of each of the putative effectors to inhibit yeast growth; many bacterial effector proteins have been identified in such a manner [144, 385-388]. Each galactose-inducible plasmid harboring an individual wBm “effector” was transformed into a yeast strain and gene expression was induced via a modified Gal4p transcriptional regulator which responds to the hormone  $\beta$ -estradiol, instead of the usual galactose (Materials and Methods), thus allowing GAL promoter induction with the same carbon source as uninduced conditions (glucose) and preventing any confounding results that may be introduced by changing carbon sources across expression conditions. Under growth conditions containing  $\beta$ -estradiol, we were able to detect full-length protein expression of 24 of the 47 putative effector proteins via the N-terminal Xpress™ epitope provided by the pYES2/NT A expression plasmid (Figure 3.1). It is likely that the total number of expressed proteins is underrepresented using this detection method, however, since N-terminal protein processing or degradation events may occur upon protein overproduction *in vivo*; further possibilities that could result in translation defects of these putative effectors were not explored. When strains harboring these plasmids were grown on minimal medium with or without  $\beta$ -estradiol, we found wBm0014, wBm0032, wBm0044, wBm0076, and wBm0284 strongly inhibit yeast growth in the presence of 1  $\mu$ M  $\beta$ -estradiol (determined by a reduction in cell titers by three orders of magnitude), but not in the absence of inducer (Figure 3.2A). Slight inhibition in yeast growth (as determined by a reduction in yeast growth by two magnitudes) was observed upon expression of wBm0070, wBm0114, and wBm0222 (Figure 3.2A). Other expressed wBm genes did not strongly inhibit the growth of yeast under these conditions (Figure 3.3).

Due to the ability of *Wolbachia* to live inside membrane-bound compartments in *B. malayi* cells [18], we next hypothesized that *Wolbachia* could secrete proteins that subvert normal endolysosomal membrane dynamics, potentially as a method of avoiding autophagic degradation [17, 396]. As yeast

strains are known to require normal endolysosomal or vacuolar function to resist high levels of zinc and caffeine [397, 398], we tested the ability of these *wBm* genes to induce growth sensitivity to 7.5 mM ZnCl<sub>2</sub> and 5 mM caffeine. As expected, putative effectors that were toxic on standard minimal media showed enhanced  $\beta$ -estradiol-dependent toxicity on zinc/caffeine plates (Figure 3.2B). Interestingly, strains harboring the *wBm0076* construct were sensitive to zinc/caffeine even under non-induction conditions (Figure 3.2B, lower left), suggesting that even low-level expression of *wBm0076* is sufficient to inhibit yeast growth under these conditions. Because expression of each of the eight above identified putative effector alone is sufficient to inhibit yeast growth under normal growth conditions, no conclusions can be drawn from the similarly defective growth observed in the presence of both  $\beta$ -estradiol and zinc/caffeine; it is not known if this observed toxicity is a result of protein-induced endolysosomal membrane trafficking defects or other protein-induced defects to yeast biology. Of note, however, was the discovery that *wBm0057*, *wBm0064*, *wBm0213*, *wBm0277*, *wBm0287* and *wBm0447* were only strongly toxic in the presence of zinc and caffeine (as determined by an observable reduction in cell titers by three orders of magnitude) (Figure 3.2B), suggesting that these strains may have defects in normal endolysosomal homeostasis, such as in defects in the TOR kinase pathway [399, 400] or protein trafficking pathways [401], although defects in DNA repair pathways may also contribute to caffeine sensitivity [402]. No other plasmids were found to induce additional sensitivity of yeast to zinc/caffeine treatment upon expression, though several others show slight inhibition of yeast growth (Figure 3.3). Taken together, we find several putative effector proteins from *Wolbachia* that inhibit the growth of yeast, suggesting these proteins may function to modulate essential eukaryotic pathways during *Wolbachia* symbiosis.

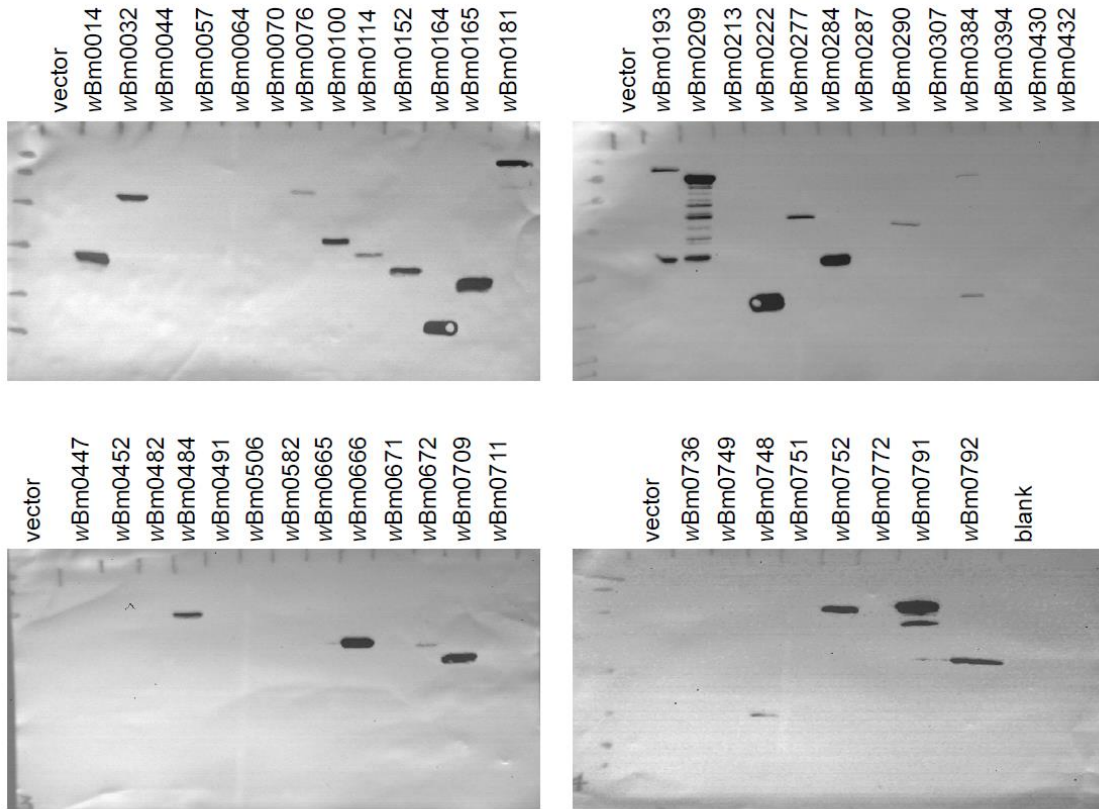


**Figure 3.1. Analysis of *wBm* effector protein expression in yeast.** BY4742 yeast strains genetically modified with GEV for  $\beta$ -estradiol-dependent induction of *GAL* promoters (Materials and Methods) were assayed for individual putative *wBm* effector expression via anti-Xpress immunoblot (Materials and Methods). Images shown are representative of three independent replicates.

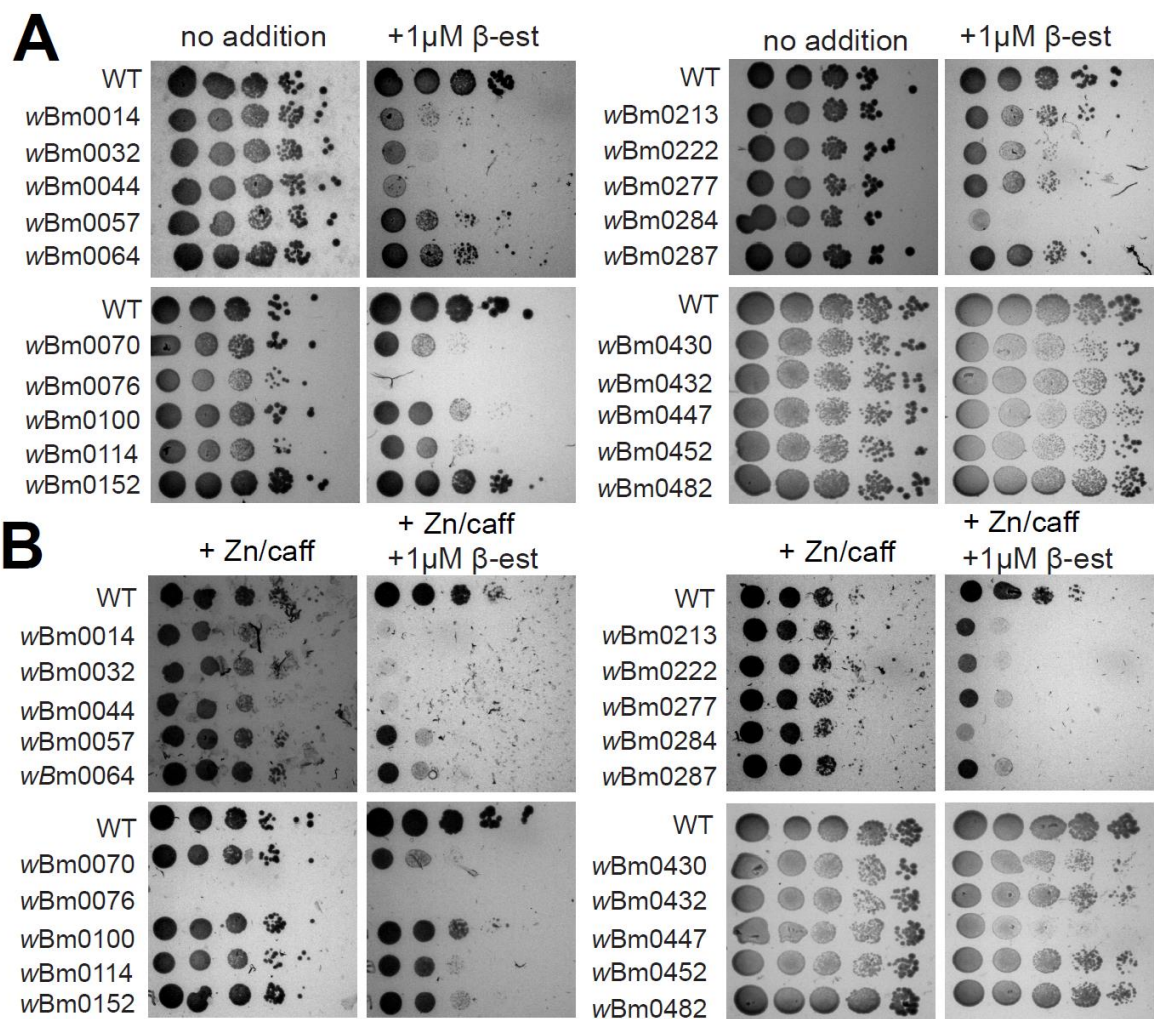


**Fig 3.2. *wBm* genes inhibit yeast growth upon expression.** **(A)** BY4742 yeast strains genetically modified with GEV for  $\beta$ -estradiol-dependent induction of *GAL* promoters (Materials and Methods) and harboring the *GAL*-inducible control plasmid pYES2/NT A, or pYES2/NT A containing the specified *wBm* open reading frame were grown to saturation in CSM-uracil medium containing 2 % glucose, and each culture was diluted to  $OD_{600} = 1.0$  in sterile 0.9% NaCl. 10-fold serial dilutions were spotted onto CSM-uracil containing 2% glucose with and without 1  $\mu$ M  $\beta$ -estradiol. Plates were incubated for 48 h at 30°C. **(B)** Strains and dilutions from **(A)** were spotted to CSM-uracil media containing 2% glucose supplemented with 7.5 mM  $ZnCl_2$ , 5 mM caffeine, and with or without 1  $\mu$ M  $\beta$ -estradiol. Plates were incubated for 72 h at 30°C. Images are representative of three independent experiments.

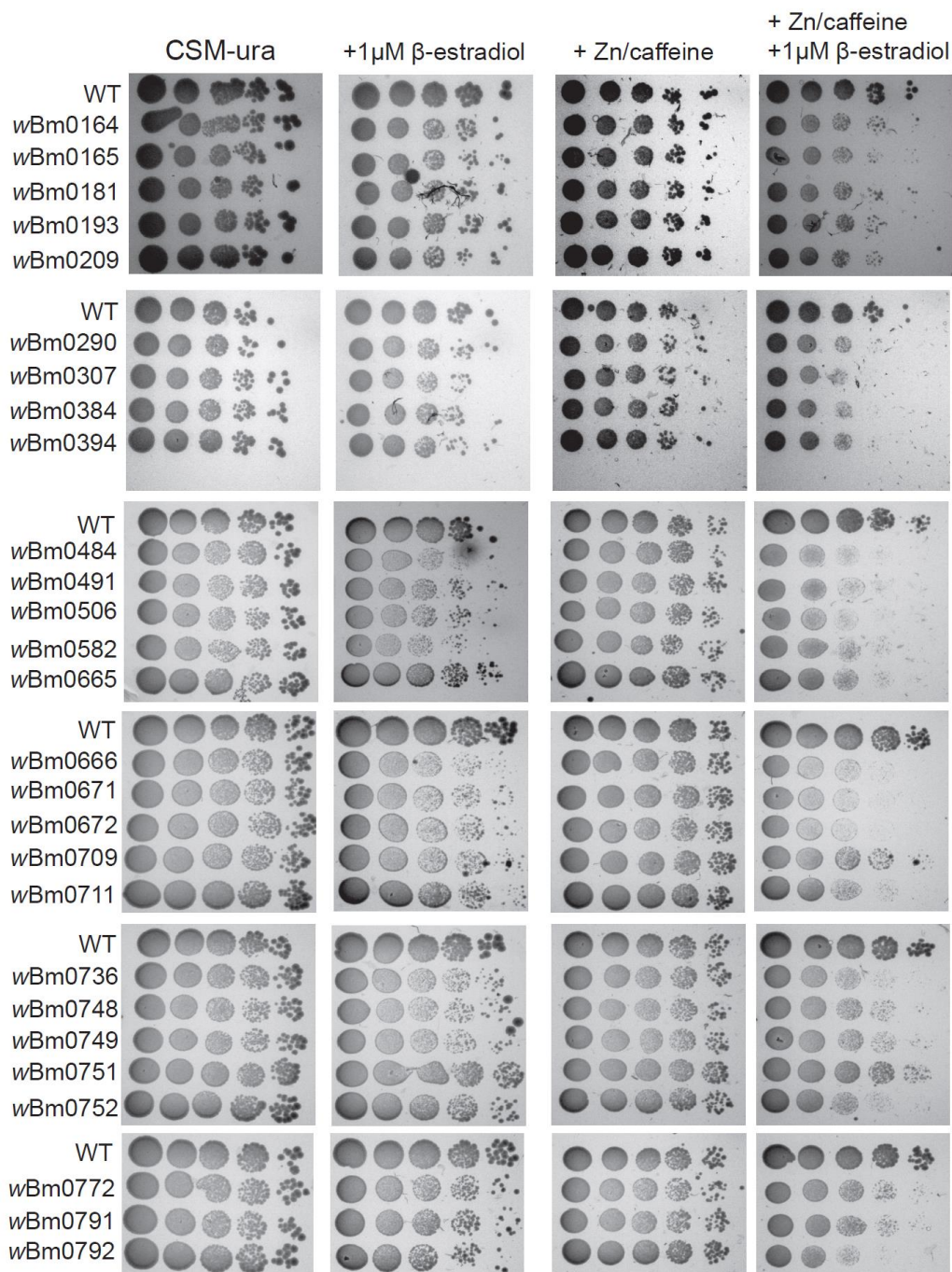


**Figure 3.3. Most individual *wBm* effector genes do not inhibit yeast growth upon expression.** BY4742 yeast strains genetically modified with GEV for  $\beta$ -estradiol-dependent induction of *GAL* promoters (Materials and Methods) and harboring the *GAL*-inducible control plasmid pYES2/NT A, or pYES2/NT A containing the specified *wBm* open reading frame were grown to saturation in CSM-uracil medium containing 2 % glucose, and each culture was diluted to  $OD_{600} = 1.0$  in sterile 0.9% NaCl. 10-fold serial dilutions were spotted onto CSM-uracil containing 2% glucose with and without 1  $\mu$ M  $\beta$ -estradiol or 7.5 mM  $ZnCl_2$ /5 mM caffeine. Plates were incubated for 48 or 72 h at 30°C; results are representative of three independent experiments.

### **Putative *Wolbachia* effectors disrupt yeast vacuole membrane dynamics.**

As reported previously, *Wolbachia* likely avoids both lysosomal and autophagic degradation pathways to survive within a membrane-bound organelle since chemical activation of autophagy results in clearance of *Wolbachia* from maturing nematodes [396]. Due to the fact that wBm must avoid normal host autophagic pathways, it is likely that wBm secretes proteins that alter normal host endolysosomal membrane trafficking pathways. The degradative vacuole of yeast has long been used as a model organelle for mammalian lysosome function and eukaryotic endolysosomal fusion dynamics [403], therefore we assayed the effects of wBm putative effector expression on yeast vacuole dynamics.

The yeast vacuole is a highly dynamic organelle that undergoes constant rounds of fission and fusion in response to the osmolarity of the extracellular environment [404]. The homotypic fusion of yeast vacuoles, like the majority of eukaryotic intracellular membrane fusion events, is governed by a conserved set of protein machinery consisting of soluble NSF attachment protein receptors (SNAREs), a Rab-family small GTPase, and a Rab/SNARE-binding multisubunit tethering factor, the homotypic vacuole fusion and protein sorting (HOPS) complex (reviewed in [233]). Yeast strains defective in the proper regulation of homotypic fusion, either directly or indirectly, generally display aberrant vacuolar morphologies. These phenotypic changes have been used to identify important regulators of endolysosomal membrane fusion and protein trafficking machineries in yeast [398, 405]. Six different classes of vacuoles have been described as A through F [359]; class A vacuoles are considered wild-type morphology. The remaining classes B-F are considered abnormal vacuole morphologies and are phenotypically described briefly: class B vacuoles represent highly fragmented vacuoles containing more than twenty vacuoles per cell, class C vacuoles are highly fragmented with no discernable vacuolar structure, class D vacuoles have a single enlarged vacuole, class E vacuoles have an enlarged prevacuolar compartment with small vesicles present, and class F vacuoles have many small vacuoles surrounding a larger prominent vacuole. Importantly, the expression of some secreted effectors from pathogenic

bacteria in yeast show the ability to both fragment the yeast vacuole *in vivo* and inhibit the fusion of yeast vacuoles *in vitro* [143, 397, 406].

Yeast strains harboring a control plasmid under induction conditions (1  $\mu$ M  $\beta$ -estradiol) show 1-5 large vacuoles per cell, as stained by the endocytic uptake of the vacuole-specific fluorescent marker, FM4-64 [389] (Figure 3.4). Under the same growth conditions, strains expressing *wBm0076* display an apparent highly fragmented, class C vacuole morphology in 75% of the cells observed, often indicative of either a complete block in vacuole biogenesis, including defects in homotypic vacuole fusion, or disruptions in the delivery of FM4-64-containing endocytic vesicles to the vacuole [193, 407]. In strains expressing *wBm0114*, approximately 40% of the observed cells display a large number of small, vacuole-like, “class B” compartments that may indicate defects in vacuolar protein sorting pathways [358, 407]. In the presence of *wBm0152*, more than half of the yeast cells contain large vacuolar compartments with accumulations of small membrane compartments immediately adjacent to the vacuolar limiting membrane; these accumulations are likely enlarged pre-vacuolar compartments (class E compartments) that arise in strains defective in endosome:vacuole fusion or endosomal sorting complexes required for transport (ESCRT) function [359, 408]. Finally, 30% of cells expressing *wBm0447* display an aberrant vacuole morphology that was not easily classified: most cells were multi-vacuolar with small membrane accumulations at the plasma membrane (Figure 3.4). No other strains harboring *wBm* genes displayed a significant defect in yeast vacuole morphology (> 85% wild type vacuoles, Figure 3.5); the ability of the selected *wBm* proteins to strongly manipulate yeast endolysosomal membrane dynamics is specific to a select few putative effectors.

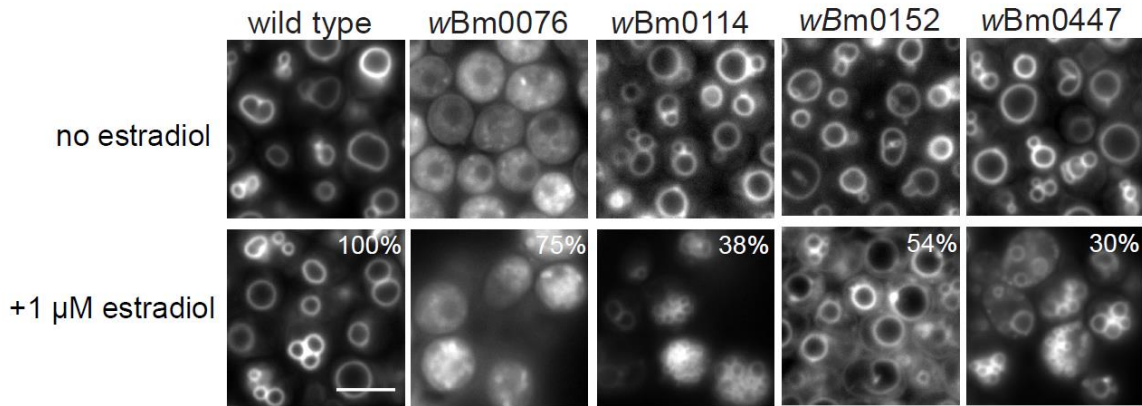


**Fig 3.4. Normal vacuole dynamics are altered upon *wBm* gene expression.** BY4742 yeast strains modified with GEV for  $\beta$ -estradiol-dependent induction of *GAL* promoters (Materials and Methods), and harboring *GAL*-inducible pYES2/NT A control plasmid or pYES2/NT A containing an individual *wBm* open reading frame were grown to saturation in CSM-uracil medium, subcultured to CSM-uracil and grown for 6h at 30°C with or without the addition of 1  $\mu$ M  $\beta$ -estradiol. Cells were stained for 20 minutes with 10  $\mu$ M FM4-64 at 30°C followed by a 1.5 h chase in CSM-uracil at 30°C. Vacuoles were visualized via microscopy, and cells displaying abnormal vacuole morphologies were counted. Percentage of cells displaying the corresponding abnormal vacuolar morphology is noted and determined from three independent experiments;  $n \geq 100$  cells per experiment. Bar = 3  $\mu$ .

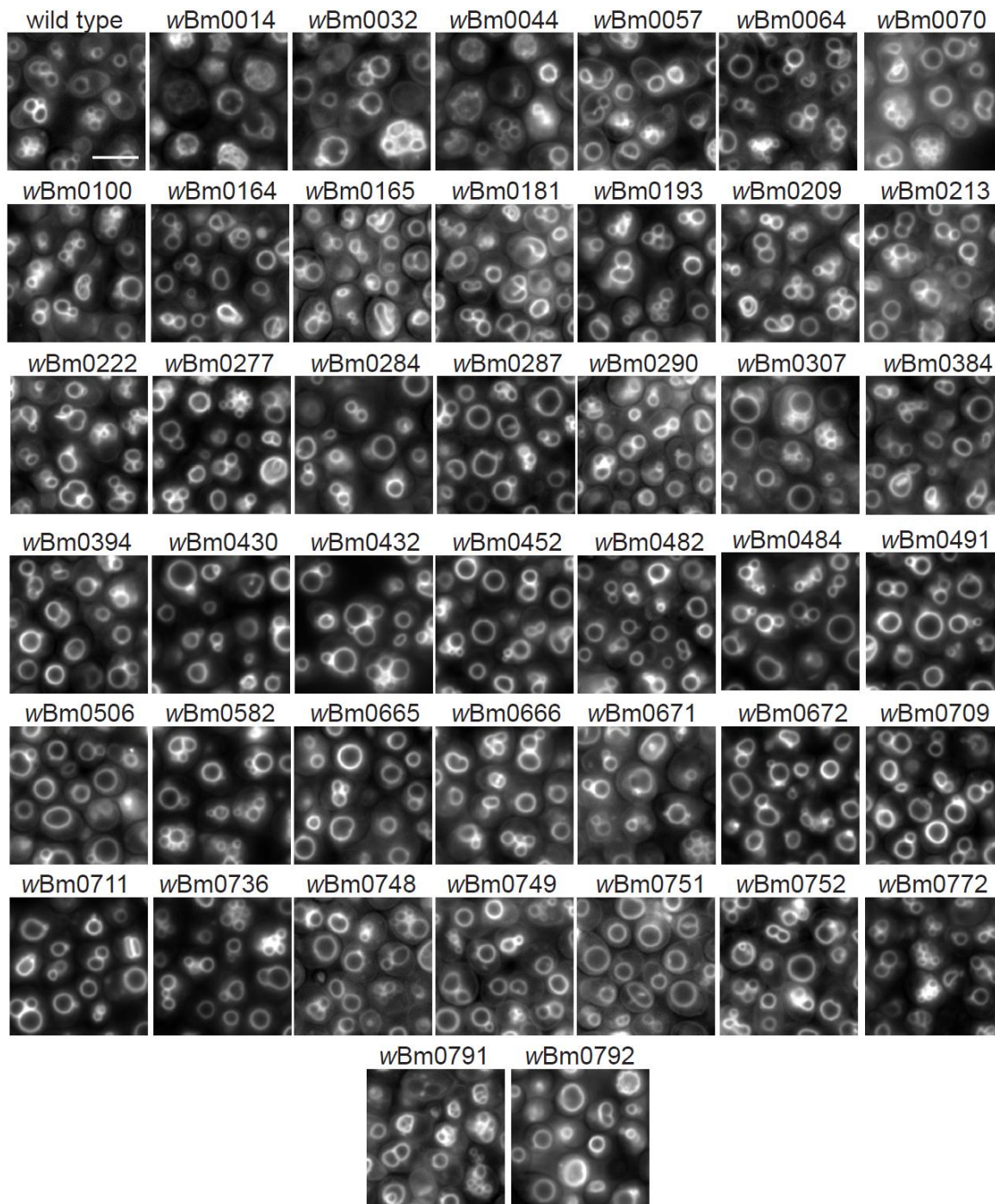
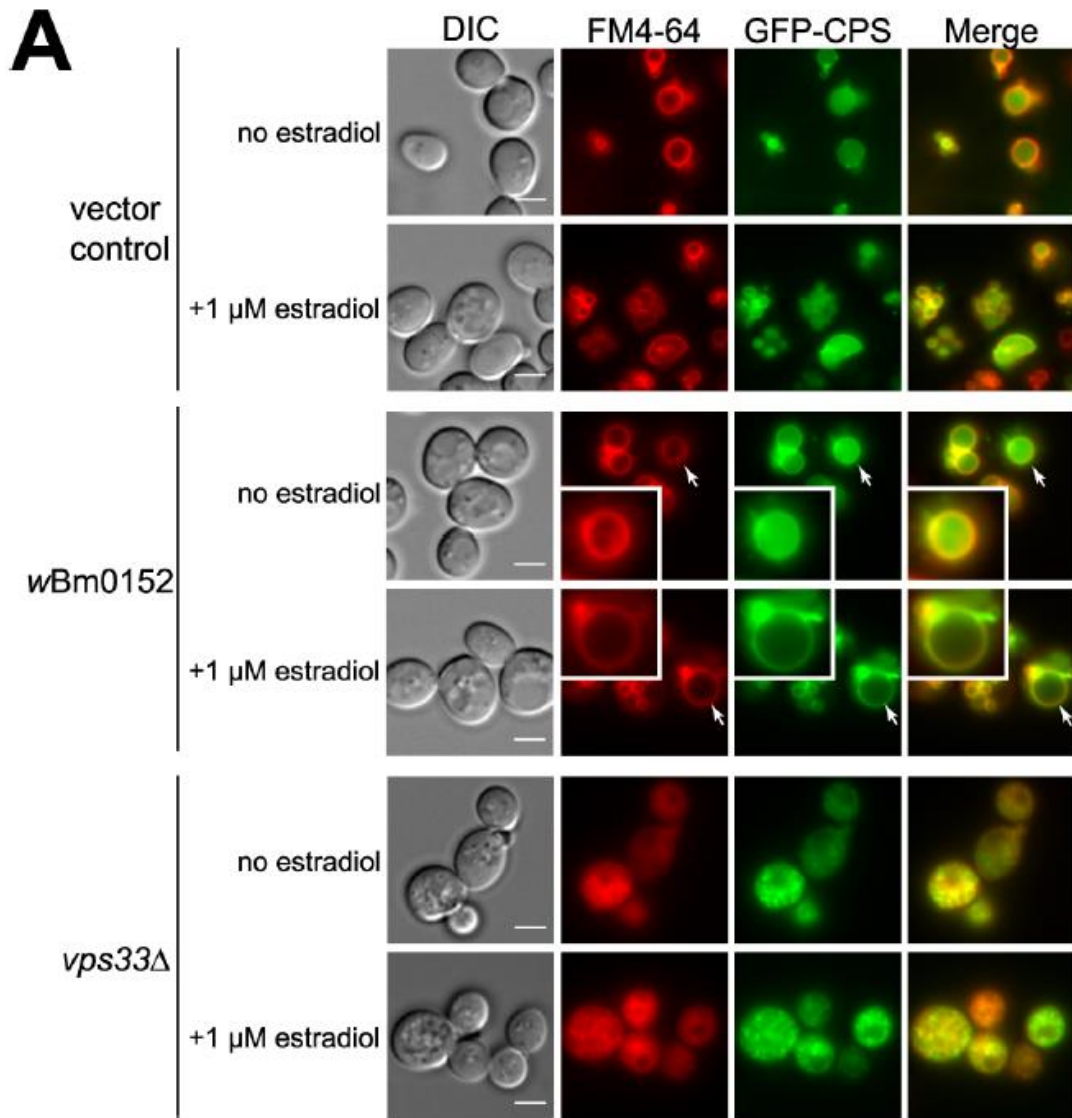


**Figure 3.5 Effects of *wBm* effector gene expression on yeast vacuole morphology.** BY4742 yeast strains modified with GEV for  $\beta$ -estradiol-dependent induction of *GAL* promoters (Materials and Methods), and harboring *GAL*-inducible pYES2/NT A control plasmid or pYES2/NT A containing an individual *wBm* open reading frame were grown to saturation in CSM-uracil medium, subcultured to CSM-uracil supplemented with 1  $\mu$ M  $\beta$ -estradiol, and grown for 6h at 30°C. Cells were stained for 20 minutes with 10  $\mu$ M FM4-64 at 30°C, followed by a 1.5 h chase in CSM-uracil at 30°C. Cells were visualized and representative crops from three independent experiments were generated; bar = 5  $\mu$ .

### **wBm0152 disrupts endosome:vacuole cargo trafficking in yeast.**

To further characterize the potential defects in endolysosomal trafficking caused by the expression of putative *wBm* effector proteins, we decided to identify *wBm* proteins that caused aberrant trafficking of endosome:vacuole cargo upon expression. We employed both GFP-tagged carboxypeptidase S (CPS), a membrane-bound vacuolar protease [302], and GFP-tagged Sna3p, a transmembrane ubiquitin ligase adapter protein involved in vacuole protein sorting [154]. It is known that both proteins cargo traffic to the yeast vacuole via an endosomal/multivesicular body (MVB) intermediate compartment [302, 390]. Under normal growth conditions of wild type strains, both GFP-CPS and Sna3-GFP localize to the yeast vacuole regardless of the presence of  $\beta$ -estradiol (Figures 3.6A&B). *VPS33* encodes for the Sec1/Munc18-family protein, which is a member of the multisubunit class C core vacuole/endosome tethering (CORVET) complex required for endosome:endosome fusion events. It is also a member of the multisubunit homotypic fusion and vacuole protein sorting (HOPS) complex required for both homotypic vacuole and late endosome:vacuole fusion [189, 190, 409, 410]. In the strain lacking *VPS33*, both GFP-CPS and Sna3-GFP were found in aberrant intracellular compartments, as expected (Figures 3.6A&B, *vps33* $\Delta$ ).

Upon induction with  $\beta$ -estradiol, most putative *wBm* effector proteins did not alter the normal vacuolar localization of either GFP-CPS (Figure 3.7) or Sna3-GFP (Figure 3.8), suggesting that expression of these proteins does not strongly alter normal endosome:vacuole traffic in yeast. Expression of the predicted peptidoglycan associated lipoprotein (PAL) *wBm0152*, however, prevented both GFP-CPS and Sna3-GFP from accumulating within the vacuole lumen (Figures 3.6A&B, respectively), suggesting that this protein is capable of modulating the MVB:vacuole fusion event, and may play some role in either preventing the degradation of *Wolbachia* in nematode lysosomes, or supporting the synthesis of the *Wolbachia*-containing vacuole from post-Golgi membranes.



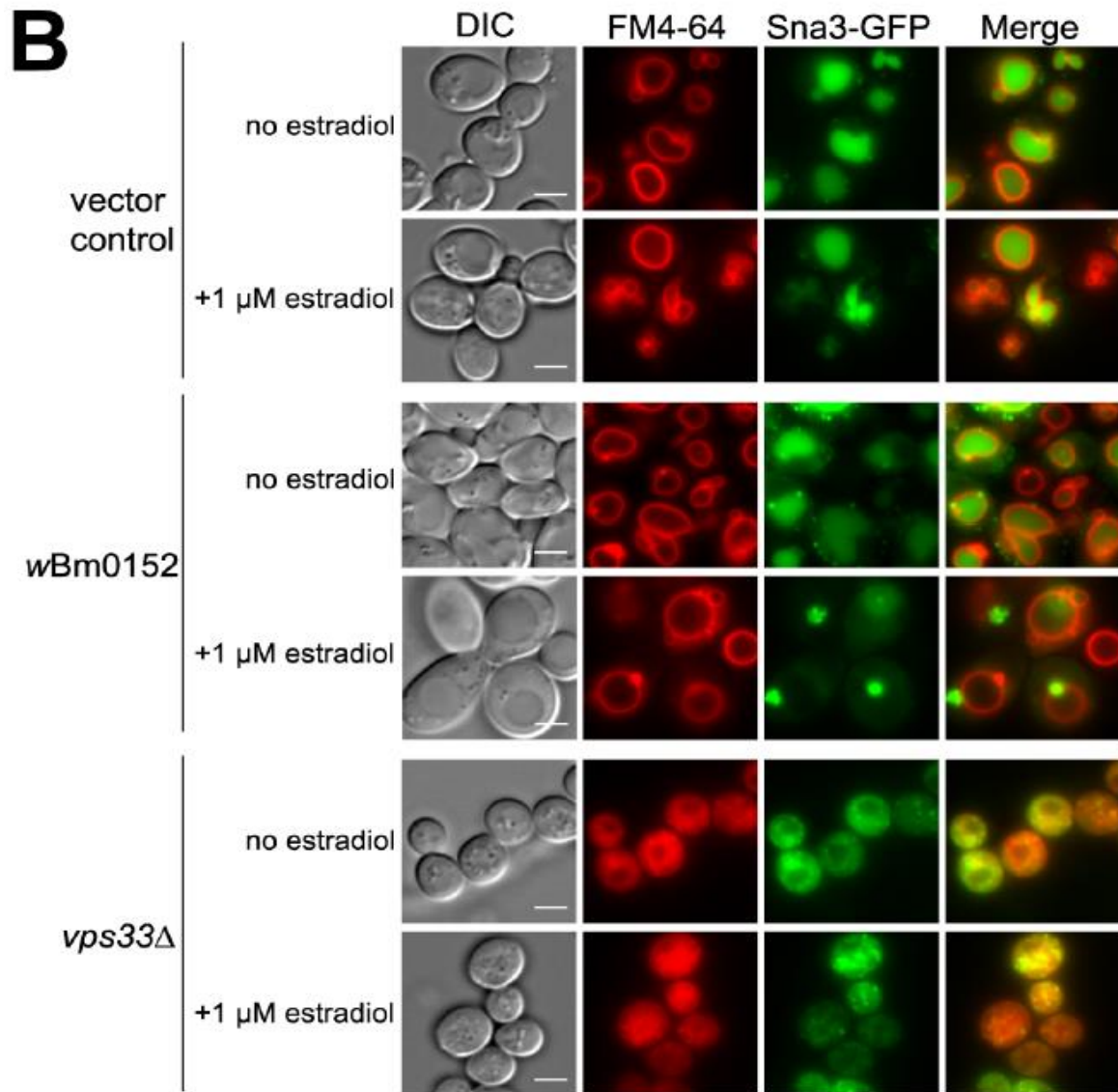


**Figure 3.6. wBm0152 expression inhibits endosomal traffic to the yeast vacuole.** BY4742 yeast strains modified with GEV for  $\beta$ -estradiol-dependent induction of *GAL* promoters (Materials and Methods), and harboring **(A)** GFP-CPS plasmid or **(B)** Sna3-GFP plasmid in addition to pYES2/NT A control plasmid or pYES2/NT A wBm0152 were grown to saturation in CSM-lysine-uracil medium. Cells were subcultured to CSM-lysine-uracil with and without the addition of 1  $\mu$ M  $\beta$ -estradiol and grown for 6h at 30°C. Cells were stained with 10  $\mu$ M FM4-64 dye for 20 minutes at 30°C and chased 1.5h in CSM-lysine-uracil medium at 30°C. Cells were visualized, and representative images are shown. Bar = 3  $\mu$ . Inset in **(A)** magnifies the cell denoted by the arrow to better visualize the GFP-CPS trafficking defect in cells expressing wBm0152; images are representative of two independent experiments

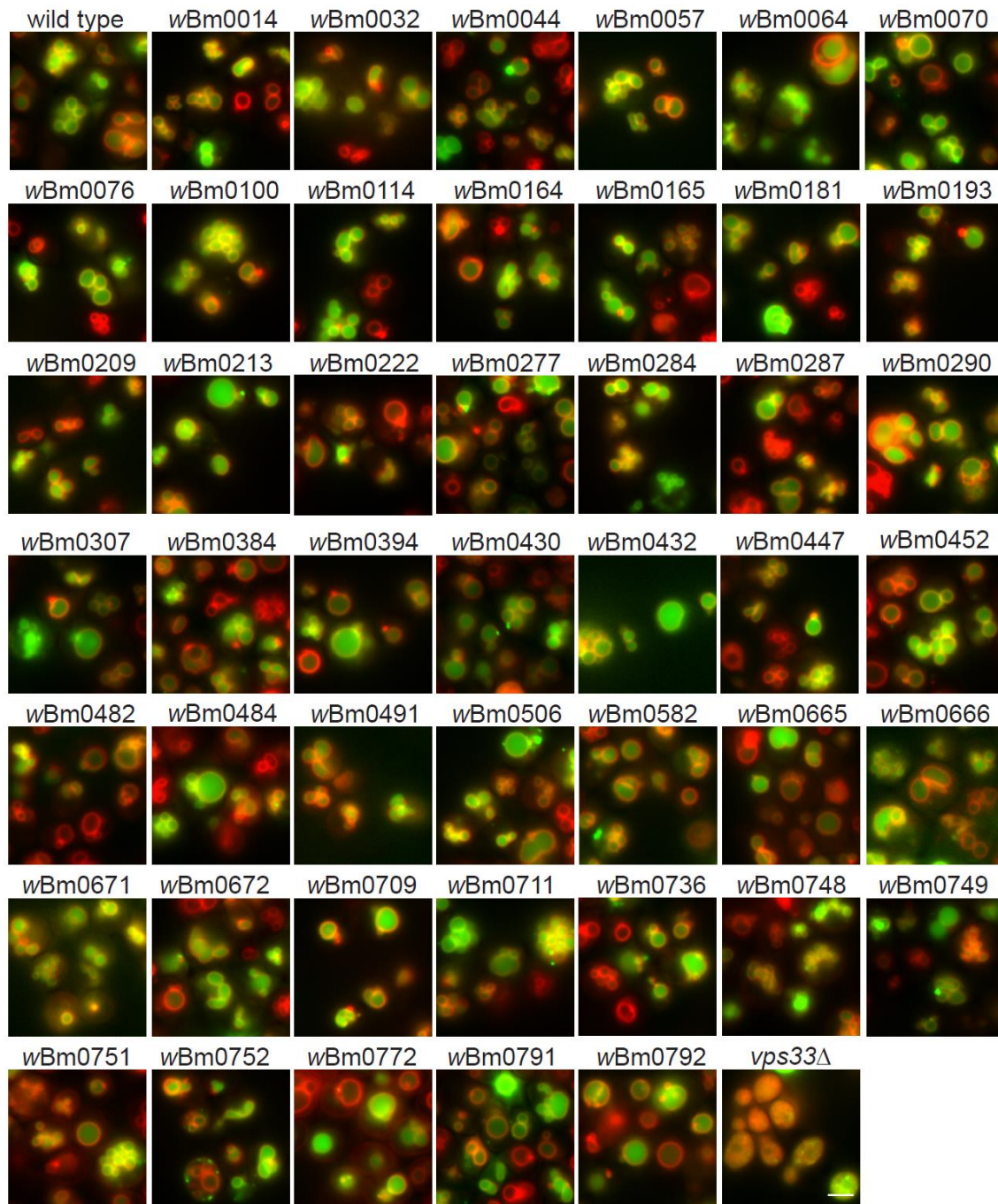


**Figure 3.7. CPS-GFP is generally not mislocalized in yeast strains expressing *wBm* genes.** BY4742 yeast strains modified with GEV for  $\beta$ -estradiol-dependent induction of *GAL* promoters (Materials and Methods), and harboring pGO45 GFP-CPS plasmid in addition to pYES2/NT A control plasmid or pYES2/NT A harboring an individual *wBm* open reading frame were grown to saturation in CSM-lysine-uracil medium. Cells were subcultured to CSM-lysine-uracil with  $1 \mu\text{M}$   $\beta$ -estradiol and grown for 6 h at  $30^\circ\text{C}$ . Cells were stained with  $10 \mu\text{M}$  FM46-4 for 20 minutes at  $30^\circ\text{C}$ , chased for 1.5 h in CSM-lysine-uracil medium at  $30^\circ\text{C}$ , then visualized. Representative crops from two independent experiments are shown; bar =  $3 \mu$ .

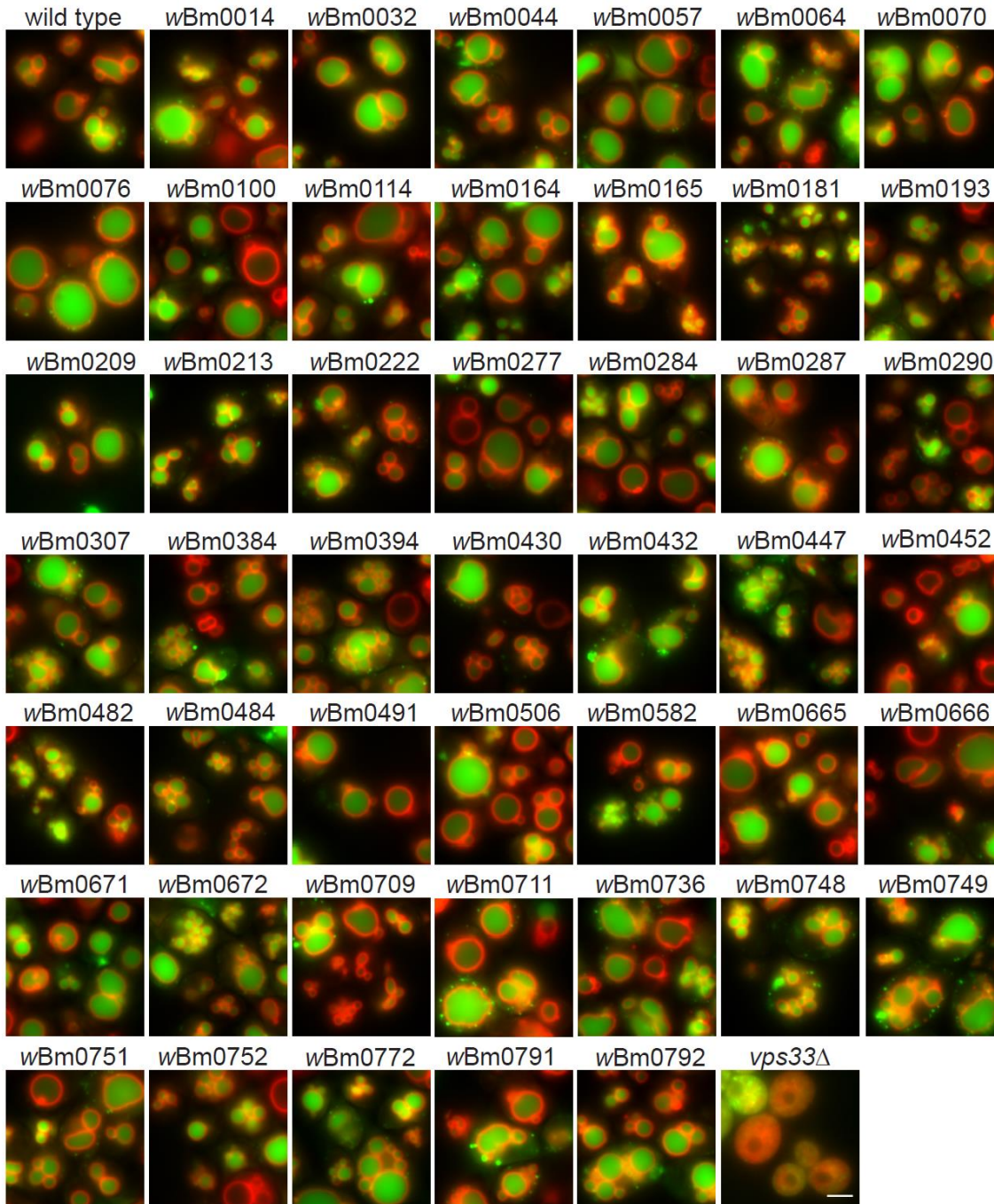


**Figure 3.8. GFP-Sna3 is generally not mislocalized in yeast strains expressing *wBm* genes.** BY4742 yeast strains modified with GEV for  $\beta$ -estradiol-dependent induction of *GAL* promoters (Materials and Methods) and harboring the Sna3-GFP plasmid in addition to pYES2/NT A control plasmid, or pYES2/NT A harboring an individual *wBm* open reading frame, were grown to saturation in CSM-lysine-uracil medium. Cells were subcultured to CSM-lysine-uracil with 1  $\mu$ M  $\beta$ -estradiol and grown for 6 h at 30°C. Cells were stained with 10  $\mu$ M FM46-4 for 20 minutes at 30°C, chased for 1.5 h in CSM-lysine-uracil medium at 30°C, then visualized. Representative images from two independent experiments are shown; bar = 3  $\mu$ .

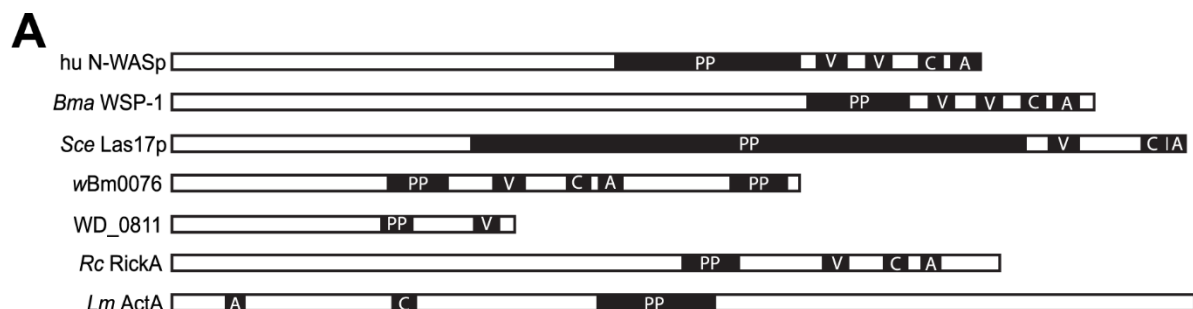
### Expression of wBm0076 disrupts the yeast actin cytoskeleton.

Expression of the wBm0076 gene is lethal to yeast (Fig 3.2). Analysis of the protein sequence via BLAST searching identifies orthologs in closely related bacteria including: *Wolbachia* of *Onchocerca volvulus* (WP\_025264345.1), *Wolbachia* of *Onchocerca ochengi* (WP\_014868845.1), *Wolbachia* of *Drosophila melanogaster* (AAS14498), and RickA from *Rickettsia conorii* (WP\_041471735.1). Wbm0076 is a protein of 392 amino acids in length, containing a putative WH2 (verprolin, V) domain, an ~18 amino acid actin-binding motif, a central  $\alpha$ -helical domain (C), an acidic region (A), and 2 proline-rich domains with homology to proteins of the eukaryotic neural Wiskott-Aldrich syndrome protein (N-WASP/WAS) family [411], including the bacterial RickA and actin-polymerizing ActA from *Listeria monocytogenes* [412] (Figures 3.9A&B). N-WASP proteins are known to bind actin monomers and the conserved eukaryotic Arp2/3 complex to stimulate branched actin filament formation in an Arp2/3-dependent manner [413, 414]. In addition, the RickA protein was determined to polymerize actin 'comet tails' on the surface of *Rickettsia* to aid in intracellular motility during infection, and to polymerize branched actin structures in a Arp2/3-dependent manner *in vitro* [415]. Based on the homology of wBm0076 protein to both eukaryotic and bacterial proteins known to modulate actin structures, we hypothesized that wBm0076 was likely modifying actin structures in yeast upon expression.

The yeast actin cytoskeleton consists of two main conformations: tight bundles of many actin filaments (cables) [416], and concentrated patches of highly branched actin that accumulate near the periphery of the yeast cell; these cortical actin patches are linked to newly-formed endocytic vesicles, thus enabling their retrograde trafficking [417]. To visualize cortical actin patches in the presence of wBm0076, we used a yeast strain expressing RFP-tagged Abp1p. Abp1p is an actin filament binding protein which interacts with Arp2/3 to stimulate Arp2/3 activity [367], and regulates the capping of barbed-end actin filaments when bound to Aim3p [418]. In a yeast strain harboring a vector control, Abp1-RFP localizes to several cortical punctae per cell, as expected (Figure 3.10A). The presence of the

*wBm0076* plasmid under non-inducing conditions does not alter the punctate localization of Abp1-RFP (Figure 3.10A). Upon addition of 1  $\mu$ M  $\beta$ -estradiol, however, yeast expressing *wBm0076* display a drastic increase in the number of Abp1-RFP punctae after 6 hours, when compared to the vector control strain (Figures 3.10A&B). While the overall number of cortical actin patches in *wBm0076*-expressing strains did not appear to increase when correcting for the estimated cell volume (Figure 3.10B, right panel), it is not yet clear if the increased number of cortical actin patches increased the cell volume, or if the increased cell volume induced a corresponding increase in cortical actin patches. When left in inducing conditions overnight, Abp1-RFP-containing punctae in the *wBm0076*<sup>+</sup> strain are no longer detected, and cells appear to lyse through a local disruption in the cell wall.

To visualize actin cables *in vivo*, we used GFP-tagged Abp140p, the actin-binding tRNA methyltransferase responsible for the addition of 3-methylcytidine in the anticodon loop of yeast tRNAs [419]. The N-terminal actin-binding domain of Abp140p is known to localize to both actin cable and cortical actin patches; control yeast expressing Abp140-3xGFP clearly mark actin cables, with a higher local concentration around the bud neck, as expected (Figure 3.10C). Upon a 6 hour induction with 1  $\mu$ M  $\beta$ -estradiol, cells harboring the *wBm0076* plasmid no longer show elongated actin cables, but rather a high concentration of discrete punctae similar to those seen in Abp1-RFP cells (Figure 3.10C); extended incubations in  $\beta$ -estradiol confirm the ability of *wBm0076* to lyse yeast cells (Figure 3.10C). Taken together, expression of *wBm0076* in yeast leads to an extensive disruption of the yeast actin cable network, an increase in the number of cortical patches containing branched actin, and cell lysis.



**B**

	WH2 domain (verprolin-like, V)	$\alpha$ -helical (C)	acidic region (A)
hu N-WASp	403 AGNKALLDQTRREGAQ--LKKVEQN	466 GIVGALMEVMQKRSKAIHSSDEDEDEDEDEDFEDDDEWED	
<i>Bma</i> WSP-1	471 G GKASLLSEIQAGVT--LKQVTN	530 GIAGALARALEERRRNMRNS--DESESEEEANNNDSEWES	
<i>Sce</i> Las17p	546 AGRDALLASTIRGAGGIGALRKVDKS	605 SLADALAAALNKRKTKV-----GAHDDMDNGDDW	
<i>wBm0076</i>	200 DSRNAMLKQIRQGTK--LTKKEER	246 YSSTALFEKLYRRLAIEFS---DSESDRSNYS DNGDWS	
WD_0811	187 NNHSTLFEOIRGGTT--LKRVGSN		
<i>Rc</i> RickA	405 IDTSDLMREIAGPKK--LKKVEFD	444 VNALSGLESIFARRAVIKVS-----DSSSSESDSGNWSD	
<i>Lm</i> ActA		137 GLPSDSA AEIKRRKAI	33 DSEDSSLNTDEWEE

**Fig 3.9. *wBm0076* is a WAS(p)-family protein.** Domain structure of *wBm0076* orthologs, including: human N-WASp (hu N-WASp; BAA20128.1), *Brugia malayi* WSP-1 (*Bma* WSP-1; CRZ22528.1), *S. cerevisiae* Las17p (*Sce* Las17p, NP\_014824.1), *wBm0076* (WP\_011256278.1), *wMel* WD\_0811 (WD\_0811; AAS14498), *Rickettsia conorii* RickA (*Rc* RickA; WP\_041471735.1), and *Listeria monocytogenes* ActA (*Lm* ActA; ABC40914.2). Domains including poly-proline motifs (PP), the WH2/verprolin-like (V), central  $\alpha$ -helical (C), and acidic regions (A) are depicted. **(B)** Sequence alignment of the conserved VCA domains of the proteins in **(A)**. Completely conserved residues are highlighted with a black box and residues conserved in more than half of the sequences are denoted with an asterisk. Only the first WH2 domains of hu N-WASP and *Bma* WSP-1 are aligned for simplicity.

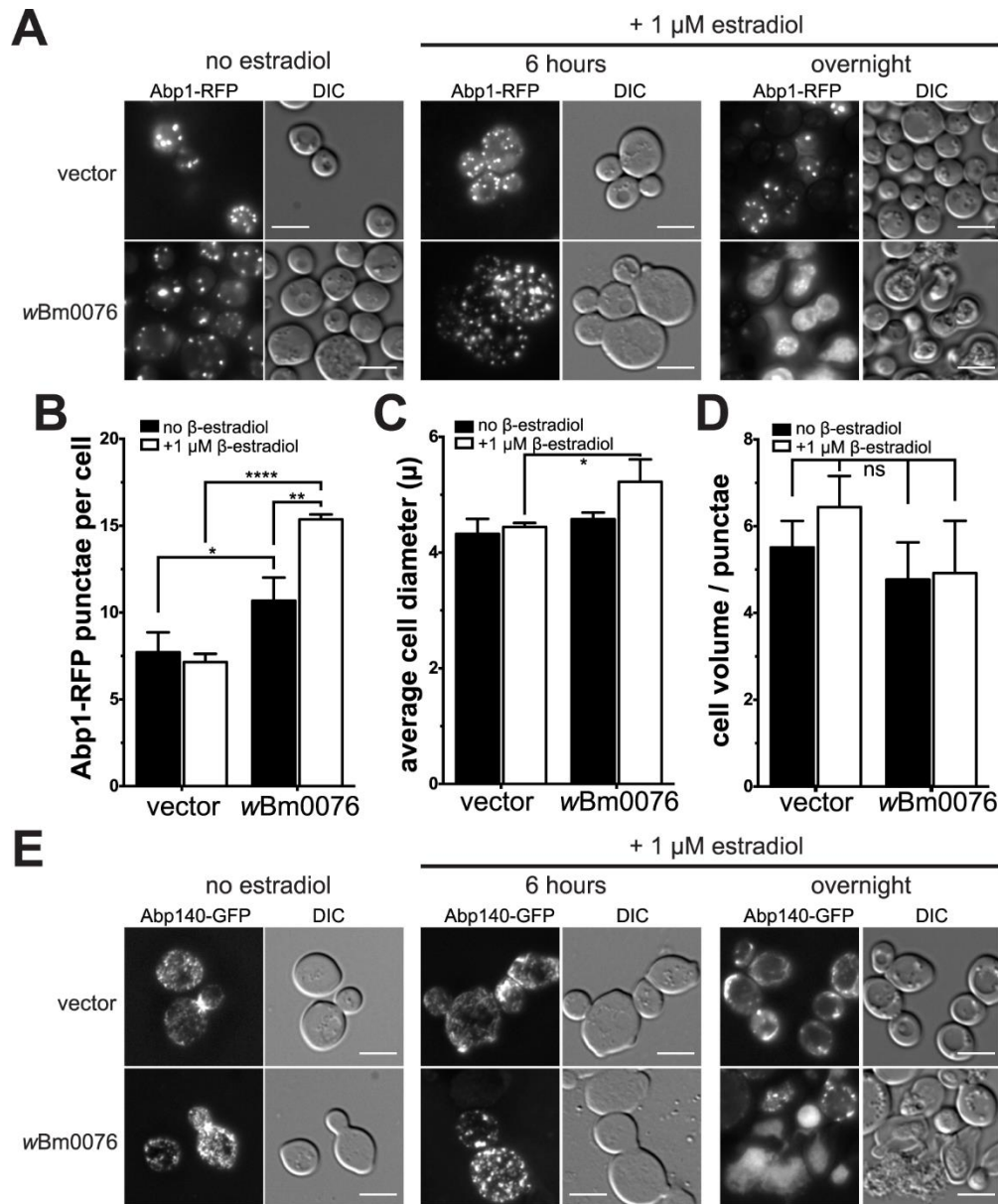


**Fig 3.10. wBm0076 expression alters yeast actin dynamics in vivo.** S288C yeast strains modified with GEV for  $\beta$ -estradiol-dependent induction of *GAL* promoters (Materials and Methods), expressing **(A)** Abp1-RFP and harboring either the pYES2/NT A control plasmid or pYES2/NT A wBm0076 were grown to saturation in CSM-uracil medium, subcultured to CSM-uracil, with or without 1  $\mu$ M  $\beta$ -estradiol, for 6h at 30°C. Cells were harvested at indicated time points and visualized. Bar = 5  $\mu$ . **(B-D)** The average Abp1-containing punctae per cell **(B)**, cell diameter **(C)**, and estimated cell volume / punctae **(D)**, (assume cell is a sphere during volume calculation) were measured from cells grown in **(A)**, and  $\geq 100$  cells each per three independent experiments were measured; ns =  $P > 0.05$  (not significant); (\*) =  $P \leq 0.05$ ; (\*\*) =  $P \leq 0.01$ ; (\*\*\*) =  $P \leq 0.0001$ . **(E)** As in **(A)**, except yeast cells harbored Abp140-3xGFP instead of Abp1-RFP.

### **Deletion of the Arp2/3-activating protein ABP1 provides resistance to wBm0076 expression.**

The isolation of yeast mutant derivatives that are no longer sensitive to wBm0076 expression could provide insight into not only the cellular processes modulated by wBm0076, but also help elucidate the protein targets or biochemical activity of wBm0076. Because wBm0076 protein displays homology to WAS(p)-family proteins and disrupts the yeast actin cytoskeleton *in vivo*, we hypothesized that deletions of genes encoding for proteins known to be involved in regulating actin dynamics may provide some resistance to wBm0076 expression in yeast.

In yeast, Las17p is the sole WAS(p)-family protein present that interacts with a large number of proteins via its conserved WH1 and proline rich domains, and plays an important role in regulating endocytosis [420-423]. We therefore assayed the toxicity of wBm0076 expression in thirty-one single gene deletion backgrounds, each of which were selected by their ability to produce proteins that either directly interact with Las17p, or otherwise regulate actin dynamics. Deletion strains harboring wBm0076 or vector only controls were serially diluted and grown on minimal media containing 1% raffinose plus either 2% glucose (uninduced condition) or 2% galactose (induced). As expected, wBm0076 was toxic to yeast upon galactose induction (Figure 3.11A; WT/0076). Of the thirty-one deletion strains tested, only *abp1Δ* strains displayed resistance to expression of wBm0076 on media containing galactose (Figures 3.11&3.12; *abp1Δ*/0076). We noted that some of these deletion strains (*arf1Δ*, *sho1Δ*, *vrp1Δ*, *las17Δ*, *bbc1Δ*, *myo5Δ*) grew very poorly on media containing galactose (Figure 3.12), even in the absence of wBm0076, and we therefore could not easily interpret these results. Importantly, expression of wBm0076 did not restore the ability of the *las17Δ* strain to grow on galactose (Figure 3.12); it is therefore unlikely that wBm0076 directly complements Las17p activity in *Saccharomyces*. However, of the thirty-one deletion strains tested, only *abp1Δ* strains displayed resistance to expression of wBm0076 on media containing galactose (Figure 3.11A&3.12; *abp1Δ*/0076).

Because Abp1p localizes to cortical actin patches and its deletion limits the toxicity of *wBm0076* expression, we considered the possibility that *wBm0076* would localize to cortical actin patches to regulate their formation *in vivo*. Accordingly, we constructed a *wBm0076*-mRuby expression construct that still maintained toxicity (and thus, activity) upon expression (Figure 3.11B). In a yeast strain harboring Abp140-3xGFP, which also localizes to cortical actin patches (Figure 3.10B), expression of *wBm0076*-mRuby induces the formation of cortical actin patches and concomitant loss of actin cables previously observed (Figure 3.11C, compare to Fig 3.10B). Additionally, we observe colocalization of *wBm0076* with these Abp140-3xGFP-positive punctae, suggesting that *wBm0076* localizes to cortical actin patches to regulate actin dynamics and may do so through direct interactions with yeast proteins directly involved in actin patch formation.

Based upon the finding that *abp1Δ* strains limit the toxicity of *wBm0076* expression, *wBm0076*-mRuby localizes to cortical actin patches, and the knowledge that Abp1p is intimately involved in activating Arp2/3 during endocytosis, we find it likely that the toxicity of *wBm0076* in yeast is directly related to its ability to alter actin dynamics *in vivo*. Given the conservation of the regulation of actin dynamics across eukaryotes, these data suggest that *wBm0076* may be important for the reorganization of actin structures in the nematode.

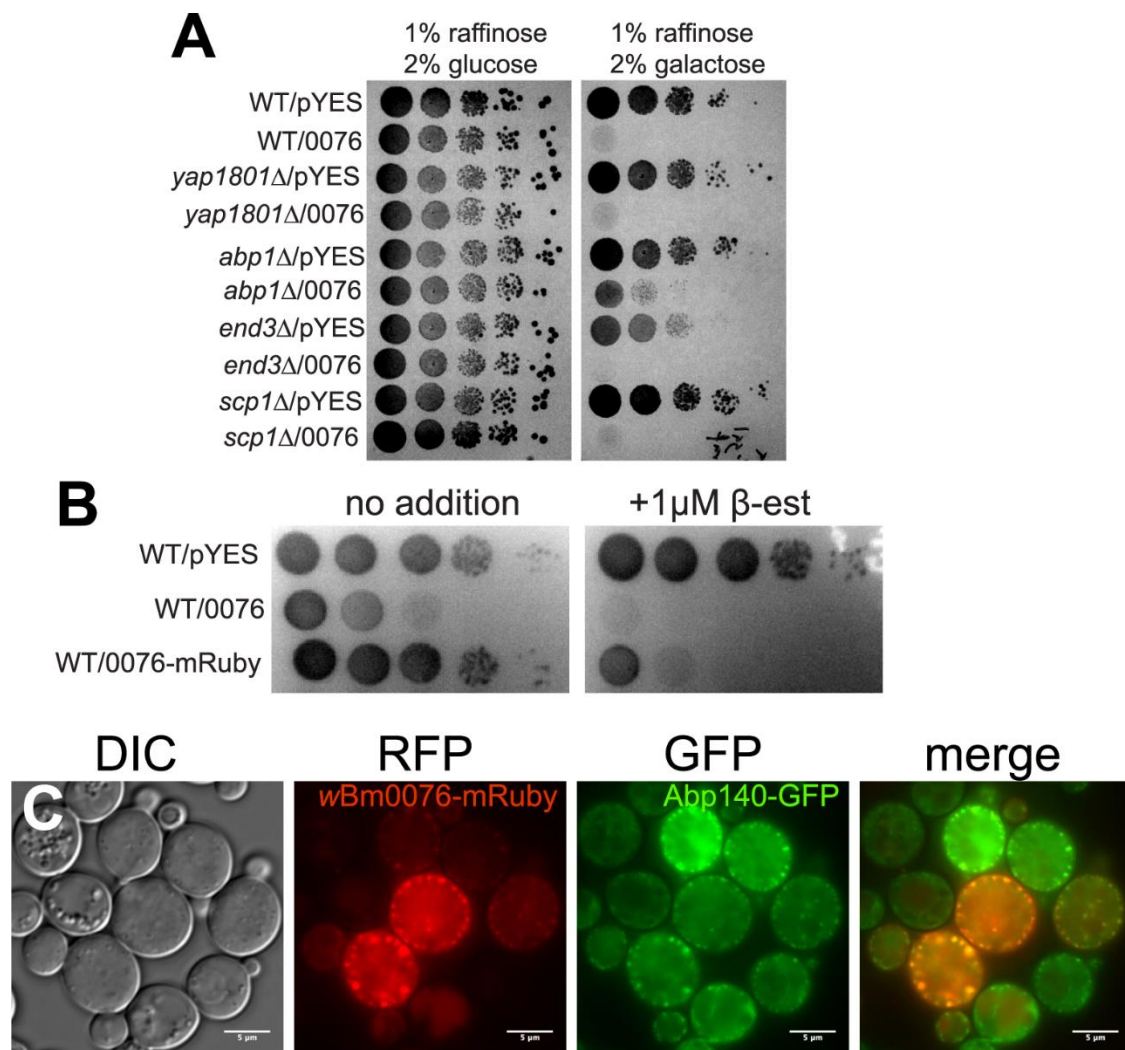


**Fig 3.11. Deletion of *ABP1* reduces the toxicity of *wBm0076* expression.** (A) BY4742 yeast strains deleted for the indicated gene and harboring either pYES2/NT A or pYES2/NT A *wBm0076* (0076) were grown overnight in CSM medium lacking uracil. Cultures were diluted to an  $OD_{600} = 1.0$  in sterile 0.9% NaCl, then spotted in 10-fold dilutions on plates containing 1% raffinose and either 2% glucose or 2% galactose to induce *wBm0076* expression. Plates were incubated for 72 h at 30°C and imaged. (B) BY4742 yeast strains modified with GEV for  $\beta$ -estradiol-dependent induction of *GAL* promoters and harboring either pYES2/NT A (pYES), pYES2/NT A *wBm0076* (0076), or pYES2/NT A *wBm0076*-mRuby2 (0076-mRuby) were grown spotted as in (A), except that plates either contained or lacked 1  $\mu$ M  $\beta$ -estradiol to induce *wBm0076* expression. Plates were incubated for 48 h and imaged. (C) Yeast strains harboring *Abp140*-3xGFP and pYES2/NT A *wBm0076*-mRuby2 were grown overnight in CSM medium lacking uracil and subcultured to fresh CSM-Ura containing 1  $\mu$ M  $\beta$ -estradiol. After 5 h outgrowth at 30°C, cells were harvested and visualized. Images are representative of three independent experiments; bar = 5  $\mu$ .

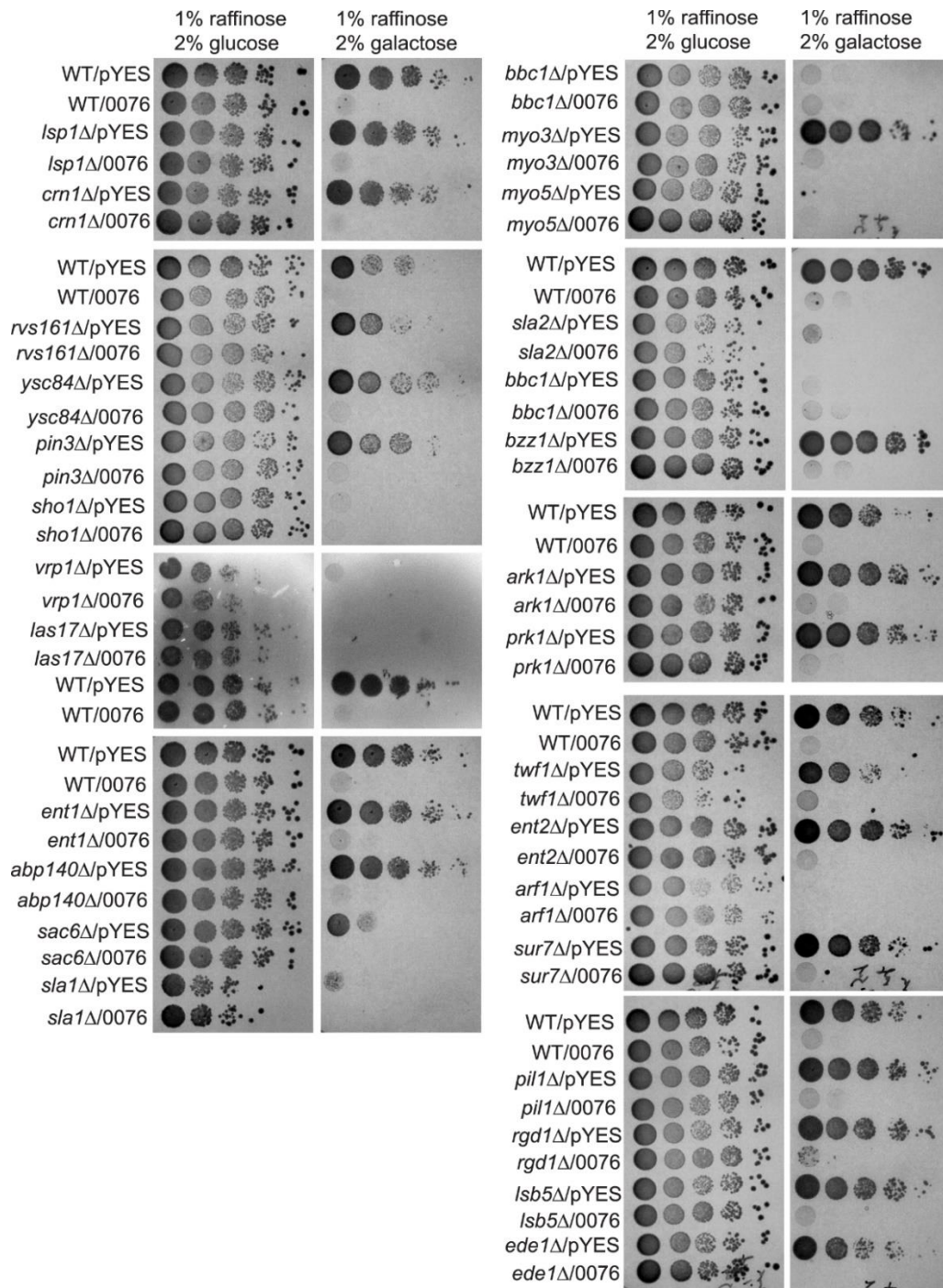


**Figure 3.12. Deletions of genes involved in yeast actin dynamics do not reduce the toxicity of wBm0076 expression.** BY4742 yeast strains deleted for the indicated gene and harboring either pYES2/NT A or pYES2/NT A wBm0076 (0076) were grown overnight in CSM medium lacking uracil. Cultures were diluted to an  $OD_{600} = 1.0$  in sterile 0.9% NaCl, then spotted in 10-fold dilutions on plates containing 1% raffinose and either 2% glucose or 2% galactose to induce *WBM0076* expression. Plates were incubated for 72 h at 30°C and imaged; results are representative of three independent experiments.

## Discussion

Though some progress has been made in understanding the *Wolbachia*:host relationship at the molecular level, much remains unknown about the mechanisms by which *Wolbachia* persists in its nematode or insect hosts. The use of *S. cerevisiae* as a highly tractable surrogate eukaryotic host provides an avenue to rapidly screen *wBm* putative T4SS effectors that may manipulate eukaryotic cell physiology and membrane trafficking pathways likely required for the persistence of *Wolbachia* in host cells. Historically, the *S. cerevisiae* model has successfully identified virulence factors from human pathogens that, upon expression in yeast, induce a growth defect and alter eukaryotic physiology, as is the case with the identification of secreted proteins from a variety of pathogenic bacteria, including *Chlamydia trachomatis*, *Legionella pneumophila*, *Pseudomonas aeruginosa*, and *Salmonella enterica* [386, 388, 424, 425]. Recently, *S. cerevisiae* was used to identify fourteen candidate effectors of the *Wolbachia* endosymbiont of *Drosophila melanogaster*, *wMel*, with each candidate effector inducing growth defects in *S. cerevisiae* [426]. Collectively, these data have verified that *S. cerevisiae* is a valuable tool to evaluate the molecular function of a number of *Wolbachia*-secreted proteins. Therefore, we have employed *S. cerevisiae* to screen 47 predicted *wBm* effectors to identify those that manipulate eukaryotic physiology. Due to the ability of some of these proteins to induce growth defects and alter growth defects in *S. cerevisiae* (Table 3.2), we propose that they may function as secreted effectors of *wBm* and may be necessary for germline cell invasion and persistence of *wBm* in its nematode host. Strikingly, two of these proteins – *wBm0076* and *wBm0152* - are particularly strong modulators of yeast physiology.

*wBm0152*, conserved across *Wolbachia* isolates of diverse hosts, is a predicted peptidoglycan associated lipoprotein (PAL) that was previously identified as a component of the *wBm* secretome [30]. PAL proteins are thought to be intimately involved in regulating Gram-negative cell envelope integrity via interactions with both periplasmic peptidoglycan and the outer membrane [427]. Relatively recent

work has found, however, that PAL proteins can exist in a so-called 'dual conformation,' where a population of these proteins are surface-exposed [428]. This particular conformation creates the possibility that these proteins may also be involved in extracellular contacts. Indeed, previous work by Melnikow and coworkers have shown that *wBm0152* was found to bind actin, and was hypothesized to be an important link between *Wolbachia* cells and host actin/tubulin during endosymbiosis, even though direct binding between *wBm0152* and actin in solution was not directly assayed [31]. In our study, we find that expression of *wBm0152* in *S. cerevisiae* induces a striking endosomal trafficking defect, as seen by aberrant class E vacuole morphologies, and in the mislocalization of the endosomal cargo proteins (CPS and Sna3p) to an enlarged prevacuolar compartment. This phenotype is reminiscent of yeast strains defective in endosomal sorting complex required for transport (ESCRT) complex proteins, which are involved in vacuolar protein sorting, Golgi protein recycling, and membrane repair/remodeling pathways [408]. Because the membrane comprising *Wolbachia* replicative vesicles in *Drosophila* appear to originate from the host Golgi [17], and because *wBm0152* seems to delay or block the delivery of Golgi-derived cargo to the vacuole in yeast, it is tempting to speculate that *wBm0152* may play a role in either the biogenesis of the *wBm* membrane-bound compartment, or preventing the degradation of the *Wolbachia*-containing vacuole by interfering with its fusion with the nematode lysosome.

*wBm0076* is a WAS family protein that likely promotes actin cytoskeletal rearrangements and has sequence homology to *RickA*, a protein expressed by *Rickettsia conorii* that is known to activate Arp2/3 and drive the polymerization of host actin to support bacterial intracellular motility during infection, similar to that of *Listeria monocytogenes* [415, 429]. In eukaryotes, Arp2/3 is a protein complex that is associated with cortical actin patches and aids in actin arrangement for the nucleation of branched actin filaments that drive processes like endocytosis and cellular motility [413, 414]. In yeast, it has been shown that the conserved Abp1p protein interacts with both actin and Arp2/3 complex to

initialize actin polymerization in *S. cerevisiae* [367, 430], specifically localizing to cortical actin patches and initiating endocytic vesicle formation and actin patch disassembly through its recruitment of other kinases [431, 432]. Our data shows *wBm0076* expression induces yeast cell lysis, in a manner similar to strains lacking F-actin[433]. Therefore, *wBm0076* may induce yeast cell lysis through the elimination of F-actin structures by either enhanced turnover of F-actin, or through the enhanced polymerization of branched actin structures and the concomitant decrease in monomeric actin required to maintain F-actin. Due to the fact that we have also identified a genetic interaction between *Abp1p* and *wBm0076*, it is possible limiting excess *Arp2/3* activation (and hence, excessive branched actin formation) by both *Abp1p* and *wBm0076* independently, is sufficient to limit cell lysis upon *wBm0076* expression. Alternatively, *Abp1p* may be the direct target of *wBm0076 in vivo* to regulate actin polymerization since the ability of *Abp1* and N-WASP to directly interact to stimulate *Arp2/3* activity has previously been shown in mammalian neuronal cells [434]. Interestingly, it has been shown that *Wolbachia* induces a reorganization of cellular F-actin structures during invasion of the germline in female nematodes, thus ensuring the vertical transmission of *Wolbachia* to offspring [435]. It is therefore possible that *wBm0076* plays a vital role in this particular process, as actin “comet tails” have not, as of yet, been detected to play a role in the mobility of *Wolbachia* in *B. malayi* [436]; *B. malayi* contains the *Abp1p* homolog *Bm4914* (20% end-to-end identity; 32% similar to yeast *Abp1p*), which could serve as the target of *wBm0076* in the nematode. Interestingly, profilin mutants of *Drosophila* are incapable of efficient maternal passage of *Wolbachia* to offspring [436], and the *Wolbachia* parasite of *Drosophila* (*wMel*) produces at least one other putative secreted effector, *WD0830*, capable of bundling actin filaments *in vivo* and *in vitro* via its  $\alpha$ -synuclein domain [437]. It is also important to note that the *wBm0076* homolog in *wMel*, *WD0811*, while containing a clear WH2 domain, lacks the conserved C and A domains usually found in WASP-family proteins (Fig 4); *WD0811* therefore may manipulate actin polymerization in *Drosophila* in a manner distinct from that of *wBm0076*. Additionally, *WD0811* has been previously

been shown to be translocated through a surrogate T4SS [438], thus providing additional evidence to support the hypothesis that *wBm0076* is an authentic T4SS effector of *wBm*. The data presented in this study provide additional mounting evidence that *Wolbachia* modulates host actin for successful transmission to offspring.

Recently, researchers have carried out a similar screen of eighty-four putative *wMel* effectors in yeast [426]. Of those eighty-four, twelve (based on sequence homology) were also screened in our study and three (*wBm0076*/*WD0811*; 36% identical, *wBm0287*/*WD0566*; 40% identical, *wBm0447*/*WD0438*; 44% identical) were moderately to severely toxic to yeast cells as determined by induced growth defects in the presence or absence of stressors. Notably, both *WD0811* and *WD0438* were identified by Rice et al. as candidate effectors of *wMel* due to induced growth defects in yeast [32]. *wMel* proteins are more similar to *Wolbachia* endosymbionts of arthropods within its same or similar clade than it is to *wBm* [32], *wBm* and *wMel* have 696 orthologous proteins and similar metabolic capacities that likely differ due to host and the relationship *Wolbachia* maintains with such host [20]. The use of yeast to identify putative effectors from *Wolbachia* endosymbionts of distinct hosts, and specifically homologous putative effectors, confirms the validity of such a screen for use as an initial characterization of protein functions in a genetically intractable system. In this work, we have furthered the characterization of two putative effectors of *wBm* that appear to have drastic effects on yeast cell biology, thus providing additional insight into their physiological function to support the intracellular survival of *Wolbachia* in *B. malayi*. Although we find individual *wBm* proteins can manipulate yeast growth and trafficking pathways, it is most likely a concerted effort of many secreted proteins is required to maintain both the intracellular colonization of *wBm* and survival of *B. malayi*. Our studies demonstrate the successful use of *S. cerevisiae* as a host system to identify putative effectors that may shed light on their roles in manipulating the cellular physiology of *B. malayi* to help maintain this essential relationship.

**Table 3.2. Summary of aberrant yeast phenotypes observed in this study.**

Growth <sup>a</sup>	Growth with Zn/caffeine <sup>a,b</sup>	Vacuole morphology <sup>c</sup>	Endosome:vacuole cargo trafficking
wBm0014 (strong)	wBm0057 (strong)	wBm0076	wBm0152
wBm0032 (strong)	wBm0064 (strong)	wBm0114	
wBm0044 (strong)	wBm0213 (strong)	wBm0152	
wBm0070 (weak)	wBm0277 (strong)	wBm0447	
wBm0076 (strong)	wBm0287 (strong)		
wBm0114 (weak)	wBm0447 (strong)		
wBm0222 (weak)			
wBm0284 (strong)			

<sup>a</sup>Inhibition of cell growth on indicated medium denoted as strong (cell titer three orders of magnitude lower in a serial dilution) or weak (two orders of magnitude), when compared to no induction controls.

<sup>b</sup>Inhibition of cell growth on medium containing ZnCl<sub>2</sub> and caffeine (Fig 1B), but not on medium lacking these additions.

<sup>c</sup>Proteins capable of producing aberrant vacuolar morphologies in ≥30% of the cells examined.

## Materials and Methods

### Yeast strains and plasmid constructions

For all growth analyses and microscopic visualization studies, yeast strain BY4742 (MAT $\alpha$  *his3 $\Delta$ 1 leu2 $\Delta$ 0 lys2 $\Delta$ 0 ura3 $\Delta$ 0*) was used for all studies. In order to create yeast strains that activate *GAL1* promoters via the addition of  $\beta$ -estradiol, strains were transformed with linearized pAGL (a gift from Dr. Daniel Gottschling, University of Washington), which introduces the gene encoding for the Gal4-estrogen receptor-VP16 (GEV) chimeric protein into the *leu2 $\Delta$ 0* locus [439]. S288C yeast strains expressing either Abp1p-RFP or Abp140-3xGFP were a kind gift from Dr. Bruce Goode (Brandeis University).

Hypothetical or eukaryotic-domain containing *Wolbachia* proteins such as ankyrin repeats or Ser/Thr kinase motifs were searched for using BLAST against the NCBI database. Proteins highly related to eukaryotes rather than bacteria were selected for this study. Coiled coil domain containing proteins were predicted using an online tool at: [https://npsa-prabi.ibcp.fr/cgi-bin/npsa\\_automat.pl?page=npsa\\_lupas.html](https://npsa-prabi.ibcp.fr/cgi-bin/npsa_automat.pl?page=npsa_lupas.html) [440]. *Rickettsia sibirica* proteins that interact with different components of its T4SS identified in a bacterial two-hybrid system [441] and proteins that potentially co-transcribed with components of T4SS were used to as query to search using TBLASTN against the *wBm* genome to identify the potential homolog in filarial *Wolbachia*. *Wolbachia* proteins identified in excretory-secretory (ES) products from *B. malayi* adult worms and microfilaria [395] were also selected. Domain structures of *wBm0076* and orthologs were determined with HHpred (MPI bioinformatics Toolkit, <https://toolkit.tuebingen.mpg.de/#/tools/hhpred>).

*Wolbachia* genes encoding for putative T4SS-secreted proteins were cloned into the galactose-inducible yeast expression vector, pYES2/NT A via the USER™ (uracil-specific excision reagent) cloning system developed at NEB. Briefly, gene-specific PCR primers were designed to clone the predicted *wBm* open reading frame into the vector expressing an amino-terminal Xpress™ epitope tag; these primers

(Table 3.3) contained a linker complementary to pYES2/NT A, with an additional uracil, and were used to amplify the target gene with *PfuTurbo* C<sub>x</sub> hotstart DNA polymerase (Stratagene). PCR products were then treated with the USER™ Enzyme (New England Biolabs) to create unique 3' single-stranded extensions which anneal and ligate to linearized pYES2/NT A, which had been previously amplified with vector-specific primers containing a complementary linker to the insert gene of interest.

In order to utilize the *URA3*<sup>+</sup> pGO45 and pMM134 plasmids, which express GFP-CPS or Sna3p-GFP, respectively [302, 442], for yeast endosome:vacuole transport studies in the presence of another *URA3*<sup>+</sup> yeast expression plasmid harboring the putative wBm effector, pGO45 and pMM134 were first converted from *URA3*<sup>+</sup> to *LYS2*<sup>+</sup> via homologous recombination methods by digesting pM2660 (ATCC) with HindIII [443], and transforming yeast strains harboring either pGO45 or pMM134 with this digest. Growth was selected on CSM medium + 2% glucose lacking lysine. Colonies from these plates were screened for lack of growth on CSM + 2% glucose medium without uracil. Plasmids from phenotypically correct strains were isolated, reintroduced into the appropriate yeast background, and confirmed for function via fluorescence microscopy.

To create the wBm0076-mRuby expressing pYES2NTA plasmid, the yomRuby2 gene was amplified from the plasmid pFA6a-link-yomRuby2-SpHis5 [444] using primers 5'-AGCTTTTCTTATAAAACAATTGATGGTGTCCAAAGGAGAGGAG and 5'-AGGGATAGGCTTAGCTGCAATTTACTTATACAATTCATCCATA, containing homology to both the C-terminus of the wBm0076 gene and the pYES2NTA-wBm0076 vector. BY4742 was co-transformed with pYES2NTA-wBm0076, previously digested with PmeI, and the mRuby2 amplicon and were plated to CSM-uracil to select for gap-repaired plasmids. Transformants were screened for red fluorescence via microscopy, and the resultant plasmid was purified and sequenced for confirmation (Eton Bioscience Inc).

### **Cell lysis and western blotting**

$\beta$ -estradiol responsive yeast strains harboring GAL-inducible pYES2/NT A control plasmid or pYES2/NT A containing an individual wBm open reading frame were grown to saturation in CSM-uracil medium, subcultured to CSM-uracil supplemented with 1  $\mu$ M  $\beta$ -estradiol, and grown for 6h at 30°C. 5.0 OD<sub>600</sub> units were harvested and protein was extracted in lysis buffer (0.1 M NaOH, 2% SDS, 2%  $\beta$ -mercaptoethanol, 0.05 M EDTA-NaOH pH 8.0) and boiled 5 minutes prior to the addition of 0.1M acetic acid. Equal volumes of extracts were separated on 13% SDS-PAGE gels and immunoblotted for wBm proteins using the commercially-available anti-Xpress monoclonal antibody (1:1000, Thermo Fisher Scientific) for 1 h, using blocking buffer containing 0.5% Tween and 5% dry non-fat milk. Goat anti-mouse IgG secondary antibody conjugated to HRP (1:20000, Thermo Fisher Scientific) was applied to the membrane for 1 h, washed, and developed with SuperSignal™ West Pico PLUS chemiluminescent substrate (Thermo Scientific).

### **Microscopy**

For evaluation of vacuole morphologies,  $\beta$ -estradiol responsive yeast strains harboring either control pYES2/NT A vector or pYES2/NT A WSPs were grown to saturation in selective medium at 30 °C, subcultured to fresh media with or without 1  $\mu$ M  $\beta$ -estradiol and grown for an additional 6 hours. After 6 hours, the entire culture was harvested via centrifugation, suspended in 50  $\mu$ L CSM lacking uracil, and FM4-64 was added to 3  $\mu$ M. Cells were incubated at 30 °C for 20 minutes, harvested, washed, then suspended in 5 mL fresh medium. This culture was incubated for an additional 90 minutes at 30 °C, harvested, washed, and suspended in 25  $\mu$ L CSM medium lacking uracil. Cell suspensions were mounted to slides that had been pre-treated with a 1:1 mixture of polylysine (10% w/v):concanavalin A (2 mg/ml) solution. Cells were visualized using a Nikon Ti-U fluorescence microscope, and images were processed using the Fiji software package [445, 446].

## **Statistical Analysis**

Statistical analysis was performed within the Prism® software package (GraphPad Software, v. 6.0b). Column statistics were performed via a 1-way ANOVA Repeated Measures test and Holm-Bonferroni post-test. Where noted in figures, ns =  $P > 0.05$  (not significant); (\*) =  $P \leq 0.05$ ; (\*\*) =  $P \leq 0.01$ ; (\*\*\*) =  $P \leq 0.0001$ .

## **Acknowledgments**

The authors would like to thank Drs. Daniel Gottschling, Bruce Goode, and Alexey Merz for providing essential reagents. E.M.C. is supported by a Graduate Research Fellowship from the National Science Foundation, and V.J.S. is supported by a grant from the National Institute of Allergy and Infectious Diseases (R01-AI100913). Z.L., C. F. and C.K.S.C. gratefully acknowledge the financial support of New England Biolabs. The Authors have no conflicts of interest to declare.

**Table 3.3. Primers used in this study.**

Gene	Forward	Reverse
pYES2NT	ATTGCAGC/ideoxyU/AAGCCTATCCCTAACCTCTCCTCGGTCT	AGCTCCT/ideoxyU/TACCTTATCGTCATCGTCGTACAGATCCCG
WBM0014	AAGGAGGC/ideoxyU/ATGCTCGAATGTGAAAATTTATCCTGTATT	AGCTGCAA/ideoxyU/TCAGCTATAACTATTGAAATTACACACGTC
WBM0032	AAGGAGGC/ideoxyU/ATGATGAACACGGATGAAACTATTTTTGC	AGCTGCAA/ideoxyU/TCACTTGCCTACACAGAAGTTATTGAATAT
WBM0044	AAGGAGGC/ideoxyU/ATGTCAAATAAAATAGGTTTTTTGGCTGT T	AGCTGCAA/ideoxyU/TTATTGTGCGGAAGCTCTTCGGTAC
WBM0057	AAGGAGGC/ideoxyU/ATGCAAGTAGTAGAAATAGTTATACGTAA TAG	AGCTGCAA/ideoxyU/CTAATCCTTTATGCACTCAATGATCTTATT
WBM0064	AAGGAGGC/ideoxyU/ATGAGTTACGACGTAATCATTTCAGGT	AGCTGCAA/ideoxyU/TTACACAAATCCCATAGCGTGCCGGAT
WBM0070	AAGGAGGC/ideoxyU/ATGGATTGGTTATTGGTTTCAATATTATCG ATA	AGCTGCAA/ideoxyU/TTAATCAATTGCTGTTACAGTATTATCAGT TTTTA
WBM0076	AAGGAGGC/ideoxyU/ATGCGTATATCTAATTTTTGGACCTTTAATT GC	AGCTGCAA/ideoxyU/CTATTGTTTTATAAGAAAAGCTCTAGATTC TTT
WBM0100	AAGGAGGC/ideoxyU/ATGATGAAAAGATCTATTGTTTTTGATGC AT	AGCTGCAA/ideoxyU/CTAAAATTAATATTAAGCCAATTTCAAT GTTATGG
WBM0114	AAGGAGGC/ideoxyU/ATGCCTAAATTATCAATTGTAGTTGCTCC	AGCTGCAA/ideoxyU/TCATCTCTCATAGTGTCTTTAACTTTTC
WBM0152	AAGGAGGC/ideoxyU/ATGTGGAGTAGATTGGTTGCAATGTGC	AGCTGCAA/ideoxyU/CTATTTTTTCATTCCAGAAAATGAAAAGCTC
WBM0164	AAGGAGGC/ideoxyU/ATGTCTAGCCAAAAGGGTGTAGATCTG	AGCTGCAA/ideoxyU/TCATGAAGTGCTCTGTATGTGCTG
WBM0165	AAGGAGGC/ideoxyU/ATGGAAGAAGCATGCAAACGTGTG	AGCTGCAA/ideoxyU/TCAATCTTTTTTGACATTTTTTTATCTT
WBM0181	AAGGAGGC/ideoxyU/ATGGACTTAAATAAATTTACCGAAAAAGC A	AGCTGCAA/ideoxyU/TTAAACCTTTTAACTAAGATTTTCATTATTA AAAGC
WBM0193	AAGGAGGC/ideoxyU/ATGAACATTGAAAATATACAACAAGAATT TTTTCC	AGCTGCAA/ideoxyU/TTATATTGATATACCTTTACCTTTTTCTTGT TGTTG
WBM0209	AAGGAGGC/ideoxyU/GTGGATACTGTTTATGTGAAATATGTTTG TCAAG	AGCTGCAA/ideoxyU/TTATCCAACACACTTAGATTTCTGAGCC
WBM0213	AAGGAGGC/ideoxyU/ATGAAAATAAAGCTGTTTTTTATTTTCACT CTACTGT	AGCTGCAA/ideoxyU/TTATTTAATAGATAAGCTATCTAAGTCAAA TTTTTGCTT
WBM0222	AAGGAGGC/ideoxyU/ATGTTCAATTTCTGAAGTTTTTGCGGCA	AGCTGCAA/ideoxyU/TTATGAAGTATTTTTACCTTTACTATCTTTC CCCT
WBM0277	AAGGAGGC/ideoxyU/ATGAATATTAATATCTTTGTTTTTTAGCT TTATCTTTT	AGCTGCAA/ideoxyU/TCAATTTATCTCAAGCTTAAAGTCTTCCG

WBM0284	AAGGAGGC/ideoxyU/ATGATGAGCAATAAAAAACATTAGCGG TTA	AGCTGCAA/ideoxyU/TTAAACCTTGCTAGCAAATGAAAAGTAA G
WBM0287	AAGGAGGC/ideoxyU/ATGCATGTTCAAGAATGTTGTAGAG	AGCTGCAA/ideoxyU/TTATTCCTTGATTAAGAAAAATTCTACAAC GTT
WBM0290	AAGGAGGC/ideoxyU/ATGAGTATATTAGACAAATTGGTAATCCT GC	AGCTGCAA/ideoxyU/TTAAACAATATTCTAAAAACTTTTCTAC GTAATT
WBM0307	AAGGAGGC/ideoxyU/ATGAGTGGCATAACAAAAGGTATAAGAC	AGCTGCAA/ideoxyU/CTATTTTATCACTGGTGGTTTTTCGAAAG
WBM0384	AAGGAGGC/ideoxyU/ATGTCCAATTATATAAAAATAGCGGAAC TA	AGCTGCAA/ideoxyU/TTAGATTAAGCTATGATCATGGTAAATATG A
WBM0394	AAGGAGGC/ideoxyU/aTGTTAGATCATAGTACTAGCTATGGGC	AGCTGCAA/ideoxyU/TTAGTTATTGACGACAGCAAAATATAAAG GA
WBM0430	AAGGAGGC/ideoxyU/ATGCGTAGTTTTTTGTATTTCTAATATTTT TTTCA	AGCTGCAA/ideoxyU/TCACCTTACGTAGCATAAATCATGCATTT
WBM0432	AAGGAGGC/ideoxyU/ATGCATTATAAAAAGTTTTTTTCAGCAACC G	AGCTGCAA/ideoxyU/TTAGAAATTAACGCTATTCCAGCTTCT
WBM0447	AAGGAGGC/ideoxyU/ATGAGTATAGATATAACTACACTAACTAC TAATACAG	AGCTGCAA/ideoxyU/TCATCGCGCCAGAGAAGAGGGTTTATT
WBM0452	AAGGAGGC/ideoxyU/ATGAATGCTGCTCTATACCATAAAGAAT	AGCTGCAA/ideoxyU/CTATGAATGATGAATCAGTATTGCTTTAAA AA
WBM0482	AAGGAGGC/ideoxyU/ATGAATAGTACTTGGCAAAAATGCATAG G	AGCTGCAA/ideoxyU/TCATGAGACATATTGTAATAAGTGATGAT ATATTAT
WBM0484	AAGGAGGC/ideoxyU/ATGTTAGAGGCGTTAAAGAGAGTAGGAA C	AGCTGCAA/ideoxyU/TCAATTATGGATTTGTGAAACACATTTATC TTGGTCTC
WBM0491	AAGGAGGC/ideoxyU/ATGGTCCCCTCTGTAAGGAGAAGCA	AGCTGCAA/ideoxyU/CTACTGTTAAGCTTAAAAAATGTATATGA TAGTG
WBM0506	AAGGAGGC/ideoxyU/ATGCGTAAGGTTTTTCATCTATAACAATAATT TCTT	AGCTGCAA/ideoxyU/CTAATTAATATTTTCATTCTTGGTTAGTTTG GTG
WBM0582	AAGGAGGC/ideoxyU/ATGAGAAGTGTTTTATACTTTACGTTGTTA TTTG	AGCTGCAA/ideoxyU/TCAGTCTTCATTGCATTGTAATTCATTATCT
WBM0665	AAGGAGGC/ideoxyU/TTGCACATCGTTACTTTGCATGGTAA	AGCTGCAA/ideoxyU/TCATACTATTTGTAGTAAAAATCTGTAACA TTTGC
WBM0666	AAGGAGGC/ideoxyU/ATGGTGACCTTGAGTGTAAGAGAAGCTTT ATGTA	AGCTGCAA/ideoxyU/TTATTTTTTTCTAAAACAGACCTGATGCAC AGT
WBM0671	AAGGAGGC/ideoxyU/ATGTATAAGGCTTTAATCACGTGCTTTA	AGCTGCAA/ideoxyU/TTACTGTTCTACAGTATTCTCTTTGAGGT

<i>WBM0672</i>	AAGGAGGC/ideoxyU/ATGACTAGTAACTTTGGAACATAAATTTCTGC	AGCTGCAA/ideoxyU/TCACATGTTTGTGCAGATATGAATCG
<i>WBM0709</i>	AAGGAGGC/ideoxyU/ATGAAAGAACAAAAATACAAGCTTTTCGA A	AGCTGCAA/ideoxyU/CTACATCCACTTAACAAGAGGTGGCAT
<i>WBM0711</i>	AAGGAGGC/ideoxyU/ATGCTTTTCAATTCTATCGCTTTTGG	AGCTGCAA/ideoxyU/CTAATCCACCCTCAATTCCTCGGC
<i>WBM0736</i>	AAGGAGGC/ideoxyU/ATGACTAGAAAAATTATACTACAATTGCT TATT	AGCTGCAA/ideoxyU/TTACTCAACAGTAGAGTGATGTGCTGCTAT TT
<i>WBM0748</i>	AAGGAGGC/ideoxyU/TTGGCTTACGCCATACGTAAGCAG	AGCTGCAA/ideoxyU/TTAAAAAAGGATCTTGACTGGCAGTAGTT CC
<i>WBM0749</i>	AAGGAGGC/ideoxyU/ATGGAAAGTGTAACCTAATTTTTTATT GATA	AGCTGCAA/ideoxyU/CTATAGCCCTAATAATTTCTTTTTGATTTCT TCCT
<i>WBM0751</i>	AAGGAGGC/ideoxyU/ATGCACATTCAATTGAATAAAGTTTTGATT TT	AGCTGCAA/ideoxyU/CTACAAGTGATACTTAATTTTTATCTTTTT TTACTAT
<i>WBM0752</i>	AAGGAGGC/ideoxyU/GTGGATGATAATGTAGCGATAGTTTTTAA TTAACA	AGCTGCAA/ideoxyU/TTAAACATGCAGTAGGCTTCTTTCATTATT AATAA
<i>WBM0772</i>	AAGGAGGC/ideoxyU/ATGGCAGAAGAGATTAACATTATGAACG	AGCTGCAA/ideoxyU/CTATCTTGATTGTGCTTCTCCTTGTC
<i>WBM0791</i>	AAGGAGGC/ideoxyU/ATGCTGCGTATTATTGCAGGAAAGTATC	AGCTGCAA/ideoxyU/TTAAGTTGATAGAGAAAGAAAAATTATTC TTGCTA
<i>WBM0792</i>	AAGGAGGC/ideoxyU/GTGAATAGGATAACAATGAAAGCTAGTA AAAA	AGCTGCAA/ideoxyU/TCAATCACTTTTTTTTTGATTTATCAACTATA TCGA

## CHAPTER 4

### MUTATIONS IN THE CONSERVED DOMAIN OF VAPA OF *RHODOCOCCUS EQUI* ALTER ITS AFFINITY FOR PHOSPHATIDIC ACID

Wright LM, Carpinone EM, Bennett TL, Hondalus MK, and Starai VJ. Mutations in the conserved domain of VapA of *Rhodococcus equi* alter its binding affinity for phosphatidic acid. To be submitted to PLoS ONE.

## Background

*Rhodococcus equi* is a Gram-positive soil-dwelling bacterium that causes pyogranulomatous pneumonia primarily in foals under six months of age though infection also occurs with diminished severity both in presentation and frequency in cattle, sheep, and immunocompromised humans [35, 447, 448]. *R. equi* is transmitted by the inhalation of aerosolized bacteria or ingestion of feces containing the bacteria [43-45] and replicates in alveolar macrophages upon its passage through mammalian airways and delivery to the lungs [49]. Replication in alveolar macrophages depends on the presence of a virulence associated plasmid (pVap) [56, 57] and by its presence, results in modulation of the phagosome to generate the *R. equi* containing vacuole (RCV) and evasion of macrophage defenses by arresting the maturation of the phagosome and preventing both its acidification and fusion with the lysosome [50-52]. To date, only one virulence associated protein (Vap), VapA, of pVapA virulence plasmid has been implicated in the arrest of phagosome maturation [72, 449].

Virulent *R. equi* possesses virulence plasmids that are predominantly host specific where pVapA is found in *R. equi* isolates of infected foals, pVapB is associated with swine, and pVapN is associated with cattle while humans may become infected with *R. equi* carrying any of the three plasmids [35, 58, 61-63]. Each virulence plasmid consists of conserved housekeeping regions, which function in conjugation and replication, and a variable region which contains a pathogenicity island (PAI) encoding Vaps that are less conserved between identified pVaps [63-65]. In addition to Vaps within the PAI, there are two transcriptional regulators, *virR* and *virS*, which are encoded in an operon and are activated in conditions of increased temperature and decreased pH [66, 71, 73-75]. The *VirR* operon activates expression of both PAI Vaps and chromosomal genes that aid in intracellular survival [66-68]. The most studied pVap is pVapA, associated with infections in foals. The PAI of pVapA specifically encodes nine Vap genes and pseudogenes: *vapG*, *-H*, *-X*, *-A*, *-I*, *-C*, *-D*, *-E*, and *-F* [64]. Of these nine genes and pseudogenes, *vapA* has been a topic of particular interest as VapA is implicated in the arrest of phagosome maturation and

binding of phosphatidic acid (PA) through analyses of *R. equi vapAΔ* infections and in vitro analysis of lipid interactions [72, 449]. Despite this, the precise method by which VapA induces such effects in macrophages remains unknown.

VapA is a lipoprotein 15-17kDa in size that, although it has not been crystalized, likely maintains a disordered/unresolved N-terminus and conserved C-terminus based on the crystal structure of VapB, which is homologous to VapA and is considered the VapA derivative of the pVapB plasmid [71, 79]. The disordered structure of VapB, like all crystalized Vaps remains unknown, however the conserved region contains eight antiparallel  $\beta$ -barrels that form two Greek key motifs and is likely present in the structure of VapA [79-81]. It has been suggested that the conserved crystal structure of Vap proteins maintains the capacity to bind ligands with its unique Greek key motifs [79]. VapA was recently shown to bind specifically phosphatidic acid (PA) containing liposomes through analysis of its interactions with liposomes of different lipid composition, providing the first evidence of a ligand of VapA [449]. Though to date there is no known PA binding domain identified in proteins, studies have identified residues that interact with PA, including arginine, histidine, lysine, and tryptophan [450, 451]. It is the goal of this work to identify residues of VapA, with a focus on arginine and lysine, that play a role in the binding capacity of VapA to PA through mutational analyses of the different regions of VapA and the interactions between such mutants and liposomes. Additionally, this work demonstrates through the use of the model eukaryotic organism, *Saccharomyces cerevisiae*, the role of charged residues in the localization of VapA to the plasma membrane. Identification of residues that bind PA can provide significant insight into the structure of VapA involved in binding membranes and may provide insight into the method by which VapA alters phagosome maturation through its interactions with PA in the macrophage.

## Results

### Mutation of VapA

VapA has a signal sequence, disordered domain that is unresolved, and conserved domain that is found across Vap proteins and its structure has been resolved. VapA contains only one residue each of arginine and lysine in its disordered domain located six residues from each other and two of each in its conserved domain, located nine or three residues apart. Mutations of VapA were performed by collaborators in the lab of Dr. Mary Hondalus to alter each of these residues to an alanine. The VapA derivatives generated are VapA<sup>K68A-R74A</sup>, designated VapA.Disordered, VapA<sup>R99A-K108A-R136A-K139A</sup>, designated VapA.Conserved, and a mutant derivative containing all six mutations, designated VapA.Full. Additionally, single mutant derivatives of VapA.Conserved were generated and are designated by their single mutation: VapA<sup>R99A</sup>, VapA<sup>K108A</sup>, VapA<sup>R136A</sup>, and VapA<sup>K139A</sup>. These mutants were each shown via immunoblot to express in *S. cerevisiae* (data not shown).

### Mutation within the conserved domain mars PA binding affinity and localization of VapA in yeast

Wild-type VapA binds PA strongly in artificial liposomes in a concentration dependent manner [449]. To determine if residue mutations in either the conserved or disordered domain of VapA altered the binding capacity of VapA to bind PA, liposomes consisting of 20% PA/80% PC (phosphatidylcholine) or 100% PC were incubated with wild-type VapA, VapA.Full, VapA.Conserved, and VapA.Disordered and examined by refloatation for interaction with PA (Figure 4.1). As expected, no construct of VapA bound 100% PC liposomes (Figure 4.1B). Interestingly, VapA.Full and VapA.Conserved mutated proteins failed to bind PA while wild-type and VapA.Disordered did bind PA (Figure 4.1A), suggesting that the PA binding domain of VapA is located within the conserved domain of the protein.

The ability of VapA to localize to the plasma membrane was also examined using GFP-VapA and its mutant derivatives. Wild-type VapA and VapA.Disordered localized to the plasma membrane as previously shown [449] (Figure 4.1C) and when quantified (Figure 4.1D) reveal that >90% of cells show

VapA or VapA.Disordered at the plasma membrane of the yeast cell. Expression of VapA.Conserved or VapA.Full resulted in a predominantly cytoplasmic distribution without clear localization to the plasma membrane in <25% of cells for VapA.Conserved and nearly no cells for VapA.Full (Figure 4.1C,D). These data confirm that mutations in the conserved domain of VapA abrogate the binding capacity of VapA to PA and suggest that the conserved domain of VapA is the PA-binding domain of VapA.

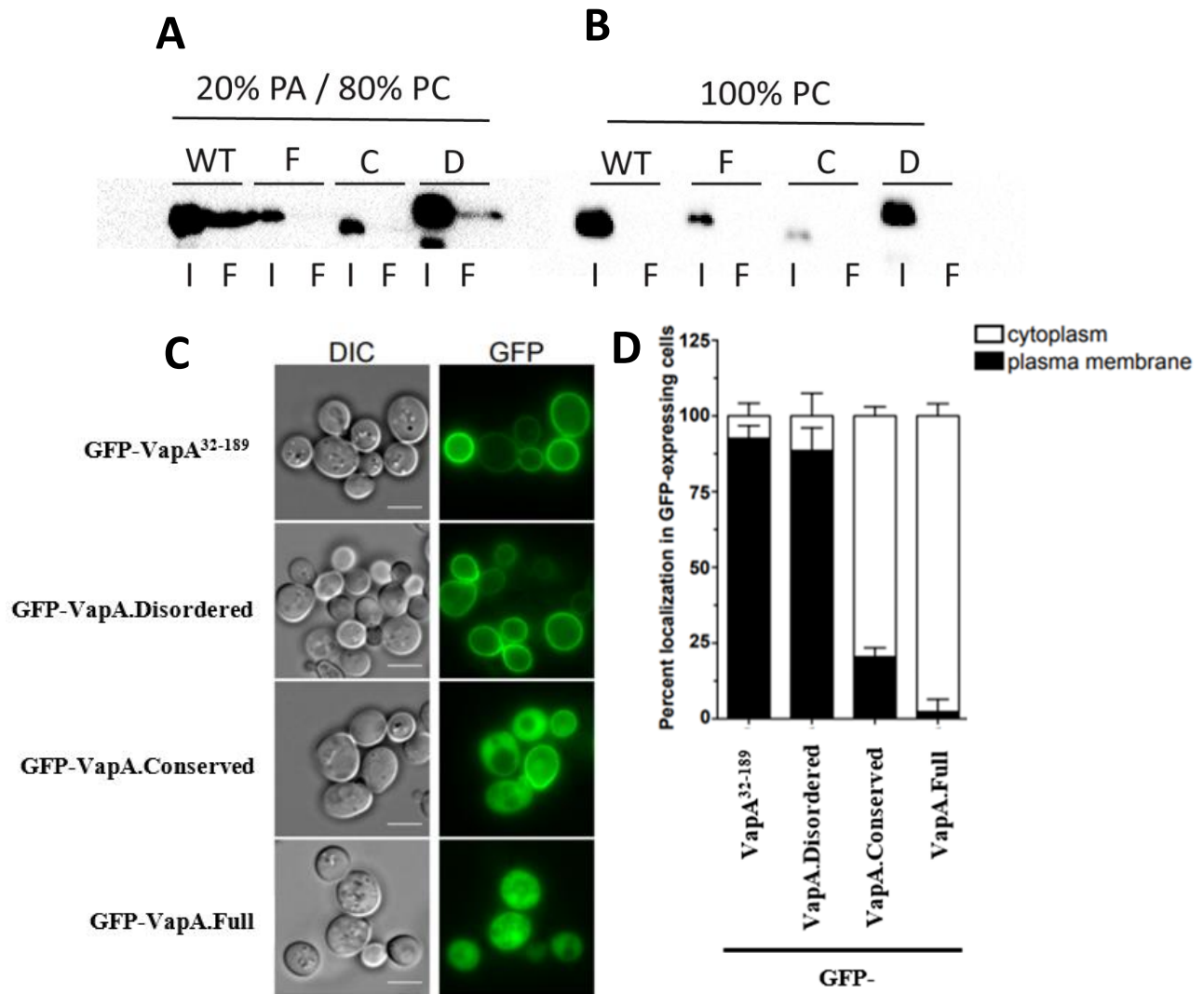


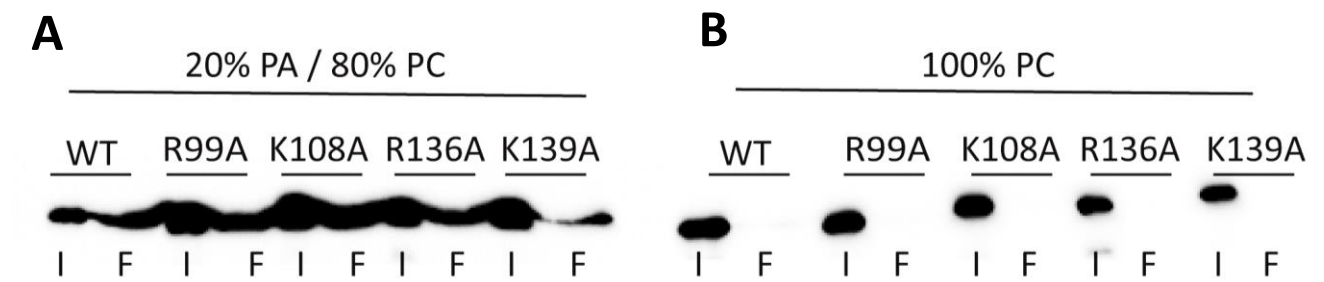
**Figure 4.1** The arginine and lysine residues in the conserved domain of VapA are necessary to bind PA and localize to the yeast plasma membrane. **A**) Wild-type VapA (WT), VapA.Full (F), VapA.Conserved (C), and VapA.Disordered (D) were reloaded with liposomes containing 20% PA or **B**) all PC after removal of 1% input of the reaction (I=input) as a control. The floated supernatant (F) was harvested and quantified via fluorescence, equal concentrations were loaded to the gel for each sample and

immunoblotted for VapA. Only wild-type VapA and VapA.Disordered were detectable in the floatation samples. No derivative of VapA bound PC upon floatation. **C)** GFP-VapA and its derivatives were expressed in *S. cerevisiae* to determine localization, if any, and **D)** quantified (100 cells were counted per sample per replicate, averaged over 3 replicates). VapA wild-type and VapA.Disordered are present at the plasma membrane of yeast while both VapA.Conserved and .Full fail to localize and are cytosolic. Scale bar=5 $\mu$ .

**Single mutations within the conserved domain do not strongly alter the binding of VapA to PA.**

VapA derivatives with single mutations within the conserved domain were similarly tested for PA binding capacity in refloatation assays with 20% PA/80% PC and 100% PC liposomes. All single mutants of VapA maintained PA binding identical with wild-type VapA, except for K139A mutant which still binds PA however qualitatively less compared to wild-type VapA (Figure 4.2A). This suggests that multiple residues or a motif is required for VapA to bind PA and therefore individual mutations fail to abrogate PA binding affinity. No derivatives of VapA bound PC, as expected (Figure 4.2B).

GFP-VapA single mutant derivatives were expressed in yeast to determine if a single mutation could alter the localization of VapA to the plasma membrane as described previously. Interestingly, one of the VapA mutants, R99A, does not localize to the plasma membrane and mimics the percent cytosolic distribution of VapA.Conserved (Figure 4.2C, D), perhaps revealing that this residue is of particular importance for its localization at the plasma membrane though it can still bind PA as shown by its refloatation with PA. All other single mutants of VapA mimicked wild-type VapA localization both qualitatively and quantitatively (Figure 4.2C, D).



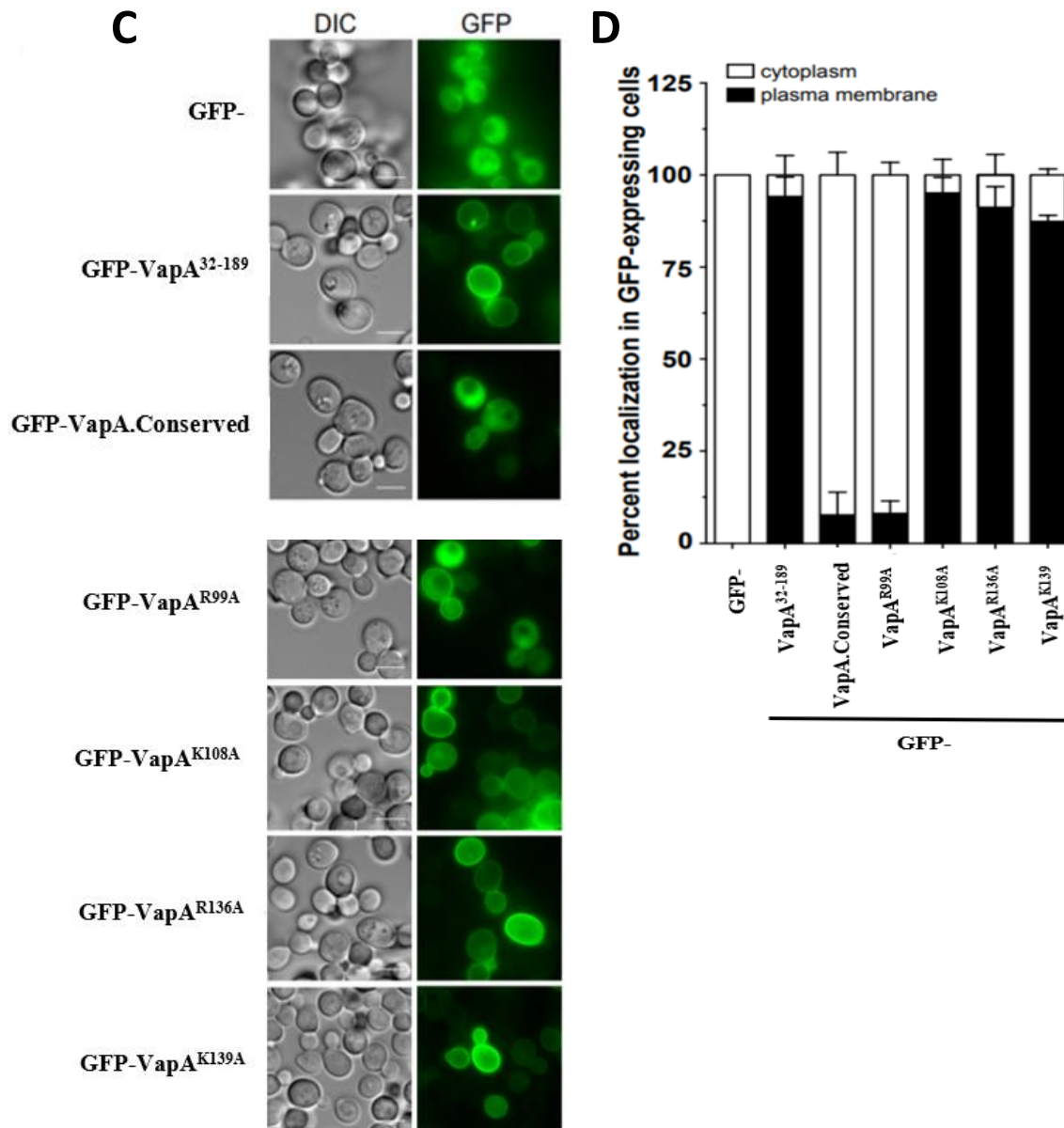


**Figure 4.2. Residue K139 aids in binding PA while R99 is necessary for plasma membrane localization in yeast. A)** Wild-type VapA (WT) and single mutant derivatives were reloaded with liposomes containing 20% PA or **B)** all PC after removal of 1% input of the reaction (I=input) as a control. The floated supernatant (F) was harvested and quantified via fluorescence, equal concentrations were loaded to the gel for each sample and immunoblotted for VapA. Each derivative of VapA bind PA though the single mutant VapA<sup>K139A</sup> is qualitatively diminished in comparison to wild-type VapA. No VapA derivative bound the control PC liposomes. **C)** GFP-VapA and its derivatives were expressed *in S. cerevisiae* to evaluate the localization ability of single mutants and cell localization was **D)** quantified (100 cells were counted per sample per replicate, averaged over 3 replicates). Only VapA<sup>R99A</sup> was incapable of localizing the yeast plasma membrane. Scale bar=5 $\mu$ .

### VapA binds PA containing membranes in a curvature dependent manner.

Because VapA is a surface protein that is present at the plasma membrane in yeast and the phagosomal membrane of macrophages, the ability of VapA to bind membranes of different curvatures was investigated. The plasma membrane, as a large membrane bilayer, is considerably less curved than intracellular vesicles, which are small and highly curved. Liposomes of different sizes were constructed to determine if the curvature of the membrane plays a role in the ability of VapA to recognize and bind PA. Liposomes containing 20% PA/ 80% PC 1 $\mu$ m, 0.4 $\mu$ m, 0.1 $\mu$ m (data not shown), and 0.05 $\mu$ m in size were constructed and incubated with wild-type VapA in refloatation assays. VapA bound membranes in a curvature dependent manner, where larger liposomes of 1 $\mu$ m qualitatively bound more VapA than smaller membranes with a drop in observed binding occurring in liposomes smaller than 0.4 $\mu$ m (Figure 4.3). This shows that VapA not only preferentially binds PA enriched membranes but less curved PA enriched membranes that are associated with the surface of the macrophage or yeast cell.

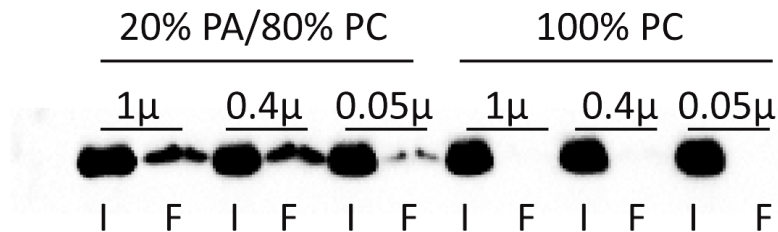


**Figure. 4.3. VapA binds larger, less curved membranes.** Wild-type VapA was incubated with liposomes containing 20% PA or PC generated at 1 $\mu$ m, 0.4 $\mu$ m, and 0.05 $\mu$ m in size. 1% input was removed (I=input) prior to refloatation on a Histodenz gradient. Floated supernatant (F) was harvested, quantified by fluorescence, and equal concentrations were run on a gel and immunoblotted for VapA. Qualitatively less VapA is bound to smaller liposomes, no VapA bound PC liposomes.

### Discussion

Charged residues within the conserved domain of VapA are necessary for VapA to bind PA as seen through the mutation of just four residues within the conserved domain. Importantly, the arginine 99 residue fails to localize as wild-type VapA to the yeast plasma membrane suggesting this residue

alone can play a role targeting the protein to large membranes with minimal curvature. Arginine 99 however still binds PA in refloatation assays, suggesting that this residue alone is not responsible for the interaction between VapA and PA but may rather be one of several residues that compose a binding motif necessary for interacting with PA. Mutation to the only other arginine, arginine 136, within the conserved domain did not alter localization of VapA to the yeast plasma membrane which shows that arginine 99 is unique and involved in either proper trafficking to the membrane by yeast trafficking machinery or for binding PA in conjunction with other charged residues as part of a PA binding motif. Mutation in the lysine 139 residue resulted in diminished, but not abolished, binding to PA via refloatation, providing evidence that VapA binds PA through interactions with several residues rather than one. Mutation in the disordered domain altered neither the localization of VapA to the yeast plasma membrane nor its capacity to bind PA, providing evidence of that the conserved domain of VapA is necessary for both such features of its activity.

The conserved domain of VapA is 87% identical to that of VapB, the homologous protein present in *R. equi* isolated from swine. Despite its similarity, VapB when expressed in yeast predominantly is distributed through the cytoplasm with only minimal localization to the plasma membrane and it does not strongly bind PA upon refloatation with 20% PA containing liposomes [449]. Of the notable differences between conserved domains of VapA and VapB proteins, residue 99 of VapB is a lysine rather than an arginine while residue 108 is methionine rather than lysine in VapA. Though both residues in the 99<sup>th</sup> position are charged, the inability of VapB to bind and localize as VapA provides further evidence that arginine 99 may be pivotal for VapA to appropriately bind eukaryotic membranes. Future studies will aim to substitute arginine 99 of VapA with lysine and/or 108 with a methionine to determine if residue charge alone or the residue itself at these positions can alter Vap protein localization in yeast.

VapA binds PA containing membranes in a curvature dependent manner. VapA is a surface protein that interacts with PA-rich alveolar macrophage derived plasma membranes that are much larger in size than that of the liposomes used in this study (human alveolar macrophage size  $\sim 21\mu$  and yeast cell size  $\sim 5\mu$  in diameter) [452] and therefore in the context of its host and replicative niche, membrane curvature is likely an important aspect for the activity of VapA. It is known that VapA is necessary for the development of the RCV and can cause endosomal swelling [72]; perhaps VapA initially uses membrane curvature and charged lipids, such as PA, to target and modulate the phagosomal membrane in such a way that induces swelling of the compartment to allow for replication. Further analyses of membrane curvature will include the use of additional membrane sizes to determine if VapA fails to bind PA containing liposomes at a certain size or binds more PA liposomes at larger sizes.

Though it is known VapA binds PA, many aspects of the activity of VapA and its function in the arrest of phagosome maturation remain unknown. Further studies using macrophages to observe the ability of *R. equi* expressing VapA and mutant derivatives to survive intracellularly are necessary and will provide in vivo evidence of potential intracellular replication or localization defects resulting from either regional or single mutations. Such analyses in macrophages can provide significant information regarding the invasion of *R. equi* and function of VapA in invasion and arrest of endosome maturation. Additionally, generating multiple mutations of charged residues within the conserved domain that are stably folded proteins, rather than just single mutations, can elucidate the residues of VapA that are necessary for PA binding and possibly the identity of a PA-binding motif.

## **Materials and Methods**

### **Liposome production**

16:0-18:1 phospholipids (Avanti Polar Lipids) were dissolved in chloroform and mixed in glass tubes to provide a final amount of 2  $\mu$ mol total lipid. For quantitation, 0.5% (mol/mol) rhodamine-phosphatidylethanolamine (Rh-PE) was added to all mixtures. Lipid mixtures were composed of 1-

palmitoyl-2-oleoyl-*sn*-glycero-3-phosphocholine (POPC) entirely or 80% POPC with 20% 1-palmitoyl-2-oleoyl-*sn*-glycero-3-phosphate (POPA) added. Chloroform was removed via a stream of argon gas. Dried lipids were suspended in 1 ml buffer containing 50 mM 2-ethanesulfonic (MES) and 3-(*N*-morpholino) propanesulfonic (MOPS) acid pH 5.5, 10% (v/v) glycerol, and 150 mM NaCl. The suspended lipids were placed in a 37°C water bath and intermittently vortexed for 60 min. After 10 freeze-thaw cycles in liquid nitrogen, suspended lipids were passaged 11 times through a Mini-Extruder (Avanti Polar Lipids) fitted with a 1µm, 0.4µm, or 0.05µm polycarbonate membrane, which had been previously equilibrated on a heating block set to 37 °C.

Liposome quantification was determined with a Rh-PE standard curve in RB150 (50mM MES pH 5.5, 150 mM NaCl, 10% (v/v) glycerol) containing 1% (v/v) Thesit; liposomes were serially diluted in this same buffer. Fluorescence of the suspensions was determined by loading 20 µl each suspension into a 384-well, low-volume, black microplate (Corning) and a computer-controlled multimode plate reader ( $\lambda_{\text{ex}} = 540 \text{ nm}$ ,  $\lambda_{\text{em}} = 585 \text{ nm}$ ; BioTek). Liposomes were stored at 4°C until the time of assay.

### **Liposome floatation**

50 µl reactions containing 500 µM total lipids and 1 µg of recombinant protein of interest were incubated for 1 hr in a 37°C water bath. Afterwards, 5 µl of the reaction was collected as an input control before adding 50µl of 80% filter-sterilized Histodenz (Sigma Aldrich) in RB150 pH 5.5 buffer. This mixture was inverted and placed into a 7 X 20 mm polycarbonate centrifuge tube (Beckman Coulter). Samples were then overlaid with 75µl of filter sterilized 30% Histodenz in RB150 and 75µl of RB150 media. Samples were centrifuged (96,000 x *g* for 2 hours at 4°C) before collecting 40µl of the floated liposomes. To analyze the samples, the harvested liposome concentrations were determined via Rh-PE fluorescence using the standard curve as previously described and equivalent amounts of liposomes were separated via SDS-PAGE and immunoblotted for VapA.

## Microscopy

BY4742 *MAT $\alpha$*  *his3 $\Delta$ 1 leu2 $\Delta$ 0 lys2 $\Delta$ 0 ura3 $\Delta$ 0* expressing pGO36-GFP-VapA or its derivatives were grown overnight in CSM-uracil. 1mL of culture was washed and resuspended in fresh CSM-uracil. 5 $\mu$ L were mounted to slides coated with a mixture of concanavalin A and poly-lysine at 1:1 ratio. Cells were visualized via fluorescence microscope (Nikon Eclipse Ti-u).

## CHAPTER 5

### THE *VIBRIO* EFFECTOR PROTEIN, VOPQ, INHIBITS FUSION OF V-ATPase CONTAINING MEMBRANES

Sreelatha A, Bennett TL, Carpinone EM, O'Brien KM, Jordan KD, Burdette DL, Orth K, Starai VJ. The *Vibrio* effector protein, VopQ, inhibits fusion of V-ATPase containing membrane. Proc Nat Acad Sci USA. 2015. Reprinted here with permission of the publisher.

## Abstract

Vesicle fusion governs many important biological processes, and imbalances in the regulation of membrane fusion can lead to a variety of diseases such as diabetes and neurological disorders. Herein, we show that the *Vibrio parahaemolyticus* effector protein, VopQ, is a potent inhibitor of membrane fusion based on an *in vitro* yeast vacuole fusion model. Previously, we demonstrated that VopQ binds to the  $V_o$  domain of the conserved V-ATPase found on acidic compartments such as the yeast vacuole. VopQ forms a nonspecific, voltage gated membrane channel of 18 angstroms resulting in neutralization of these compartments. We now present data that shows that VopQ inhibits yeast vacuole fusion. Furthermore, we identified a unique mutation in VopQ that delineates its two functions, deacidification and inhibition of membrane fusion. The use of VopQ as a membrane fusion inhibitor in this manner now provides new and convincing evidence that vacuole fusion occurs independently of luminal acidification *in vitro*.

## Significance Statement

Fusion of intracellular membranes is involved in many critical cellular processes, such as neurotransmission, protein trafficking, and in the lysosomal degradation of invading bacterial pathogens. Accordingly, some intracellular bacterial pathogens use protein effectors to directly alter host membrane fusion as a survival mechanism. In this study, we show that the *Vibrio* secreted effector, VopQ, is a potent inhibitor of yeast homotypic vacuole fusion *in vitro*. While VopQ was shown to deacidify yeast vacuoles via its known V-ATPase-binding and channel-forming activities, its ability to inhibit vacuole fusion does not depend on channel-forming activity. Our studies suggest that yeast vacuole fusion is not regulated by luminal acidification, and identify a new reagent to study the V-ATPase role in some membrane fusion events.

## Introduction

Vesicle fusion governs many important physiological processes including neurotransmitter release and exocytosis. As such, many studies have focused on understanding this process and the proteins involved in fusion using various models such as yeast vacuoles and *Drosophila* synaptic vesicles [233, 453]. Yeast vacuoles are an established and elegant model to study eukaryotic membrane fusion, due to the ease of their isolation and the conserved nature of the fusion machinery required for their homotypic fusion [454]. While the core SNARE and Rab GTPase fusion machinery alone can drive the physiologically-relevant fusion of liposomes *in vitro* [233], genetic and biochemical experiments have identified a number of additional regulators of vacuole fusion, including the membrane sector of the highly conserved V-type H<sup>+</sup>-ATPase (V-ATPase) [455, 456].

The eukaryotic V-ATPase is the main electrogenic proton pump involved in the acidification of many intracellular organelles such as endosomes, lysosomes, and the yeast vacuole [305]. The V-ATPase consists of two conserved, multi-subunit domains: the cytoplasmic V<sub>1</sub> domain and the membrane bound V<sub>o</sub> domain. The V<sub>1</sub> domain hydrolyzes ATP, providing the energy for proton translocation through the membrane-bound V<sub>o</sub> proteolipid proton channel, thus acidifying the lumen of the vesicle. The loss of V-ATPase subunits is lethal in higher eukaryotes, highlighting the importance of this vital protein complex for normal eukaryotic physiology. However, yeast that lack subunits of the V-ATPase exhibit conditional lethality that is rescued by growth on acidic media, thus providing a unique and powerful system for the study of V-ATPase functions *in vivo*. Besides its acidification function, the V-ATPase has been implicated in a broad range of biological processes, including the proper trafficking of secreted and endocytosed cargos [457], viral fusion [458], exocytosis [453, 459, 460], and the SNARE-dependent membrane fusion of yeast vacuoles [455, 456, 461, 462]. Even though the role of V-ATPase in fusion has been demonstrated in various model organisms, its role in this process remains controversial [349, 455, 463-465].

Recent work has shown that a bacterial protein, VopQ (also VP1680 or VepA), forms an outward rectifying, gated channel in membranes that contain the V-ATPase, resulting in the collapse of ion gradients and the disruption of autophagic flux [125]. VopQ is a Type III effector protein from the marine bacterium *Vibrio parahaemolyticus* that strongly associates with the  $V_o$  domain of the eukaryotic V-ATPase [125, 466]. Given the proposed role of the  $V_o$  domain in fusion, we sought to examine the effect of VopQ on fusion using the well-defined biochemical model of eukaryotic membrane fusion from the budding yeast *S. cerevisiae*. In this study, we demonstrate that expression of VopQ causes extensive yeast vacuolar fragmentation, indicative of a defect in homotypic vacuole fusion. *In vitro* vacuole fusion assays confirmed VopQ is a potent inhibitor of a conserved Rab GTPase and SNARE-dependent membrane fusion. Furthermore, we identify a mutant of VopQ, VopQ<sup>S200P</sup> that deacidifies the vacuole via its known channel-forming activity, but no longer inhibits vacuole fusion *in vitro* due to its reduced affinity for the V-ATPase  $V_o$  domain. Therefore, by using a novel bacterial effector protein with yeast vacuoles containing wild type V-ATPase machinery, we show that yeast vacuole fusion does not require luminal acidification *in vitro*.

## Results

### VopQ inhibits yeast homotypic vacuole fusion

VopQ directly interacts with the  $V_o$  domain of the V-ATPase on the yeast vacuole. To assess whether this interaction alters vacuole morphology *in vivo*, we stained and visualized the vacuolar membrane of VopQ-expressing yeast. Normally, yeast cells contain 1-3 large vacuoles (Figure 5.1A, *WT*). The Vps33p protein, a component of the endosomal (CORVET) and vacuolar (HOPS) membrane tethering complexes, is required for normal vacuolar morphology and fusion [196]. Yeast strains lacking Vps33p display highly fragmented vacuoles typical of strains with defects in homotypic vacuole fusion (Figure 5.1A, *vps33Δ*). When VopQ was expressed in yeast under a galactose-inducible promoter, yeast

are viable (Figure 5.1B) but have fragmented vacuoles similar to that seen in *vps33Δ* strains (Figure 5.1A, *VopQ*<sup>+</sup>). Therefore, *VopQ* appears to modulate vacuolar membrane dynamics *in vivo*.

To assay whether this fragmentation is mediated through inhibition of the known yeast vacuole fusion machinery, we measured the effect of *VopQ* on a purified, well-studied homotypic vacuole fusion system. As this system is known to be sensitive to a full complement of Rab GTPase, SNARE, and lipid-directed reagents, observations made in the context of this system are often found to be conserved in lysosomal fusion events in higher organisms [233]. Yeast vacuoles were isolated from two strains of yeast: one lacking *Pho8p*, the normal vacuolar alkaline phosphatase (ALP), and one lacking *Pep4p*, required for the activation of the luminal vacuolar protease (*Prb1p*) responsible for activating *Pho8p in vivo*. While neither of these purified vacuoles has alkaline phosphatase activity alone, upon successful fusion, active proteases gain access to the catalytically inactive *Pho8p*, thereby activating *Pho8p* phosphatase activity to be measured colorimetrically [467]. Recombinant *VopQ* protein was a powerful inhibitor of vacuole fusion in a dose-dependent manner (Figure 5.2A, closed squares), on par with standard inhibitors of the fusion reaction including antisera against the *Sec17p* ( $\alpha$ -SNAP) SNARE chaperone and the *Vam3p* syntaxin [468]. Therefore, *VopQ* is capable of directly inhibiting homotypic vacuole fusion *in vitro*.

Since *VopQ* is known to form channels in the vacuolar membrane, we wanted to confirm that *VopQ* does not disrupt the vacuolar membrane during fusion. We routinely include the ~8 kDa inhibitor of *Prb1p*, *Pbi2p*, in these assays to prevent aberrant pro*Pho8p* activation; *Pbi2p* access to the vacuole lumen would be measured as fusion inhibition. ALP reactions performed in the absence of *Pbi2p* continue to display potent *VopQ*-dependent fusion inhibition (Figure 5.3A), and vacuoles treated with *VopQ* do not release additional luminal GFP during fusion, unlike reactions treated with the soluble *Vam7p* SNARE and HOPS tethering complex (Figure 5.3B), a condition known to disrupt the integrity of yeast vacuoles [469]. Therefore, *VopQ* does not disrupt vacuolar integrity during fusion.

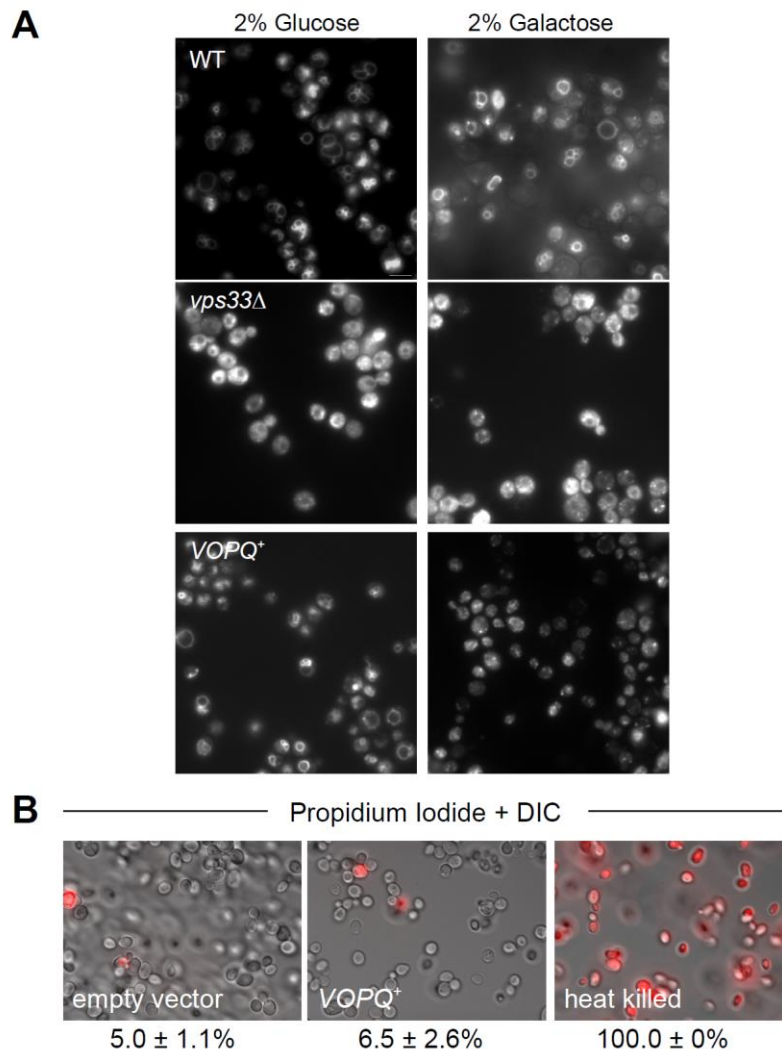


**Figure 5.1. VopQ induces vacuole fragmentation (A)** BY4742 yeast strains harboring the galactose-inducible vector pRS413-Gal1 (WT), pRS413-Gal1-*VOPQ* (*VopQ*<sup>+</sup>), or with deletions in *VPS33* (*vps33Δ*) were visualized via FM4-64 staining [389]. Images are larger fields of those presented in Figure 1A. Bar = 10 μ (B) Prior to FM4-64 staining of the galactose-grown cells, aliquots of BY4742 harboring either pRS413-Gal1 or pRS413-Gal1-*VOPQ* were assayed for cell wall integrity. A small sample of the WT cells were incubated at 100°C for 10 min for a heat killed control. Cells were stained with 25 μM propidium iodide for 30 min at 30 °C then washed, and visualized. At least 200 cells from each sample were scored for propidium iodide retention; representative micrographs for each condition are shown. Mean percentage of cells displaying fluorescence is denoted (*n*=3).

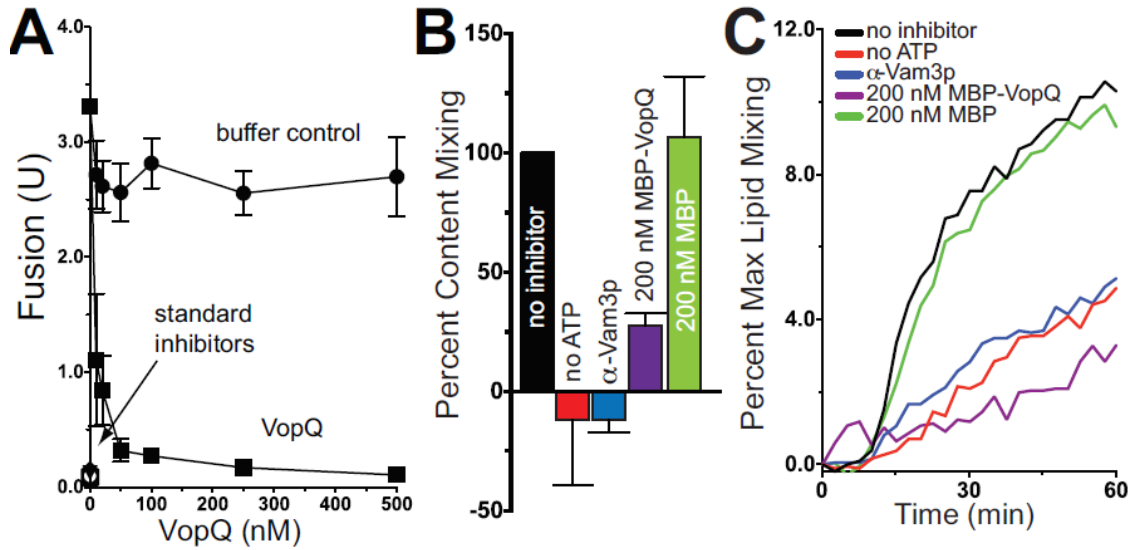


**Figure 5.2. VopQ inhibits yeast homotypic vacuole fusion.** (A) Alkaline phosphatase (ALP) vacuole fusion reactions in the absence or presence of increasing concentrations of recombinant His<sub>6</sub>-VopQ. Standard fusion inhibitors:  $\alpha$ -Vam3p,  $\alpha$ -Sec17p, 1  $\mu$ M Gdi1p and Gyp1-46, or ice incubation. Error is SD from mean,  $n = 4$ . (B)  $\beta$ -lactamase content mixing assay was performed in parallel with (C) Rh-PE dequenching lipid mixing assay in the absence of ATP or including  $\alpha$ -Vam3p, MBP-VopQ or MBP. Content mixing is SD from mean,  $n = 3$ . Rh-PE dequenching plot is a representative curve measured from the same three experiments used for content mixing.

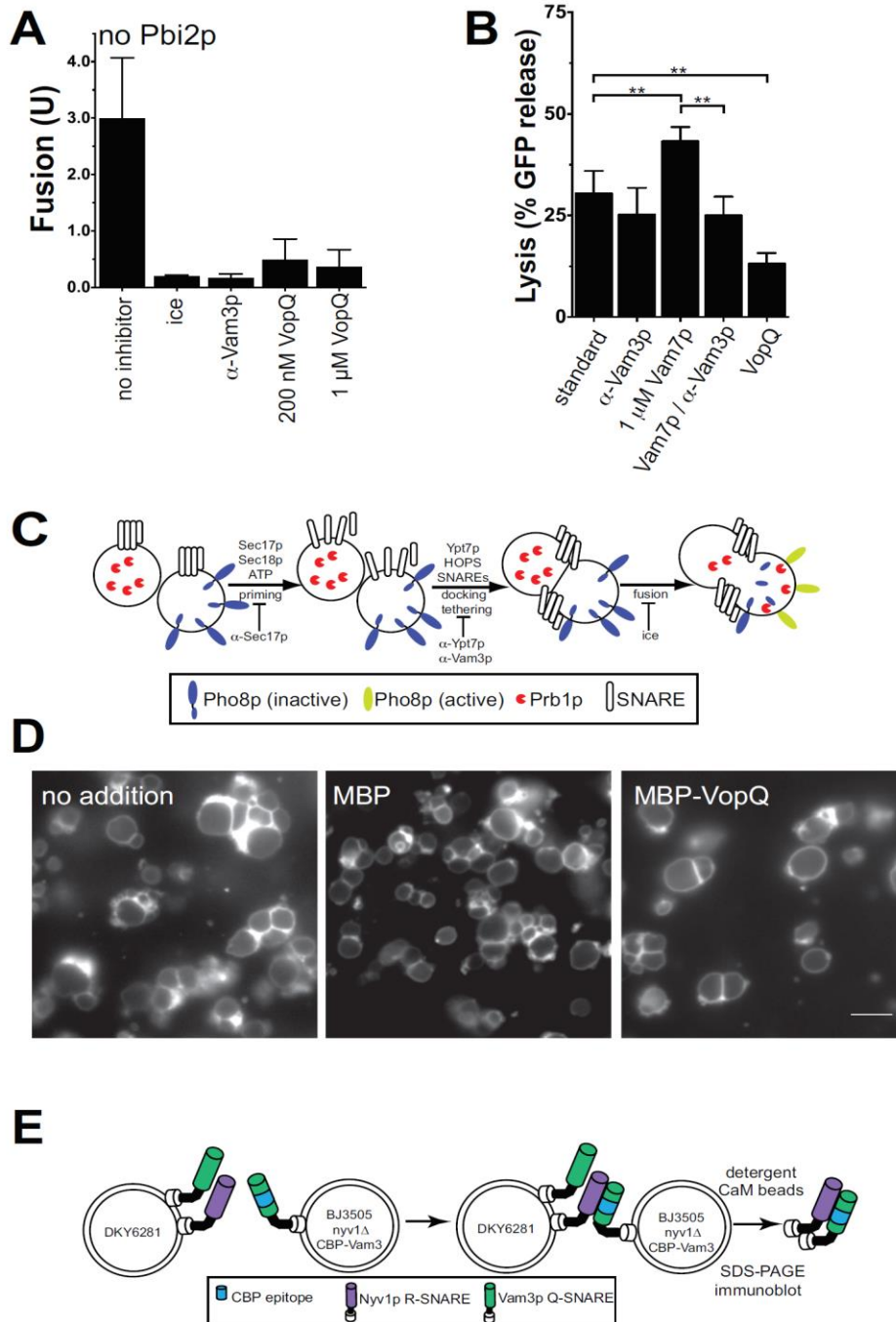


**Figure 5.3. VopQ does not disrupt vacuolar integrity.** (A) Standard Pho8p-dependent vacuole fusion reactions were performed in the absence of the protease inhibitor Pbi2p. (B) Luminal GFP release (lysis) was measured for GFP containing vacuoles either untreated (standard) or treated with  $\alpha$ -Vam3p, Vam7p, or 200 nM MBP-VopQ;  $n = 3$ . 1-way ANOVA Repeated Measures Test and Tukey's Multiple Comparison Post-test; (\*\*) =  $0.001 < p < 0.01$ . (C) Ordered model of vacuole priming, docking and fusion. Known inhibitors of each stage are listed below the arrows. (D) Representative vacuole morphologies observed with FM4-64 staining during the 'docking' of yeast vacuoles in the absence or presence of 500 nM MBP or 500 nM MBP-VopQ. Bar = 5  $\mu$ . (E) Model of trans-SNARE assay using CBP-Vam3p:Nyv1p pull-down.

### **VopQ inhibits vacuole content mixing**

The proteolytic processing and activation of the alkaline phosphatase can be used as a measure for successful yeast vacuolar fusion. However, luminal proteases that cleave the phosphatase require an acidic environment for proper trafficking and optimal activity *in vitro* [470]. Previous work with the purified homotypic vacuole fusion system has shown that V-ATPase inhibitors that inhibit acidification of the vacuole, such as bafilomycin, also inhibit *in vitro* vacuolar fusion reaction as measured by ALP activity; therefore vacuolar acidification appears to be required for homotypic fusion [471]. Because VopQ deacidifies yeast vacuoles and our readout for fusion may be sensitive to luminal pH, we chose to revisit VopQ's ability to inhibit membrane fusion with assays that do not depend acidification.

Yeast homotypic vacuole fusion can be measured by reconstituting the activity of a soluble, vacuole lumen-directed bifurcated enzyme,  $\beta$ -lactamase [472]. When vacuolar contents are mixed as a result of fusion, the domains of  $\beta$ -lactamase are brought together by interacting leucine zipper domains of the c-Jun and c-Fos proteins resulting in an active  $\beta$ -lactamase enzyme that can be assayed via its hydrolytic activity [472]. Fusion observed in the absence of inhibitors is used to standardize the effects of each biochemical inhibitor of the reaction (Figure 5.2B). Vacuolar fusion is strongly inhibited in the presence of fusion inhibitors (no ATP,  $\alpha$ -Vam3p; Figure 5.2B). Addition of MBP-VopQ protein, but not MBP alone, inhibited vacuolar fusion, demonstrating that VopQ still inhibits homotypic vacuole fusion in an acidification-independent manner using an alternative ALP-independent fusion assay.

### **VopQ inhibits lipid mixing**

We next measured the ability of VopQ to inhibit lipid bilayer mixing during *in vitro* vacuole fusion. Purified vacuolar membranes containing the components for the  $\beta$ -lactamase reconstitution fusion assay can be labeled with Rhodamine-PE and fused to unlabeled vacuoles to measure lipid bilayer mixing via fluorescence dequenching [473] and content mixing via nitrocefin hydrolysis (Figure 5.2B & C). Fusion inhibitors prevent both content and lipid mixing (Figure 5.2B & C, red and blue, respectively).

MBP-VopQ, but not MBP, inhibited both content and lipid mixing (Figure 5.2B & C, purple and green respectively). Coupled with its ability to inhibit Pho8p activation,  $\beta$ -lactamase reconstitution, and vacuolar lipid mixing, VopQ was validated as an authentic inhibitor of yeast vacuole fusion *in vitro* (Figure 5.2).

### **VopQ inhibits docking and trans-SNARE complex formation**

We next took advantage of the fact that fusion must occur in three biochemically-distinct stages: 1. Priming, where the SNARE chaperones Sec17p and Sec18p ( $\alpha$ -soluble NSF attachment protein ( $\alpha$ -SNAP) and N-ethylmaleimide sensitive fusion (NSF) protein, respectively) disassemble cis-SNARE complexes in an ATP-dependent manner [474]; 2. Docking, which requires the activities of the Rab-GTPase Ypt7p and a multi-subunit tethering complex called the HOPS (homotypic fusion and vacuole protein sorting) complex, to tether vacuoles and enable the formation of the essential trans-SNARE complexes composed of Vam3p, Vti1p, Vam7p, and Nyv1p across opposing membranes [468, 475, 476]; 3. Fusion, where trans-SNARE complexes catalyze the mixing of lipid bilayers, and luminal contents are exchanged [477, 478] (Figure 5.3C). Fusion can be analyzed using a kinetic assay designed to determine the step at which the vacuole fusion reaction becomes resistant to particular sub-reaction inhibitors [479]. The kinetic profiles for blocking the priming, docking, and fusion steps in vacuole fusion were exemplified by the addition of antibodies to Sec17p, Ypt7p and Vam3p, or ice respectively, over the course of the Pho8p-dependent fusion reaction. Addition of the priming inhibitor,  $\alpha$ -Sec17p, to the reaction after 20 minutes did not inhibit fusion, indicating that the priming step has been surpassed (Figure 5.4A, closed circles). Similarly, the addition of the docking inhibitors,  $\alpha$ -Ypt7p and  $\alpha$ -Vam3p, after 45 minutes did not inhibit fusion indicating the completion of docking by this time (Figure 5.4A, open diamond and black triangle, respectively). Placing reactions on ice inhibited the final stage of fusion, lipid mixing (Figure 5.4A, open squares). We find that vacuoles become resistant to VopQ inhibition (Figure 5.4A, closed squares) after resistance to the priming inhibitor  $\alpha$ -Sec17p, but before the final stage of

lipid and content exchange, as measured by incubation on ice. Vacuoles display kinetic resistance to VopQ similar to the docking/tethering inhibitors  $\alpha$ -Ypt7p and  $\alpha$ -Vam3p, suggesting that VopQ may inhibit vacuole docking and the formation of *trans*-SNARE complexes.

To further analyze the effect of VopQ on the Rab GTPase and SNARE-dependent tethering of yeast vacuoles, we employed a visual “docking” assay that measures the number of vacuoles in clusters [480]. Addition of MBP-VopQ or MBP does not disrupt the integrity of vacuoles (Figure 5.3D). Incubation with MBP results in clusters of 5 or more vacuoles approximately 30% of the time (Figure 5.4B, black bars). Fewer vacuoles were observed in clusters upon treatment with a combination of GDI and Gyp1-46, which causes the release of Ypt7p and inhibits docking (Figure 5.4B, white bars). Addition of MBP-VopQ closely mimicked GDI / Gyp1-46 activity (Figure 5.4B, gray bars), indicating that VopQ inhibits the docking of yeast vacuoles.

To test the effect of VopQ on *trans*-SNARE complex formation during fusion, we measured the extent of *trans*-SNARE complex formation using an epitope-tagged Vam3p SNARE (CBP-Vam3p) with its cognate vacuolar R-SNARE, Nyv1p (Figure 5.3E) [468]. Under normal fusion conditions, CBP-Vam3p and Nyv1p interact (Figure 5.4C, lane 5). This SNARE interaction was strongly disrupted by incubation on ice (Figure 5.4C, lane 6), and with GDI/Gyp1-46 (Figure 5.4C, lane 7). Addition of VopQ prevented the formation of *trans*-SNARE complexes (Figure 5.4C, lane 8), consistent with its distinct mechanism of vacuole fusion inhibition observed in the kinetic fusion assay (Figure 5.4A).

The kinetic assay along with the docking and *trans*-SNARE assay suggests that VopQ inhibits fusion downstream of priming but upstream of *trans*-SNARE complex formation. In an attempt to reverse VopQ inhibition by increasing *trans*-SNARE complex formation, we provided an excess of the soluble SNARE Vam7p and the HOPS tethering complex; these proteins are known to bypass inhibitors that prevent SNARE complex assembly [476, 481]. In the absence of HOPS and Vam7p, VopQ inhibits vacuole fusion similar to the addition of Vam3p antibody (Figure 5.4D). Upon addition of HOPS or Vam7

alone, only modest effects on VopQ inhibition are observed. However, upon addition of HOPS and Vam7p, VopQ mediated inhibition is reversed; this reversal remains sensitive to the fusion inhibitor  $\alpha$ -Vam3p. Taken together, these data suggest VopQ may hinder trans-SNARE complex assembly, thus inhibiting membrane fusion.

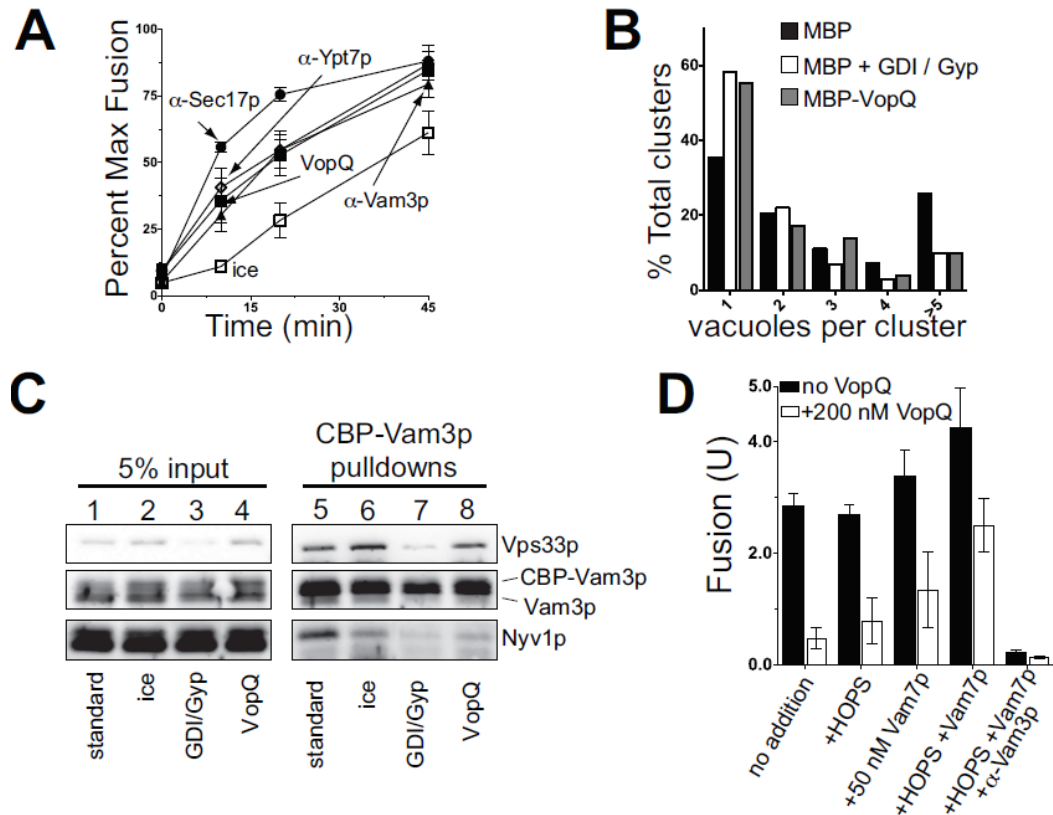


**Fig. 5.4. VopQ inhibits trans-SNARE complex formation. (A)** At 0, 10, 20 and 45 minute intervals, alkaline phosphatase vacuole fusion reaction was incubated on ice or one of the following fusion inhibitors was added:  $\alpha$ -Sec17p,  $\alpha$ -Ypt7p,  $\alpha$ -Vam3p or 200 nM VopQ. After 90 minutes, fusion was measured and compared with the fusion of an uninhibited fusion reaction. Error is SD from mean,  $n = 3$ . **(B)** Quantitative docking assay was performed in the presence of 500 nM MBP, 2.8  $\mu$ M Gdi1p and 11.4  $\mu$ M Gyp1-46, or 500 nM MBP-VopQ. At least 130 clusters were scored for each condition from 10 random fields. **(C)** Trans-SNARE assays were performed without or with the following inhibitors: ice incubation, 1  $\mu$ M Gdi1p / 1  $\mu$ M Gyp1-46, or 200 nM VopQ. **(D)** ALP vacuole fusion reactions were performed in the absence or presence of 200 nM MBP-VopQ. Recombinant 50 nM Vam7p SNARE, 20 nM HOPS complex, or  $\alpha$ -Vam3p was added where indicated.

### **Vacuolar acidification and electrochemical gradient is not required for fusion**

VopQ deacidifies the lumen of vacuoles through the rapid formation of an 18Å channel in the membrane after direct interactions with  $V_o$  subunits of the V-ATPase [125]. A recent publication by Coonrod et al shows that acidification of the yeast vacuole by the V-ATPase is absolutely required for vacuole fusion *in vivo* [349]. Therefore, we tested if VopQ inhibits fusion simply through the collapse of the vacuole pH gradient.

Previously, the specific V-ATPase inhibitor bafilomycin was shown to be an inhibitor of yeast vacuole fusion *in vitro* using the alkaline phosphatase assay [471]. We therefore compared VopQ and bafilomycin activities in ALP-dependent and -independent fusion assays and found that MBP-VopQ inhibited both the alkaline phosphatase (Figure 5.5A, black bars) and  $\beta$ -lactamase fusion assays (Figure 5.5A, white bars). In contrast, bafilomycin inhibited the alkaline phosphatase assay to approximately 60% of the maximal fusion level (Figure 5.5A, black bars), but had no effect on the activation of  $\beta$ -lactamase (Figure 5.5A, white bars). Therefore, in contrast to VopQ, bafilomycin does inhibit vacuole fusion based on the alkaline phosphatase assay, but does not inhibit vacuole fusion based on  $\beta$ -lactamase reconstitution.

The possibility remained that the lumen of the vacuole retained acidification due to V-ATPase activity prior to vacuole isolation, and this was sufficient for driving homotypic fusion *in vitro*. Furthermore, the V-ATPase generates an electrochemical gradient ( $\Delta\psi$ ) that could also be the driving force in vacuole fusion. To address the role of acidification and electrochemical gradient in yeast vacuole fusion, we used a pair of well-studied ionophores, valinomycin and nigericin, in combination with bafilomycin. Valinomycin is a neutral  $K^+$ -specific ionophore, which transports  $K^+$  across the membrane down the concentration gradient [482, 483], and nigericin is an electroneutral  $K^+/H^+$  antiporter [484]. In the presence of V-ATPase activity, valinomycin and nigericin together equilibrate  $H^+$  and  $K^+$  ions to collapse both the electrochemical and pH gradients of the vacuole (Figure 5.5B). Valinomycin and

nigericin, in combination with bafilomycin, will collapse any pre-existing electrochemical and pH gradient and inhibit any further V-ATPase-dependent translocation of H<sup>+</sup>.

First, we measured vacuole acidification by measuring the change in absorbance of acridine orange upon protonation [485]. Similar to the no inhibitor control,  $\alpha$ -Vam3p fusion inhibitor did not inhibit H<sup>+</sup> translocation (Figure 5.5C, black and blue curves). When added individually, bafilomycin and nigericin inhibited H<sup>+</sup> translocation (Figure 5.5C, orange and purple curves). Valinomycin did not completely inhibit proton translocation (pink curve), as expected for a K<sup>+</sup>-specific ionophore. However, valinomycin in combination with nigericin (green curve) inhibited luminal acidification. Likewise, no acidification was detected when a cocktail of all three inhibitors was added (brown curve). These results indicate that these inhibitors are capable of neutralizing the yeast vacuole.

Next, we measured vacuole fusion in the presence of these inhibitors to study the role of electrochemical and pH gradients in fusion. As expected, bafilomycin inhibited the alkaline phosphatase but not the  $\beta$ -lactamase fusion assay (Figure 5.5D). Combinations containing valinomycin and nigericin partially inhibit the alkaline phosphatase fusion assay (Figure 5.5D, black bars) but do not inhibit the  $\beta$ -lactamase fusion assay (white bars). Vacuole fusion detected in the presence of these inhibitors is authentic, SNARE-dependent fusion, as the addition of  $\alpha$ -Vam3p inhibited this fusion to baseline levels in both the alkaline phosphatase (Figure 5.6A) and  $\beta$ -lactamase (Figure 5.6B) assays. Therefore, vacuoles fuse normally in the absence of pH and electrochemical gradients *in vitro*. Furthermore, ALP-dependent fusion proceeds normally when KCl is completely replaced with the lysomotrophic, weakly basic NH<sub>4</sub>Cl [486] in the fusion reaction to neutralize the lumen of vacuoles (Figure 5.6C); vacuoles do not acidify in the presence of NH<sub>4</sub>Cl in contrast to KCl (Figure 5.6D,E).

To address the role of  $\Delta\psi$  in fusion, we measured the ability of the vacuole to quench the potential-sensitive dye, Oxonol V. Dye quenching occurs as Oxonol V changes its membrane association in response to an inside-positive electrochemical gradient [487]. In the absence of inhibitors, vacuoles

rapidly quench Oxonol V fluorescence (Figure 5.6F, black curve). Inhibiting V-ATPase activity eliminates most Oxonol V quenching (blue curve). Similar to bafilomycin, MBP-VopQ inhibits Oxonol V quenching (Figure 5.6G, purple curve), showing that VopQ can inhibit the formation of  $\Delta\psi$  during vacuole fusion. Finally, in a reconstituted proteoliposome fusion system that lacks the V-ATPase and depends solely on the activities of vacuolar SNAREs, the Rab GTPase Ypt7p, HOPS, and SNARE chaperones (Figure 5.7A) [488], VopQ is completely unable to inhibit both content (Figure 5.7B) and lipid (Figure 5.7C) mixing. These data support the proposal that VopQ requires the V-ATPase to bind to the vacuole and inhibit fusion, because we observe that VopQ does not directly inhibit the “core” SNARE/Rab GTPase/HOPS membrane fusion machinery.

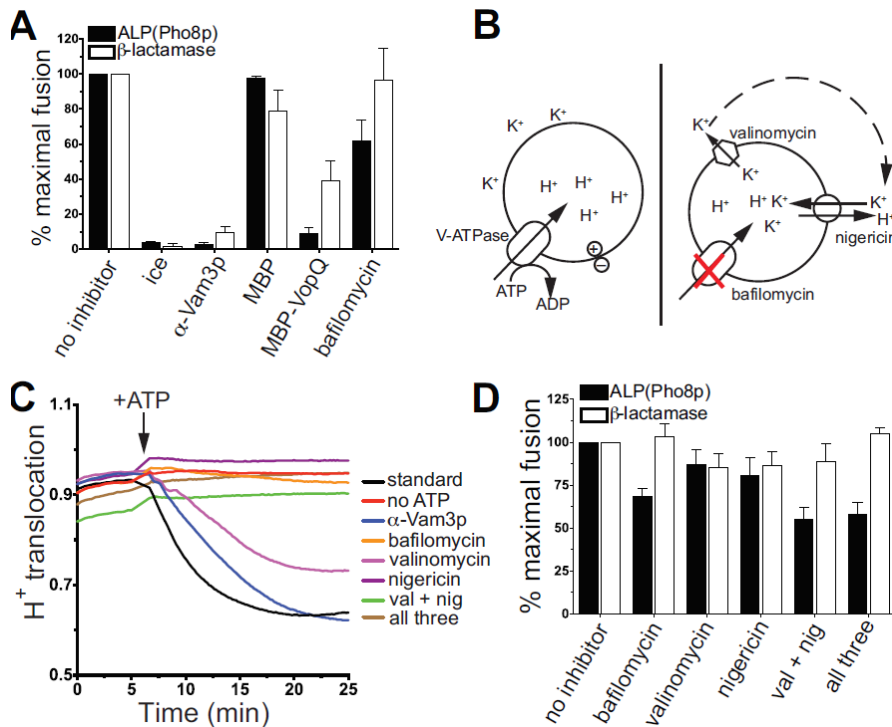


**Fig. 5.5. pH gradient is not required for vacuole fusion.** (A) ALP or  $\beta$ -lactamase fusion reactions were performed in parallel, using standard inhibitors or 200 nM MBP, 200 nM MBP-VopQ, or 500 nM bafilomycin. Maximal fusion was set to the extent of fusion of the “no inhibitor” reaction; error is SD from mean,  $n = 3$ . (B) Schematic diagram of the mechanism of action of the ionophores used. (C) Proton translocation activity of vacuoles was assayed in the absence or presence of ATP,  $\alpha$ -Vam3p, 500 nM bafilomycin, 1  $\mu$ M valinomycin, 1  $\mu$ M nigericin, or combinations of ionophores and bafilomycin. Curves are representative of three independent experiments. (D) ALP or  $\beta$ -lactamase fusion reactions were performed in parallel, using a combination of ionophores at concentrations used in (C). Maximal fusion was set to the “no inhibitor” reaction, error is SD from mean;  $n = 3$ .

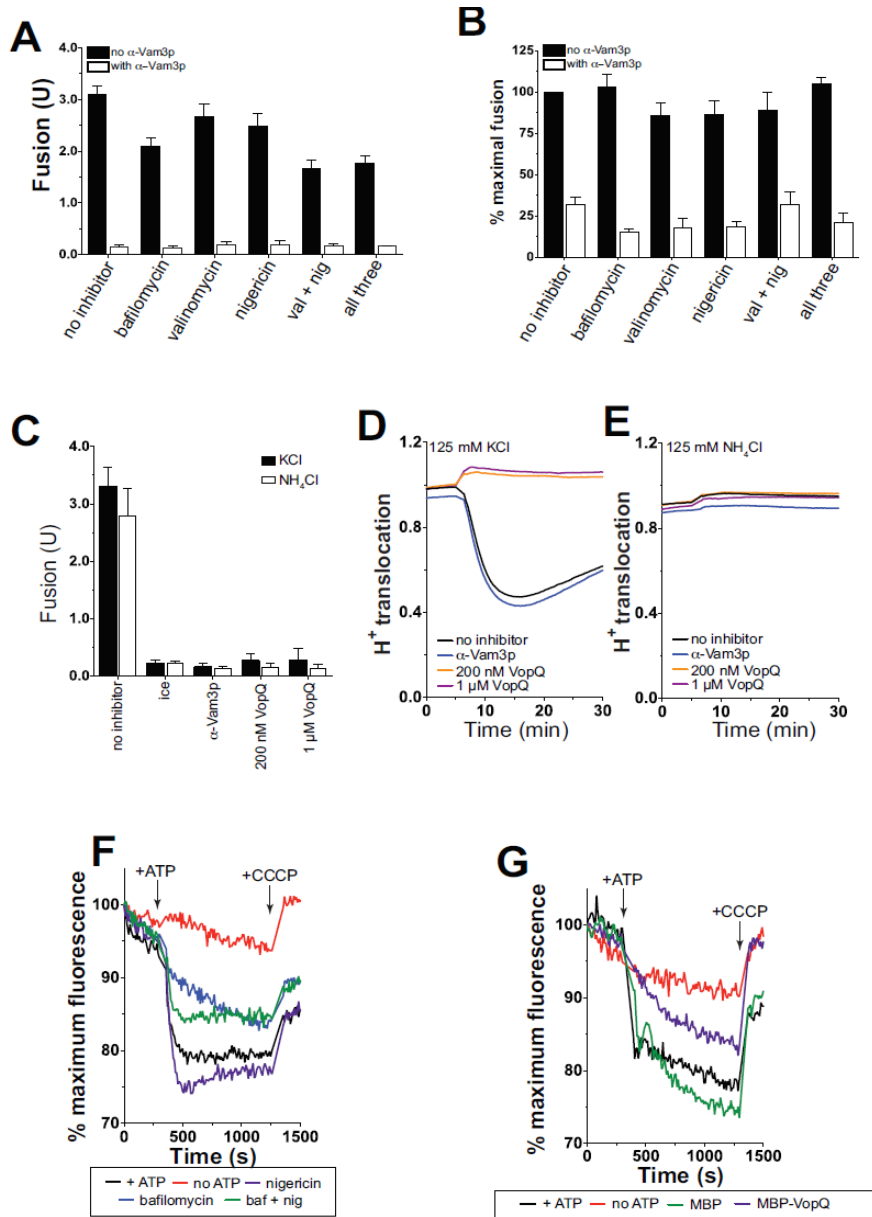


**Fig. 5.6. pH gradient is not required for vacuole fusion.** (A) Standard ALP dependent vacuole fusion reactions (black bars), were performed in the presence of 500 nM bafilomycin, 1  $\mu$ M valinomycin, 1  $\mu$ M nigericin, or combinations thereof. These reactions either lacked (black bars) or contained (white bars) 450 nM  $\alpha$ -Vam3p to inhibit trans-SNARE complex formation. Error is SD from mean,  $n = 3$ . (B)  $\beta$ -lactamase fusion assay under the same condition as Panel (A). Maximal fusion (100%) is defined as the “no inhibitor” reaction; error is SD from mean,  $n = 3$ . (C) ALP fusion reactions were performed with either 125 mM KCl or 125 mM NH<sub>4</sub>Cl, and assayed for VopQ sensitivity. Error is SD from mean;  $n = 3$ . (D) Proton translocation activity of vacuoles in the absence or presence of  $\alpha$ -Vam3p or MBP-VopQ was measured in 125 mM KCl or (E) 125 mM NH<sub>4</sub>Cl. Curves are representative of three independent experiments. (F) Vacuolar membrane potential in the presence of bafilomycin and nigericin was measured via Oxonol V fluorescence. Loss of fluorescence due to dye quenching is dependent on an inside-positive membrane potential. (G) Vacuolar membrane potential in the presence of 500 nM MBP or MBP-VopQ is measured using Oxonol V.

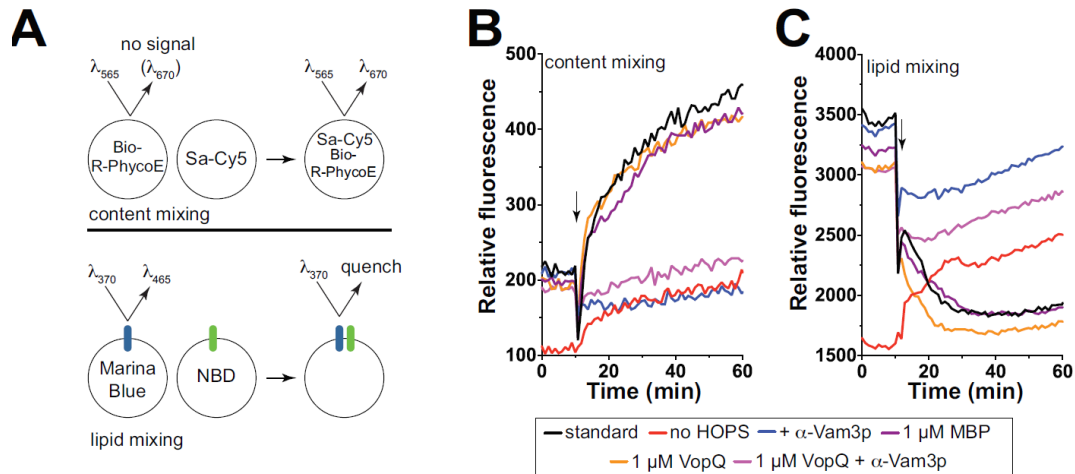


**Fig. 5.7. VopQ does not inhibit V-ATPase independent proteoliposome fusion. (A)** Content and lipid mixing scheme for SNARE and Rab-dependent liposome fusion detection. **(B)** Content and **(C)** lipid mixing of reconstituted SNARE/Ypt7p-containing proteoliposomes in the presence of MBP-VopQ.

### VopQ does not inhibit vacuole fusion via channel-forming activity

With the knowledge that VopQ binds  $V_o$  subunits, we sought to identify mutants of VopQ that were defective in V-ATPase binding to better characterize the mechanism by which VopQ inhibits vacuole fusion. VopQ expression arrests yeast cell growth, and this effect appears to be mediated through the interaction of VopQ with Vma3p; *vma3 $\Delta$*  strains are fully resistant to VopQ growth repression (Figure 5.8A) [125, 466]. Furthermore, VopQ-dependent vacuolar fragmentation *in vivo* was also completely dependent on the presence of Vma3p (Figure 5.8B). Therefore, we hypothesized that mutants of VopQ defective in V-ATPase binding would be less toxic upon expression in wild type yeast. Using this as a genetic selection, the galactose-inducible VopQ expression plasmid was transformed into an error-prone *E. coli* mutator strain to create a library of random *vopQ* mutants. Sequencing of the mutants that did not arrest growth identified a plasmid containing a missense mutation in the *vopQ* coding sequence: a T to C transition at position 598. This mutation produced a mutant protein substituting a proline for serine at position 200 (VopQ<sup>S200P</sup>). In contrast to wild type VopQ, the mutant VopQ<sup>S200P</sup> allowed yeast growth (Figure 5.9A), despite being more highly expressed than the wild type

VopQ protein (Figure 5.9A). Furthermore, the VopQ<sup>S200P</sup> mutant, unlike the wild type protein, did not cause extensive fragmentation of yeast vacuoles *in vivo* (Figures 5.9B and 5.11), suggesting that the mutant VopQ<sup>S200P</sup> protein might be defective in its ability to inhibit homotypic vacuole fusion *in vivo*.

To examine the activity of VopQ<sup>S200P</sup> in comparison to wild type, recombinant proteins were purified (Figure 5.12) and assayed for both inhibition of vacuole fusion and vacuolar deacidification *in vitro*. Strikingly, recombinant VopQ<sup>S200P</sup> protein did not inhibit the alkaline phosphatase (Figure 5.10A) or  $\beta$ -lactamase (Figure 5.10B) fusion assays at concentrations up to 1  $\mu$ M. Even concentrations of VopQ<sup>S200P</sup> up to 10  $\mu$ M were no more effective at fusion inhibition than MBP alone (Figure 5.12B). To study the S200P mutant for the known vacuolar channel-forming activity of VopQ [125], we assayed the ability of VopQ<sup>S200P</sup> to inhibit vacuolar acidification *in vitro*. VopQ<sup>S200P</sup> completely inhibited vacuolar acidification when added prior to the ATP addition (Figure 5.10C), and deacidified the lumen after the vacuoles have been fully acidified (Figure 5.12C). To eliminate the possibility that MBP interfered with VopQ<sup>S200P</sup> fusion inhibition, we utilized the channel-forming His-tagged version of VopQ<sup>S200P</sup> (Figures 5.12D and E) and observed it is also incapable of inhibiting vacuole fusion (Figure 5.12F). Accordingly, VopQ<sup>S200P</sup> still associates with yeast vacuoles in a V-ATPase-dependent manner, as vacuoles lacking the V-ATPase no longer bind VopQ or VopQ<sup>S200P</sup> at pH 7.5 (Figure 5.12G), confirming previous observations of VopQ:vacuole interactions [125]. Therefore, VopQ<sup>S200P</sup> still has some affinity for the V-ATPase, which is required for its channel forming activity *in vitro*.

While the rate of vacuolar deacidification induced by VopQ<sup>S200P</sup> was slower when compared to VopQ, the extent of deacidification was nearly identical over time and broad concentration range (Figure 5.13). We used a dye release assay that measures the release of self-quenching concentration of carboxyfluorescein dye encapsulated in liposomes. As these are protein-free liposomes, this assay tests for VopQ channel activity independent of its V-ATPase-dependent targeting activity [125]. Interestingly, VopQ<sup>S200P</sup> induced carboxyfluorescein release from protein-free liposomes [125] with rates identical to

wild type VopQ (Figure 5.14A). Therefore, VopQ<sup>S200P</sup> appears to retain the channel-forming and deacidification activities of VopQ on both vacuoles and liposomes, but is unable to inhibit *in vitro* vacuole fusion.

Because we noticed a reduction in the ability of VopQ<sup>S200P</sup> to induce the release of protons from yeast vacuoles when compared to wild type VopQ, but not in the release of carboxyfluorescein from protein-free liposomes, we hypothesized that VopQ<sup>S200P</sup> has a lower affinity for the V-ATPase. Accordingly, VopQ<sup>S200P</sup>-GFP does not localize to the yeast vacuole as was observed for VopQ-GFP (Figure 5.14B). Furthermore, much lower levels of the V<sub>o</sub> subunits Vph1p and Vma6p were found in co-precipitation with VopQ<sup>S200P</sup> when compared to VopQ (Figure 5.14C). Therefore, VopQ<sup>S200P</sup> binds more weakly to V-ATPase subunits when compared to VopQ, but still retains its channel-forming activity on yeast vacuoles. The weak binding of VopQ<sup>S200P</sup> is sufficient to completely neutralize the vacuole *in vitro*, but is insufficient to inhibit vacuolar fusion. These facts support the model that VopQ inhibits homotypic vacuole fusion through its direct interaction with the V-ATPase V<sub>o</sub> domain, and not via its deacidification activity.

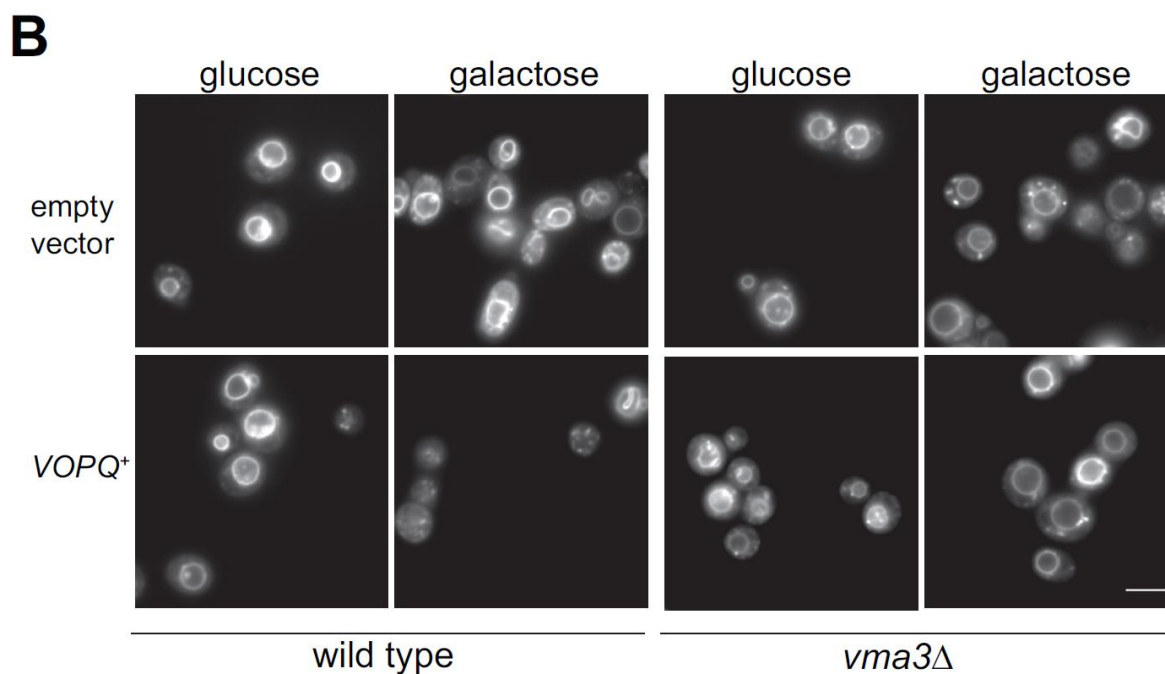
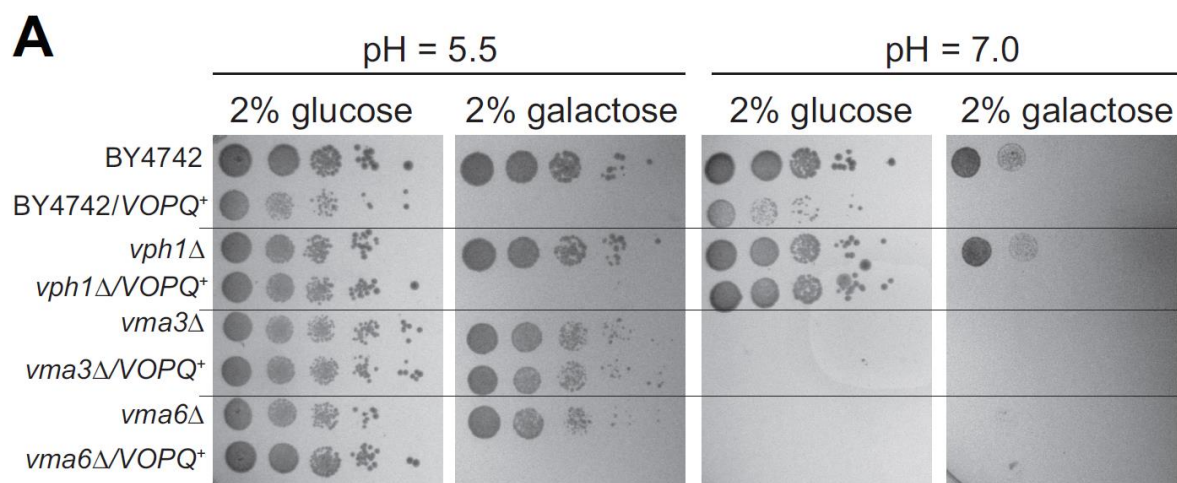


**Fig. 5.8. VopQ does not phenocopy *vma* mutants.** **(A)** Serial dilutions (1:10 dilutions from a starting OD<sub>600</sub> = 1.0) of BY4742 or *vma* strains harboring either pRS413-Gal or pRS413-Gal1-VopQ (10μl) to CSM medium lacking histidine supplemented with either 2% glucose or 2% galactose. Plates were buffered with 50 mM MES/50 mM MOPS to either pH 5.5 or 7.0. **(B)** Vacuoles from BY4742 or *vma3*Δ strains harboring either pRS413-Gal1 control or pRS413-Gal1-VOPQ plasmids were visualized via FM4-64 staining [389]. Cells were incubated with 8 μM FM4-64 were 1 h. Bar = 5 μ.

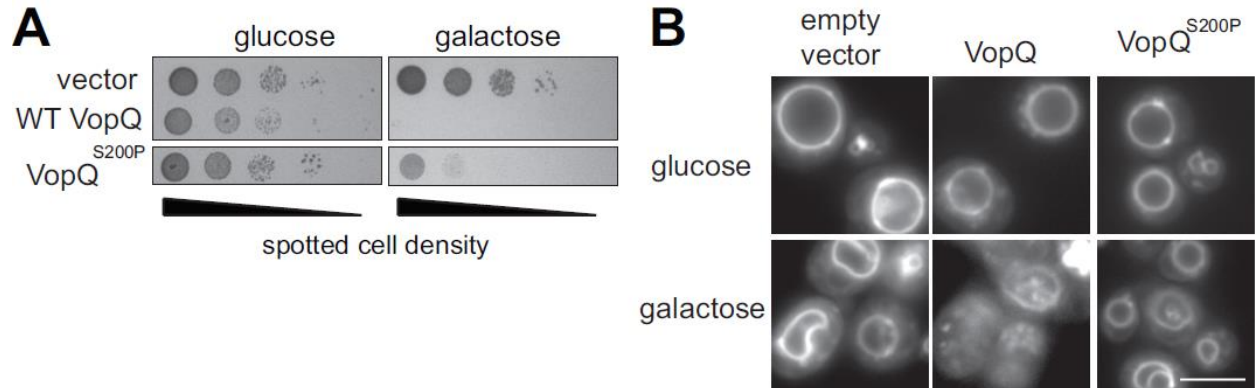


**Fig. 5.9. VopQ<sup>S200P</sup> does not induce vacuole fragmentation.** (A) Serial dilutions of yeast strain BY4742 harboring either pRS413-Gal1, pRS413-Gal1-VopQ, or pRS413-Gal1-VopQ<sup>S200P</sup> to CSM medium lacking histidine, supplemented with either 2% glucose or 2% galactose. (B) Vacuolar morphology of BY4742 strain harboring pRS413-Gal1, pRS413-Gal1-VopQ or pRS413-Gal1-VopQ<sup>S200P</sup> was visualized via FM4-64 staining. Bar = 5  $\mu$ .

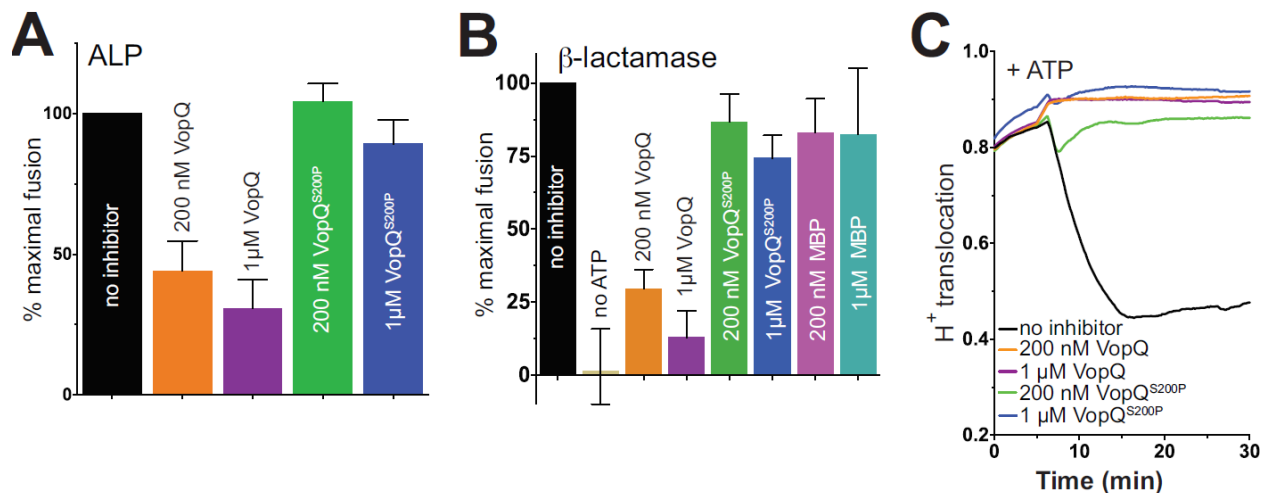


**Fig. 5.10. VopQ<sup>S200P</sup> deacidifies the vacuole but does not inhibit fusion.** (A) ALP vacuole fusion reactions or (B)  $\beta$ -lactamase fusion reactions were performed using standard inhibitors, MBP-VopQ or MBP-VopQ<sup>S200P</sup>. (C) Proton translocation activity was measured in the presence of MBP-VopQ or MBP-VopQ<sup>S200P</sup> when proteins were added prior to ATP addition.

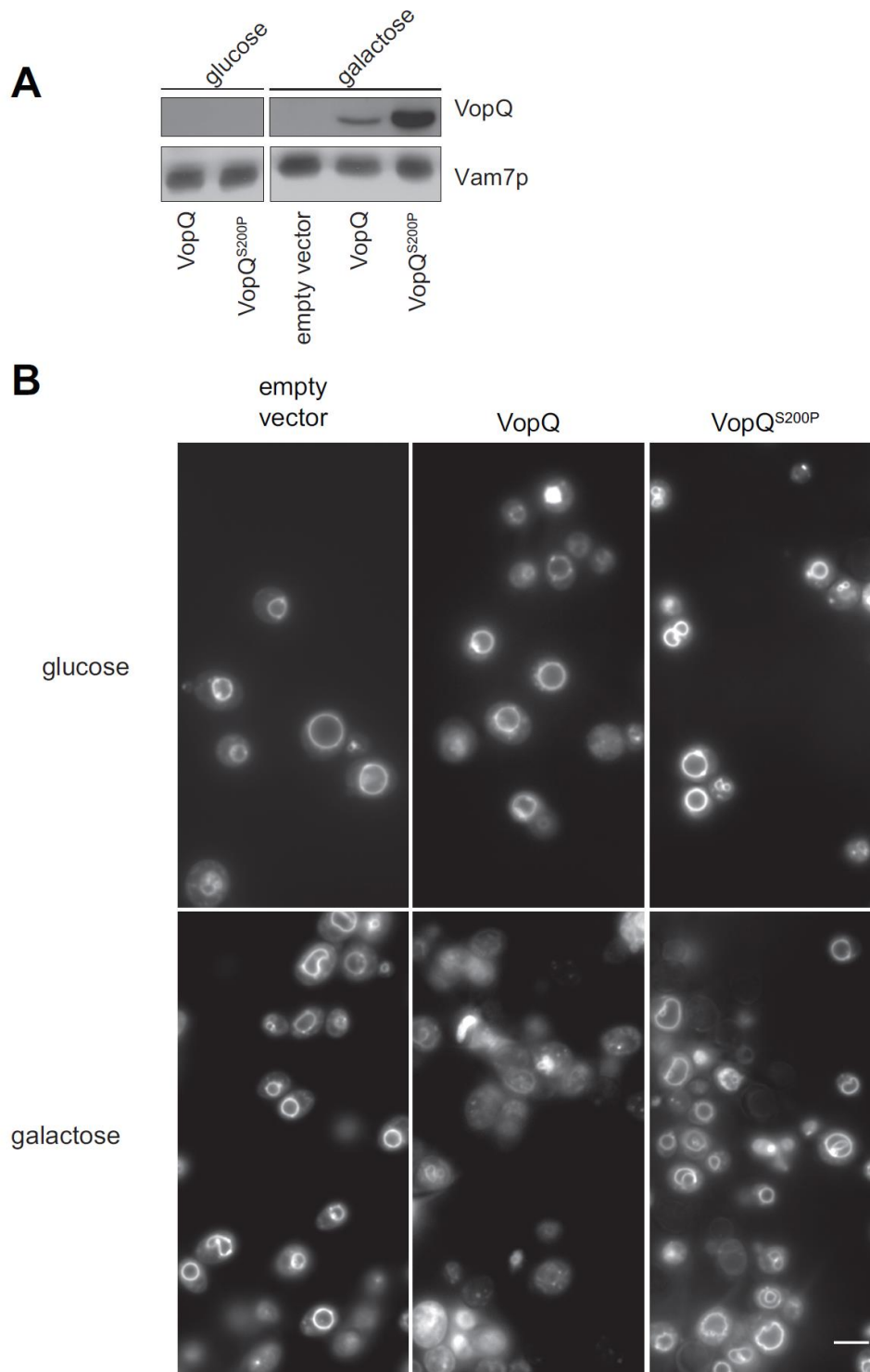


**Fig. 5.11. VopQ<sup>S200P</sup> does not fragment the yeast vacuole.** (A) VopQ protein expression was assayed in overnight cultures of the same strains in Fig. 4A. (B) BY4742 yeast strains harboring the galactose-inducible vector pRS413-Gal1 (WT), pRS413-Gal1-*VOPQ* (VopQ), or pRS413-Gal1-*VOPQ*<sup>S200P</sup> (VopQ<sup>S200P</sup>) were visualized via FM4-64 staining [389]. Images are larger fields of those presented in Figure 4C. Bar = 5  $\mu$

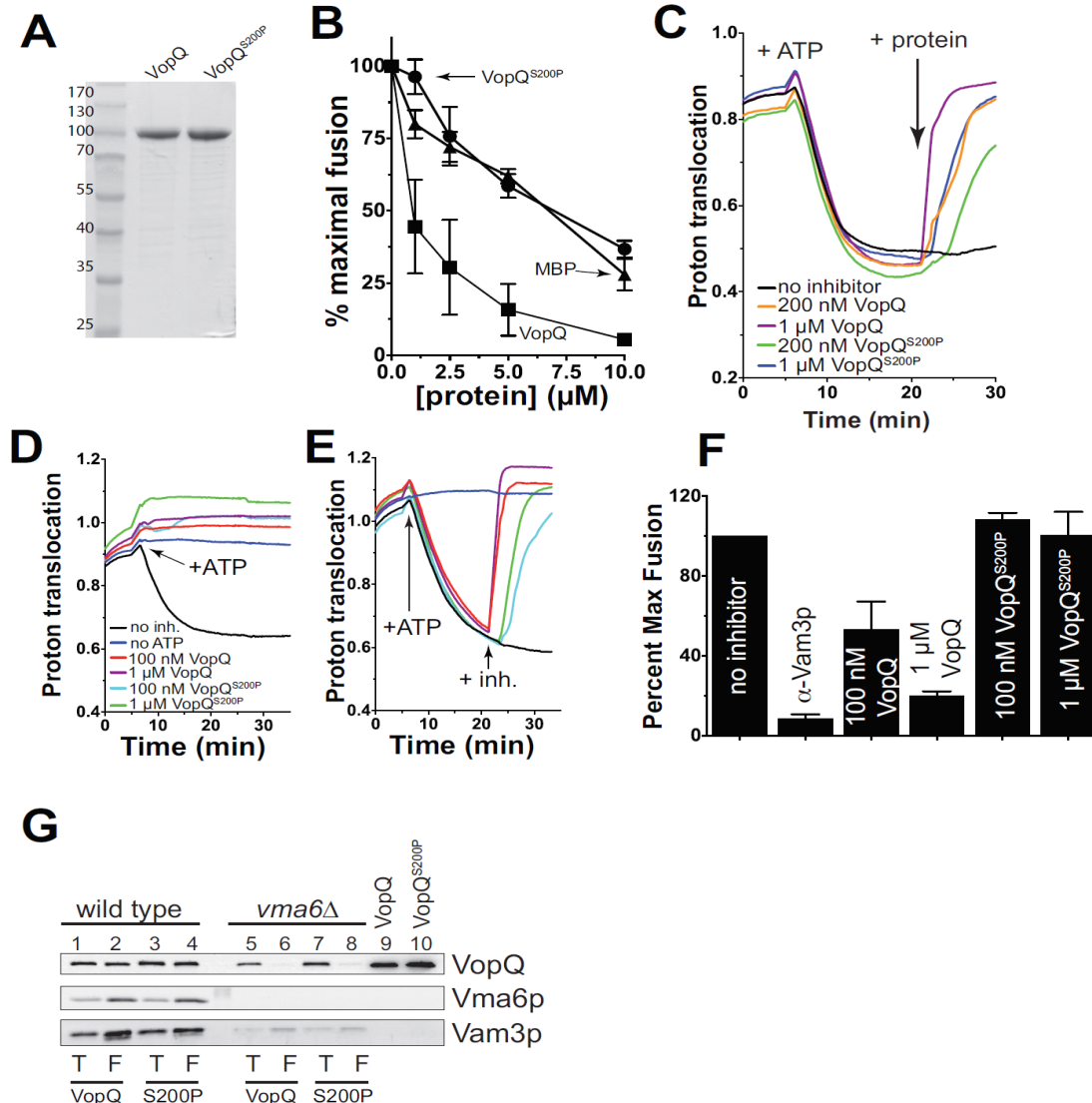


**Fig. 5.12. VopQ<sup>S200P</sup> does not inhibit vacuole fusion.** (A) 4 μg of purified MBP-VopQ and MBP-VopQ<sup>S200P</sup> visualized via SDS-PAGE and Coomassie staining. (B) Standard ALP-dependent vacuole fusion reactions were performed in the presence of the indicated concentrations of recombinant MBP, MBP-VopQ, or MBP-VopQ<sup>S200P</sup>. Maximal fusion was set to the “no inhibitor” reaction conditions, error is SD from mean;  $n = 3$ . (C) Vacuolar proton translocation activity was measured in the presence of MBP-VopQ or MBP-VopQ<sup>S200P</sup> when proteins were added 15 minutes after ATP addition. (D) Proton translocation activity was measured in the presence of His<sub>6</sub>-VopQ or His<sub>6</sub>-VopQ<sup>S200P</sup> when proteins were added either (D) prior to, or (E) 15 minutes after ATP addition. Curves representative of three independent experiments. (F) Standard ALP-dependent vacuole fusion reactions were performed in the presence of the indicated concentrations of recombinant His<sub>6</sub>-VopQ, or His<sub>6</sub>-VopQ<sup>S200P</sup>. Maximal fusion was set to the “no inhibitor” reaction conditions, error is SD from mean;  $n = 3$ . (G) Vacuoles purified from either BY4742 (wild type) or *vma6Δ* strains were assayed for MBP-VopQ or MBP-VopQ<sup>S200P</sup> associations at pH 7.5. 0.5 μg of vacuoles from either pre- (T) or post-flotation (F) were separated via SDS-PAGE and immunoblotted for the indicated proteins.

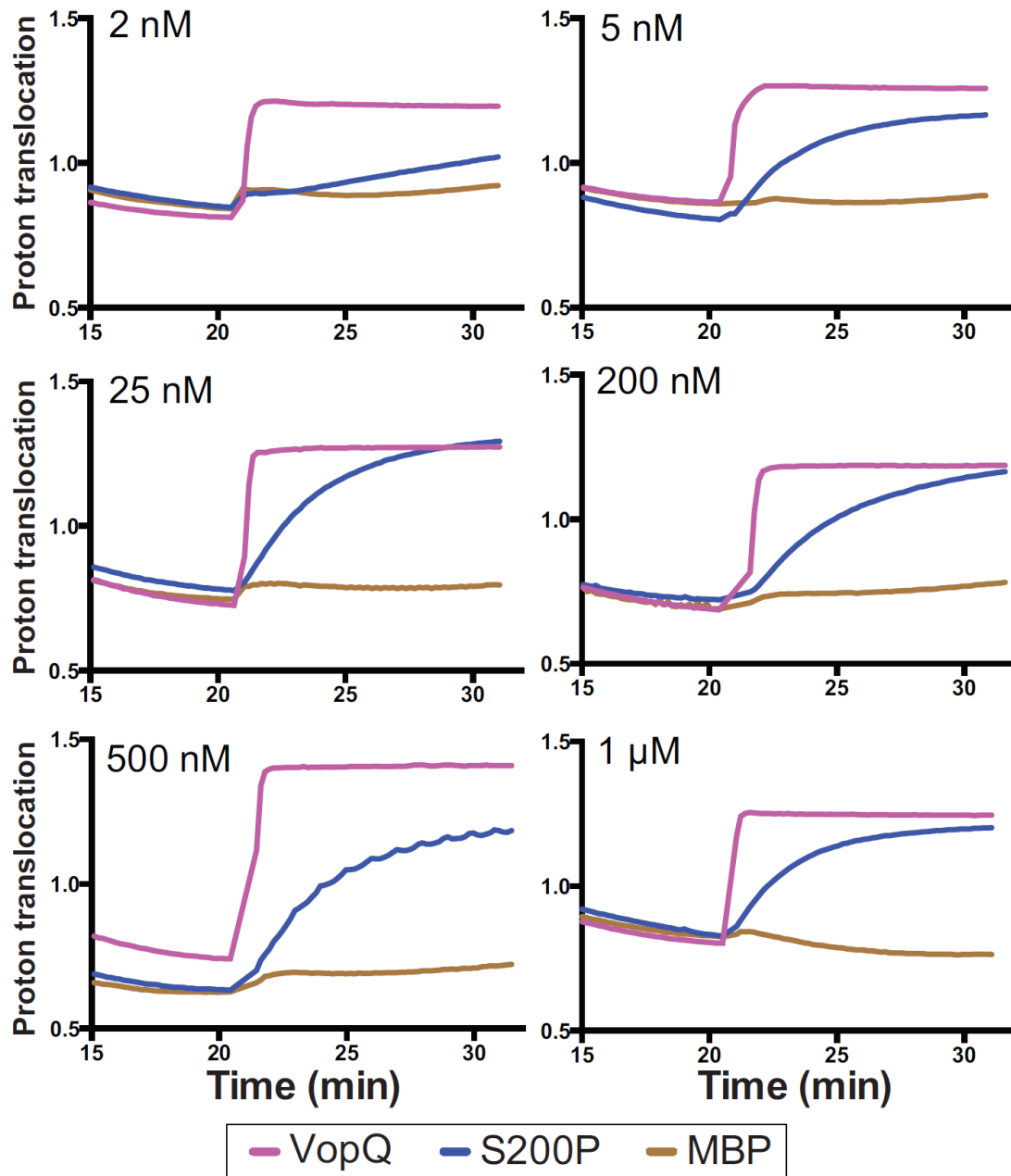


**Fig. 5.13. Characterization of VopQ<sup>S200P</sup> vacuolar deacidification rates.** Proton translocation activity of vacuoles was measured in the presence of the indicated concentrations of MBP-VopQ (pink curves), MBP-VopQ<sup>S200P</sup> (blue curves), or MBP (brown curves). Proteins were added 15 minutes after ATP addition (t = 20 min), and acridine orange absorbance was followed for an additional 10 min. Curves are representative of three independent experiments.

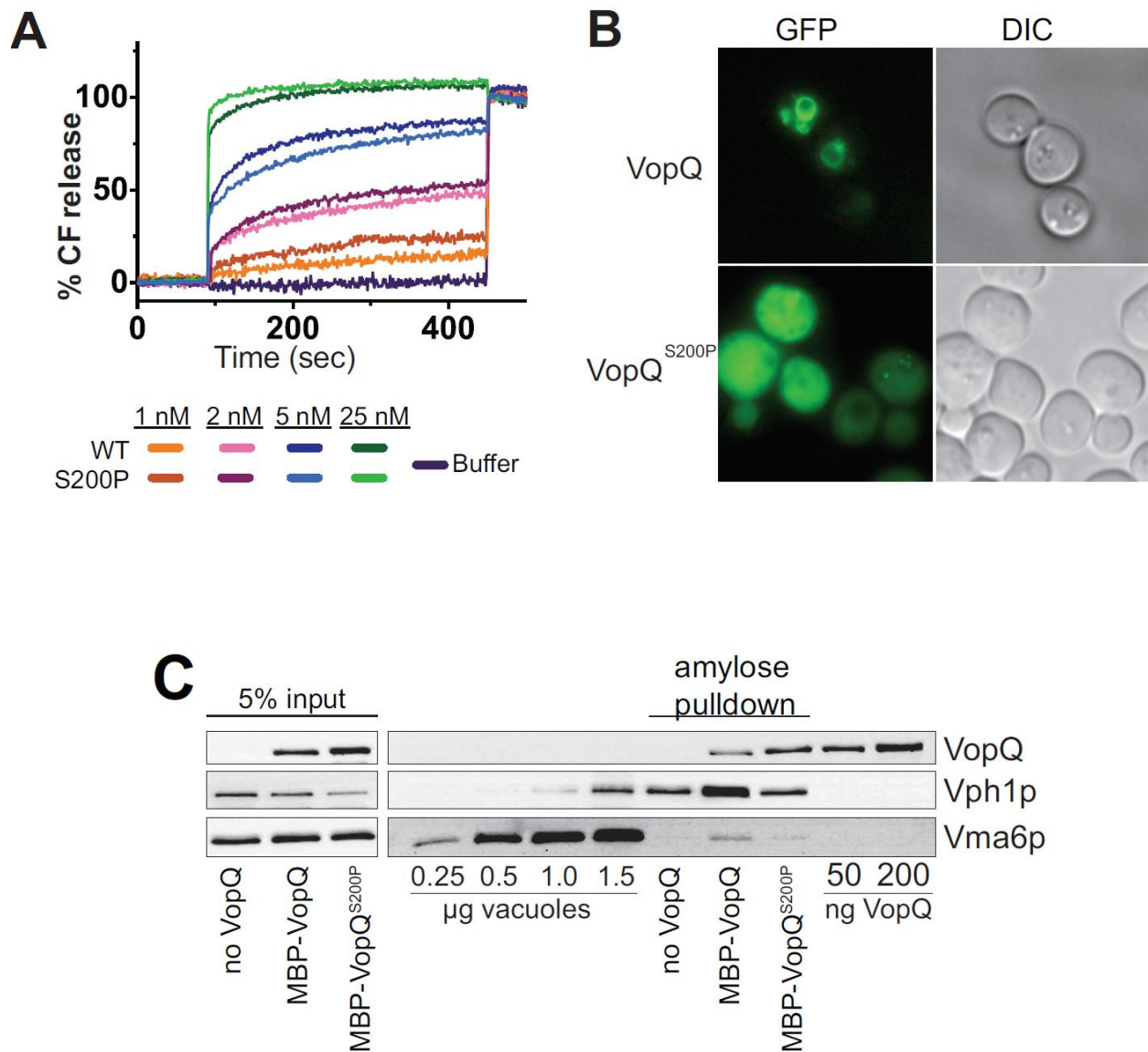


**Fig. 5.14. VopQ<sup>S200P</sup> displays channel forming activity but weaker V-ATPase binding.** (A) Carboxyfluorescein dye release from liposomes upon the addition of buffer, MBP-VopQ or MBP-VopQ<sup>S200P</sup>. (B) BY4742 strain harboring either the galactose-inducible vector VopQ-GFP or VopQ<sup>S200P</sup>-GFP was grown in CSM-uracil supplemented with 1% raffinose / 2% galactose for 8 hours, harvested, and visualized. Bar = 5 µ. (C) MBP-VopQ or MBP-VopQ<sup>S200P</sup> was precipitated from BY4742 vacuole lysates and eluates were separated via SDS-PAGE and immunoblotted for VopQ and the known VopQ-interacting subunits of V<sub>o</sub> (Vph1p and Vma6p).

## Discussion

VopQ is a 53 kD bacterial effector protein that binds to the conserved eukaryotic V-ATPase and forms a voltage-gated channel in the vacuolar membrane to disrupt ion homeostasis [125]. We now show that nanomolar amounts of VopQ inhibit the homotypic fusion of yeast vacuoles, a biochemical model of Rab GTPase and SNARE-dependent membrane fusion. Furthermore, we identified a VopQ mutant, VopQ<sup>S200P</sup>, that retained V-ATPase binding and membrane channel forming activities, but no longer inhibited vacuole fusion *in vitro*. Co-precipitation assays between VopQ<sup>S200P</sup> and V<sub>o</sub> domain subunits show a weaker overall interaction when compared to the wild type VopQ protein, and thus we speculate that the direct interaction of VopQ with the V<sub>o</sub> membrane sector is required to inhibit vacuole fusion. Importantly, the use of VopQ as a channel-forming reagent for the study of membrane fusion regulation shows that yeast vacuoles do not require active acidification or  $\Delta\psi$  for homotypic fusion *in vitro*.

This finding contrasts recent work showing that yeast vacuole fusion absolutely requires acidification *in vivo*, as was measured by protein maturation in an elegant *in vivo* protein localization assay during haploid cell mating and subsequent vacuolar membrane fusion [349]. However, both of these assays were completely dependent upon the localization and maturation of the vacuolar alkaline phosphatase. The physiological readout of these assays may be sensitive to vesicular ion concentrations, and therefore could be completely independent of physiological membrane fusion. Consistent with this theory, we show that the yeast ALP-dependent content mixing assay is sensitive to a number of ionophores, while an alternative  $\beta$ -lactamase content mixing assay is unaffected by these reagents. Furthermore, the previous study showed that a mutation in Vph1p (V<sub>o</sub> a subunit) that disrupts the ability of the V-ATPase to translocate protons, Vph1p<sup>R735Q</sup>, was unable to support the fusion of intracellular vacuoles [349]. This finding was also in contrast to studies in *Drosophila*, which show that a mutant *v100* a1 subunit with the corresponding arginine disrupted (*v100*<sup>R755A</sup>) restored vesicular trafficking and

synaptic transmission in *v100* null mutant flies, confirming an acidification-independent role of the  $\alpha 1$  subunit in membrane fusion events [459]. Further research demonstrated that  $\text{Ca}^{2+}$ -calmodulin interactions with  $\alpha 1$  subunit positively regulate the formation of some SNARE complexes at the synapse in an acidification-independent fashion [463], thereby highlighting an important acidification-independent role of  $V_o$  upstream of SNARE complex formation.

Previous studies have indicated that the role of the  $V_o$  sector in vacuole fusion is required after the formation of the trans-SNARE complexes, but before content mixing has occurred [455]. In this study, when VopQ binds to  $V_o$ , we see inhibition of the trans-SNARE complex formation during homotypic vacuole fusion *in vitro*. These data could help point to two distinct roles for the  $V_o$  sector in membrane fusion, each implicating fusion-promoting activities upstream and downstream of SNARE pairing. Furthermore, by binding a large protein (VopQ) to the  $V_o$  channel, we may be imposing a fusion block distinct from other studies. It is important to note that VopQ does not inhibit V-ATPase activity [125], which could account for some of the SNARE complex staging discrepancies between this study and others.

Most published studies measuring the role of the V-ATPase in acidification and fusion events relied on mutant derivatives of the V-ATPase  $V_o$  domain, making a direct link of V-ATPase activities to membrane fusion regulation difficult. By using a specific  $V_o$  binding, channel-forming protein from a pathogenic bacterium, we now separate the role of acidification and electrochemical gradient formation in regulating SNARE-dependent membrane fusion. Yeast vacuoles unable to acidify due to inhibitors or the activity of VopQ<sup>S200P</sup> protein are perfectly capable of fusing *in vitro* and *in vivo* indicating that luminal acidification and membrane potential is not necessary for fusion. It remains possible, however, that additional unknown factors for efficient *in vivo* vacuolar fusion require acidification, and that purification of vacuolar membranes removes this biochemical requirement. Many studies using reconstituted proteoliposomes containing cognate SNAREs, Rab GTPase, and tethering factors confirm

that the V-ATPase (or acidification and  $\Delta\psi$ ) is not explicitly required to drive fusion [488-490]; we see that VopQ is incapable of inhibiting fusion in these systems.

We therefore propose that the physical interaction of VopQ with the  $V_o$  domain is responsible for inhibiting membrane fusion in a V-ATPase-dependent manner, distinct from its deacidification activity. The  $V_o$  domain may simply serve as a receptor for VopQ, and VopQ could inhibit docking of vacuoles via several possible mechanisms including simple steric hindrance of vacuolar docking, uncoupling Vam3p SNARE: $V_o$  interactions during fusion [462] or by inhibiting a previously uncharacterized activity for  $V_o$ . Interestingly, it has been shown that the lack of the V-ATPase  $V_o$  a1 subunit induces an accumulation of autophagic vesicles without altering lysosomal acidity [491], and it has been proposed that functional V-ATPase may be required for membrane:membrane contacts between yeast autophagosomes and vacuoles [461]. Given that VopQ was also shown to induce an accumulation of autophagic vesicles in HeLa cells [125], it is possible that this VopQ:V-ATPase interaction may also induce autophagosome accumulation by directly blocking autophagosome:lysosome fusion. Studies to address these possibilities are currently underway, and may provide important new insights into the mechanisms by which  $V_o$  domains or VopQ may regulate some intracellular membrane fusion events between V-ATPase-containing membranes. To the best of our knowledge, VopQ is the first bacterial V-ATPase-binding effector shown to inhibit membrane fusion, and as observed with other virulence factors, provides valuable insight into eukaryotic cellular signaling [492].

## Materials and Methods

### Yeast strains

Yeast strains BY4742 (*MAT $\alpha$  his3 $\Delta$ 1 leu2 $\Delta$ 0 lys2 $\Delta$ 0 ura3 $\Delta$ 0*), BJ3505 (*MAT $\alpha$  ura3-52 trp1- $\Delta$ 101 his3- $\Delta$ 200 lys2-801 gal2 (gal3) can1 prb1- $\Delta$ 1.6R pep4::HIS3*)[493], DKY6281 (*MAT $\alpha$  ura3-52 leu2-3,112 trp1- $\Delta$ 901 his3- $\Delta$ 200 lys2-801 suc2- $\Delta$ 9 pho8::TRP1*) [494], BJ3505-Fos- $\omega$  and BJ3505- $\alpha$ -Jun [472] were

used for vacuole production. pRS4xx-Gal1-VOPQ were constructed as described previously [495, 496]. For GFP localization studies in yeast, VopQ was cloned into the BamHI and KpnI sites of the pDGFP vector [497].

### **Reagent preparation**

Purified recombinant yeast proteins Pbi2p [498], Gyp1-46 [499], Gdi1p [500], and Sec18p [501] were isolated as previously described. Inhibitory antibodies against Vam3p and Ypt7p were purified from serum, as previously described [499], and routinely used in fusion assays at 450 nM and 467 nM, respectively. Antisera against Nyv1p, Vam3p, and Vps33p were generous gifts from Dr. William Wickner (Geisel School of Medicine at Dartmouth); antiserum against Vma6p was a gift from Dr. Christian Ungermann (University of Osnabrück). Nitrocefin was a generous gift from Dr. Shahriar Mobashery (University of Notre Dame). All other chemicals were purchased from Sigma-Aldrich. Monoclonal antiserum against yeast Vph1p (clone 10D7A7B2) was purchased from Life Technologies.

MBP-VopQ was purified using standard nickel-affinity purification protocol, as previously described [125], buffer exchanged into storage buffer (10 mM Tris-HCl pH 8.0, 50 mM NaCl), and stored at -80°C. MBP-VopQ<sup>S200P</sup> was purified in the same manner.

### *Vacuole isolation and in vitro alkaline phosphatase fusion assay*

Vacuoles were freshly prepared from BJ3505 (*pep4Δ*) and DKY6281 (*pho8Δ*) yeast strains on discontinuous Ficoll gradients, as previously reported [502]. Standard *in vitro* vacuole fusion assays (30 μl final volume, 27°C, 90 min) contained 3 μg each BJ3505 and DKY6281 vacuoles (6 μg total), fusion reaction buffer [20 mM piperazine-*N,N'*-bis(2-ethanesulfonic acid) (PIPES)-KOH (pH 6.8), 200 mM sorbitol, 10 μM coenzyme A, 125 mM KCl, 5 mM MgCl<sub>2</sub>], 815 nM Pbi2p (I<sub>2</sub><sup>B</sup>), and ATP regenerating system [1 mM ATP, 1 mg/ml creatine kinase, and 29 mM creatine phosphate]. Reactions were assayed for Pho8p alkaline phosphatase activity as a measure of vacuole fusion as described [502], except CaCl<sub>2</sub> was omitted from the development solution. Units of fusion are reported as nmol *p*-nitrophenylate

formed  $\text{min}^{-1} \mu\text{g } pep4\Delta \text{ vacuole}^{-1}$ .

### **Yeast vacuolar staining**

BY4742 yeast strains harboring either the galactose-inducible pRS413-Gal1 (WT), pRS413-Gal1-*VOPQ* (*VopQ*<sup>+</sup>), or deletions in *VPS33* (*vps33* $\Delta$ ) were grown overnight in CSM-histidine medium, supplemented with 2% glucose. Saturated cultures were subcultured to fresh 5 mL CSM-histidine medium supplemented with either 2% glucose or 2% galactose, and grown for 16 h at 30°C with shaking. Cells in mid-logarithmic phase were suspended in YPD with 8  $\mu\text{M}$  FM4-64 and incubated at 30°C for 30 min. After incubation, cells were pelleted, suspended in minimal media, and shaken for an additional 30 min. Cells were then harvested and visualized using fluorescence microscopy.

### **$\beta$ -lactamase vacuole fusion assay**

Assays of homotypic vacuole fusion via the fusion-dependent reconstitution of  $\beta$ -lactamase enzyme were performed as previously described [472]. Briefly, vacuoles were prepared from BJ3505-Fos- $\omega$  and BJ3505- $\alpha$ -Jun strains, and 6  $\mu\text{g}$  of each vacuole type was incubated under standard fusion conditions (above) in a 60  $\mu\text{l}$  volume, except that Pbi2p was replaced with 4.3  $\mu\text{M}$  recombinant GST-Fos protein to quench fusion-independent reconstitution of  $\beta$ -lactamase. After 90 min at 27°C, tubes were removed to ice for 5 min, 140  $\mu\text{l}$  developer solution (0.1 M sodium phosphate pH 7.0, 150  $\mu\text{M}$  nitrocefin, and 0.2% Triton X-100) was added to each tube, and 150  $\mu\text{l}$  sample was removed to a clear 96-well plate. A blank well for reference consisted of 6  $\mu\text{g}$  each vacuole type, 4.3  $\mu\text{M}$  GST-Fos, and 140  $\mu\text{l}$  developer solution in a final volume of 200  $\mu\text{l}$ .  $\beta$ -lactamase-dependent hydrolysis of nitrocefin was measured via change in absorbance ( $\lambda = 492 \text{ nm}$ ) over 10 min (30 sec intervals) in a Synergy MX plate-reading spectrophotometer (Bio-Tek). Rates of hydrolysis were calculated over the interval, and “no inhibitor” fusion condition rates were set to 100 % fusion.

### **Tandem content and lipid mixing assay**

800 µg vacuoles purified from BJ3505-Fos- $\omega$  were incubated with 200 µM Rhodamine-DHPE (Rh-PE, Life Technologies), as in [472]. After harvesting labeled vacuolar membranes, 300 µl (10 x) standard  $\beta$ -lactamase reactions were performed with 30 µg vacuoles isolated from BJ3505- $\alpha$ -Jun, 23.3 µg vacuoles isolated from BJ3505-Fos- $\omega$ , and 6.7 µg Rh-PE labeled vacuoles, and containing either 200 nM MBP-VopQ or 200 nM MBP control protein. For content mixing assay, 60 µl of the master reaction was transferred to individual tubes, and the  $\beta$ -lactamase content mixing fusion assay was assayed. For lipid mixing, 180 µl of the master reaction was transferred to a 96-well black plate and Rh-PE fluorescence was followed over 90 min at 27 °C ( $\lambda_{\text{ex}}$  = 544;  $\lambda_{\text{em}}$  = 590, 150 s intervals, 10 s shaking between readings). Maximal dequenching (100% fusion) was set by the addition of 0.33% (v/v) Triton X-100 to each well, then averaging the final 10 fluorescence reads over 10 min (1 min intervals).

### **Random mutagenesis of vopQ**

To identify VopQ mutant derivatives which are no longer toxic to yeast, pRS416-Gal1-VOPQ was transformed into the highly mutagenic *E. coli* strain XL1-Red (Stratagene), 100 µl of the transformation mixture was plated to LB + 100 µl/ml ampicillin and incubated at 37°C for 36 h. All colonies (>200) were scraped into 10 mL fresh LB + 100 µg / ml ampicillin, incubated at 37°C with shaking for 16 h, and plasmid was isolated.

Mutagenized plasmid was transformed into *S. cerevisiae* BY4742, selecting for growth on CSM medium lacking uracil and supplemented with 2% galactose. Colonies appearing under these conditions were likely defective in VopQ activity *in vivo*. Thirty independent colonies were isolated in this manner, and plasmid phenotypes were confirmed via introduction into a fresh BY4742 background. Of the original 30, eleven plasmids continued to display a defect in VopQ activity *in vivo*, and the VOPQ locus from these vectors was sequenced (University of Georgia).

### **Measurement of vacuolar proton translocation**

Acidification of the vacuolar lumen by V-ATPase-dependent proton translocation was measured by the change in absorbance of acridine orange upon protonation, as previously described [485], with modifications. Vacuole fusion reactions (6 x, 180  $\mu$ l final volume) containing 6  $\mu$ g vacuoles (3  $\mu$ g each *pep4 $\Delta$*  and *pho8 $\Delta$*  per 180  $\mu$ l reaction), standard fusion buffer, 815 nM Pbi2p, 15  $\mu$ M acridine orange, and indicated reagents were preincubated for 5 min in a SynergyMX microplate reader (BioTek) prewarmed to 27°C, in a 96-well clear plate (Corning). Acridine orange absorbance (490 nm and 540 nm) was measured every minute with path length correction enabled. Acidification was initiated with the addition of 2 mM ATP, and absorbance measurements were followed every 10 sec over 20 min. Absorbance is plotted as ( $A_{490} - A_{540}$ ); the loss of absorbance indicates protonation of acridine orange and acidification of the vacuole lumen.

### **Trans-SNARE assay**

Vacuoles from BJ3505 *nyv1 $\Delta$  CBP-VAM3* and DKY6281 were used to detect trans-SNARE complex formation during fusion, as described in [468]. Interactions between CBP-Vam3p Q-SNARE and Nyv1p R-SNARE are indicative of a proper trans-SNARE complex assembly. Reactions contained either no inhibitor, left on ice, 1  $\mu$ M Gdi1p and 1  $\mu$ M Gyp1-46, or 200 nM rVopQ. After 45 min, reactions were removed to ice for 5 min, and a 30- $\mu$ l aliquot was removed to measure fusion via Pho8p activity. Remaining vacuoles were precipitated (7600 x *g*, 5 min, 4°C), solubilized, and calmodulin-affinity pulldown was performed. Vps33p, Vam3p and Nyv1p were detected using immunoblotting.

### **Vacuole docking assay**

Docking reactions were carried out as previously described [480]. Briefly, 6  $\mu$ g vacuoles purified from BY4742 were incubated for 30 min at 27°C in 30  $\mu$ l docking buffer [20 mM PIPES-KOH pH 6.8, 200 mM sorbitol, 100 mM KCl, 0.5 mM MgCl<sub>2</sub>] and 0.3x ATP regenerating system [0.3 mM ATP, 9.7 mM creatine phosphate, and 0.3 mg/ml creatine kinase] containing 815 nM Pbi2p, 20  $\mu$ M coenzyme A, and 8

nM Sec18p. After incubation, vacuoles were placed on ice, mixed with FM4-64 (3  $\mu$ M final), and were vortexed (3 s, medium speed) into an equal volume of molten 0.6% agarose. A 15  $\mu$ l aliquot of this mixture was mounted to glass slides, allowed to solidify, and visualized via epifluorescent microscopy.

### **GFP release (Lysis) assay**

Lysis of vacuoles was assayed via measuring the release of a luminal GFP protein after fusion, as previously described [500]. Briefly, fluorescent vacuoles were isolated from yeast strain VSY39, a protease-deficient BJ3505 strain constitutively expressing GFP targeted to the vacuolar lumen via fusion to an N-terminal signal sequence from the *Saccharomyces carlsbergensis*  $\beta$ -galactosidase, *MEL1* [503]. These vacuoles were premixed in a 1:1 (fluorescent *pep4* $\Delta$  / nonfluorescent *pho8* $\Delta$ ) ratio before the addition of other reaction components. Standard vacuole fusion reactions were used for the GFP release assay, with the following modifications: reactions contained 0.1X protease inhibitor mixture (50X stock: 13  $\mu$ g/ml leupeptin, 25  $\mu$ g/ml pepstatin A, and 5 mM Pefabloc SC) to stabilize GFP after vacuolar release. Each reaction was performed on a 3X scale (90  $\mu$ l), and fused for 60 min at 27 °C. Fusion detection and vacuolar pellet / supernatant separation was performed as described [477, 500]; GFP signal in each 20  $\mu$ l vacuole membrane pellet or supernatant sample was measured in a BioTek SynergyMX plate reader (Bio-Tek) ( $\lambda_{\text{ex}}$ =462 nm;  $\lambda_{\text{em}}$ =510 nm, Read Height = 8.00 mm, gain = 100). The amount of GFP released (lysis) was calculated as: RFU supernatant / (RFU supernatant + RFU pellet) \* 100 %.

### **Oxonol V membrane potential assay**

For each condition, 2.5 total  $\mu$ g purified vacuoles from BJ3505 and DKY6281 (1.25  $\mu$ g vacuoles each type) were incubated in 180  $\mu$ l reactions in PS buffer containing 125 mM KCl, 5 mM MgCl<sub>2</sub>, 10  $\mu$ M coenzyme A, 815 nM Pbi2p, and 0.5  $\mu$ M bis-(3-Phenyl-5-Oxoisoxazol-4-yl)Pentamethine Oxonol (Life Technologies). Where indicated, 0.5  $\mu$ M bafilomycin, 1  $\mu$ M nigericin, 1  $\mu$ M valinomycin, 500 nM MBP, or 500 nM MBP-VopQ was added at t = 0. Reactions were incubated in a SynergyMX plate reader (Bio-Tek), and fluorescence was measured every 10 s for 5 min at 27°C ( $\lambda_{\text{ex}}$ =580 nm;  $\lambda_{\text{em}}$ =620 nm). After 5 min, ATP

was added to 2 mM, and reaction fluorescence was measured for an additional 20 min every 10 s. After 25 min, the protonophore carbonyl cyanide *m*-chlorophenyl hydrazone (CCCP) was added to 25  $\mu$ M to collapse the remaining electrochemical gradient. Average fluorescence readings over the first 5 min for each condition were set to 100% fluorescence.

### **Reconstituted SNARE- and Rab GTPase-dependent liposome fusion**

“Vacuole-mimic’ liposomes harboring the critical homotypic fusion SNARE proteins (Nyv1p, Vam3p, Vam7p, Vti1p) and the Rab family GTPase Ypt7p were a kind gift from Dr. William Wickner (Geisel School of Medicine at Dartmouth), and were of two distinct types: ‘donor’ liposomes contained the membrane-bound fluor 7-nitrobenz-2-oxa-1,3-diazole [NBD]–1,2-di- palmitoyl-sn-glycero-3-phosphatidylethanolamine (NBD-DPPE) and encapsulated Cy5-derivatized streptavidin, and ‘acceptor’ liposomes contained the membrane-bound Marina-Blue-DPPE fluorescent probe, and entrapped soluble biotinylated R-phycoerythrin. Fusion and content mixing of proteoliposomes was described previously [504]. Briefly, 20  $\mu$ l total volume reactions containing 0.25 mM each liposome type in RB150 + Mg buffer [20 mM HEPES-NaOH, pH 7.4, 150 mM NaCl, 10% (v/v) glycerol, 1 mM MgCl<sub>2</sub>] were incubated in a 384-well low-volume, round bottom black plate (Corning) with 1 mM ATP and 9.6  $\mu$ M streptavidin. After 5 min at 27°C, reactions were initiated with the addition of premixed Sec17p/Sec18p/HOPS, so that the final concentrations of each are 1  $\mu$ M, 1 $\mu$ M, and 165 nM in the 20  $\mu$ l reaction, respectively. Fluorescence wavelengths corresponding to liposome content mixing ( $\lambda_{\text{ex}}$ =565 nm;  $\lambda_{\text{em}}$ =670 nm) and lipid mixing ( $\lambda_{\text{ex}}$ =370 nm;  $\lambda_{\text{em}}$ =465 nm) were measured every 1 min over 1 h at 27°C.

### **Liposome leakage assay**

Carboxyfluorescein encapsulated liposomes were prepared as mentioned previously [505, 506]. Briefly, dried lipid film of 85% POPC:15%DOPS (Avanti Polar Lipids) was hydrated using 100 mM carboxyfluorescein dye solution to constitute final 15 mM lipid composition. Liposomes were disrupted by 5 freeze-thaw cycles in liquid nitrogen and then extruded using Avanti mini-extruder and 80 nm

polycarbonate membranes. Extruded liposomes were passed through a PD-10 desalting column to remove excess dye. For liposome leakage assay, 100  $\mu$ M of liposomes in 10 mM MES pH5.5, 25 mM NaCl were added to a quartz cuvette, and fluorescence intensity ( $\lambda_{ex}$ =480nm,  $\lambda_{em}$ =514nm) was measured using PTI Felix32 Software. Carboxyfluorescein leakage is expressed as percent of total lysis upon addition of 1% final (v/v) n-octyl- $\beta$ -D-glucopyranoside detergent.

### **Vacuolar V-ATPase:VopQ interaction studies**

To test the association of MBP-VopQ or MBP-VopQ<sup>S200P</sup> with the vacuolar membrane in a V-ATPase-dependent manner, 150  $\mu$ g vacuoles from either BY4742 or BY4742 *vma6 $\Delta$*  [125] strains were added to 25 nM purified MBP-VopQ or MBP-VopQ<sup>S200P</sup> protein in MMS buffer [50 mM 2-(N-morpholino)ethanesulfonic acid (MES) / 50 mM 3-(N-morpholino)propanesulfonic acid (MOPS), pH = 5.5 or 7.5, 200 mM sorbitol] containing 125 mM KCl, 815 nM Pbi2p, and 2 x protease inhibitor (10 x stock from Protease Inhibitor Tablet – EDTA, Thermo Scientific), in a final volume of 300  $\mu$ l. Vacuoles were incubated for 30 min at 27  $^{\circ}$ C, removed to ice for 5 min, and 10  $\mu$ l each reaction was withdrawn for assaying pre-flotation conditions. The remaining sample was gently mixed with 262.5  $\mu$ l 15% (w/v) Ficoll solution (made in the appropriate MMS pH buffer), and overlaid sequentially with 200  $\mu$ l each 8%, 4%, and 0% Ficoll solutions in MMS. Vacuoles were re-isolated by flotation (TLS-55, 173000 x g, 30 min, 4  $^{\circ}$ C), harvested from the 0%-4% interface, and assayed for protein content.

To measure V<sub>o</sub> subunit associations with purified MBP-VopQ derivatives via co-precipitation, 400  $\mu$ g vacuoles isolated from BY4742 (2 x protease inhibitor added immediately after isolation to reduce Vph1p degradation) were added to 10  $\mu$ g recombinant MBP-VopQ or MBP-VopQ<sup>S200P</sup> in PS buffer containing 125 mM KCl, 5 mM MgCl<sub>2</sub>, 0.5 mM PMSF, 1 x protease inhibitor and 815 nM Pbi2p. Reactions were placed at 30 $^{\circ}$ C for 30 min, removed to 22 $^{\circ}$ C for 30 min, and 1 M Tris-HCl pH 7.5 was added to 20 mM. Reactions remained at 22 $^{\circ}$ C for 15 min, and were solubilized with 0.5% Triton X-100. Insoluble material was removed via centrifugation, input samples were removed, and the remaining lysate was

applied to 25  $\mu$ l equilibrated amylose resin. Beads were washed extensively, and MBP-VopQ co-precipitates were eluted with 50 mM maltose.

### **Acknowledgments**

We thank W. Wickner, C. Ungermann, R. Fratti, R. Hiesinger, and the Orth Lab for insightful discussions and supply of reagents. K.O. and A.S. are supported by grants from NIH-Allergy and Infectious Disease (R01-AI056404 and R01-AI087808) and the Welch Foundation (I-1561). A.S. is a HHMI Med into Grad Scholar. K.O. is a Burroughs Wellcome Investigator in Pathogenesis of Infectious Disease and a W.W. Caruth Jr. Biomedical Scholar. V.J.S. is supported by University of Georgia Startup Funds and a grant from NIH-Allergy and Infectious Disease (R01-AI100913).

### **Author contribution**

A.S., T.L.B., E.M.C., K.M.O, K.D.J., D.L.B., and V.J.S performed the experiments; A.S., K.O., and V.J.S. designed the study, analyzed the data, and wrote the manuscript. All authors discussed the results and commented on the manuscript.

### **Conflict of interest**

The authors declare that they have no conflict of interest.

## CHAPTER 6

### CONCLUSIONS

With the ever-looming threat of destruction by eukaryotic host defenses, bacteria, particularly those that replicate intracellularly, must evolve their own methods of evasion and defense to ensure survival. Among the many methods of eukaryotic defenses, trafficking and degradation of foreign material in the lysosome is the cornerstone, not only in the context of eukaryotic survival but also as a target for bacterial defenses. In the case of each organism presented in this work, modulation of trafficking has been identified as one function, of potentially many, of a single protein. Further, in the case of proteins VopQ and VapA, that although are one of several transcribed effectors or virulence associated proteins, each has been identified as independently necessary for bacterial pathogenicity and predominantly the cause of toxicity in eukaryotic cells [69, 124], demonstrating the importance and potency of targeting membrane trafficking as a bacterial defense mechanism. In addition to evading degradation in the lysosome, the use of proteins to reorganize the eukaryotic cytoskeleton undoubtedly aids in bacterial survival and in many cases, works in tandem with proteins such as wBm0152, VapA, and VopQ to prevent degradation. Importantly, much of the work to characterize the activity of the proteins described in this work was performed in *S. cerevisiae*, showing the value of using a well-established model organism to glean both the activity of foreign proteins and enhanced understanding of native trafficking pathways.

wBm0152, VapA, and VopQ each blocks the fusion of endosomes with the lysosome or vacuole and alters the pH of a degradative organelle for survival. wBm0152 prevents the fusion of late endosomes (MVBs) with vacuole [507], VapA specifically arrests the maturation of the phagosome/late endosome [72], and VopQ inhibits fusion with the vacuole directly in yeast [406]. Upon expression in *S.*

*cerevisiae*, *wBm0152* appears to modulate the VPS trafficking pathway in such a way that prevents the ultimate fusion of the MVB with the vacuole. Through analysis of microscopy [507], MVB:vacuole fusion assays (data not shown), and temperature-sensitivity growth assays (data not shown), this activity, though phenotypically similar to ESCRT defects, appears to be unlike a block or deletion in ESCRT machinery, which is necessary for the trafficking of membrane bound proteins to the vacuole (*wBm0152* maintains a transmembrane domain), and rather a direct result of the presence and activity of *wBm0152* either in the MVB or another unacidified vesicle associated with the vacuole membrane. Consideration of *wBm0152* as a modulator of the VPS pathway in yeast translates to its possible mechanism of action in its nematode host. As the VPS pathway is the primary pathway that delivers Golgi-derived vesicles to the vacuole (via delivery of the MVB to the vacuole) in yeast, in the context of *Wolbachia*, it has been shown that its replicative niche is Golgi-derived as well [17, 18] and therefore *wBm0152* may be the primary inhibitor of fusion and necessary for the *wBm* replicative niche to evade degradation in the nematode vacuole. Upon analysis of the phenotype observed upon expression of *wBm0152* in yeast expressing *Sna3-GFP* and vacuoles stained with FM4-64, *Sna3-GFP* was identified in unstained compartments, meaning these compartments are unacidified as FM4-64 only stains acidic membranes. Interestingly, *wBm0152-mRuby2* regularly associates with *Sna3-GFP* punctae at the vacuole (Appendix I), suggesting that *wBm0152* alters the pH of that compartment, making it more suitable to bacterial replication. *wBm0152* is a predicted OmpA PAL-like protein that has some sequence identity (~39%) to both *Ehrlichia* spp. and *Anaplasma* spp., each of which are members of the Rickettsiales order. Though the precise activity of these OmpA proteins are also unknown in *Anaplasma* spp. and *Ehrlichia* spp., several reports show they function as adhesins, aid in invasion, and are upregulated by *virB-virD4* operon during iron starvation [508-510]. Quite possibly, *wBm0152* similarly binds nematode membranes as an anchor or tether to both maintain the stability of the replicative niche and block its fusion with the vacuole through yet unknown activity. Similar tethering activity of secreted proteins has been identified

in other organisms such as *S. enterica* serovar Typhimurium and have been shown to facilitate the rapid intracellular replication of intracellular bacteria [511]. If OmpA proteins of *Anaplasma* and *Ehrlichia* spp. are upregulated in response to external stimuli, wBm0152 may also respond to extracellular stimuli, perhaps those that are involved in signaling transfer of nutrients between host and endosymbiont or those involved in worm maturation to act as a signal to other wBm proteins to initiate the movement of wBm containing vesicles to the adult female germline, though this is highly speculative. There is still little known about not only wBm but *Wolbachia* of other host organisms and many *Wolbachia* do not maintain mutualistic relationships, limiting the parallels that can be drawn between wBm0152 and other homologues across *Wolbachia*. One avenue of future work with wBm0152 should focus on its ability to inhibit MVB:vacuole fusion by determining if wBm0152 interacts with fusion specific proteins (SNAREs, Rabs, tethering complexes) or lipids that are enriched at the vacuole and MVB as potential binding partners, as well as its ability to alter or prevent membrane acidification through analysis of protease maturation. Specifically, there are well-established assays to determine if *trans*-SNARE pairing is inhibited in the presence of a foreign protein, in this case wBm0152. SNAREs that are present at the vacuole and MVB can be used in this assay to determine if wBm0152 inhibits specific SNARE activity. Performing pulldowns using tagged wBm0152 with yeast lysate or nematode lysate can elucidate protein:protein interactions which can begin to reveal the method by which fusion is inhibited if it is through inhibition or blockage of native proteins. Refloatation assays using liposomes of different lipid content (perhaps with a focus on different phosphatidylinositols at the late endosome) and charge would reveal if wBm0152 preferentially binds lipids that are enriched at different stages of endosomes. Finally, well-established assays in yeast that evaluate protease maturation can determine if wBm0152 does in fact alter the proteolytic capabilities by managing the pH of late endosomes.

Much like wBm0152, the mechanism of action of VapA is unknown though its ability to arrest phagosome maturation is known [72]. Through the arrest of phagosome maturation, the phagosome

fails to fuse with the lysosome, thereby providing *R. equi* with a replicative niche with a less acidic pH safe from macrophage defenses. The ability of VapA to prevent acidification of the phagosome can also prevent the maturation of many proteolytic enzymes that exist as zymogens and require processing and an acidic compartment for rapid maturation, thereby providing an additional defense against lysosomal degradation. To verify this, analysis of protease maturation in yeast can be examined. VapA is a surface protein of *R. equi* that binds PA strongly in relatively large membranes ([449], Chapter 4), which provides evidence that VapA has a lipid ligand that is present at the macrophage membrane. The preference VapA maintains for limited membrane curvature may be a reflection of yet another role of VapA in maintaining stability of the RCV and providing significant space by swelling of the phagosome for intracellular replication. The presumed  $\beta$ -barrel structure of VapA is unique and no crystallized proteins have significant identity to the Greek key motif that its conserved domain maintains [79] but perhaps the expense of the predicted structure of VapA is in part responsible for its preference for less curved membranes. Determining if VapA does in fact prevent maturation of proteases and evaluating other possible interactions it maintains with proteins, likely those present at the phagosomal membrane, would aid in elucidating the mechanism of activity of VapA. Analysis of potential protein binding partners can be done through pulldowns and genetic deletion of PM associated proteins (such as those involved in Golgi to PM trafficking or homologues to macrophage PM proteins) in yeast, as this is where VapA is trafficked upon expression in yeast. Continued work with VapA mutants in both macrophages to evaluate *R. equi* replicative ability and in yeast will be essential to determine the PA binding domain or other potential protein binding motifs of VapA.

Unlike either wBm0152 and VapA, VopQ is recognized as a pore-forming protein through its interaction with the V-ATPase at the vacuole membrane and as an inducer of autophagy through an unknown process. The interaction VopQ maintains with the  $V_o$  domain is fascinating, particularly its specific interaction with and requirement of Vma3p for its toxicity. Comparison of the sequences of

Vma3p and VopQ reveal some identity in the transmembrane domains of Vma3p (29% identity, 41% positives, 65% coverage), however such similarity does not exist in other c-ring subunits, Vma11p and Vma16p, despite that fact that Vma3p is similar in sequence to both Vma11p and Vma16p (56% identity/78% positive and 33% identity/54% positive, respectively with over 90% coverage for either). It is unknown if the similarity is simply due to fact that VopQ behaves as a transmembrane protein upon recognition of the vacuole membrane or if there is a more complex interaction between VopQ and Vma3p. Regardless, the sequence similarity may be telling in terms of the behavior of VopQ at the membrane. There are eight Vma3p subunits that make up the c-ring, each crossing through the vacuole membrane four times and forming a complex with other c-ring subunits. VopQ may bind Vma3p and form a VopQ “ring” by oligomerizing with other copies of VopQ on either the exterior or interior of the c-ring. The concept of forming a multi-subunit complex also aids in the explanation of pore size because VopQ forms an 18Å pore which is large given that VopQ is 54kDa. Though it is possible that VopQ exists as a monomeric pore-forming protein, other proteins that generate a similarly sized pore are frequently documented to exist in multi-copy complexes [512, 513]. Generating mutant derivatives of VopQ specifically by mutating single residues within the region with similarity to Vma3p could begin to pull apart whether this region is necessary for the interaction between VopQ and Vma3p as well as the pore-forming activity of VopQ. Vma3p single mutations can additionally be generated within its transmembrane domain to determine if the binding motif between Vma3p and VopQ is shared and again, necessary for the activity of VopQ. Vma3p can also be generated with an ER retention signal to evaluate if by forcing Vma3p to stay at the ER, if VopQ loses its toxicity and targeted interaction with the vacuole membrane despite the presence of Vma3p within the yeast cell. Although the pore-forming activity of VopQ is important in disrupting cellular homeostasis, particularly as it destroys the pH and electrochemical gradient and causes the passage of ions and small molecules across the vacuole membrane, this activity alone is not enough to inhibit fusion at the vacuole or induce autophagy, leaving

a significant gap in the understanding of the mechanism of action of VopQ [406]. Perhaps VopQ acts as an autophagy inducer merely by its ability to alter the vacuole storage of ions and molecules. Many components stored in the vacuole act as signaling molecules for other pathways, many of which are involved in stress responses such as autophagic pathways. If this is the case, then the induction of autophagy and resulting accumulation of autophagic vesicles are a result of the interaction VopQ maintains with the V-ATPase. To date, only limited work has been performed to understand VopQ as an autophagy inducer (described in [124]) and future studies in yeast can focus on identifying essential autophagy genes necessary for the activity of VopQ, at least in a genetic capacity, and which pathway(s) of autophagy VopQ may be hijacking (i.e. using Ape1p to evaluate VopQ in the Cvt pathway) either directly through unknown means or indirectly by the release of vacuolar signaling molecules. Additionally, it would be interesting to block, by gene deletion or mutation, proteins that respond to ionic changes to signal autophagy in the presence of VopQ to discern if its autophagy induction is merely due to ion release or is in fact inherent in the activity of VopQ. One consideration to evaluate the fusion-inhibitory activity of VopQ is the pH and ionic environment in which fusion assays are performed. VopQ preferentially binds acidic membranes but what about the ionic gradient present at such membranes? Liposome fusion assays using vacuole mimic liposomes either lacking or containing purified V<sub>o</sub> and both in low pH and physiological pH can reveal if VopQ is capable of inhibiting fusion only in certain ionic or pH conditions. As a putative transmembrane protein, VopQ has access to the vacuole lumen and therefore, presenting it with different ionic concentrations with emphasis on calcium, chloride, and potassium would be telling in evaluating ion gradient requirement as a means to aid in recognition of target membranes. Similarly, this would be useful while evaluating VopQ induced gating events. The electrophysiology described in Appendix III utilizes very low salt conditions to prevent background and membrane collapse, perhaps in future analyses of VopQ gating across a pH and electrochemical range would be helpful in determining how it targets membranes in vivo and if there

are external conditions that facilitate the gating of VopQ. Though no other binding partners have been identified as of yet, VopQ may be capable of blocking or binding necessary fusion components by its presence at the vacuole and exacerbate its many other consequences by its mere presence in the vacuole membrane.

Although arguably the most important aspect of bacterial survival, preventing the acidification and fusion of endosomes containing bacteria often occurs in addition to other modulation of eukaryotic trafficking, namely actin modulation. *V. parahaemolyticus* expresses VopS and *wBm* expresses *wBm0076*, both of which induce significant changes to host actin [126, 507]. VopS, though dispensable for invasion, has been shown to induce cell rounding through its AMPylation activity [124, 126]. *wBm0076* is highly toxic to yeast cells, causing the cell lysis presumably as a result of its ability to increase branched actin at cortical actin patches and overall cell volume [507]. No actin modulator has been identified as a virulence protein of *R. equi* though the function of the Vaps outside of VapA are largely unknown which doesn't preclude the possibility of a Vap exhibiting such a function. Importantly, actin modulating proteins have been identified in many bacteria, including *Listeria* spp., *Mycobacterium* spp., *Rickettsia* spp., *Salmonella* spp., and *Yersinia* spp. [415, 514-517], each use this as a method of survival in conjunction with other proteins. *wBm0076* may be pivotal to the movement of *wBm* containing vesicles within the nematode by controlling actin rearrangements of the nematode and providing means for intracellular motility, as is the case with proteins of *Listeria*, *Shigella*, and *Rickettsia* spp. [361, 415, 518]. Actin polymerization and depolymerization assays will prove important in determining the activity of *wBm0076* and if it does in fact act to stimulate Arp2/3 during actin filamentation. It is not known how the *wBm* containing vesicle is capable of motility within the nematode or what triggers the increased presence of *wBm* in adult female germ cells but *wBm0076* as a WASP family protein with homology to other known actin modulators (namely, RickA of *R. conorii*), is undoubtedly essential for the nematode cytoskeletal rearrangements to aid in at least the survival of

wBm and more likely, the intracellular mobility of wBm vesicles. The use of the nematode model, *Caenorhabditis elegans*, though not naturally colonized with *Wolbachia*, to examine modulation of actin specifically during nematode growth may provide evidence of how nematode cells are altered in its presence and if/where it localizes in nematode cells. Additionally, performing pulldown assays with wBm0076 and nematode cell lysate can determine if wBm0076 interacts with proteins outside of actin. The ability to modulate cytoskeletal components in orchestration with the ability to modulate membrane trafficking provides bacteria with an excellent chance of survival and depending on the relationship between bacteria and host, may significantly impede eukaryotic host cell health and survival.

Through the use of model eukaryotic mock host, *S. cerevisiae*, this work has identified proteins secreted by three different organisms that live in vastly different environments and yet for survival, similarly target eukaryotic membrane dynamics through the modulation of vesicle traffic, pH, and actin dynamics. Despite vast differences in such proteins, three – wBm0152, VapA, and VopQ - cause failed fusion with the degradative organelle and two – wBm0076 and VopS – work in tandem with membrane trafficking modulators to induce significant cytoskeletal alterations. Indubitably, the activities of these proteins are well-orchestrated events that occur in either response to host cues or by the timely upregulation and/or translocation of such proteins. How bacteria are capable of orchestrating such finely tuned events is a natural phenomenon that enables bacteria to gain a modicum of control over a eukaryotic cell to ensure survival.

## REFERENCES

1. Hilgenboecker, K., et al., *How many species are infected with Wolbachia?--A statistical analysis of current data*. FEMS Microbiol Lett, 2008. **281**(2): p. 215-20.
2. Hertig, M., *The Rickettsia, Wolbachia pipientis (gen. et sp.n.) and Associated Inclusions of the Mosquito, Culex pipiens*. Parasitology, 1936. **28**(4): p. 453-486.
3. Glowska, E., et al., *New Wolbachia supergroups detected in quill mites (Acari: Syringophilidae)*. Infect Genet Evol, 2015. **30**: p. 140-146.
4. Zhou, W., F. Rousset, and S. O'Neill, *Phylogeny and PCR-based classification of Wolbachia strains using wsp gene sequences*. Proc. R. Soc. Lond., 1998. **265**: p. 509-515.
5. Baldo, L., et al., *Multilocus sequence typing system for the endosymbiont Wolbachia pipientis*. Appl Environ Microbiol, 2006. **72**(11): p. 7098-110.
6. Hoffmann, A.A., P.A. Ross, and G. Rasic, *Wolbachia strains for disease control: ecological and evolutionary considerations*. Evol Appl, 2015. **8**(8): p. 751-68.
7. O'Neill, S., et al., *16S rRNA phylogenetic analysis of the bacterial endosymbionts associated with cytoplasmic incompatibility in insects*. Proc. Natl. Acad. Sci., 1992. **89**: p. 2699-2702.
8. Lo, N., et al., *Taxonomic status of the intracellular bacterium Wolbachia pipientis*. Int J Syst Evol Microbiol, 2007. **57**(Pt 3): p. 654-7.
9. Stouthamer, R., J.A.J. Breeuwer, and G.D.D. Hurst, *Wolbachia pipientis: Microbial Manipulator of Arthropod Reproduction*. Annu. Rev. Microbiol., 1999. **53**: p. 71-102.
10. Bhattacharya, T. and I.L.G. Newton, *Mi Casa es Su Casa: how an intracellular symbiont manipulates host biology*. Environ Microbiol, 2017.
11. Genty, L.M., et al., *Wolbachia infect ovaries in the course of their maturation: last minute passengers and priority travellers?* PLoS One, 2014. **9**(4): p. e94577.
12. Scientific Working Group on Serious Adverse Events in Loa Loa endemic, a., *Report of a Scientific Working Group on Serious Adverse Events following Mectizan(R) treatment of onchocerciasis in Loa loa endemic areas*. Filaria J, 2003. **2 Suppl 1**: p. S2.
13. Debrah, A.Y., et al., *Macrofilaricidal Activity in Wuchereria bancrofti after 2 Weeks Treatment with a Combination of Rifampicin plus Doxycycline*. J Parasitol Res, 2011. **2011**: p. 201617.

14. Debrah, A.Y., et al., *Macrofilaricidal effect of 4 weeks of treatment with doxycycline on Wuchereria bancrofti*. Trop Med Int Health, 2007. **12**(12): p. 1433-41.
15. Hoerauf, A., et al., *Depletion of Wolbachia endobacteria in Onchocerca volvulus by doxycycline and microfilaridermia after ivermectin treatment*. Lancet, 2001. **357**(9266): p. 1415-6.
16. Taylor, M.J., et al., *Macrofilaricidal activity after doxycycline treatment of Wuchereria bancrofti: a double-blind, randomised placebo controlled trial*. Lancet, 2005. **365**(9477): p. 2116-21.
17. Cho, K.O., G.W. Kim, and O.K. Lee, *Wolbachia bacteria reside in host Golgi-related vesicles whose position is regulated by polarity proteins*. PLoS One, 2011. **6**(7): p. e22703.
18. Fischer, K., et al., *High pressure freezing/freeze substitution fixation improves the ultrastructural assessment of Wolbachia endosymbiont-filarial nematode host interaction*. PLoS One, 2014. **9**(1): p. e86383.
19. Fischer, K., et al., *Tissue and stage-specific distribution of Wolbachia in Brugia malayi*. PLoS Negl Trop Dis, 2011. **5**(5): p. e1174.
20. Foster, J., et al., *The Wolbachia genome of Brugia malayi: endosymbiont evolution within a human pathogenic nematode*. PLoS Biol, 2005. **3**(4): p. e121.
21. Darby, A.C., et al., *Analysis of gene expression from the Wolbachia genome of a filarial nematode supports both metabolic and defensive roles within the symbiosis*. Genome Res, 2012. **22**(12): p. 2467-77.
22. Li, Z. and C.K. Carlow, *Characterization of transcription factors that regulate the type IV secretion system and riboflavin biosynthesis in Wolbachia of Brugia malayi*. PLoS One, 2012. **7**(12): p. e51597.
23. Warbrick, E., et al., *The effect of invertebrate hormones and potential hormone inhibitors on the third larval moult of the filarial nematode, Diofilaria immitis in vitro*. Parasitology, 1993. **107**: p. 459-463.
24. Barker, G., et al., *The effect of ecdysteroids on the microfilarial production of Brugia pahangi and the control of meiotic reinitiation in the oocytes of Diofilaria immitis*. Parasitol Res, 1991. **77**: p. 65-71.
25. Rances, E., et al., *Genetic and functional characterization of the type IV secretion system in Wolbachia*. J Bacteriol, 2008. **190**(14): p. 5020-30.
26. Christie, P.J., et al., *Biogenesis, architecture, and function of bacterial type IV secretion systems*. Annu Rev Microbiol, 2005. **59**: p. 451-85.
27. Waksman, G. and E.V. Orlova, *Structural organisation of the type IV secretion systems*. Curr Opin Microbiol, 2014. **17**: p. 24-31.

28. Masui, S., T. Sasaki, and H. Ishikawa, *Genes for the Type IV Secretion System in an Intracellular Symbiont, Wolbachia, a Causative Agent of Various Sexual Alterations in Arthropods*. J Bacteriol, 2000. **182**(22): p. 6529-6531.
29. Cheng, Z., X. Wang, and Y. Rikihisa, *Regulation of type IV secretion apparatus genes during Ehrlichia chaffeensis intracellular development by a previously unidentified protein*. J Bacteriol, 2008. **190**(6): p. 2096-105.
30. Voronin, D., et al., *Wolbachia lipoproteins: abundance, localisation and serology of Wolbachia peptidoglycan associated lipoprotein and the Type IV Secretion System component, VirB6 from Brugia malayi and Aedes albopictus*. Parasit Vectors, 2014. **7**: p. 462.
31. Melnikow, E., et al., *A potential role for the interaction of Wolbachia surface proteins with the Brugia malayi glycolytic enzymes and cytoskeleton in maintenance of endosymbiosis*. PLoS Negl Trop Dis, 2013. **7**(4): p. e2151.
32. Rice, D.W., K.B. Sheehan, and I.L.G. Newton, *Large-Scale Identification of Wolbachia pipientis Effectors*. Genome Biol Evol, 2017. **9**(7): p. 1925-1937.
33. Siozios, S., et al., *The Diversity and Evolution of Wolbachia Ankyrin Repeat Domain Genes*. PLoS One, 2013. **8**(2).
34. Takai, S., *Epidemiology of Rhodococcus equi infections: a review*. Vet Microbiol, 1997. **56**(3-4): p. 167-76.
35. Vazquez-Boland, J.A., et al., *Rhodococcus equi: the many facets of a pathogenic actinomycete*. Vet Microbiol, 2013. **167**(1-2): p. 9-33.
36. Goodfellow, M. and G. Alderson, *The actinomycete-genus Rhodococcus: a home for the "rhodochrous" complex*. J Gen Microbiol, 1977. **100**(1): p. 99-122.
37. Goodfellow, M., et al., *Charting stormy waters: A commentary on the nomenclature of the equine pathogen variously named Prescottella equi, Rhodococcus equi and Rhodococcus hoagii*. Equine Veterinary Journal, 2015. **47**(5): p. 508-509.
38. Jones, A.L., I.C. Sutcliffe, and M. Goodfellow, *Prescottia equi: a new home for an old pathogen*. Antonie van Leeuwenhoek, 2013. **103**(3): p. 655-671.
39. Chaffin, M.K., et al., *Evaluation of the efficacy of gallium maltolate for chemoprophylaxis against pneumonia caused by Rhodococcus equi infection in foals*. Am J Vet Res, 2011. **72**: p. 945-57.
40. Zink, M.C., J.A. Yager, and N.L. Smart, *Corynebacterium equi infections in horses, 1958-1984: A review of 131 cases*. Can J Vet Res, 1986. **27**: p. 213-217.
41. Takai, S., et al., *Identification of intermediately virulent Rhodococcus equi isolates from pigs*. Journal of Clinical Microbiology, 1996. **34**(4): p. 1034.
42. Cohen, N.D., *Rhodococcus equi Foal Pneumonia*. Veterinary Clinics of North America: Equine Practice, 2014. **30**(3): p. 609-622.

43. Martens, R.J., R.A. Fiske, and H.W. Renshaw, *Experimental subacute foal pneumonia induced by aerosol administration of Corynebacterium equi*. Equine Veterinary Journal, 1982. **14**: p. 111-116.
44. Johnson, J.A., J.F. Prescott, and R.J. Markham, *The pathology of experimental Corynebacterium equi infection in foals following intrabronchial challenge* Vet Pathol, 1983. **20**: p. 440-449.
45. Johnson, J.A., J.F. Prescott, and R.J. Markham, *The pathology of experimental Corynebacterium equi infection in foals following intragastric challenge*. Vet Pathol, 1983. **20**: p. 450-459.
46. Muscatello, G., et al., *Associations between the ecology of virulent Rhodococcus equi and the epidemiology of R. equi pneumonia on Australian thoroughbred farms*. Appl Environ Microbiol, 2006. **72**(9): p. 6152-60.
47. Kuskie, K.R., et al., *Associations between the Exposure to Airborne Virulent Rhodococcus equi and the Incidence of R equi Pneumonia among Individual Foals*. Journal of Equine Veterinary Science, 2011. **31**(8): p. 463-469.
48. Cohen, N.D., et al., *Association of perinatal exposure to airborne Rhodococcus equi with risk of pneumonia caused by R equi in foals*. American Journal of Veterinary Research, 2012. **74**(1): p. 102-109.
49. Hondalus, M.K. and D.M. Mosser, *Survival and replication of Rhodococcus equi in macrophages*. Infect Immun, 1994. **62**(10): p. 4167-75.
50. Fernandez-Mora, E., et al., *Maturation of Rhodococcus equi-containing vacuoles is arrested after completion of the early endosome stage*. Traffic, 2005. **6**(8): p. 635-53.
51. Toyooka, K., S. Takai, and T. Kirikae, *Rhodococcus equi can survive a phagolysosomal environment in macrophages by suppressing acidification of the phagolysosome*. J Med Microbiol, 2005. **54**(Pt 11): p. 1007-15.
52. von Bargen, K., et al., *Rhodococcus equi virulence-associated protein A is required for diversion of phagosome biogenesis but not for cytotoxicity*. Infect Immun, 2009. **77**(12): p. 5676-81.
53. Lührmann, A., et al., *Necrotic death of Rhodococcus equi-infected macrophages is regulated by virulence-associated plasmids*. Infect Immun, 2004. **72**: p. 853-62.
54. Haas, A., *Reprogramming the phagocytic pathway—intracellular pathogens and their vacuoles (Review)*. Molecular Membrane Biology, 1998. **15**(3): p. 103-121.
55. Uribe-Querol, E. and C. Rosales, *Control of Phagocytosis by Microbial Pathogens*. Frontiers in Immunology, 2017. **8**: p. 1368.
56. Takai, S., et al., *Identification of 15- to 17-kilodalton antigens associated with virulent Rhodococcus equi*. J Clin Microbiol, 1991. **29**(3): p. 439-43.

57. Giguere, S., et al., *Role of the 85-kilobase plasmid and plasmid-encoded virulence-associated protein A in intracellular survival and virulence of Rhodococcus equi*. *Infect Immun*, 1999. **67**(7): p. 3548-57.
58. Ocampo-Sosa, A.A., et al., *Molecular Epidemiology of Rhodococcus equi Based on traA, vapA, and vapB Virulence Plasmid Markers*. *The Journal of Infectious Diseases*, 2007. **196**(5): p. 763-769.
59. Makrai, L., et al., *Characterization of virulence plasmid types in Rhodococcus equi isolates from foals, pigs, humans and soil in Hungary*. *Veterinary Microbiology*, 2002. **88**(4): p. 377-384.
60. Tripathi, V.N., et al., *Conjugal Transfer of a Virulence Plasmid in the Opportunistic Intracellular Actinomycete Rhodococcus equi*. *Journal of Bacteriology*, 2012. **194**(24): p. 6790.
61. Takai, S., et al., *Virulence-associated plasmids in Rhodococcus equi*. *Journal of Clinical Microbiology*, 1993. **31**(7): p. 1726.
62. Tkachuk-Saad, O. and J. Prescott, *Rhodococcus equi plasmids: isolation and partial characterization*. *Journal of Clinical Microbiology*, 1991. **29**(12): p. 2696.
63. Valero-Rello, A., et al., *An Invertron-Like Linear Plasmid Mediates Intracellular Survival and Virulence in Bovine Isolates of Rhodococcus equi*. *Infect Immun*, 2015. **83**(7): p. 2725-37.
64. Letek, M., et al., *Evolution of the Rhodococcus equi vap pathogenicity island seen through comparison of host-associated vapA and vapB virulence plasmids*. *J Bacteriol*, 2008. **190**(17): p. 5797-805.
65. Takai, S., et al., *DNA Sequence and Comparison of Virulence Plasmids from Rhodococcus equi ATCC 33701 and 103*. *Infection and Immunity*, 2000. **68**(12): p. 6840.
66. Letek, M., et al., *The Genome of a Pathogenic Rhodococcus: Cooptive Virulence Underpinned by Key Gene Acquisitions*. *PLOS Genetics*, 2010. **6**(9): p. e1001145.
67. Wang, X., et al., *IcgA is a virulence factor of Rhodococcus equi that modulates intracellular growth*. *Infect Immun*, 2014. **82**(5): p. 1793-800.
68. Kakuda, T., et al., *VirS, an OmpR/PhoB subfamily response regulator, is required for activation of vapA gene expression in Rhodococcus equi*. *BMC Microbiol*, 2014. **14**: p. 243.
69. Jain, S., B.R. Bloom, and M.K. Hondalus, *Deletion of vapA encoding Virulence Associated Protein A attenuates the intracellular actinomycete Rhodococcus equi*. *Mol Microbiol*, 2003. **50**(1): p. 115-28.
70. Coulson, G.B., S. Agarwal, and M.K. Hondalus, *Characterization of the role of the pathogenicity island and vapG in the virulence of the intracellular actinomycete pathogen Rhodococcus equi*. *Infect Immun*, 2010. **78**(8): p. 3323-34.

71. Takai, S., et al., *Virulence-associated 15- to 17-kilodalton antigens in Rhodococcus equi: temperature-dependent expression and location of the antigens*. Infect Immun, 1992. **60**(7): p. 2995-7.
72. Rofe, A.P., et al., *The Rhodococcus equi virulence protein VapA disrupts endolysosome function and stimulates lysosome biogenesis*. Microbiologyopen, 2016.
73. Benoit, S., et al., *Induction of vap genes encoded by the virulence plasmid of Rhodococcus equi during acid tolerance response*. Res Microbiol, 2001. **152**(5): p. 439-49.
74. Byrne, B.A., et al., *Virulence Plasmid of Rhodococcus equi Contains Inducible Gene Family Encoding Secreted Proteins*. Infection and Immunity, 2001. **69**(2): p. 650.
75. Ren, J. and J. Prescott, *Analysis of virulence plasmid gene expression of intra-macrophage and in vitro grown Rhodococcus equi ATCC 33701*. Vet Microbiol, 2003. **94**: p. 167-82.
76. Ren, J. and J. Prescott, *The effect of mutation of Rhodococcus equi virulence plasmid gene expression and mouse virulence*. Vet Microbiol, 2004. **103**: p. 219-230.
77. Byrne, G.A., et al., *Transcriptional regulation of the virR operon of the intracellular pathogen Rhodococcus equi*. J Bacteriol, 2007. **189**: p. 5082-89.
78. Russell, D.A., et al., *The LysR-type transcriptional regulator VirR is required for expression of the virulence gene vapA of Rhodococcus equi ATCC 33701*. J Bacteriol, 2004. **186**: p. 5576-84.
79. Geerds, C., et al., *Structure of Rhodococcus equi virulence-associated protein B (VapB) reveals an eight-stranded antiparallel beta-barrel consisting of two Greek-key motifs*. Acta Crystallogr F Struct Biol Commun, 2014. **70**(Pt 7): p. 866-71.
80. Whittingham, J.L., et al., *Structure of the virulence-associated protein VapD from the intracellular pathogen Rhodococcus equi*. Acta Crystallogr D Biol Crystallogr, 2014. **70**(Pt 8): p. 2139-51.
81. Okoko, T., et al., *Structural characterisation of the virulence-associated protein VapG from the horse pathogen Rhodococcus equi*. Vet Microbiol, 2015. **179**(1-2): p. 42-52.
82. Sydor, T., et al., *Diversion of phagosome trafficking by pathogenic Rhodococcus equi depends on mycolic acid chain length*. Cell Microbiol, 2013. **15**: p. 458-73.
83. Garton, N.J., et al., *A Novel Lipoarabinomannan from the Equine Pathogen Rhodococcus equi: Structure and Effect on Macrophage Cytokine Production*. Journal of Biological Chemistry, 2002. **277**(35): p. 31722-31733.
84. Wall, D.M., et al., *Isocitrate lyase activity is required for virulence of the intracellular pathogen Rhodococcus equi*. Infect Immun, 2005. **73**: p. 6736-41.
85. Darrah, P.A., et al., *Cooperation between reactive oxygen and nitrogen intermediates in killing of Rhodococcus equi by activated macrophages*. Infect Immun, 2000. **68**(6): p. 3587-93.

86. Pei, Y., et al., *Mutation and virulence assessment of chromosomal genes of Rhodococcus equi 103*. Can J Vet Res, 2007. **71**(1): p. 1-7.
87. Wessling-Resnick, M., *Nramp1 and Other Transporters Involved in Metal Withholding during Infection*. The Journal of Biological Chemistry, 2015. **290**(31): p. 18984-18990.
88. Miranda-CasoLuengo, R., et al., *The Hydroxamate Siderophore Rhequichelin Is Required for Virulence of the Pathogenic Actinomycete Rhodococcus equi*. Infection and Immunity, 2012. **80**(12): p. 4106.
89. Miranda-CasoLuengo, R., et al., *The Intracellular Pathogen Rhodococcus equi Produces a Catecholate Siderophore Required for Saprophytic Growth*. Journal of Bacteriology, 2008. **190**(5): p. 1631.
90. Richards, J.C., *Stereochemical aspects of the antigenic determinants of bacterial polysaccharides: the Rhodococcus equi capsular polysaccharides*. Carbohydrate Polymers, 1994. **25**(4): p. 253-267.
91. Zhang, L. and K. Orth, *Virulence determinants for Vibrio parahaemolyticus infection*. Current Opinion in Microbiology, 2013. **16**(1): p. 70-77.
92. Broberg, C.A., T.J. Calder, and K. Orth, *Vibrio parahaemolyticus cell biology and pathogenicity determinants*. Microbes and Infection, 2011. **13**(12): p. 992-1001.
93. McCarter, L., *The multiple identities of Vibrio parahaemolyticus* J Mol Microbiol Biotechnol, 1999. **1**: p. 51-57.
94. Fujino, T., et al., *On the bacteriological examination of shirasu-food poisoning*. Med J Osaka Univ, 1953. **4**: p. 299-304.
95. Shinoda, S., *Sixty Years from the Discovery of Vibrio parahaemolyticus and Some Recollections*. Biocontrol Science, 2011. **16**(4): p. 129-137.
96. Newton, A., et al., *Increasing Rates of Vibriosis in the United States, 1996–2010: Review of Surveillance Data From 2 Systems*. Clinical Infectious Diseases, 2012. **54**(suppl\_5): p. S391-S395.
97. Elmahdi, S., L.V. DaSilva, and S. Parveen, *Antibiotic resistance of Vibrio parahaemolyticus and Vibrio vulnificus in various countries: A review*. Food Microbiology, 2016. **57**: p. 128-134.
98. Daniels, N.A., et al., *Vibrio parahaemolyticus infections in the United States, 1973-1998*. J Infect Dis, 2000. **181**(5): p. 1661-6.
99. *National Enteric Disease Surveillance: COVIS Annual Summary, 2014*. Centers for Disease Control and Prevention: Atlanta, Georgia, 2014. <https://www.cdc.gov/vibrio/surveillance.html>.
100. *Multistate Outbreak of Vibrio parahaemolyticus Infections Linked to Fresh Crab Meat Imported from Venezuela*. Center for Disease Control: Atlanta, Georgia, 2018. <https://www.cdc.gov/vibrio/investigations/vibriop-07-18/index.html>.

101. O'Boyle, N. and A. Boyd, *Manipulation of intestinal epithelial cell function by the cell contact-dependent type III secretion systems of Vibrio parahaemolyticus*. Front Cell Infect Microbiol, 2014. **3**: p. 114.
102. Ham, H. and K. Orth, *The role of type III secretion System 2 in Vibrio parahaemolyticus pathogenicity*. Journal of Microbiology, 2012. **50**(5): p. 719-725.
103. Gonzalez-Escalona, N., et al., *Genome sequence of a clinical O4:K12 serotype Vibrio parahaemolyticus strain 10329*. J Bacteriol, 2011. **10**: p. 10.1128/JB.05044-05011.
104. Raghunath, P., *Roles of thermostable direct hemolysin (TDH) and TDH-related hemolysin (TRH) in Vibrio parahaemolyticus*. Frontiers in Microbiology, 2015. **5**: p. 805.
105. Honda, T., et al., *The thermostable direct hemolysin of Vibrio parahaemolyticus is a pore-forming toxin*. Can J Microbiol, 1992. **38**(11): p. 1175-80.
106. Matsuda, S., et al., *Association of Vibrio parahaemolyticus Thermostable Direct Hemolysin with Lipid Rafts Is Essential for Cytotoxicity but Not Hemolytic Activity*. Infection and Immunity, 2010. **78**(2): p. 603.
107. Yanagihara, I., et al., *Structure and Functional Characterization of Vibrio parahaemolyticus Thermostable Direct Hemolysin*. Journal of Biological Chemistry, 2010. **285**(21): p. 16267-16274.
108. Takahashi, A., et al., *Cl(-) secretion in colonic epithelial cells induced by the vibrio parahaemolyticus hemolytic toxin related to thermostable direct hemolysin*. Infect Immun, 2000. **68**(9): p. 5435-38.
109. Honda, T., Y. Ni, and T. Miwatani, *Purification and characterization of a hemolysin produced by a clinical isolate of Kanagawa phenomenon-negative Vibrio parahaemolyticus and related to the thermostable direct hemolysin*. Infect Immun, 1988. **56**(4): p. 961-65.
110. Krachler, A.M., H. Ham, and K. Orth, *Outer membrane adhesion factor multivalent adhesion molecule 7 initiates host cell binding during infection by Gram-negative pathogens*. Proceedings of the National Academy of Sciences, 2011. **108**(28): p. 11614.
111. Krachler, A.M. and K. Orth, *Functional Characterization of the Interaction between Bacterial Adhesin Multivalent Adhesion Molecule 7 (MAM7) Protein and Its Host Cell Ligands*. Journal of Biological Chemistry, 2011. **286**(45): p. 38939-38947.
112. Park, K.S., et al., *Functional characterization of two type III secretion systems of Vibrio parahaemolyticus*. Infection and immunity, 2004. **72**(11): p. 6659-65.
113. Okada, N., et al., *Presence of genes for type III secretion system 2 in Vibrio mimicus strains*. BMC Microbiology, 2010. **10**: p. 302-302.
114. Okada, N., et al., *Identification and Characterization of a Novel Type III Secretion System in Vibrio parahaemolyticus Strain TH3996 Reveal Genetic Lineage and Diversity of Pathogenic Machinery beyond the Species Level*. Infection and Immunity, 2009. **77**(2): p. 904.

115. Salomon, D., et al., *Vibrio parahaemolyticus* Type VI Secretion System 1 Is Activated in Marine Conditions to Target Bacteria, and Is Differentially Regulated from System 2. PLOS ONE, 2013. **8**(4): p. e61086.
116. Yu, Y., et al., Putative type VI secretion systems of *Vibrio parahaemolyticus* contribute to adhesion to cultured cell monolayers. Archives of Microbiology, 2012. **194**(10): p. 827-835.
117. Boyd, E.F., et al., Molecular analysis of the emergence of pandemic *Vibrio parahaemolyticus*. BMC Microbiology, 2008. **8**: p. 110-110.
118. Wang, L., et al., Cell Density- and Quorum Sensing-Dependent Expression of Type VI Secretion System 2 in *Vibrio parahaemolyticus*. PLOS ONE, 2013. **8**(8): p. e73363.
119. Zhang, Y., et al., Transcriptional Regulation of the Type VI Secretion System 1 Genes by Quorum Sensing and ToxR in *Vibrio parahaemolyticus*. Frontiers in Microbiology, 2017. **8**: p. 2005.
120. Galán, J.E. and G. Waksman, Protein-Injection Machines in Bacteria. Cell, 2018. **172**(6): p. 1306-1318.
121. Ono, T., et al., Identification of proteins secreted via *Vibrio parahaemolyticus* type III secretion system 1. Infection and immunity, 2006. **74**(2): p. 1032-42.
122. Zhou, X., M.E. Konkel, and D.R. Call, Regulation of type III secretion system 1 gene expression in *Vibrio parahaemolyticus* is dependent on interactions between ExsA, ExsC, and ExsD. Virulence, 2010. **1**(4): p. 260-272.
123. Burdette, D.L., et al., *Vibrio parahaemolyticus* orchestrates a multifaceted host cell infection by induction of autophagy, cell rounding, and then cell lysis. Proceedings of the National Academy of Sciences of the United States of America, 2008. **105**(34): p. 12497-502.
124. Burdette, D.L., J. Seemann, and K. Orth, *Vibrio* VopQ induces PI3-kinase-independent autophagy and antagonizes phagocytosis. Molecular Microbiology, 2009. **73**(4): p. 639-49.
125. Sreelatha, A., et al., *Vibrio* effector protein, VopQ, forms a lysosomal gated channel that disrupts host ion homeostasis and autophagic flux. Proc Natl Acad Sci U S A, 2013. **110**(28): p. 11559-64.
126. Yarbrough, M.L., et al., AMPylation of Rho GTPases by *Vibrio* VopS disrupts effector binding and downstream signaling. Science, 2009. **323**(5911): p. 269-72.
127. Hall, A., Rho family GTPases. Biochemical Society Transactions, 2012. **40**(6): p. 1378-82.
128. Broberg, C.A., et al., A *Vibrio* effector protein is an inositol phosphatase and disrupts host cell membrane integrity. Science, 2010. **329**(5999): p. 1660-2.
129. Li, P., et al., Bile salt receptor complex activates a pathogenic type III secretion system. Elife, 2016. **5**(e15718): p. doi: 10.7554/eLife.15718.

130. Gotoh, K., et al., *Bile acid-induced virulence gene expression of Vibrio parahaemolyticus reveals a novel therapeutic potential for bile acid sequestrants*. PLoS One, 2010. **5**(e13365): p. doi:10.1371/journal.pone.0013365.
131. Zhang, L., et al., *Type III Effector VopC Mediates Invasion for Vibrio Species*. Cell Reports, 2012. **1**(5): p. 453-460.
132. Kodama, T., et al., *Identification and characterization of VopT, a novel ADP-ribosyltransferase effector protein secreted via the Vibrio parahaemolyticus type III secretion system 2*. Cellular Microbiology, 2007. **9**(11): p. 2598-2609.
133. Trosky, J.E., et al., *VopA Inhibits ATP Binding by Acetylating the Catalytic Loop of MAPK Kinases*. Journal of Biological Chemistry, 2007. **282**(47): p. 34299-34305.
134. Nishimura, M., et al., *A repeat unit of Vibrio diarrheal T3S effector subverts cytoskeletal actin homeostasis via binding to interstrand region of actin filaments*. Sci Reps, 2015. **5**: p. 10870.
135. Liverman, A.D., et al., *Arp2/3-independent assembly of actin by Vibrio type III effector VopL*. Proc Natl Acad Sci U S A, 2007. **104**(43): p. 17117-22.
136. Schu, P., et al., *Phosphatidylinositol 3-kinase encoded by yeast VPS34 gene essential for protein sorting*. Science, 1993. **260**: p. 88-91.
137. Matsuda, S., et al., *A cytotoxic type III secretion effector of Vibrio parahaemolyticus targets vacuolar H<sup>+</sup>-ATPase subunit c and ruptures host cell lysosomes*. PLoS Pathog, 2012. **8**(7): p. e1002803.
138. Matlawska-Wasowska, K., et al., *The Vibrio parahaemolyticus Type III Secretion Systems manipulate host cell MAPK for critical steps in pathogenesis*. BMC microbiology, 2010. **10**: p. 329.
139. Shimohata, T., et al., *Vibrio parahaemolyticus infection induces modulation of IL-8 secretion through dual pathway via VP1680 in Caco-2 cells*. The Journal of infectious diseases, 2011. **203**(4): p. 537-44.
140. Bickel, M., *The role of interleukin-8 in inflammation and mechanisms of regulation*. J Periodontol, 1993. **64**(5): p. 456-60.
141. Siggers, K.A. and C.F. Lesser, *The Yeast Saccharomyces cerevisiae: a versatile model system for the identification and characterization of bacterial virulence proteins*. Cell Host Microbe, 2008. **4**(1): p. 8-15.
142. Campodonico, E.M., L. Chesnel, and C.R. Roy, *A yeast genetic system for the identification and characterization of substrate proteins transferred into host cells by the Legionella pneumophila Dot/Icm system*. Mol Microbiol, 2005. **56**(4): p. 918-33.
143. Lesser, C.F. and S.I. Miller, *Expression of microbial virulence proteins in Saccharomyces cerevisiae models mammalian infection*. EMBO J, 2001. **20**(8): p. 1840-9.

144. Slagowski, N.L., et al., *A functional genomic yeast screen to identify pathogenic bacterial proteins*. PLoS Pathog, 2008. **4**(1): p. e9.
145. Aridor, M. and L. Hannan, *Traffic Jam: A Compendium of Human Diseases that Affect Intracellular Transport Processes*. Traffic, 2000. **1**: p. 836-851.
146. Feyder, S., et al., *Membrane trafficking in the yeast *Saccharomyces cerevisiae* model*. Int J Mol Sci, 2015. **16**(1): p. 1509-25.
147. Gomez-Navarro, N. and E. Miller, *Protein sorting at the ER-Golgi interface*. J Cell Biol, 2016. **215**(6): p. 769-778.
148. Bowers, K. and T.H. Stevens, *Protein transport from the late Golgi to the vacuole in the yeast *Saccharomyces cerevisiae**. Biochim Biophys Acta, 2005. **1744**(3): p. 438-54.
149. Phan, H., et al., *The *Saccharomyces cerevisiae* APS1 gene encodes a homolog of the small subunit of the mammalian clathrin AP-1 complex: evidence for functional interaction with clathrin at the Golgi complex*. EMBO J, 1994. **13**(7): p. 1706-1717.
150. Conibear, E. and T.H. Stevens, *Multiple sorting pathways between the late Golgi and the vacuole in yeast*. Biochim Biophys Acta, 1998. **1404**: p. 211-230.
151. Marcusson, E., et al., *The sorting receptor for yeast vacuolar carboxypeptidase Y is encoded by the VPS10 gene*. Cell, 1994. **77**: p. 579-586.
152. Schuh, A.L. and A. Audhya, *The ESCRT machinery: from the plasma membrane to endosomes and back again*. Crit Rev Biochem Mol Biol, 2014. **49**(3): p. 242-61.
153. Katzmann, D., M. Babst, and S. Emr, *Ubiquitin-Dependent Sorting into the Multivesicular Body Pathway Requires the Function of a Conserved Endosomal Protein Sorting Complex, ESCRT-I*. Cell, 2001. **106**: p. 145-155.
154. MacDonald, C., D. Stringer, and R. Piper, *Sna3 is an Rsp5 adaptor protein that relies on ubiquitination for its MVB sorting*. Traffic, 2012. **13**(4): p. 586-98.
155. Cowles, C., et al., *Novel Golgi to vacuole delivery pathway in yeast: identification of a sorting determinant and required transport component*. EMBO J, 1997. **16**(10): p. 2769-2782.
156. He, B. and W. Guo, *The exocyst complex in polarized exocytosis*. Curr Opin Cell Biol, 2009. **21**(4): p. 537-42.
157. TerBush, D., et al., *The Exocyst is a multiprotein complex required for exocytosis in *Saccharomyces cerevisiae**. EMBO J, 1996. **15**(23): p. 6483-6494.
158. Boyd, C., et al., *Vesicles carry most exocyst subunits to exocytic sites marked by the remaining two subunits, Sec3p and Exo70p*. J Cell Biol, 2004. **167**(5): p. 889-901.
159. Tokarev, A., A. Alfonso, and N. Segev, *Overview of Intracellular Compartments and Trafficking Pathways*. Madame Curie Bioscience Database, 2013. **Landes Bioscience; 2000-2013**.

160. Moreau, V., et al., *The Yeast Actin-related Protein Arp2p Is Required for the Internalization Step of Endocytosis*. Mol Biol Cell, 1997. **8**: p. 1361-1373.
161. Madania, A., et al., *The Saccharomyces cerevisiae Homologue of Human Wiskott–Aldrich Syndrome Protein Las17p Interacts with the Arp2/3 Complex*. Mol Biol Cell, 1999. **10**: p. 3521-3538.
162. Munn, A., et al., *end5, end6, and end7: Mutations that Cause Actin Delocalization and Block the Internalization Step of Endocytosis in Saccharomyces cerevisiae*. Mol Biol Cell, 1995. **6**: p. 1721-1742.
163. Reggiori, F. and D.J. Klionsky, *Autophagic processes in yeast: mechanism, machinery and regulation*. Genetics, 2013. **194**(2): p. 341-61.
164. Deffieu, M., et al., *Glutathione participates in the regulation of mitophagy in yeast*. J Biol Chem, 2009. **284**(22): p. 14828-37.
165. Oku, M., et al., *Peroxisome degradation requires catalytically active sterol glucosyltransferase with a GRAM domain*. EMBO J, 2003. **22**(13): p. 3231-3241.
166. Roberts, P., et al., *Piecemeal microautophagy of nucleus in Saccharomyces cerevisiae*. Mol Biol Cell, 2003. **14**(1): p. 129-41.
167. Oda, M.N., et al., *Identification of a cytoplasm to vacuole targeting determinant in aminopeptidase I*. J Cell Biol, 1996. **132**: p. 999-1010.
168. Segui-Real, B., M. Martinez, and I.V. Sandoval, *Yeast aminopeptidase I is post-translationally sorted from the cytosol to the vacuole by a mechanism mediated by its N-terminal extension*. EMBO J, 1995. **14**: p. 5476-5484.
169. Scott, S., et al., *Cvt19 is a receptor for the cytoplasm-to-vacuole targeting pathway*. Mol Cell, 2001. **7**: p. 1131-1141.
170. Shintani, T., et al., *Mechanism of Cargo Selection in the Cytoplasm to Vacuole Targeting Pathway*. Dev Cell, 2002. **3**: p. 825-837.
171. Baba, M., et al., *Two distinct pathways for targeting proteins from the cytoplasm to the vacuole/lysosome*. J Cell Biol, 1997. **139**: p. 1687-1695.
172. Scott, S.V., et al., *Aminopeptidase I is targeted to the vacuole by a nonclassical vesicular mechanism*. J Cell Biol, 1997. **138**: p. 37-44.
173. Kim, J. and D. Klionsky, *Autophagy, Cytoplasm-to-vacuole targeting pathway, and pexophagy in yeast and mammalian cells* Annu Rev Biochem, 2000. **69**: p. 303-342.
174. Stenmark, H., *Rab GTPases as coordinators of vesicle traffic*. Nat Rev Mol Cell Biol, 2009. **10**(8): p. 513-25.

175. Bock, J., et al., *A genomic perspective on membrane compartment organization*. Nature, 2001. **409**: p. 839-841.
176. Muller, M.P. and R.S. Goody, *Molecular control of Rab activity by GEFs, GAPs and GDI*. Small GTPases, 2018. **9**(1-2): p. 5-21.
177. Kinsella, B. and W. Maltese, *rab GTP-binding proteins implicated in vesicular transport are isoprenylated in vitro at cysteines within a novel carboxyl-terminal motif*. J Biol Chem, 1991. **266**(13): p. 8540-4.
178. Khosravi-Far, R., et al., *Ras (CXXX) and Rab (CC/CXC) prenylation signal sequences are unique and functionally distinct*. J Biol Chem, 1992. **267**(34): p. 24363-8.
179. Fujimura, K., et al., *The Saccharomyces cerevisiae MSI4 gene encodes the yeast counterpart of component A of Rab geranylgeranyltransferase*. J Biol Chem, 1994. **269**: p. 9205-9212.
180. Waldherr, M., et al., *MRS6 — yeast homologue of the choroideaemia gene*. Nature Genetics, 1993. **3**: p. 193-194.
181. Stenmark, H., et al., *Inhibition of rab5 GTPase activity stimulates membrane fusion in endocytosis*. EMBO J, 1994. **13**: p. 1287-1296.
182. Pfeffer, S., *Structural clues to Rab GTPase functional diversity*. J Biol Chem, 2005. **280**: p. 15485-15488.
183. Ullrich, O., et al., *Membrane association of Rab5 mediated by GDP-dissociation inhibitor and accompanied by GDP/GTP exchange*. Nature, 1994. **368**(6467): p. 157-160.
184. Nakatsukasa, K., et al., *The nutrient stress-induced small GTPase Rab5 contributes to the activation of vesicle trafficking and vacuolar activity*. J Biol Chem, 2014. **289**(30): p. 20970-8.
185. Buvelot Frei, S., et al., *Bioinformatic and comparative localization of Rab proteins reveals functional insights into the uncharacterized GTPases Ypt10p and Ypt11p*. Mol Cell Biol, 2006. **26**(19): p. 7299-317.
186. Brocker, C., S. Engelbrecht-Vandre, and C. Ungermann, *Multisubunit tethering complexes and their role in membrane fusion*. Curr Biol, 2010. **20**(21): p. R943-52.
187. Chia, P.Z. and P.A. Gleeson, *Membrane tethering*. F1000Prime Rep, 2014. **6**: p. 74.
188. Balderhaar, H.J. and C. Ungermann, *CORVET and HOPS tethering complexes - coordinators of endosome and lysosome fusion*. J Cell Sci, 2013. **126**(Pt 6): p. 1307-16.
189. Peplowska, K., et al., *The CORVET Tethering Complex Interacts with the Yeast Rab5 Homolog Vps21 and Is Involved in Endo-Lysosomal Biogenesis*. Dev Cell, 2007. **12**(5): p. 739-750.
190. Seals, D.F., et al., *A Ypt/Rab effector complex containing the Sec1 homolog Vps33p is required for homotypic vacuole fusion*. Proc Natl Acad Sci U S A, 2000. **97**(17): p. 9402-9407.

191. Brocker, C., et al., *Molecular architecture of the multisubunit homotypic fusion and vacuole protein sorting (HOPS) tethering complex*. Proc Natl Acad Sci U S A, 2012. **109**(6): p. 1991-6.
192. Lurick, A., et al., *The Habc domain of the SNARE Vam3 interacts with the HOPS tethering complex to facilitate vacuole fusion*. J Biol Chem, 2015. **290**(9): p. 5405-13.
193. Sato, T.K., et al., *Class C Vps protein complex regulates vacuolar SNARE pairing and is required for vesicle docking/fusion*. Mol Cell, 2000. **6**(3): p. 661-71.
194. Robinson, J., T. Graham, and S. Emr, *A Putative Zinc Finger Protein, Saccharomyces cerevisiae Vps18p, Affects Late Golgi Functions Required for Vacuolar Protein Sorting and Efficient  $\alpha$ -Factor Prohormone Maturation*. Mol Cell Biol, 1991. **12**(12): p. 5813-5824.
195. Rieder, S. and S. Emr, *A Novel RING Finger Protein Complex Essential for a Late Step in Protein Transport to the Yeast Vacuole*. Mol Biol Cell, 1997. **8**: p. 2307-2327.
196. Nickerson, D.P., C.L. Brett, and A.J. Merz, *Vps-C complexes: gatekeepers of endolysosomal traffic*. Curr Opin Cell Biol, 2009. **21**(4): p. 543-51.
197. Baker, R.W., et al., *A direct role for the Sec1/Munc18-family protein Vps33 as a template for SNARE assembly*. Science, 2015. **349**(6252): p. 1111-4.
198. Stroupe, C., et al., *Purification of active HOPS complex reveals its affinities for phosphoinositides and SNARE Vam7p*. EMBO J, 2006. **25**(8): p. 1579-89.
199. Kramer, L. and C. Ungermann, *HOPS drives vacuole fusion by binding the vacuolar SNARE complex and the Vam7 PX domain via two distinct sites*. Mol Biol Cell, 2011. **22**(14): p. 2601-11.
200. Lobingier, B.T. and A.J. Merz, *Sec1/Munc18 protein Vps33 binds to SNARE domains and the quaternary SNARE complex*. Mol Biol Cell, 2012. **23**(23): p. 4611-22.
201. Zick, M. and W. Wickner, *The tethering complex HOPS catalyzes assembly of the soluble SNARE Vam7 into fusogenic trans-SNARE complexes*. Mol Biol Cell, 2013. **24**: p. 3746-53.
202. Starai, V.J., C.M. Hickey, and W. Wickner, *HOPS proofreads the trans-SNARE complex for yeast vacuole fusion*. Mol Biol Cell, 2008. **19**(6): p. 2500-8.
203. Xu, H., et al., *HOPS prevents the disassembly of trans-SNARE complexes by Sec17p/Sec18p during membrane fusion*. EMBO J, 2010. **29**(12): p. 1948-60.
204. Nordmann, M., et al., *The Mon1-Ccz1 complex is the GEF of the late endosomal Rab7 homolog Ypt7*. Curr Biol, 2010. **20**(18): p. 1654-9.
205. Brett, C.L., et al., *Efficient termination of vacuolar Rab GTPase signaling requires coordinated action by a GAP and a protein kinase*. J Cell Biol, 2008. **182**(6): p. 1141-51.
206. Sun, B., et al., *The yeast casein kinase Yck3p is palmitoylated, then sorted to the vacuolar membrane with AP-3-dependent recognition of a YXXPhi adaptin sorting signal*. Mol Biol Cell, 2004. **15**(3): p. 1397-406.

207. Cabrera, M., et al., *Phosphorylation of a membrane curvature-sensing motif switches function of the HOPS subunit Vps41 in membrane tethering*. J Cell Biol, 2010. **191**(4): p. 845-59.
208. Cabrera, M., et al., *Vps41 phosphorylation and the Rab Ypt7 control the targeting of the HOPS complex to endosome-vacuole fusion sites*. Mol Biol Cell, 2009. **20**(7): p. 1937-48.
209. LaGrassa, T.J. and C. Ungermann, *The vacuolar kinase Yck3 maintains organelle fragmentation by regulating the HOPS tethering complex*. J Cell Biol, 2005. **168**(3): p. 401-14.
210. Angers, C.G. and A.J. Merz, *HOPS interacts with Apl5 at the vacuole membrane and is required for consumption of AP-3 transport vesicles*. Mol Biol Cell, 2009. **20**(21): p. 4563-74.
211. Plemel, R.L., et al., *Subunit organization and Rab interactions of Vps-C protein complexes that control endolysosomal membrane traffic*. Mol Biol Cell, 2011. **22**(8): p. 1353-63.
212. Andag, U. and H.D. Schmitt, *Dsl1p, an essential component of the Golgi-endoplasmic reticulum retrieval system in yeast, uses the same sequence motif to interact with different subunits of the COPI vesicle coat*. J Biol Chem, 2003. **278**: p. 51722-51734.
213. Zink, S., et al., *A link between ER tethering and COP-I vesicle uncoating*. Dev Cell, 2009. **17**: p. 403-416.
214. Whyte, J.R. and S. Munro, *The Sec34/35 Golgi transport complex is related to the exocyst, defining a family of complexes involved in multiple steps of membrane traffic*. Dev Cell, 2001. **1**: p. 527-537.
215. Conibear, E. and T.H. Stevens, *Vps52p, Vps53p, and Vps54p form a novel multisubunit complex required for protein sorting at the yeast late Golgi*. Mol Biol Cell, 2000. **11**: p. 305-323.
216. Wiederkehr, A., et al., *Functional specialization within a vesicle tethering complex: bypass of a subset of exocyst deletion mutants by Sec1p or Sec4p*. J Cell Biol, 2004. **167**: p. 875-887.
217. Sivaram, M.V., et al., *Dimerization of the exocyst protein Sec6p and its interaction with the t-SNARE Sec9p*. Biochemistry, 2005. **44**: p. 6302-6311.
218. Sacher, M., et al., *TRAPP, a highly conserved novel complex on the cis-Golgi that mediates vesicle docking and fusion*. EMBO J, 1998. **17**: p. 2494-2503.
219. Barrowman, J., M. Sacher, and S. Ferro-Novick, *TRAPP stably associates with the Golgi and is required for vesicle docking*. EMBO J, 2000. **19**: p. 862-869.
220. Jones, S., et al., *The TRAPP complex is a nucleotide exchanger for Ypt1 and Ypt31/32*. Mol Biol Cell, 2000. **11**: p. 4403-4411.
221. Cai, H., et al., *Mutants in trs120 disrupt traffic from the early endosome to the late Golgi*. J Cell Biol, 2005. **171**: p. 823-833.
222. Morozova, N., et al., *TRAPP II subunits are required for the specificity switch of a Ypt-Rab GEF*. Nat Cell Biol, 2006. **8**: p. 1263-1269.

223. Lynch-Day, M.A., et al., *Trs85 directs a Ypt1 GEF, TRAPPIII, to the phagophore to promote autophagy*. Proc Natl Acad Sci U S A, 2010. **107**: p. 7811-7816.
224. Wang, W., M. Sacher, and S. Ferro-Novick, *TRAPP stimulates guanine nucleotide exchange on Ypt1p*. J Cell Biol, 2000. **151**: p. 289-296.
225. Fasshauer, D., et al., *Conserved structural features of the synaptic fusion complex: SNARE proteins reclassified as Q- and R-SNAREs*. Proc Natl Acad Sci U S A, 1998. **95**: p. 15781-15786.
226. Söllner, T., et al., *A Protein Assembly-Disassembly Pathway In Vitro That May Correspond to Sequential Steps of Synaptic Vesicle Docking, Activation, and Fusion*. Cell, 1993. **75**: p. 409-418.
227. Sutton, R., et al., *Crystal structure of a SNARE complex involved in synaptic exocytosis at 2.4Å resolution*. Nature, 1998. **395**(6700): p. 347-353.
228. Hong, W., *SNAREs and traffic*. Biochim Biophys Acta, 2005. **1744**(2): p. 120-44.
229. Fernandez, I., et al., *Three-Dimensional Structure of an Evolutionarily Conserved N-Terminal Domain of Syntaxin 1A*. Cell, 1998. **94**: p. 841-849.
230. Misura, K., R. Scheller, and W. Weis, *Three-dimensional structure of the neuronal-Sec1-syntaxin 1a complex*. Nature, 2000. **404**: p. 356-362.
231. Paumet, F., et al., *Concerted auto-regulation in yeast endosomal t-SNAREs*. J Biol Chem, 2005. **280**(22): p. 21137-43.
232. Fukasawa, M., et al., *Localization and activity of the SNARE Ykt6 determined by its regulatory domain and palmitoylation*. Proc Natl Acad Sci U S A, 2004. **101**(14): p. 4815-4820.
233. Wickner, W., *Membrane fusion: five lipids, four SNAREs, three chaperones, two nucleotides, and a Rab, all dancing in a ring on yeast vacuoles*. Annu Rev Cell Dev Biol, 2010. **26**: p. 115-36.
234. Mayer, A., W. Wickner, and A. Haas, *Sec18p (NSF)-Driven Release of Sec17p ( $\alpha$ -SNAP) Can Precede Docking and Fusion of Yeast Vacuoles*. Cell, 1996. **85**: p. 83-94.
235. Kato, M. and W. Wickner, *Ergosterol is required for the Sec18/ATP-dependent priming step of homotypic vacuole fusion*. EMBO J, 2001. **20**(15): p. 4035-40.
236. Barnard, R.J.O., A. Morgan, and R.D. Burgoyne, *Stimulation of NSF ATPase Activity by  $\alpha$ -SNAP Is Required for SNARE Complex Disassembly and Exocytosis*. The Journal of Cell Biology, 1997. **139**(4): p. 875.
237. Subramaniam, V.N., E. Loh, and W. Hong, *N-Ethylmaleimide-sensitive Factor (NSF) and  $\alpha$ -Soluble NSF Attachment Proteins (SNAP) Mediate Dissociation of GS28-Syntaxin 5 Golgi SNAP Receptors (SNARE) Complex*. Journal of Biological Chemistry, 1997. **272**(41): p. 25441-25444.
238. Collins, K.M. and W. Wickner, *trans-SNARE complex assembly and yeast vacuole membrane fusion*. Proc Natl Acad Sci U S A, 2007. **104**(21): p. 8755-8760.

239. Burri, L. and T. Lithgow, *A Complete Set of SNAREs in Yeast*. Traffic, 2004. **5**(1): p. 45-52.
240. Liu, Y. and V.A. Bankaitis, *Phosphoinositide phosphatases in cell biology and disease*. Prog Lipid Res, 2010. **49**(3): p. 201-17.
241. Huijbregts, R., L. Topalof, and V.A. Bankaitis, *Lipid Metabolism and Regulation of Membrane Trafficking*. Traffic, 2000. **1**: p. 195-202.
242. Burd, C., M. Babst, and S.D. Emr, *Novel pathways, membrane coats and PI kinase regulation in yeast lysosomal trafficking*. Semin Cell Dev Biol, 1998. **9**(527-533).
243. Di Paolo, G. and P. De Camilli, *Phosphoinositides in cell regulation and membrane dynamics*. Nature, 2006. **443**(7112): p. 651-7.
244. Kutateladze, T.G., *Phosphatidylinositol 3-phosphate recognition and membrane docking by the FYVE domain*. Biochim Biophys Acta, 2006. **1761**(8): p. 868-77.
245. Simonsen, A., et al., *EEA1 links PI(3)K function to rab5 regulation of endosome fusion*. Nature, 1998. **394**: p. 494-498.
246. Tall, G., et al., *The phosphatidylinositol 3-phosphate binding protein Vac1p interacts with a Rab GTPase and a Sec1p homologue to facilitate vesicle-mediated vacuolar protein sorting*. Mol Biol Cell, 1999. **10**: p. 1873-79.
247. Weisman, L. and W. Wickner, *Molecular characterization of VAC1, a gene required for vacuolar inheritance and vacuole protein sorting*. J Biol Chem, 1992. **267**(618-23).
248. Piper, R., et al., *VPS27 controls vacuolar and endocytic traffic through a prevacuolar compartment in Saccharomyces cerevisiae*. J Cell Biol, 1995. **131**: p. 603-617.
249. Cheever, M., et al., *Phox domain interaction with PtdIns(3)P targets the Vam7 t-SNARE to vacuole membranes*. Nat Cell Biol, 2001. **3**: p. 613-618.
250. He, B., et al., *Exo70 interacts with phospholipids and mediates the targeting of the exocyst to the plasma membrane*. EMBO J, 2007. **26**: p. 4053-65.
251. Zhang, X., et al., *Membrane association and functional regulation of Sec3 by phospholipids and Cdc42*. J Cell Biol, 2008. **180**: p. 145-158.
252. Baek, K., et al., *Structure-function study of the N-terminal domain of exocyst subunit Sec3*. J Biol Chem, 2010. **285**(14): p. 10424-33.
253. Harlan, J., et al., *Pleckstrin homology domains bind to phosphatidylinositol-4,5-bisphosphate*. Nature, 1994. **371**: p. 168-170.
254. Desrivieres, S., et al., *MSS4, a phosphatidylinositol-4-phosphate 5-kinase required for organization of the actin cytoskeleton in Saccharomyces cerevisiae*. J Biol Chem, 1998. **273**(25): p. 15787-93.

255. Mayer, A., et al., *Phosphatidylinositol 4,5-Bisphosphate Regulates Two Steps of Homotypic Vacuole Fusion*. Mol Biol Cell, 2000. **11**: p. 807-17.
256. Audhya, A., M. Foti, and S.D. Emr, *Distinct Roles for the Yeast Phosphatidylinositol 4-Kinases, Stt4p and Pik1p, in Secretion, Cell Growth, and Organelle Membrane Dynamics*. Mol Biol Cell, 2000. **11**(8): p. 2673-89.
257. DeMatteis, M., A. Di Campli, and A. Godi, *The role of the phosphoinositides at the Golgi complex*. Biochim Biophys Acta, 2005. **1744**: p. 396-405.
258. Gaynor, E., et al., *ARF is required for maintenance of yeast Golgi and endosome structure and function*. Mol Biol Cell, 1998. **9**: p. 653-670.
259. Dove, S., et al., *Svp1p defines a family of phosphatidylinositol 3,5-bisphosphate effectors*. EMBO J, 2004. **23**(9): p. 1922-33.
260. Duncan, M., G. Costaguta, and G. Payne, *Yeast epsin-related proteins required for Golgi-endosome traffic define a gamma-adaptin ear-binding motif*. Nat Cell Biol, 2003. **5**: p. 77-81.
261. Legendre-Guillemain, V., et al., *ENTH/ANTH proteins and clathrin-mediated membrane budding*. J Cell Sci, 2004. **117**: p. 9-18.
262. Eugster, A., et al., *Ent5p is required with Ent3p and Vps27p for ubiquitin-dependent protein sorting into the multivesicular body*. Mol Biol Cell, 2004. **15**: p. 3031-41.
263. Friant, S., et al., *Ent3p Is a PtdIns(3,5)P2 effector required for protein sorting to the multivesicular body*. Dev Cell, 2003. **5**: p. 499-511.
264. Jun, Y., R.A. Fratti, and W. Wickner, *Diacylglycerol and its formation by phospholipase C regulate Rab- and SNARE-dependent yeast vacuole fusion*. J Biol Chem, 2004. **279**(51): p. 53186-95.
265. Mima, J. and W. Wickner, *Complex lipid requirements for SNARE- and SNARE chaperone-dependent membrane fusion*. J Biol Chem, 2009. **284**(40): p. 27114-22.
266. Mima, J., et al., *Reconstituted membrane fusion requires regulatory lipids, SNAREs and synergistic SNARE chaperones*. EMBO J, 2008. **27**(15): p. 2031-42.
267. Mima, J. and W. Wickner, *Phosphoinositides and SNARE chaperones synergistically assemble and remodel SNARE complexes for membrane fusion*. Proc Natl Acad Sci U S A, 2009. **106**(38): p. 16191-96.
268. Weber, T., et al., *SNAREpins: minimal machinery for membrane fusion*. Cell, 1998. **92**: p. 759-772.
269. Ohya, T., et al., *Reconstitution of Rab- and SNARE-dependent membrane fusion by synthetic endosomes*. Nature, 2009. **459**: p. 1091-97.
270. Wang, L., et al., *Hierarchy of protein assembly at the vertex ring domain for yeast vacuole docking and fusion*. J Cell Biol, 2003. **160**(3): p. 365-74.

271. Jun, Y. and W. Wickner, *Assays of vacuole fusion resolve the stages of docking, lipid mixing, and content mixing*. Proceedings of the National Academy of Sciences, 2007. **104**: p. 13010-13015.
272. Wang, L., et al., *Vacuole fusion at a ring of vertex docking sites leaves membrane fragments within the organelle* Cell, 2002. **108**(357-69).
273. Mattie, S., et al., *How and why intraluminal membrane fragments form during vacuolar lysosome fusion*. Mol Biol Cell, 2017. **28**(2): p. 309-321.
274. Chernomordik, L. and M. Kozlov, *Mechanics of membrane fusion*. Nat Struct Mol Biol, 2008. **15**(7): p. 675-683.
275. Warner, J. and B. O'Shaughnessy, *Evolution of the Hemifused Intermediate on the Pathway to Membrane Fusion*. Biophys J, 2012. **103**(4): p. 689-701.
276. Risselada, H., G. Bubnis, and H. Grubmuller, *Expansion of the fusion stalk and its implication for biological membrane fusion*. Proc Natl Acad Sci U S A, 2014. **111**(30): p. 11043-48.
277. Li, S.C. and P.M. Kane, *The yeast lysosome-like vacuole: endpoint and crossroads*. Biochim Biophys Acta, 2009. **1793**(4): p. 650-63.
278. Preston, R., R. Murphy, and E. Jones, *Assay of vacuolar pH in yeast and identification of acidification-defective mutants* Proc Natl Acad Sci U S A, 1989. **86**: p. 7027-31.
279. Yamashiro, C., et al., *Role of vacuolar acidification in protein sorting and zymogen activation: a genetic analysis of the yeast vacuolar proton-translocating ATPase*. Mol Cell Biol, 1990. **10**: p. 3737-49.
280. Hecht, K.A., A.F. O'Donnell, and J.L. Brodsky, *The proteolytic landscape of the yeast vacuole*. Cell Logist, 2014. **4**(1): p. e28023.
281. Klionsky, D.J., P.K. Herman, and S.D. Emr, *The Fungal Vacuole: Composition, Function, and Biogenesis*. Microbiol Rev, 1990. **54**(3): p. 266-292.
282. Haas, A., *A quantitative assay to measure homotypic vacuole fusion in vitro*. Methods in Cell Science, 1995. **17**(4): p. 283-294.
283. Russnak, R., D. Konczal, and S.L. McIntire, *A Family of Yeast Proteins Mediating Bidirectional Vacuolar Amino Acid Transport*. Journal of Biological Chemistry, 2001. **276**(26): p. 23849-23857.
284. Thomas, M.R. and E.K. O'Shea, *An intracellular phosphate buffer filters transient fluctuations in extracellular phosphate levels*. Proceedings of the National Academy of Sciences of the United States of America, 2005. **102**(27): p. 9565-9570.
285. Freimoser, F.M., et al., *Systematic screening of polyphosphate (poly P) levels in yeast mutant cells reveals strong interdependence with primary metabolism*. Genome Biology, 2006. **7**(11): p. R109-R109.

286. Carroll, A.S. and E.K. O'Shea, *Pho85 and signaling environmental conditions*. Trends in Biochemical Sciences, 2002. **27**(2): p. 87-93.
287. Denis, V. and M.S. Cyert, *Internal Ca(2+) release in yeast is triggered by hypertonic shock and mediated by a TRP channel homologue*. The Journal of Cell Biology, 2002. **156**(1): p. 29-34.
288. Yoshimoto, H., et al., *Genome-wide Analysis of Gene Expression Regulated by the Calcineurin/Crz1p Signaling Pathway in Saccharomyces cerevisiae*. Journal of Biological Chemistry, 2002. **277**(34): p. 31079-31088.
289. Cyert, M.S., *Calcineurin signaling in Saccharomyces cerevisiae: how yeast go crazy in response to stress*. Biochemical and Biophysical Research Communications, 2003. **311**(4): p. 1143-1150.
290. Dove, S.K., et al., *Osmotic stress activates phosphatidylinositol-3,5-bisphosphate synthesis*. Nature, 1997. **390**: p. 187.
291. Duex, J.E., F. Tang, and L.S. Weisman, *The Vac14p-Fig4p complex acts independently of Vac7p and couples PI3,5P(2) synthesis and turnover*. The Journal of Cell Biology, 2006. **172**(5): p. 693-704.
292. Dong, X.-p., et al., *PI(3,5)P(2) Controls Membrane Traffic by Direct Activation of Mucolipin Ca(2+) Release Channels in the Endolysosome*. Nature communications, 2010. **1**(4): p. 38.
293. Wilson, Z.N., et al., *PI(3,5)P2 controls vacuole potassium transport to support cellular osmoregulation*. Molecular Biology of the Cell, 2018. **29**(14): p. 1718-1731.
294. Cooke, F.T., et al., *The stress-activated phosphatidylinositol 3-phosphate 5-kinase Fab1p is essential for vacuole function in S. cerevisiae*. Curr Biol, 1998. **8**(0960-9822 (Print)): p. 1219-22.
295. Dove, S., et al., *Vac14 controls PtdIns(3,5)P(2) synthesis and Fab1-dependent protein trafficking to the multivesicular body*. Curr Biol, 2002. **12**(0960-9822 (Print)): p. 885-93.
296. Bonangelino, C.J., et al., *Osmotic stress-induced increase of phosphatidylinositol 3,5-bisphosphate requires Vac14p, an activator of the lipid kinase Fab1p*. J Cell Biol, 2002. **156**(0021-9525 (Print)): p. 1015-28.
297. Yamamoto, A., et al., *Novel PI(4)P5-Kinase Homologue, Fab1p, Essential for Normal Vacuole Function and Morphology in Yeast*. Mol Biol Cell, 1995. **6**(525-539).
298. Efe, J.A., R.J. Botelho, and S.D. Emr, *The Fab1 phosphatidylinositol kinase pathway in the regulation of vacuole morphology*. Current Opinion in Cell Biology, 2005. **17**(4): p. 402-408.
299. Bonangelino, C.J., N.L. Catlett, and L.S. Weisman, *Vac7p, a novel vacuolar protein, is required for normal vacuole inheritance and morphology*. Mol Biol Cell, 1997. **17**(12): p. 6847-58.
300. Shaw, J.D., et al., *PtdIns(3,5)P2 is Required for Delivery of Endocytic Cargo into the Multivesicular Body*. Traffic, 2003. **4**(7): p. 479-490.

301. Fernandez-Borja, M., et al., *Multivesicular body morphogenesis requires phosphatidylinositol 3-kinase activity*. *Current Biology*, 1999. **9**(1): p. 55-58.
302. Odorizzi, G., M. Babst, and S.D. Emr, *Fab1p PtdIns(3)P 5-kinase function essential for protein sorting in the multivesicular body*. *Cell*, 1998. **95**(6): p. 847-58.
303. Sarry, J.E., et al., *Analysis of the vacuolar luminal proteome of Saccharomyces cerevisiae*. *FEBS J*, 2007. **274**(16): p. 4287-305.
304. Wiederhold, E., et al., *The yeast vacuolar membrane proteome*. *Mol Cell Proteomics*, 2009. **8**(2): p. 380-92.
305. Forgac, M., *Vacuolar ATPases: rotary proton pumps in physiology and pathophysiology*. *Nat Rev Mol Cell Biol*, 2007. **8**(11): p. 917-29.
306. Kitagawa, N., et al., *Stoichiometry of the Peripheral Stalk Subunits E and G of Yeast V1-ATPase Determined by Mass Spectrometry*. *Journal of Biological Chemistry*, 2008. **283**(6): p. 3329-3337.
307. Couoh-Cardel, S., et al., *Yeast V-ATPase Proteolipid Ring Acts as a Large-conductance Transmembrane Protein Pore*. *Sci Reps*, 2016. **6**(24774).
308. Benlekbir, S., S.A. Bueler, and J.L. Rubinstein, *Structure of the vacuolar-type ATPase from Saccharomyces cerevisiae at 11-Å resolution*. *Nature Structural & Molecular Biology*, 2012. **19**: p. 1356.
309. Cotter, K., et al., *Recent Insights into the Structure, Regulation, and Function of the V-ATPases*. *Trends Biochem Sci*, 2015. **40**(10): p. 611-622.
310. Maher, M.J., et al., *Crystal structure of A3B3 complex of V-ATPase from Thermus thermophilus*. *The EMBO Journal*, 2009. **28**(23): p. 3771.
311. Oot, R.A., et al., *Breaking up and making up: The secret life of the vacuolar H(+) -ATPase*. *Protein Sci*, 2017. **26**(5): p. 896-909.
312. Zhao, J., S. Benlekbir, and J.L. Rubinstein, *Electron cryomicroscopy observation of rotational states in a eukaryotic V-ATPase*. *Nature*, 2015. **521**(7551): p. 241-5.
313. Drory, O., F. F., and N. Nelson, *Crystal structure of yeast V-ATPase subunit C reveals its stator function*. *EMBO Rep*, 2004. **5**(12): p. 1148-52.
314. Oot, R.A. and S. Wilkens, *Domain Characterization and Interaction of the Yeast Vacuolar ATPase Subunit C with the Peripheral Stator Stalk Subunits E and G*. *Journal of Biological Chemistry*, 2010. **285**(32): p. 24654-24664.
315. Oot, Rebecca A., et al., *Crystal Structure of the Yeast Vacuolar ATPase Heterotrimeric EGC head Peripheral Stalk Complex*. *Structure*, 2012. **20**(11): p. 1881-1892.
316. Oot, R.A. and S. Wilkens, *Subunit Interactions at the V1-Vo Interface in Yeast Vacuolar ATPase*. *Journal of Biological Chemistry*, 2012. **287**(16): p. 13396-13406.

317. Parsons, L.S. and S. Wilkens, *Probing Subunit-Subunit Interactions in the Yeast Vacuolar ATPase by Peptide Arrays*. PLOS ONE, 2012. **7**(10): p. e46960.
318. Hirata, R., et al., *VMA11 and VMA16 Encode Second and Third Proteolipid Subunits of the Saccharomyces cerevisiae Vacuolar Membrane H<sup>+</sup>-ATPase*. Journal of Biological Chemistry, 1997. **272**(8): p. 4795-4803.
319. Noumi, T., et al., *Mutational analysis of yeast vacuolar H<sup>(+)</sup>-ATPase*. Proceedings of the National Academy of Sciences, 1991. **88**(5): p. 1938-1942.
320. Roh, S.H., et al., *The 3.5-Å CryoEM Structure of Nanodisc-Reconstituted Yeast Vacuolar ATPase Vo Proton Channel*. Mol Cell, 2018. **69**(6): p. 993-1004 e3.
321. Kawasaki-Nishi, S., T. Nishi, and M. Forgac, *Arg-735 of the 100-kDa subunit a of the yeast V-ATPase is essential for proton translocation*. Proceedings of the National Academy of Sciences, 2001. **98**(22): p. 12397-12402.
322. Kawasaki-Nishi, S., et al., *The Amino-terminal Domain of the Vacuolar Proton-translocating ATPase a Subunit Controls Targeting and in Vivo Dissociation, and the Carboxyl-terminal Domain Affects Coupling of Proton Transport and ATP Hydrolysis*. Journal of Biological Chemistry, 2001. **276**(50): p. 47411-47420.
323. Finnigan, G.C., et al., *Sorting of the Yeast Vacuolar-type, Proton-translocating ATPase Enzyme Complex (V-ATPase): Identification of a Necessary and Sufficient Golgi/Endosomal Retention Signal in Stv1p*. Journal of Biological Chemistry, 2012. **287**(23): p. 19487-19500.
324. Bauerle, C., et al., *The Saccharomyces cerevisiae VMA6 gene encodes the 36-kDa subunit of the vacuolar H<sup>(+)</sup>-ATPase membrane sector*. Journal of Biological Chemistry, 1993. **268**(17): p. 12749-12757.
325. Bueler, S.A. and J.L. Rubinstein, *Vma9p Need Not Be Associated with the Yeast V-ATPase for Fully-Coupled Proton Pumping Activity in Vitro*. Biochemistry, 2015. **54**(3): p. 853-858.
326. Graham, L.A., K.J. Hill, and T.H. Stevens, *Assembly of the Yeast Vacuolar H<sup>+</sup>-ATPase Occurs in the Endoplasmic Reticulum and Requires a Vma12p/Vma22p Assembly Complex*. The Journal of Cell Biology, 1998. **142**(1): p. 39.
327. Hill, K.J. and T.H. Stevens, *Vma21p is a yeast membrane protein retained in the endoplasmic reticulum by a di-lysine motif and is required for the assembly of the vacuolar H<sup>(+)</sup>-ATPase complex*. Molecular Biology of the Cell, 1994. **5**(9): p. 1039-1050.
328. Hirata, R., et al., *VMA12 is essential for assembly of the vacuolar H<sup>(+)</sup>-ATPase subunits onto the vacuolar membrane in Saccharomyces cerevisiae*. Journal of Biological Chemistry, 1993. **268**(2): p. 961-967.
329. Moriyama, Y. and N. Nelson, *Cold inactivation of vacuolar proton-ATPases*. Journal of Biological Chemistry, 1989. **264**(6): p. 3577-3582.

330. Puopolo, K. and M. Forgac, *Functional reassembly of the coated vesicle proton pump*. Journal of Biological Chemistry, 1990. **265**(25): p. 14836-14841.
331. Gräf, R., W.R. Harvey, and H. Wiczorek, *Purification and Properties of a Cytosolic V1-ATPase*. Journal of Biological Chemistry, 1996. **271**(34): p. 20908-20913.
332. Parra, K.J., K.L. Keenan, and P.M. Kane, *The H Subunit (Vma13p) of the Yeast V-ATPase Inhibits the ATPase Activity of Cytosolic V1 Complexes*. Journal of Biological Chemistry, 2000. **275**(28): p. 21761-21767.
333. Zhang, J., Y. Feng, and M. Forgac, *Proton conduction and bafilomycin binding by the VO domain of the coated vesicle V-ATPase*. Journal of Biological Chemistry, 1994. **269**(38): p. 23518-23523.
334. Oot, R.A., et al., *Crystal structure of yeast V-ATPase in the autoinhibited state*. The EMBO Journal, 2016. **35**(15): p. 1694.
335. Kane, P.M., *Disassembly and reassembly of the yeast vacuolar H(+)-ATPase in vivo*. J Biol Chem, 1995. **270**: p. 17025-32.
336. Couoh-Cardel, S., E. Milgrom, and S. Wilkens, *Affinity Purification and Structural Features of the Yeast Vacuolar ATPase Vo Membrane Sector*. Journal of Biological Chemistry, 2015. **290**(46): p. 27959-27971.
337. Smardon, A.M. and P.M. Kane, *RAVE Is Essential for the Efficient Assembly of the C Subunit with the Vacuolar H+ATPase*. Journal of Biological Chemistry, 2007. **282**(36): p. 26185-26194.
338. Bond, S. and M. Forgac, *The Ras/cAMP/protein kinase A pathway regulates glucose-dependent assembly of the vacuole (H+)-ATPase in yeast*. J Biol Chem, 2008. **283**: p. 36513-21.
339. Lu, M., et al., *Physical interaction between aldolase and H+ATPase is essential for the assembly and activity of the proton pump*. J Biol Chem, 2007. **282**(34): p. 24495-503.
340. Chan, C.-Y. and K.J. Parra, *Yeast phosphofuctokinase-1 subunit Pfk2p is necessary for pH homeostasis and glucose-dependent vacuole ATPase reassembly* J Biol Chem, 2014. **289**: p. 19448-57.
341. Dechant, R., et al., *Cytosolic pH is a second messenger for glucose and regulates the PKA pathway through V-ATPase*. EMBO J, 2010. **29**(15): p. 2515-26.
342. Nelson, H. and N. Nelson, *Disruption of genes encoding subunits of yeast vacuolar H(+)-ATPase causes conditional lethality*. Proceedings of the National Academy of Sciences, 1990. **87**(9): p. 3503.
343. Ohya, Y., et al., *Calcium-sensitive cls mutants of Saccharomyces cerevisiae showing a Pet-phenotype are ascribable to defects of vacuolar membrane H(+)-ATPase activity*. Journal of Biological Chemistry, 1991. **266**(21): p. 13971-13977.
344. Huang, C. and A. Chang, *pH-dependent Cargo Sorting from the Golgi*. Journal of Biological Chemistry, 2011. **286**(12): p. 10058-10065.

345. Stevens, T.H. and M. Forgac, *Structure, function, and regulation of the vacuolar (H<sup>+</sup>)-ATPase*. Annual Review of Cell and Developmental Biology, 1997. **13**(1): p. 779-808.
346. Futai, M., et al., *Diverse Roles of Single Membrane Organelles: Factors Establishing the Acid Lumenal pH*. J Biochem, 1998. **124**: p. 259-267.
347. Peters, C., et al., *Trans-complex formation by proteolipid channels in the terminal phase of membrane fusion*. Nature, 2001. **409**: p. 581-588.
348. Ungermann, C., W. Wickner, and Z. Xu, *Vacuole acidification is required for trans-SNARE pairing, LMA1 release, and homotypic fusion*. Proceedings of the National Academy of Sciences, 1999. **96**(20): p. 11194.
349. Coonrod, E.M., et al., *Homotypic vacuole fusion in yeast requires organelle acidification and not the V-ATPase membrane domain*. Dev Cell, 2013. **27**(4): p. 462-8.
350. Desfougeres, Y., et al., *Organelle acidification negatively regulates vacuole membrane fusion in vivo*. Sci Reps, 2016. **6**: p. 29045.
351. Stroupe, C., et al., *Minimal membrane docking requirements revealed by reconstitution of Rab GTPase-dependent membrane fusion from purified components*. Proceedings of the National Academy of Sciences, 2009. **106**(42): p. 17626.
352. Peters, C. and A. Mayer, *Ca<sup>2+</sup>/calmodulin signals the completion of docking and triggers a late step of vacuole fusion*. Nature, 1998. **396**: p. 575-580.
353. Starai, V.J., et al., *Ion regulation of homotypic vacuole fusion in Saccharomyces cerevisiae*. J Biol Chem, 2005. **280**(17): p. 16754-62.
354. Merz, A.J. and W.T. Wickner, *Trans-SNARE interactions elicit Ca<sup>2+</sup> efflux from the yeast vacuole lumen*. The Journal of Cell Biology, 2004. **164**(2): p. 195.
355. Strasser, B., et al., *The V-ATPase proteolipid cylinder promotes the lipid-mixing stage of SNARE-dependent fusion of yeast vacuoles*. The EMBO Journal, 2011. **30**(20): p. 4126.
356. Reese, C., F. Heise, and A. Mayer, *Trans-SNARE pairing can precede a hemifusion intermediate in intracellular membrane fusion*. Nature, 2005. **436**: p. 410.
357. Bankaitis, V.A., L.M. Johnson, and S.D. Emr, *Isolation of yeast mutants defective in protein sorting to the vacuole*. Proc Natl Acad Sci U S A, 1986. **83**: p. 9075-79.
358. Rothman, J.H. and T.H. Stevens, *Protein sorting in yeast: mutants defective in vacuole biogenesis mislocalize vacuolar proteins into the late secretory pathway*. Cell, 1986. **47**(6): p. 1041-51.
359. Raymond, C.K., et al., *Morphological classification of the yeast vacuolar protein sorting mutants: evidence for a prevacuolar compartment in class E vps mutants*. Mol Biol Cell, 1992. **3**(12): p. 1389-402.

360. Pollard, T.D., L. Blanchoin, and R.D. Mullins, *Molecular mechanisms controlling actin filament dynamics in nonmuscle cells*. Annu Rev Biophys Biomol Struct, 2000. **29**: p. 545-576.
361. Pollard, T.D. and G.G. Borisy, *Cellular motility driven by assembly and disassembly of actin filaments*. Cell, 2003. **112**(453-465).
362. Adams, A.E. and J.R. Pringle, *Relationship of actin and tubulin distribution to bud growth in wild-type and morphogenetic-mutant Saccharomyces cerevisiae*. J Cell Biol, 1984. **98**: p. 934-945.
363. Kilmartin, J.V. and A.E. Adams, *Structural rearrangements of tubulin and actin during the cell cycle of the yeast Saccharomyces*. J Cell Biol, 1984. **98**: p. 922-933.
364. Marks, J., I.M. Hagan, and J.S. Hyams, *Growth polarity and cytokinesis in fission yeast: the role of cytoskeleton* J Cell Sci Suppl, 1986. **5**: p. 229-241.
365. Mishra, M., J. Huang, and M.K. Balasubramanian, *The yeast actin cytoskeleton*. FEMS Microbiol Rev, 2014. **38**(2): p. 213-27.
366. Pollard, T.D., *Regulation of Actin Filament Assembly by Arp2/3 Complex and Formins*. Annual Review of Biophysics and Biomolecular Structure, 2007. **36**(1): p. 451-477.
367. Goode, B.L., et al., *Activation of the Arp2/3 complex by the actin filament binding protein Abp1p*. J Cell Biol, 2001. **153**(3): p. 627-34.
368. Pruyne, D., et al., *Mechanisms of polarized growth and organelle segregation in yeast*. Annual Review of Cell and Developmental Biology, 2004. **20**(1): p. 559-591.
369. Buttery, S.M., et al., *Yeast Formins Bni1 and Bnr1 Utilize Different Modes of Cortical Interaction during the Assembly of Actin Cables*. Molecular Biology of the Cell, 2007. **18**(5): p. 1826-1838.
370. Oh, Y. and E. Bi, *Septin structure and function in yeast and beyond*. Trends in Cell Biology, 2011. **21**(3): p. 141-148.
371. Stolk, W.A., et al., *Between-Country Inequalities in the Neglected Tropical Disease Burden in 1990 and 2010, with Projections for 2020*. PLoS Negl Trop Dis, 2016. **10**(5): p. e0004560.
372. Taylor, M.J., A. Hoerauf, and M. Bockarie, *Lymphatic filariasis and onchocerciasis*. Lancet, 2010. **376**(9747): p. 1175-85.
373. Molyneux, D.H., et al., *Mass drug treatment for lymphatic filariasis and onchocerciasis*. Trends in Parasitology, 2003. **19**(11): p. 516-522.
374. Taylor, M.J., et al., *16S rDNA Phylogeny and Ultrastructural Characterization of Wolbachia Intracellular Bacteria of the Filarial Nematodes Brugia malayi, B. pahangi, and Wuchereria bancrofti*. Experimental Parasitology, 1999. **91**: p. 356-361.
375. Taylor, M.J., et al., *Anti-Wolbachia drug discovery and development: safe macrofilaricides for onchocerciasis and lymphatic filariasis*. Parasitology, 2014. **141**(1): p. 119-27.

376. Landmann, F., et al., *Asymmetric Wolbachia segregation during early Brugia malayi embryogenesis determines its distribution in adult host tissues*. PLoS Negl Trop Dis, 2010. **4**(7): p. e758.
377. Landmann, F., et al., *Anti-filarial activity of antibiotic therapy is due to extensive apoptosis after Wolbachia depletion from filarial nematodes*. PLoS Pathog, 2011. **7**(11): p. e1002351.
378. Melnikow, E., et al., *Interaction of a Wolbachia WSP-like protein with a nuclear-encoded protein of Brugia malayi*. Int J Parasitol, 2011. **41**(10): p. 1053-61.
379. Voth, D.E., L.J. Broederdorf, and J.G. Graham, *Bacterial Type IV secretion systems: versatile virulence machines*. Future Microbiol, 2012. **7**(2): p. 241-57.
380. Du, J., et al., *The type III secretion system apparatus determines the intracellular niche of bacterial pathogens*. Proc Natl Acad Sci U S A, 2016. **113**(17): p. 4794-9.
381. Renvoise, A., et al., *Intracellular Rickettsiales: Insights into manipulators of eukaryotic cells*. Trends Mol Med, 2011. **17**(10): p. 573-83.
382. Hicke, L. and R. Schekman, *Molecular machinery required for protein transport from the endoplasmic reticulum to the Golgi complex*. Bioessays, 1990. **12**(6): p. 253-8.
383. Pelham, H.R., *Insights from yeast endosomes*. Curr Opin Cell Biol, 2002. **14**(4): p. 454-62.
384. Stamnes, M., *Regulating the actin cytoskeleton during vesicular transport*. Curr Opin Cell Biol, 2002. **14**(4): p. 428-33.
385. Aleman, A., et al., *A yeast-based genetic screen for identification of pathogenic Salmonella proteins*. FEMS Microbiol Lett, 2009. **296**(2): p. 167-77.
386. Shohdy, N., et al., *Pathogen effector protein screening in yeast identifies Legionella factors that interfere with membrane trafficking*. Proc Natl Acad Sci U S A, 2005. **102**(13): p. 4866-71.
387. de Felipe, K.S., et al., *Legionella eukaryotic-like type IV substrates interfere with organelle trafficking*. PLoS Pathog, 2008. **4**(8): p. e1000117.
388. Sisko, J.L., et al., *Multifunctional analysis of Chlamydia-specific genes in a yeast expression system*. Mol Microbiol, 2006. **60**(1): p. 51-66.
389. Vida, T.A. and S.D. Emr, *A new vital stain for visualizing vacuolar membrane dynamics and endocytosis in yeast*. J Cell Biol, 1995. **128**(5): p. 779-92.
390. Katzmann, D.J., Sarkar, S., Chu, T., Audhya A., Emr, S.D, *Multivesicular Body Sorting: Ubiquitin Ligase Rsp5 Is Required for the Modification and Sorting of Carboxypeptidase S*. Molecular Biology of the Cell, 2004. **15**: p. 468-480.
391. de Felipe, K.S., et al., *Evidence for acquisition of Legionella type IV secretion substrates via interdomain horizontal gene transfer*. J Bacteriol, 2005. **187**(22): p. 7716-26.

392. Schulein, R., et al., *A bipartite signal mediates the transfer of type IV secretion substrates of Bartonella henselae into human cells*. Proc Natl Acad Sci U S A, 2005. **102**(3): p. 856-61.
393. Pan, X., et al., *Ankyrin repeat proteins comprise a diverse family of bacterial type IV effectors*. Science, 2008. **320**(5883): p. 1651-4.
394. Malek, J.A., et al., *Protein interaction mapping on a functional shotgun sequence of Rickettsia sibirica*. Nucleic Acids Res, 2004. **32**(3): p. 1059-64.
395. Bennuru, S., et al., *Stage-Specific Transcriptome and Proteome Analyses of the Filarial Parasite Onchocerca volvulus and Its Wolbachia Endosymbiont*. MBio, 2016. **7**(6).
396. Voronin, D., et al., *Autophagy regulates Wolbachia populations across diverse symbiotic associations*. Proc Natl Acad Sci U S A, 2012. **109**(25): p. E1638-46.
397. Bennett, T.L., et al., *LegC3, an effector protein from Legionella pneumophila, inhibits homotypic yeast vacuole fusion in vivo and in vitro*. PLoS One, 2013. **8**(2): p. e56798.
398. Seeley, E.S., et al., *Genomic analysis of homotypic vacuole fusion*. Mol Biol Cell, 2002. **13**(3): p. 782-94.
399. Reinke, A., et al., *Caffeine targets TOR complex I and provides evidence for a regulatory link between the FRB and kinase domains of Tor1p*. J Biol Chem, 2006. **281**(42): p. 31616-26.
400. Banuelos, M.G., et al., *Genomic analysis of severe hypersensitivity to hygromycin B reveals linkage to vacuolar defects and new vacuolar gene functions in Saccharomyces cerevisiae*. Curr Genet, 2010. **56**(2): p. 121-37.
401. Webb, G.C., et al., *Genetic interactions between a pep7 mutation and the PEP12 and VPS45 genes: evidence for a novel SNARE component in transport between the Saccharomyces cerevisiae Golgi complex and endosome*. Genetics, 1997. **147**(2): p. 467-78.
402. Kucharczyk R, et al., *Disruption of six novel yeast genes located on chromosome II reveals one gene essential for vegetative growth and two required for sporulation and conferring hypersensitivity to various chemicals*. Yeast, 1999. **15**(10B): p. 987-1000.
403. Matile, P. and A. Wiemken, *The vacuole as the lysosome of the yeast cell*. Arch Mikrobiol, 1967. **56**(2): p. 148-55.
404. Bone, N., et al., *Regulated vacuole fusion and fission in Schizosaccharomyces pombe: an osmotic response dependent on MAP kinases*. Curr Biol, 1998. **8**(3): p. 135-144.
405. Wada, Y., Y. Ohsumi, and Y. Anraku, *Genes for directing vacuolar morphogenesis in Saccharomyces cerevisiae: Isolation and characterization of two classes of vam mutants*. J Biol Chem, 1992. **267**(26): p. 18665-70.
406. Sreelatha, A., et al., *Vibrio effector protein VopQ inhibits fusion of V-ATPase-containing membranes*. Proc Natl Acad Sci U S A, 2015. **112**(1): p. 100-5.

407. Banta, L.M., et al., *Organelle assembly in yeast: characterization of yeast mutants defective in vacuolar biogenesis and protein sorting*. J Cell Biol, 1988. **107**(4): p. 1369-83.
408. Babst, M., *MVB vesicle formation: ESCRT-dependent, ESCRT-independent and everything in between*. Curr Opin Cell Biol, 2011. **23**(4): p. 452-7.
409. Wurmser, A.E., T.K. Sato, and S.D. Emr, *New Component of the Vacuolar Class C-Vps Complex Couples Nucleotide Exchange on the Ypt7 Gtpase to Snare-Dependent Docking and Fusion*. J Cell Biol, 2000. **151**(3): p. 551-562.
410. Peterson, M.R. and S.D. Emr, *The class C Vps complex functions at multiple stages of the vacuolar transport pathway*. Traffic, 2001. **2**(7): p. 476-86.
411. Veltman, D. and R. Insall, *WASP family proteins: their evolution and its physiological implications*. Mol Biol Cell, 2010. **16**: p. 2880-2893.
412. Welch, M., et al., *Interaction of human Arp2/3 complex and the Listeria monocytogenes ActA protein in actin filament nucleation*. Science, 1998. **281**(5373): p. 105-108.
413. Higgs, H.N. and T.D. Pollard, *Regulation of actin filament network formation through ARP2/3 complex: activation by a diverse array of proteins*. Annu Rev Biochem, 2001. **70**: p. 649-76.
414. Takenawa, T. and H. Miki, *WASP and WAVE family proteins: key molecules for rapid rearrangement of cortical actin filaments and cell movement*. J Cell Sci, 2001. **114**(Pt 10): p. 1801-9.
415. Gouin, E., et al., *The RickA protein of Rickettsia conorii activates the Arp2/3 complex*. Nature, 2004. **427**(6973): p. 457-61.
416. Mulholland, J., et al., *Ultrastructure of the yeast actin cytoskeleton and its association with the plasma membrane*. J Cell Biol, 1994. **125**(2): p. 381-91.
417. Kaksonen, M., Y. Sun, and D.G. Drubin, *A pathway for association of receptors, adaptors, and actin during endocytic internalization*. Cell, 2003. **115**(4): p. 475-87.
418. Michelot, A., et al., *Actin filament elongation in Arp2/3-derived networks is controlled by three distinct mechanisms*. Dev Cell, 2013. **24**(2): p. 182-95.
419. D'Silva, S., S.J. Haider, and E.M. Phizicky, *A domain of the actin binding protein Abp140 is the yeast methyltransferase responsible for 3-methylcytidine modification in the tRNA anti-codon loop*. RNA, 2011. **17**(6): p. 1100-10.
420. Colwill, K., et al., *In vivo analysis of the domains of yeast Rvs167p suggests Rvs167p function is mediated through multiple protein interactions*. Genetics, 1999. **152**(3): p. 881-93.
421. Gourlay, C.W., et al., *An interaction between Sla1p and Sla2p plays a role in regulating actin dynamics and endocytosis in budding yeast*. J Cell Sci, 2003. **116**(Pt 12): p. 2551-64.

422. Naqvi, S.N., et al., *The WASp homologue Las17p functions with the WIP homologue End5p/verprolin and is essential for endocytosis in yeast*. *Curr Biol*, 1998. **8**(17): p. 959-62.
423. Rodal, A.A., et al., *Negative regulation of yeast WASp by two SH3 domain-containing proteins*. *Curr Biol*, 2003. **13**(12): p. 1000-8.
424. Fernandez-Pinar, P., et al., *The Salmonella Typhimurium effector SteC inhibits Cdc42-mediated signaling through binding to the exchange factor Cdc24 in Saccharomyces cerevisiae*. *Mol Biol Cell*, 2012. **23**(22): p. 4430-43.
425. Zrieg, R., et al., *Genome-wide Screen of Pseudomonas aeruginosa in Saccharomyces cerevisiae Identifies New Virulence Factors*. *Front Cell Infect Microbiol*, 2015. **5**: p. 81.
426. Rice, D.W., Sheehan, K.B., Newton, I.L.G., *Large-Scale Identification of Wolbachia pipientis Effectors*. *Genome Biol. Evol.* , 2017. **9**(7): p. 1925-1937.
427. Lloubes, R., et al., *The Tol-Pal proteins of the Escherichia coli cell envelope: an energized system required for outer membrane integrity?* *Res Microbiol*, 2001. **152**(6): p. 523-9.
428. Michel, L.V., et al., *Dual orientation of the outer membrane lipoprotein Pal in Escherichia coli*. *Microbiology*, 2015. **161**(6): p. 1251-9.
429. Ireton, K. and P. Cossart, *Host-pathogen interactions during entry and actin-based movement of Listeria monocytogenes*. *Annu Rev Genet*, 1997. **31**: p. 113-38.
430. Sun, Y., A.C. Martin, and D.G. Drubin, *Endocytic internalization in budding yeast requires coordinated actin nucleation and myosin motor activity*. *Dev Cell*, 2006. **11**(1): p. 33-46.
431. Aghamohammadzadeh, S., R. Smaczynska-de, II, and K.R. Ayscough, *An Abp1-dependent route of endocytosis functions when the classical endocytic pathway in yeast is inhibited*. *PLoS One*, 2014. **9**(7): p. e103311.
432. Huckaba, T.M., et al., *Live cell imaging of the assembly, disassembly, and actin cable-dependent movement of endosomes and actin patches in the budding yeast, Saccharomyces cerevisiae*. *J Cell Biol*, 2004. **167**(3): p. 519-30.
433. Sahin, A., B. Daignan-Fornier, and I. Sagot, *Polarized growth in the absence of F-actin in Saccharomyces cerevisiae exiting quiescence*. *PLoS One*, 2008. **3**(7): p. e2556.
434. Pinyol, R., et al., *Regulation of N-WASP and the Arp2/3 complex by Abp1 controls neuronal morphology*. *PLoS One*, 2007. **2**(5): p. e400.
435. Landmann, F., et al., *Both asymmetric mitotic segregation and cell-to-cell invasion are required for stable germline transmission of Wolbachia in filarial nematodes*. *Biol Open*, 2012. **1**(6): p. 536-47.
436. Newton, I.L.G., Savytskyy O., Sheehan, K.B, *Wolbachia Utilize Host Actin for Efficient Maternal Transmission in Drosophila melanogaster*. *PLoS Pathog*, 2015. **11**(4): p. e1004798.

437. Sheehan, K.B., et al., *Identification and Characterization of a Candidate Wolbachia pipientis Type IV Effector That Interacts with the Actin Cytoskeleton*. MBio, 2016. **7**(4).
438. Whitaker, N., et al., *Chimeric Coupling Proteins Mediate Transfer of Heterologous Type IV Effectors through the Escherichia coli pKM101-Encoded Conjugation Machine*. J Bacteriol, 2016. **198**(19): p. 2701-2718.
439. Gao, C.Y. and J.L. Pinkham, *Tightly regulated, beta-estradiol dose-dependent expression system for yeast*. Biotechniques, 2000. **29**(6): p. 1226-31.
440. Lupas, A., M. Van Dyke, and J. Stock, *Predicting coiled coils from protein sequences*. Science, 1991. **252**(5009): p. 1162-1164.
441. Malek, J., et al., *Protein interaction mapping on a functional shotgun sequence of Rickettsia sibirica*. Nucleic Acids Res, 2004. **32**(3): p. 1059-1064.
442. McNatt, M., et al., *Direct Binding to Rsp5 Mediates Ubiquitin-independent Sorting of Sna3 via the Multivesicular Body Pathway*. Mol Biol Cell, 2007. **18**(2): p. 697-706.
443. Voth, W.P., Y.W. Jiang, and D.J. Stillman, *New 'marker swap' plasmids for converting selectable markers on budding yeast gene disruptions and plasmids*. Yeast, 2003. **20**(11): p. 985-93.
444. Lee, S., W. Lim, and K. Thorn, *Improved blue, green, and red fluorescent protein tagging vectors for S. cerevisiae*. PLoS One, 2013. **8**(7): p. e67902.
445. Schindelin, J., et al., *Fiji: an open-source platform for biological-image analysis*. Nat Methods, 2012. **9**(7): p. 676-82.
446. Schneider, C.A., W.S. Rasband, and K.W. Eliceiri, *NIH Image to ImageJ: 25 years of image analysis*. Nat Methods, 2012. **9**(7): p. 671-5.
447. Weinstock, D.M. and A.E. Brown, *Rhodococcus equi: an emerging pathogen*. Clin Infect Dis, 2002. **34**(10): p. 1379-85.
448. Giguere, S., et al., *Rhodococcus equi: clinical manifestations, virulence, and immunity*. J Vet Intern Med, 2011. **25**(6): p. 1221-30.
449. Wright, L.M., et al., *VapA of Rhodococcus equi binds phosphatidic acid*. Mol Microbiol, 2017. **107**(3): p. 428-44.
450. Putta, P., et al., *Phosphatidic acid binding proteins display differential binding as a function of membrane curvature stress and chemical properties*. Biochimica et Biophysica Acta (BBA) - Biomembranes, 2016. **1858**(11): p. 2709-2716.
451. Lemmon, M.A., *Membrane recognition by phospholipid-binding domains*. Nat Rev Mol Cell Biol, 2008. **9**(2): p. 99-111.
452. Krombach, F., et al., *Cell size of alveolar macrophages: an interspecies comparison*. Environmental Health Perspectives, 1997. **105**(Suppl 5): p. 1261-1263.

453. Hiesinger, P.R., et al., *The v-ATPase V0 subunit a1 is required for a late step in synaptic vesicle exocytosis in Drosophila*. Cell, 2005. **121**(4): p. 607-20.
454. Armstrong, J., *Yeast vacuoles: more than a model lysosome*. Trends Cell Biol, 2010. **20**(10): p. 580-5.
455. Strasser, B., et al., *The V-ATPase proteolipid cylinder promotes the lipid-mixing stage of SNARE-dependent fusion of yeast vacuoles*. EMBO J, 2011. **30**(20): p. 4126-41.
456. Bayer, M.J., et al., *Vacuole membrane fusion: V0 functions after trans-SNARE pairing and is coupled to the Ca<sup>2+</sup>-releasing channel*. J Cell Biol, 2003. **162**(2): p. 211-22.
457. Nishi, T. and M. Forgac, *The vacuolar (H<sup>+</sup>)-ATPases--nature's most versatile proton pumps*. Nat Rev Mol Cell Biol, 2002. **3**(2): p. 94-103.
458. van der Goot, F.G. and J. Gruenberg, *Intra-endosomal membrane traffic*. Trends Cell Biol, 2006. **16**(10): p. 514-21.
459. Williamson, W.R., et al., *A dual function of V0-ATPase a1 provides an endolysosomal degradation mechanism in Drosophila melanogaster photoreceptors*. J Cell Biol, 2010. **189**(5): p. 885-99.
460. Di Giovanni, J., et al., *V-ATPase membrane sector associates with synaptobrevin to modulate neurotransmitter release*. Neuron, 2010. **67**(2): p. 268-79.
461. Mijaljica, D., M. Prescott, and R.J. Devenish, *V-ATPase engagement in autophagic processes*. Autophagy, 2011. **7**(6): p. 666-8.
462. Peters, C., et al., *Trans-complex formation by proteolipid channels in the terminal phase of membrane fusion*. Nature, 2001. **409**(6820): p. 581-8.
463. Wang, D., et al., *Ca<sup>2+</sup>-Calmodulin regulates SNARE assembly and spontaneous neurotransmitter release via v-ATPase subunit V0a1*. J Cell Biol, 2014. **205**(1): p. 21-31.
464. El Far, O. and M. Seagar, *A role for V-ATPase subunits in synaptic vesicle fusion?* J Neurochem, 2011. **117**(4): p. 603-12.
465. Wang, D. and P.R. Hiesinger, *The vesicular ATPase: a missing link between acidification and exocytosis*. J Cell Biol, 2013. **203**(2): p. 171-3.
466. Matsuda, S., et al., *A cytotoxic type III secretion effector of Vibrio parahaemolyticus targets vacuolar H<sup>+</sup>-ATPase subunit c and ruptures host cell lysosomes*. PLoS pathogens, 2012. **8**(7): p. e1002803.
467. Haas, A., et al., *The GTPase Ypt7p of Saccharomyces cerevisiae is required on both partner vacuoles for the homotypic fusion step of vacuole inheritance*. EMBO J, 1995. **14**(21): p. 5258-70.
468. Collins, K.M. and W.T. Wickner, *Trans-SNARE complex assembly and yeast vacuole membrane fusion*. Proc Natl Acad Sci U S A, 2007. **104**(21): p. 8755-60.

469. Starai, V.J., Y. Jun, and W. Wickner, *Excess vacuolar SNAREs drive lysis and Rab bypass fusion*. Proc Natl Acad Sci U S A, 2007. **104**(34): p. 13551-8.
470. Sorensen, S.O., et al., *pH-dependent processing of yeast procarboxypeptidase Y by proteinase A in vivo and in vitro*. Eur J Biochem, 1994. **220**(1): p. 19-27.
471. Ungermann, C., W. Wickner, and Z. Xu, *Vacuole acidification is required for trans-SNARE pairing, LMA1 release, and homotypic fusion*. Proc Natl Acad Sci U S A, 1999. **96**(20): p. 11194-9.
472. Jun, Y. and W. Wickner, *Assays of vacuole fusion resolve the stages of docking, lipid mixing, and content mixing*. Proc Natl Acad Sci U S A, 2007. **104**(32): p. 13010-5.
473. Reese, C., F. Heise, and A. Mayer, *Trans-SNARE pairing can precede a hemifusion intermediate in intracellular membrane fusion*. Nature, 2005. **436**(7049): p. 410-4.
474. Ungermann, C., et al., *A vacuolar v-t-SNARE complex, the predominant form in vivo and on isolated vacuoles, is disassembled and activated for docking and fusion*. J Cell Biol, 1998. **140**(1): p. 61-9.
475. Mayer, A. and W. Wickner, *Docking of yeast vacuoles is catalyzed by the Ras-like GTPase Ypt7p after symmetric priming by Sec18p (NSF)*. J Cell Biol, 1997. **136**(2): p. 307-17.
476. Stroupe, C., et al., *Purification of active HOPS complex reveals its affinities for phosphoinositides and the SNARE Vam7p*. EMBO J, 2006. **25**(8): p. 1579-89.
477. Merz, A.J. and W.T. Wickner, *Trans-SNARE interactions elicit Ca<sup>2+</sup> efflux from the yeast vacuole lumen*. J Cell Biol, 2004. **164**(2): p. 195-206.
478. Peters, C. and A. Mayer, *Ca<sup>2+</sup>/calmodulin signals the completion of docking and triggers a late step of vacuole fusion*. Nature, 1998. **396**(6711): p. 575-80.
479. Ungermann, C. and W. Wickner, *Vam7p, a vacuolar SNAP-25 homolog, is required for SNARE complex integrity and vacuole docking and fusion*. EMBO J, 1998. **17**(12): p. 3269-76.
480. Fratti, R.A., et al., *Interdependent assembly of specific regulatory lipids and membrane fusion proteins into the vertex ring domain of docked vacuoles*. J Cell Biol, 2004. **167**(6): p. 1087-98.
481. Thorngren, N., et al., *A soluble SNARE drives rapid docking, bypassing ATP and Sec17/18p for vacuole fusion*. EMBO J, 2004. **23**(14): p. 2765-76.
482. Andreoli, T.E., M. Tieffenberg, and D.C. Tosteson, *The effect of valinomycin on the ionic permeability of thin lipid membranes*. J Gen Physiol, 1967. **50**(11): p. 2527-45.
483. Tosteson, D.C., et al., *The effect of valinomycin on potassium and sodium permeability of HK and LK sheep red cells*. J Gen Physiol, 1967. **50**(11): p. 2513-25.
484. Pressman, B.C., *Biological applications of ionophores*. Annu Rev Biochem, 1976. **45**: p. 501-30.

485. Perzov, N., et al., *Characterization of yeast V-ATPase mutants lacking Vph1p or Stv1p and the effect on endocytosis*. J Exp Biol, 2002. **205**(Pt 9): p. 1209-19.
486. Miesenbock, G., D.A. De Angelis, and J.E. Rothman, *Visualizing secretion and synaptic transmission with pH-sensitive green fluorescent proteins*. Nature, 1998. **394**(6689): p. 192-5.
487. Cooper, C.E., D. Bruce, and P. Nicholls, *Use of oxonol V as a probe of membrane potential in proteoliposomes containing cytochrome oxidase in the submitochondrial orientation*. Biochemistry, 1990. **29**(16): p. 3859-65.
488. Zucchi, P.C. and M. Zick, *Membrane fusion catalyzed by a Rab, SNAREs, and SNARE chaperones is accompanied by enhanced permeability to small molecules and by lysis*. Mol Biol Cell, 2011. **22**(23): p. 4635-46.
489. Mima, J. and W. Wickner, *Phosphoinositides and SNARE chaperones synergistically assemble and remodel SNARE complexes for membrane fusion*. Proc Natl Acad Sci U S A, 2009. **106**(38): p. 16191-6.
490. Zick, M., et al., *Membranes linked by trans-SNARE complexes require lipids prone to non-bilayer structure for progression to fusion*. Elife, 2014. **3**: p. e01879.
491. Hsin, I.L., et al., *Inhibition of lysosome degradation on autophagosome formation and responses to GMI, an immunomodulatory protein from Ganoderma microsporium*. Br J Pharmacol, 2012. **167**(6): p. 1287-300.
492. Alto, N.M. and K. Orth, *Subversion of cell signaling by pathogens*. Cold Spring Harb Perspect Biol, 2012. **4**(9): p. a006114.
493. Jones, E.W., *Vacuolar proteases and proteolytic artifacts in Saccharomyces cerevisiae*. Methods Enzymol, 2002. **351**: p. 127-50.
494. Haas, A., B. Conradt, and W. Wickner, *G-protein ligands inhibit in vitro reactions of vacuole inheritance*. J Cell Biol, 1994. **126**(1): p. 87-97.
495. Mumberg, D., R. Muller, and M. Funk, *Regulatable promoters of Saccharomyces cerevisiae: comparison of transcriptional activity and their use for heterologous expression*. Nucleic Acids Research, 1994. **22**(25): p. 5767-8.
496. Yoon, S., et al., *Yersinia effector YopJ inhibits yeast MAPK signaling pathways by an evolutionarily conserved mechanism*. Journal of Biological Chemistry, 2003. **278**(4): p. 2131-5.
497. Salomon, D., et al., *Effectors of animal and plant pathogens use a common domain to bind host phosphoinositides*. Nat Commun, 2013. **4**: p. 2973.
498. Slusarewicz, P., et al., *I2B is a small cytosolic protein that participates in vacuole fusion*. Proc Natl Acad Sci U S A, 1997. **94**(11): p. 5582-7.
499. Wang, L., et al., *Hierarchy of protein assembly at the vertex ring domain for yeast vacuole docking and fusion*. The Journal of cell biology, 2003. **160**(3): p. 365-74.

500. Starai, V.J., Y. Jun, and W. Wickner, *Excess vacuolar SNAREs drive lysis and Rab bypass fusion*. Proceedings of the National Academy of Sciences of the United States of America, 2007. **104**(34): p. 13551-8.
501. Haas, A. and W. Wickner, *Homotypic vacuole fusion requires Sec17p (yeast alpha-SNAP) and Sec18p (yeast NSF)*. EMBO J, 1996. **15**(13): p. 3296-305.
502. Haas, A., *A quantitative assay to measure homotypic fusion in vitro*. Methods Cell Sci, 1995. **17**: p. 283-294.
503. Li, J., et al., *Impediments to secretion of green fluorescent protein and its fusion from Saccharomyces cerevisiae*. Biotechnology progress, 2002. **18**(4): p. 831-8.
504. Zick, M. and W. Wickner, *Phosphorylation of the effector complex HOPS by the vacuolar kinase Yck3p confers Rab nucleotide specificity for vacuole docking and fusion*. Mol Biol Cell, 2012. **23**(17): p. 3429-37.
505. Arac, D., et al., *Close membrane-membrane proximity induced by Ca(2+)-dependent multivalent binding of synaptotagmin-1 to phospholipids*. Nature Structural and Molecular Biology, 2006. **13**(3): p. 209-17.
506. Chen, X., et al., *SNARE-mediated lipid mixing depends on the physical state of the vesicles*. Biophysical Journal, 2006. **90**(6): p. 2062-74.
507. Carpinone, E.M., et al., *Identification of putative effectors of the Type IV secretion system from the Wolbachia endosymbiont of Brugia malayi*. PLoS One, 2018.
508. Cheng, Z., et al., *Insights into the CtrA regulon in development of stress resistance in obligatory intracellular pathogen Ehrlichia chaffeensis*. Molecular Microbiology, 2011. **82**(5): p. 1217-1234.
509. Hebert, K.S., et al., *Anaplasma marginale Outer Membrane Protein A Is an Adhesin That Recognizes Sialylated and Fucosylated Glycans and Functionally Depends on an Essential Binding Domain*. Infection and Immunity, 2017. **85**(3).
510. Moumène, A., et al., *Iron Starvation Conditions Upregulate Ehrlichia ruminantium Type IV Secretion System, tr1 Transcription Factor and map1 Genes Family through the Master Regulatory Protein ErxR*. Frontiers in Cellular and Infection Microbiology, 2017. **7**: p. 535.
511. Yu, X.-J., M. Liu, and D.W. Holden, *Salmonella Effectors SseF and SseG Interact with Mammalian Protein ACBD3 (GCP60) To Anchor Salmonella-Containing Vacuoles at the Golgi Network*. mBio, 2016. **7**(4): p. e00474-16.
512. Vachon, V., D.N. Kristjanson, and J.W. Coulton, *Outer membrane porin protein of Haemophilus influenzae type b: pore size and subunit structure*. Can J Microbiol, 1988. **34**(2): p. 134-140.
513. Abdali, N., et al., *Identification and characterization of smallest pore-forming protein in the cell wall of pathogenic Corynebacterium urealyticum DSM 7109*. BMC Biochemistry, 2018. **19**: p. 3.

514. Lambrechts, A., et al., *Listeria comet tails: the actin-based motility machinery at work*. Trends in Cell Biology, 2008. **18**(5): p. 220-227.
515. Guérin, I. and C. de Chastellier, *Pathogenic Mycobacteria Disrupt the Macrophage Actin Filament Network*. Infection and Immunity, 2000. **68**(5): p. 2655-2662.
516. Galán, J.E. and D. Zhou, *Striking a balance: Modulation of the actin cytoskeleton by Salmonella*. Proceedings of the National Academy of Sciences, 2000. **97**(16): p. 8754.
517. Salomon, D. and K. Orth, *Lost after translation: post-translational modifications by bacterial type III effectors*. Current opinion in microbiology, 2013. **16**(2): p. 213-220.
518. Frischknecht, F. and M. Way, *Surfing pathogens and the lessons learned for actin polymerization*. Trends in Cell Biology, 2001. **11**(1): p. 30-38.
519. Flynn, O., et al., *Virulence-associated protein characterisation of Rhodococcus equi isolated from bovine lymph nodes*. Veterinary Microbiology, 2001. **78**(3): p. 221-228.
520. Komijn, R.E., et al., *Granulomatous lesions in lymph nodes of slaughter pigs bacteriologically negative for Mycobacterium avium subsp. avium and positive for Rhodococcus equi*. Veterinary Microbiology, 2007. **120**(3): p. 352-357.
521. Barton, M.D. and K.L. Hughes, *Ecology of Rhodococcus equi*. Vet Microbiol, 1984. **9**(1): p. 65-76.
522. Giguere, S., *Treatment of Infections Caused by Rhodococcus equi*. Vet Clin North Am Equine Pract, 2017. **33**(1): p. 67-85.
523. Flannagan, R.S., G. Cosio, and S. Grinstein, *Antimicrobial mechanisms of phagocytes and bacterial evasion strategies*. Nat Rev Microbiol, 2009. **7**(5): p. 355-66.
524. Coulson, G.B., et al., *Transcriptome reprogramming by plasmid-encoded transcriptional regulators is required for host niche adaptation of a macrophage pathogen*. Infect Immun, 2015. **83**(8): p. 3137-45.
525. Kakuda, T., et al., *Transcriptional regulation by VirR and VirS of members of the Rhodococcus equi virulence-associated protein multigene family*. Microbiol Immunol, 2015. **59**(8): p. 495-9.
526. Jacks, S., S. Giguere, and J.F. Prescott, *In vivo expression of and cell-mediated immune responses to the plasmid-encoded virulence-associated proteins of Rhodococcus equi in foals*. Clin Vaccine Immunol, 2007. **14**(4): p. 369-74.
527. Hooper-McGrevy, K.E., B.N. Wilkie, and J.F. Prescott, *Immunoglobulin G Subisotype Responses of Pneumonic and Healthy, Exposed Foals and Adult Horses to Rhodococcus equi Virulence-Associated Proteins*. Clinical and Diagnostic Laboratory Immunology, 2003. **10**(3): p. 345.
528. Tan, C., et al., *Molecular characterization of a lipid-modified virulence-associated protein of Rhodococcus equi and its potential in protective immunity*. Can J Vet Res, 1995. **59**(1): p. 51-9.

529. Botstein, D. and G.R. Fink, *Yeast: an experimental organism for 21st Century biology*. Genetics, 2011. **189**(3): p. 695-704.
530. Burd, C.G. and S.D. Emr, *Phosphatidylinositol(3)-phosphate signaling mediated by specific binding to RING FYVE domains*. Mol Cell, 1998. **2**(1): p. 157-62.
531. Vieira, O.V., R.J. Botelho, and S. Grinstein, *Phagosome maturation: aging gracefully*. Biochem J, 2002. **366**(Pt 3): p. 689-704.
532. Sangkanjanavanich, N., et al., *Rescue of an intracellular avirulent Rhodococcus equi replication defect by the extracellular addition of virulence-associated protein A*. Journal of Veterinary Medical Science, 2017. **79**(8): p. 1323-1326.
533. Deng, W., et al., *Assembly, structure, function and regulation of type III secretion systems*. Nature Reviews Microbiology, 2017. **15**: p. 323.
534. Zinser, E., et al., *Phospholipid synthesis and lipid composition of subcellular membranes in the unicellular eukaryote Saccharomyces cerevisiae*. Journal of Bacteriology, 1991. **173**(6): p. 2026.
535. Shin, J.J.H. and C.J.R. Loewen, *Putting the pH into phosphatidic acid signaling*. BMC Biology, 2011. **9**(1): p. 85.
536. Kooijman, E.E., et al., *Spontaneous curvature of phosphatidic acid and lysophosphatidic acid*. Biochemistry, 2005. **44**(6): p. 2097-102.
537. Corrotte, M., et al., *Dynamics and function of phospholipase D and phosphatidic acid during phagocytosis*. Traffic, 2006. **7**(3): p. 365-77.
538. Fang, Y., et al., *Phosphatidic acid-mediated mitogenic activation of mTOR signaling*. Science, 2001. **294**(5548): p. 1942-5.
539. Frondorf, K., et al., *Phosphatidic acid is a leukocyte chemoattractant that acts through S6 kinase signaling*. J Biol Chem, 2010. **285**(21): p. 15837-47.
540. Lim, H.K., et al., *Phosphatidic acid regulates systemic inflammatory responses by modulating the Akt-mammalian target of rapamycin-p70 S6 kinase 1 pathway*. J Biol Chem, 2003. **278**(46): p. 45117-27.
541. Schlam, D., et al., *Diacylglycerol kinases terminate diacylglycerol signaling during the respiratory burst leading to heterogeneous phagosomal NADPH oxidase activation*. J Biol Chem, 2013. **288**(32): p. 23090-104.
542. Wang, X., et al., *Signaling functions of phosphatidic acid*. Prog Lipid Res, 2006. **45**(3): p. 250-78.
543. Giguere, S. and J.F. Prescott, *Cytokine induction in murine macrophages infected with virulent and avirulent Rhodococcus equi*. Infect Immun, 1998. **66**(5): p. 1848-54.
544. Flinn, R.J., et al., *The late endosome is essential for mTORC1 signaling*. Mol Biol Cell, 2010. **21**(5): p. 833-41.

545. Zoncu, R., et al., *mTORC1 senses lysosomal amino acids through an inside-out mechanism that requires the vacuolar H(+)-ATPase*. *Science*, 2011. **334**(6056): p. 678-83.
546. Makrai, L., et al., *Characterization of Virulence Plasmids and Serotyping of Rhodococcus equi Isolates from Submaxillary Lymph Nodes of Pigs in Hungary*. *Journal of Clinical Microbiology*, 2005. **43**(3): p. 1246.
547. Willingham-Lane, J.M., et al., *Influence of Plasmid Type on the Replication of Rhodococcus equi in Host Macrophages*. *mSphere*, 2016. **1**(5).
548. Burton, A.J., et al., *Efficacy of liposomal gentamicin against Rhodococcus equi in a mouse infection model and colocalization with R. equi in equine alveolar macrophages*. *Vet Microbiol*, 2015. **176**(3-4): p. 292-300.
549. Takai, S., et al., *Correlation of In Vitro Properties of Rhodococcus (Corynebacterium) equi with Virulence for Mice*. *Microbiology and Immunology*, 1985. **29**(12): p. 1175-1184.
550. Sheffield, P., S. Garrard, and Z. Derewenda, *Overcoming expression and purification problems of RhoGDI using a family of "parallel" expression vectors*. *Protein Expr Purif*, 1999. **15**(1): p. 34-9.
551. Gietz, R.D. and R.A. Woods, *Transformation of yeast by lithium acetate/single-stranded carrier DNA/polyethylene glycol method*. *Methods Enzymol*, 2002. **350**: p. 87-96.

## APPENDIX I

### WBM0152 ASSOCIATES WITH SNA3-GFP CONTAINING COMPARTMENTS

In order to evaluate the localization of *wBm0152* in *S. cerevisiae*, a C-terminally tagged *wBm0152-mRuby2* construct under the control of an inducible promoter was generated and expressed in the previously described *Sna3-GFP* expression strain [507]. It is evident that the *wBm0152-mRuby2* construct does not induce as strong a trafficking defect as untagged however with increased induction time (24 hours), yeast cells predominantly show modulation of *Sna3-GFP* trafficking and accumulation in vacuole-associated compartments equivalent to untagged *wBm0152*. *wBm0152-mRuby2* mostly colocalizes in *Sna3-GFP* compartments (Figure AI.1), however not exclusively, and in several cells *wBm0152-mRuby2* is associated but not necessarily colocalized with *Sna3-GFP* compartments. This may be a result of the tag or it may be that *wBm0152* resides in vesicles associated with the vacuole that by its presence, block fusion of late endosomes with the vacuole.

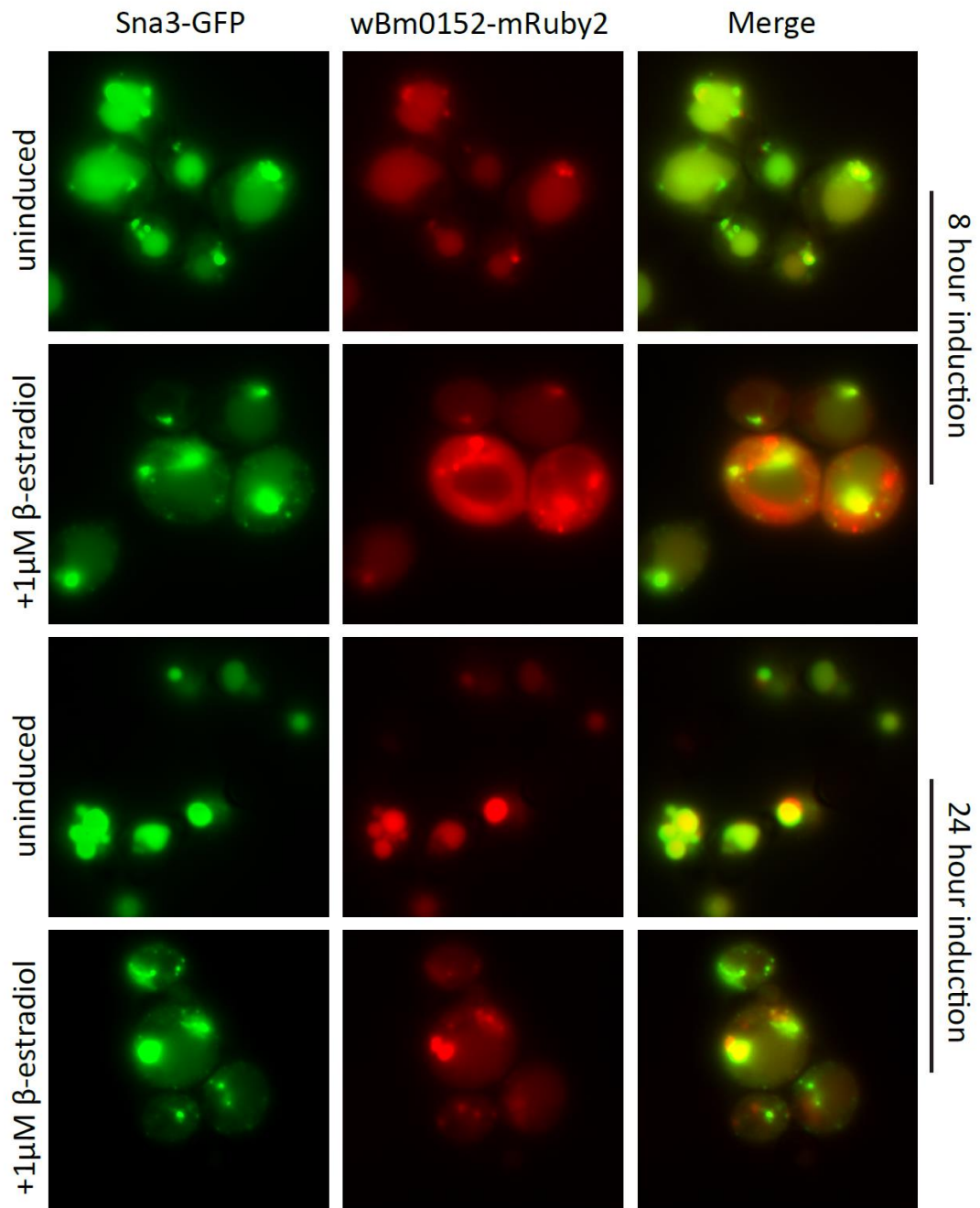


**Figure AI.1. wBm0152-mRuby2 associates with Sna3-GFP containing compartments.** *S. cerevisiae* harboring plasmids for both constitutively expressed Sna3-GFP and wBm0152-mRuby2 under control of the *GAL4* promoter was visualized either at 8 hours or 24 hours in both uninduced or induced conditions (+1μM β-estradiol). wBm0152-mRuby2 is observed in association with Sna3-GFP containing compartments.

## APPENDIX II

### VAPA OF *RHODOCOCCUS EQUI* BINDS PHOSPHATIDIC ACID

Wright LM, Carpinone EM, Bennett TL, Hondalus MK, and Starai VJ. VapA of *Rhodococcus equi* binds phosphatidic acid. *Mol Microbiol.* 2017. 107(3):428-444. Reprinted here with permission of the publisher.

## Summary

*Rhodococcus equi* is a multi-host, facultative intracellular bacterial pathogen that primarily causes pneumonia in foals less than six months in age and immunocompromised people. Previous studies determined that the major virulence determinant of *R. equi* is the surface bound virulence associated protein A (VapA). The presence of VapA inhibits the maturation of *R. equi*-containing phagosomes and promotes intracellular bacterial survival, as determined by the inability of *vapA* deletion mutants to replicate in host macrophages. While the mechanism of action of VapA remains elusive, we show that soluble recombinant VapA<sup>32-189</sup> both rescues the intramacrophage replication defect of a wild type *R. equi* strain lacking the *vapA* gene and enhances the persistence of nonpathogenic *Escherichia coli* in macrophages. During macrophage infection, VapA was observed at both the bacterial surface and at the membrane of the host-derived *R. equi* containing vacuole, thus providing an opportunity for VapA to interact with host constituents and promote alterations in phagolysosomal function. In support of the observed host membrane binding activity of VapA, we also found that rVapA<sup>32-189</sup> interacted specifically with liposomes containing phosphatidic acid *in vitro*. Collectively, these data demonstrate a lipid binding property of VapA, which may be required for its function during intracellular infection.

## Introduction

The Gram-positive coccobacillus *Rhodococcus equi* is a causative agent of pyogranulomatous pneumonia in foals less than six months in age and in immunocompromised people [35, 447, 448]. Cattle and swine are also occasional hosts but disease presentation in these species is different and typically manifests as respiratory lymph node abscessation and sub-maxillary lymphadenitis respectively [63, 519, 520]. Delayed type hypersensitivity testing of horses has determined that exposure to *R. equi* is widespread. Disease however, is either sporadic or endemic depending on the horse farm [34, 521]. While a significant portion of subclinical disease resolves naturally, the unrestrained use of antibiotics on

some horse farms has led to the emergence of antimicrobial resistant strains of the bacterium, complicating treatment during disease progression [522]. Additionally, the rise in human immunocompromised populations, whether it be from chemotherapy or HIV, has allowed the bacterium to become a relevant opportunistic pathogen of humans [447].

*R. equi* exposure of foals typically occurs through inhalation of aerosolized bacteria from contaminated soil, wherein the bacterium is introduced to the lower airway [46]. Delivery of the bacterium to the lungs allows alveolar macrophages to recognize and phagocytose the bacterium. Thereafter, the macrophage will attempt to kill the bacterium through a variety of antimicrobial mechanisms, including the production of reactive oxygen and nitrogen species, activation of hydrolytic enzymes, generation of an acidified vacuolar compartment, and depletion of essential nutrients [523]. Despite these tactics, *R. equi* is able to survive and replicate within macrophages of susceptible hosts, designating the bacterium a facultative intracellular pathogen [49].

Initial studies indicated that there are both virulent and avirulent strains of *R. equi*, differing in the possession of a virulence-associated plasmid [57]. Subsequent work has shown that the type of virulence plasmid carried by disease-causing strains of *R. equi* is host specific; wherein pVapA is the plasmid type carried by *R. equi* isolates infecting equine and is the most studied of the virulence plasmid types [58]. pVapB and pVapN comprise the remainder of the sequenced virulence plasmids and are carried by *R. equi* strains infecting swine and bovine species respectively [63]. Human infection can arise from *R. equi* carrying any of the aforementioned virulence associated plasmids, but the most commonly detected pathogen is *R. equi* harboring the pVapB type virulence plasmid [58]. The ability of multiple *R. equi* strains harboring different virulence plasmids to cause disease in immunocompromised humans confirms the opportunistic capacity of this bacterium. Sequence analysis of these virulence plasmids revealed the presence of four common regions known as the conjugation, replication, unknown function and the virulence or pathogenicity island (PAI) regions [63, 64]. Within the PAI region of these plasmids,

members of a novel gene family, the *vap* (virulence associated protein) family reside. Deletion of the plasmid pathogenicity island renders the bacterium incapable of replication in macrophages [70].

Further experimentation on the pVapA type virulence plasmid has shown that, of the twenty open reading frames present in the PAI, only three are required for intramacrophage replication: *virR*, *virS*, and *vapA* [63, 69, 524].

*virR* and *virS* encode for transcriptional regulators crucial for the expression of *vapA* as well as a number of other genes found on both the virulence-associated plasmid and the *R. equi* chromosome. The *vapA* gene produces the highly immunogenic protein, virulence associated protein A (VapA) [56, 69, 524, 525]. There are five other open reading frames located in the pVapA PAI encoding for proteins with a high degree of identity to *vapA*: *vapG*, *vapH*, *vapC*, *vapD*, and *vapE* [64]. Targeted deletion studies of each of these *vap* genes have determined that deletion of *vapA* alone attenuates the bacterium's ability to replicate within macrophages [67, 69, 70]. Therefore, VapA activity does not appear to be shared among these related Vap homologs even though many of these Vap-family proteins appear to be expressed during *R. equi* infection [74, 526, 527]. While the mechanism of action of VapA has yet to be discerned, it has been determined that VapA is localized on the surface of *R. equi*, giving it the capability to directly interact with the host [71]. Studies have shown that virulent *R. equi* reside within an enlarged neutral compartment in the macrophage and that the presence of *vapA* inhibits the acidification of the *R. equi* containing vacuole (RCV), thereby supporting the intracellular survival of the bacterium [50-52].

Direct visualization of *R. equi* after phagocytic uptake has determined that the recruitment of early trafficking markers to the bacteria-laden phagosome is unaffected. The early endosomal markers Rab5 and early endosomal antigen 1 (EEA1) are gained and lost by the RCV in a timely manner. Late endosomal markers lysobisphosphatidic acid, Rab7, and lysosomal-associated membrane proteins (LAMP) 1 and 2 increase subsequently, suggesting that maturation of these endosomal compartments to late endosomes proceeds unhindered by the presence of the bacterium [50]. The two aberrant

phenotypes associated with *R. equi* infection of macrophages are the lack of acidification of, and replication within, an enlarged phagosomal compartment [50-52].

Sequence characterization of the Vap proteins suggests that they can be broken into three domains, designated as the signal sequence, disordered, and conserved domains [64]. Molecular work on the Vap proteins has determined the protein structure of the conserved domain of VapG, VapD, and VapB; VapB is a virulence associated protein located in the PAI of pVapB [41, 59, 63, 79-81]. Solved structures resolved an eight stranded anti-parallel  $\beta$ -barrel connected by an  $\alpha$ -helix for each of the preceding proteins, although the solved structures could not provide much insight into the function of these Vaps [79-81]. Attempts to crystallize VapA have been unsuccessful, but it is presumed that the protein obtains a similar structure to the other Vaps due to high sequence homology. More recent work on endocytosed recombinant VapA has determined that the protein does not directly inhibit acidification but can reduce hydrolytic capacity and cause endolysosomal swelling of normal rat kidney cells; however, a mechanism for how VapA alters cellular trafficking remains to be determined [72].

This study further characterizes VapA, the major virulence determinant of *Rhodococcus equi* isolates carrying pVapA. Experiments focused on localizing the protein during both macrophage infection and *in vitro* expression in yeast show a distinct membrane-binding activity of VapA, which may be critical for its ability to alter endolysosomal traffic in host cells during infection. Additionally, the ability of rVapA to bind to liposomes of varying lipid composition was analyzed, and provides evidence that membrane phosphatidic acid is a ligand for VapA.

## **Results**

### ***Recombinant VapA complements the intramacrophage replication defect of an R. equi strain lacking vapA.***

In order to survive and replicate intracellularly, *R. equi* harboring the pVapA-type virulence plasmid requires only the activity of *vapA*, and two transcriptional regulators, *virR* and *virS*, all residing

within the plasmid-borne pathogenicity island [524]. Since VapA appears to be the only pVapA-encoded Vap family protein essential for the growth of *R. equi* in macrophages [69], and considering a recent study that showed that VapA could directly alter lysosomal activity when endocytosed by the normal rat kidney cell line [72], we assessed whether macrophages pre-treated with purified recombinant VapA lacking the putative N-terminal signal sequence, rVapA<sup>32-189</sup>, could rescue the intramacrophage replication defect of *R. equi*  $\Delta vapA$ . It is important to note that this fragment of the VapA protein is known to be functional, as mature VapA lacks the first 31 N-terminal amino acids [528]. In these experiments, bacterial intracellular growth in the J774A.1 macrophage cell line was followed over time by traditional lysis and plating of infected monolayer lysates. As anticipated, intracellular bacterial loads of wild type *R. equi* (103S) increased ~17 fold over 48 hr. This was in contrast to bacteria lacking the pVapA-type virulence plasmid (103<sup>P</sup>), whose growth was reduced 10-fold over the same time frame (Figures All.1A and B). Similar to 103<sup>P</sup>, the wild type *R. equi* strain lacking *vapA* ( $\Delta vapA$ ) was unable to replicate intracellularly, although intracellular bacterial loads persisted over the course of the infection (Figures All.1A and B). Strikingly, the addition of rVapA<sup>32-189</sup> restored the ability of the  $\Delta vapA$  strain to replicate in a dose-dependent manner, wherein macrophages pre-treated with 100nM of rVapA<sup>32-189</sup> could replicate to levels comparable to that of the wild type strain (Figures All.1A and B). Thus, exogenous addition of soluble recombinant VapA could compensate for the loss of the bacterially-encoded VapA protein during *R. equi* intramacrophage growth.

To assess the specificity of rVapA<sup>32-189</sup> activity, other recombinant Vap-family proteins lacking their putative signal sequences were tested in their ability to rescue the intramacrophage replication defect of  $\Delta vapA$ . Of the five other functional *vap* open reading frames (*vapG*, *vapH*, *vapE*, *vapC* and *vapD*) located in the PAI of pVapA, VapG displays the highest sequence identity to VapA at 48%, and is known to have high mRNA expression levels during *R. equi* infection of foals [63, 64, 81, 526]. Despite

these characteristics, purified recombinant VapG<sup>27-172</sup> was unable to rescue the replication defect of  $\Delta vapA$  bacteria (Figures All.1C and D).

Isolates of *R. equi* that harbor a pVapB-type plasmid contain six distinct *vap* genes (*vapJ*, *vapK1*, *vapL*, *vapK2*, *vapM*, and *vapB*) [63, 64]. Because of the high sequence identity (78%) between the VapB and VapA proteins, it has been proposed that the VapB protein in *R. equi* strains harboring pVapB would be functionally equivalent to VapA during pathogenesis [64]. Despite this, a recent report speculates that VapK1/K2, with 59% identity to VapA, is the functional equivalent of VapA in pVapB-carrying *R. equi* strains [63, 64]. Interestingly, in support of the latter, we found that while the addition of rVapB<sup>35-197</sup> was unable to reverse the intracellular replication defect of  $\Delta vapA$ , rVapK2<sup>32-202</sup> addition resulted in a 10-fold increase of  $\Delta vapA$  bacterial loads 48 hours post-infection (Figures All.1C and D). Importantly, this increase was in-line with the overall magnitude of intracellular replication displayed by that of the wild type pVapB-carrying *R. equi* strain 33705 (Figures All.1C and D), although the overall extent of bacterial replication was reduced when compared to the growth displayed by the  $\Delta vapA$  strain in the presence of rVapA<sup>32-189</sup>. To assess whether the lack of effect of rVapG and rVapB could be explained by improper folding of the recombinant proteins, all of the recombinant Vap proteins used in these studies were subjected to Proteinase K digestion and analyzed by gel electrophoresis, as previously performed by Geerds and coworkers, who described the presence of a properly-folded ~12 kDa core domain of VapA and VapB that was resistant to proteolytic degradation [79]. Upon exposure to Proteinase K digestion, we detected this Proteinase K-resistant core domain in each of the rVaps used in this study; this protease-resistant fragment was lost upon the denaturation of the protein in SDS (Figure All.2). These data suggest that each of the Vap proteins tested was appropriately folded and that the inability of rVapB<sup>35-197</sup> or rVapG<sup>27-271</sup> to rescue the intracellular growth defect of a *R. equi*  $\Delta vapA$  strain was likely not due to improperly folded recombinant protein. Taken together, these data show that exogenous addition of either rVapA<sup>32-189</sup> or rVapK2<sup>32-202</sup> can reverse the  $\Delta vapA$  replication defect in macrophages,

whereas related Vap-family proteins do not share this property. Surprisingly, VapA does not need to be directly produced by *R. equi* for its activity, likely because this virulence factor directly alters macrophage physiology.

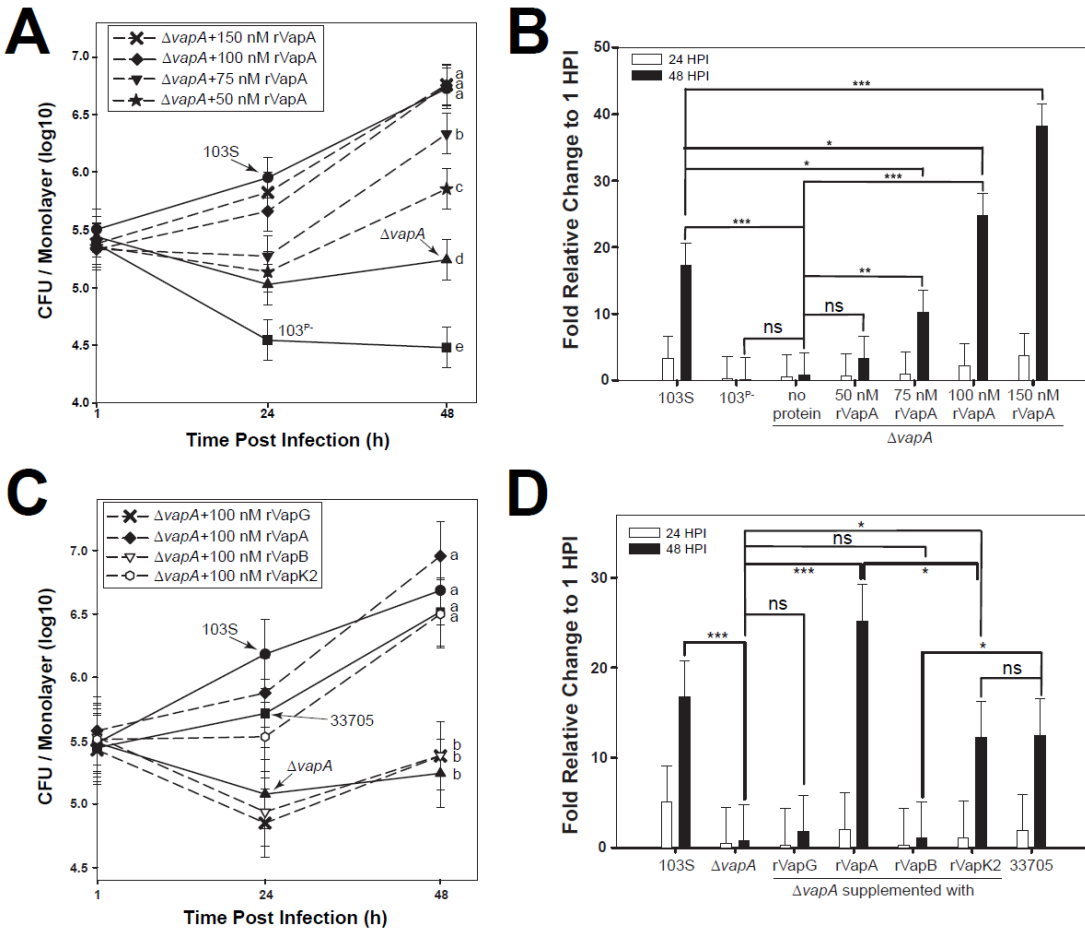


**Figure AII.1. Recombinant VapA<sup>32-189</sup> and VapK2<sup>32-202</sup> complement the replication defect of *R. equi* ΔvapA.** Symbols denote the mean number of bacteria observed and the bars denote the mean bacterial fold change. Error bars represent the standard deviation using a two-way analysis of variation (ANOVA) by way of the Holm-Sidak test. (A,C) Letters to the right of each curve denote statistical significance; the same letter signifies no statistical difference, while different letters signify statistical difference at  $P \leq 0.05$ . (B,D) ns = not significant; (\*) =  $P < 0.05$ ; (\*\*) =  $P < 0.01$ ; (\*\*\*) =  $P < 0.001$ .  $n=3$ .

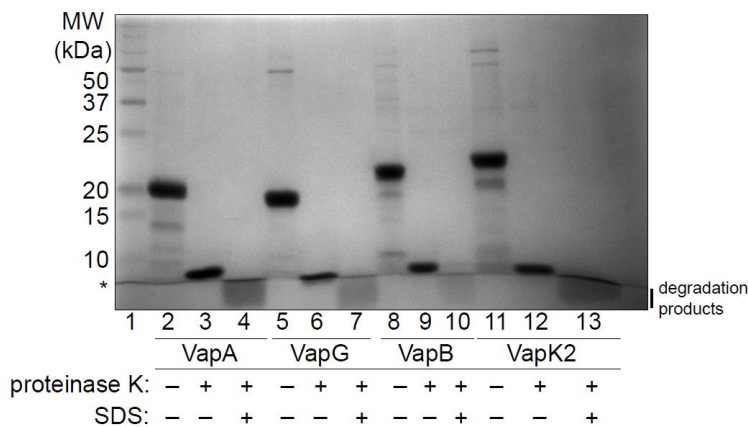


**Figure AII.2. Proteinase K digestion of each recombinant Vap shows a stable protein core.** 3 $\mu$ g protein was incubated with Proteinase K at 500:1 molar ratio. \*represents dye front.

***rVapA promotes the intramacrophage persistence of nonpathogenic Escherichia coli.***

It is known that *R. equi* expressing *vapA* has the ability to both neutralize the pH of the RCV during infection and to inhibit the degradative capacity of host macrophages [50-52]. Because exogenous addition of *rVapA*<sup>32-189</sup> was able to reverse the intramacrophage replication defect of the  $\Delta$ *vapA* strain, we hypothesized that *rVapA*<sup>32-189</sup> could directly alter the killing capacity of macrophages. Thus, we questioned whether the effect was broad in scope, and therefore, we assessed the impact of the presence of *rVapA*<sup>32-189</sup> on the intracellular survival of a nonpathogenic *E. coli* strain. As expected, the nonpathogenic *E. coli* strain was unable to replicate or persist in J774A.1 cells, with intracellular bacterial loads reduced by ~80% at 12 hours post infection (Figures AII.3A and B). Upon preincubation of macrophages with *rVapA*<sup>32-189</sup>, however, the survival of *E. coli* was greatly enhanced and bacterial numbers were only reduced by 40% at 12 hours post infection (Figures AII.3A and B). In contrast, macrophages incubated with *rVapG*<sup>27-271</sup> were not significantly different from untreated macrophages in their ability to kill *E. coli* under these conditions (Figures AII.3A and B). In order to support the intracellular persistence of a nonpathogenic bacterium, it is likely that *rVapA*<sup>32-189</sup> directly alters host phagolysosomal function.

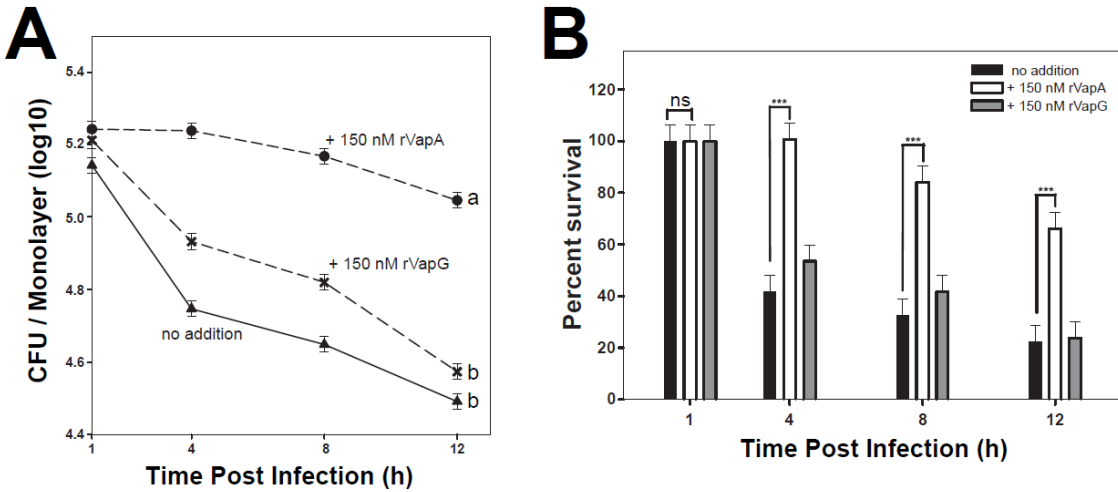


**Figure AII.3. Recombinant VapA<sup>32-189</sup> enhances intracellular persistence of nonpathogenic *E. coli* in J774A.1 cells.** J774A.1 macrophage monolayers were incubated overnight with either media (triangles) or 150 nM recombinant Vap protein (VapA, circles; VapG, crosses), and infected with *E. coli*. Symbols delineate the mean bacterial number and bars denote the mean percent survival. The error bars represent the standard deviation calculated using a two-way ANOVA via the Holm-Sidak method. Each experimental condition was performed in triplicate per infection;  $n = 3$ . **(A)** Statistical significance is expressed as letters to the right of the curve, with same letters defining a lack of significant difference, and different letters defining significance with  $P \leq 0.05$ . **(B)** Percent of viable *E. coli* cells detected, as compared to 1 hour post infection (HPI) is shown; ns = not significant; (\*\*\*) =  $P < 0.001$ .

**Localization of VapA during *R. equi* infection shows the protein at the bacterial surface and the RCV membrane.**

Because rVapA<sup>32-189</sup> appeared to be able to directly modulate the activity of host phagolysosomal compartments, we sought to localize *R. equi*-produced VapA over the course of an infection. For these studies, we utilized murine bone marrow-derived macrophages (BMDMs) as the host for *R. equi*. Both wild type 103S and  $\Delta vapA$  *R. equi* strains harboring a GFP expression plasmid were utilized to locate bacteria during infection of BMDM monolayers, and intracellular bacterial loads were measured via direct visualization and enumeration. As expected, the 103S-GFP wild type strain was capable of replicating intracellularly over 72 hr, and the  $\Delta vapA$ -GFP strain was cleared from these macrophages over the same timeframe (Figures AII.4A and B). As previously observed, supplementation

with exogenous rVapA<sup>32-189</sup> restored the ability of the  $\Delta vapA$ -GFP strain to survive and replicate intracellularly (Figures AII.4A and B). Of note, these results (Figure AII.4B) likely underestimate the total number of intracellular bacteria because of the clumping nature of *R. equi* and the fact that macrophages containing more than 10 organisms were quantified as containing only 10 bacteria. Therefore, the number of macrophages containing ten or more bacteria was also followed over time. After 72 hr, 35 of 200 macrophages infected with 103S harbored  $\geq 10$  intracellular bacteria, compared to 1 macrophage infected with the  $\Delta vapA$  strain. In the presence of exogenous rVapA<sup>32-189</sup>, almost 80 of 200 macrophages assessed contained 10 or more  $\Delta vapA$  bacteria, thus directly confirming the ability of rVapA<sup>32-189</sup> to support the intracellular replication of  $\Delta vapA$  *R. equi* (Figure AII.4C).

Visualization of monolayers infected with 103S *R. equi* showed the presence of VapA at the bacterial surface throughout the course of infection (Figure AII.4A). After 48 hours, however, in addition to remaining on the surface of the bacterium, we found that VapA was also observed to accumulate on the membrane of the *R. equi*-containing vacuole (RCV) (Figure AII.4A, arrows and insets). In  $\Delta vapA$ -infected monolayers supplemented with rVapA<sup>32-189</sup>, the recombinant protein displayed a highly punctate staining pattern at 1 hour post-infection, reminiscent of vesicular packaging upon endocytic or pinocytotic uptake (Figure AII.4A, T1). After 48 hr, rVapA<sup>32-189</sup> appears to accumulate around and within RCVs, suggesting that not only is rVapA<sup>32-189</sup> eventually trafficked to bacteria-laden compartments within these cells, but that its activity is needed within (or on) the RCV to support the replication of the *R. equi*  $\Delta vapA$  strain. Taken together, these images indicate that VapA likely functions in the lumen of the RCV, and that VapA may begin to associate with the membrane of bacteria-laden host vacuoles by 48 hr after infection.

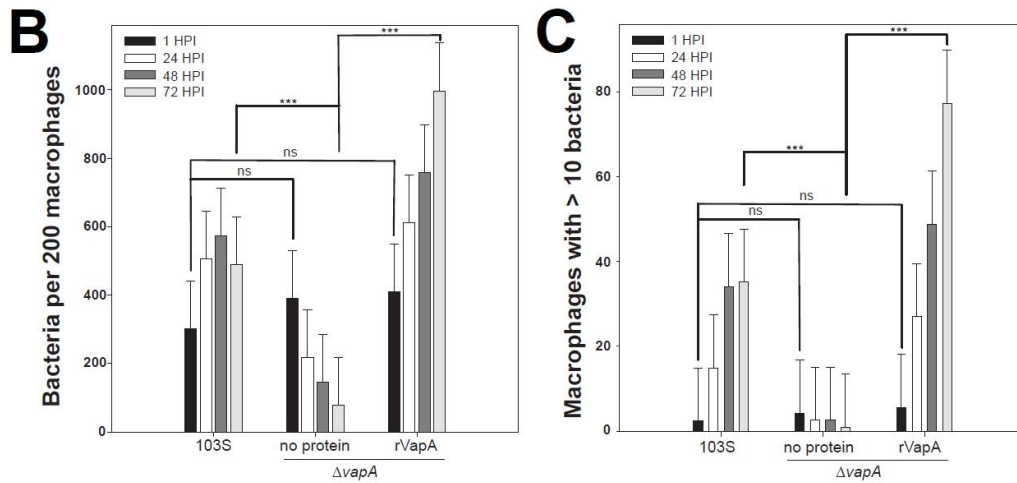
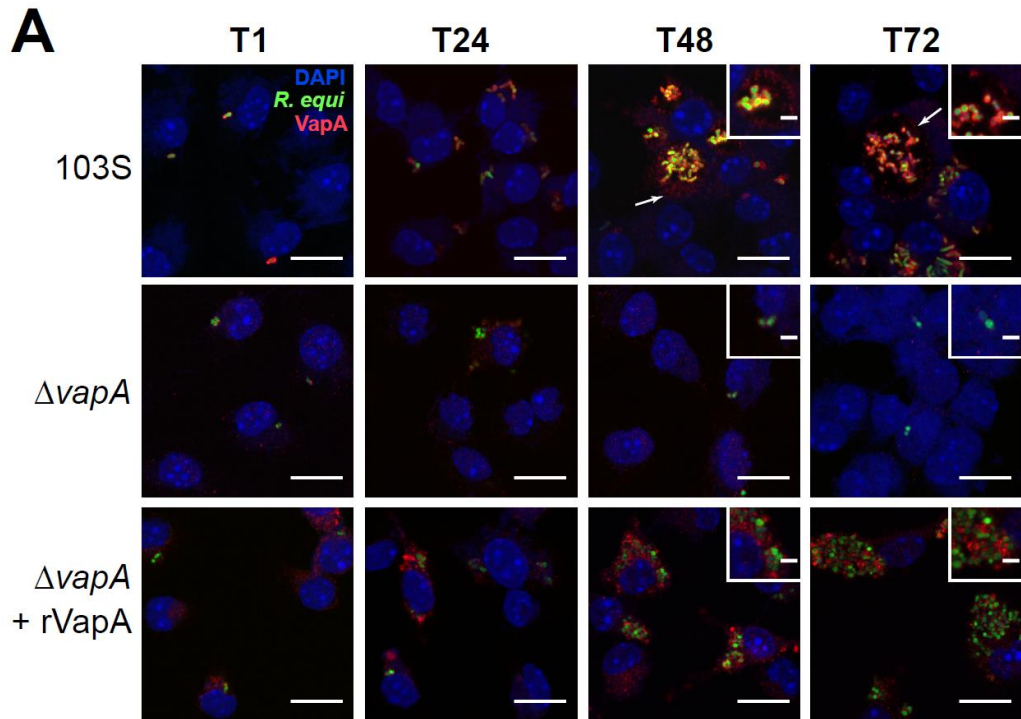


**Figure AII.4. VapA associates with the RCV membrane during infection.** Murine bone marrow-derived macrophages (BMDMs) were infected with *R. equi* 103S or  $\Delta vapA$  strains harboring the GFP expression plasmid, pGFPmut2. Where indicated, 100 nM rVapA was added to the BMDM monolayer the night before the infection. *R. equi* (GFP, green), BMDM nucleus (DAPI, blue), and VapA (anti-VapA, red) were observed. **(A)** Representative confocal images of infection, bar = 5  $\mu$ , inset bar = 1  $\mu$ . Arrows indicate VapA detected at the RCV membrane. **(B)** Bacterial numbers per 200 macrophages were quantified by direct visualization at the indicated time points. **(C)** Macrophages containing ten or more bacteria, discerned via direct visualization. **(B,C)** Bars indicate the mean number of quantified bacteria or macrophages, while the error bars represent the standard deviation calculated by a two-way ANOVA using the Holm-Sidak method.  $n = 3$ ; ns = not significant and (\*\*\*) =  $P \leq 0.001$ .

***VapA localizes to the yeast plasma membrane.***

Because of the discovery that VapA appears to localize to the limiting membrane of mature RCVs during *R. equi* infection, we decided to exploit a model eukaryotic system to aid in characterizing the cellular localization of the various Vap-family proteins. The budding yeast *Saccharomyces cerevisiae* is a robust model system for essential eukaryotic processes and has often been used to study the biochemical activities of secreted bacterial effector proteins that alter eukaryotic physiology [141, 529]. N-terminal GFP fusions to full-length VapA, VapA<sup>32-189</sup>, VapG<sup>27-172</sup>, VapB<sup>35-197</sup>, and VapK2<sup>32-202</sup> were constructed in the yeast GFP expression vector pGO35 [302, 530], and protein expression of each of these constructs in yeast was examined via immunoblot (Figure AII.5A). Each GFP-Vap construct, with the exception of GFP-VapG<sup>27-172</sup>, generated the expected ~44kDa band upon exposure with the polyclonal and cross-reactive anti-VapA antibody. Subsequently, the localization of each GFP-Vap fusion (other than GFP-VapG) within *S. cerevisiae* was examined. Expression of GFP alone showed a diffuse cytosolic staining, as expected (Figure AII.5B). However, expression of either GFP-tagged VapA construct (VapA or VapA<sup>32-189</sup>) resulted in a striking localization of GFP to the yeast plasma membrane. In fact, plasma membrane localization of GFP was observed in 100% of the GFP-VapA expressing yeast cells (Figure AII.5C). In contrast, yeast expressing either GFP-VapK2<sup>32-202</sup> or GFP-VapB<sup>35-197</sup>, showed a marked decrease in the amount of GFP localized to the plasma membrane (Figure AII.5B). Only ~40% of the GFP-VapK2<sup>32-202</sup> expressing yeast cells showed GFP at the plasma membrane, while ~23% of GFP-VapB<sup>35-197</sup> expressing yeast cells displayed plasma membrane-localized GFP (Figure AII.5C). Cumulatively, VapA membrane localization in both BMDM infection and upon expression in yeast suggest that VapA can either directly bind to cellular lipids or a conserved membrane-bound receptor. That GFP-VapK2<sup>32-202</sup> can also moderately localize to membranes in yeast may be relevant in its capacity to rescue the intramacrophage growth impairment of the *vapA* deletion mutant.

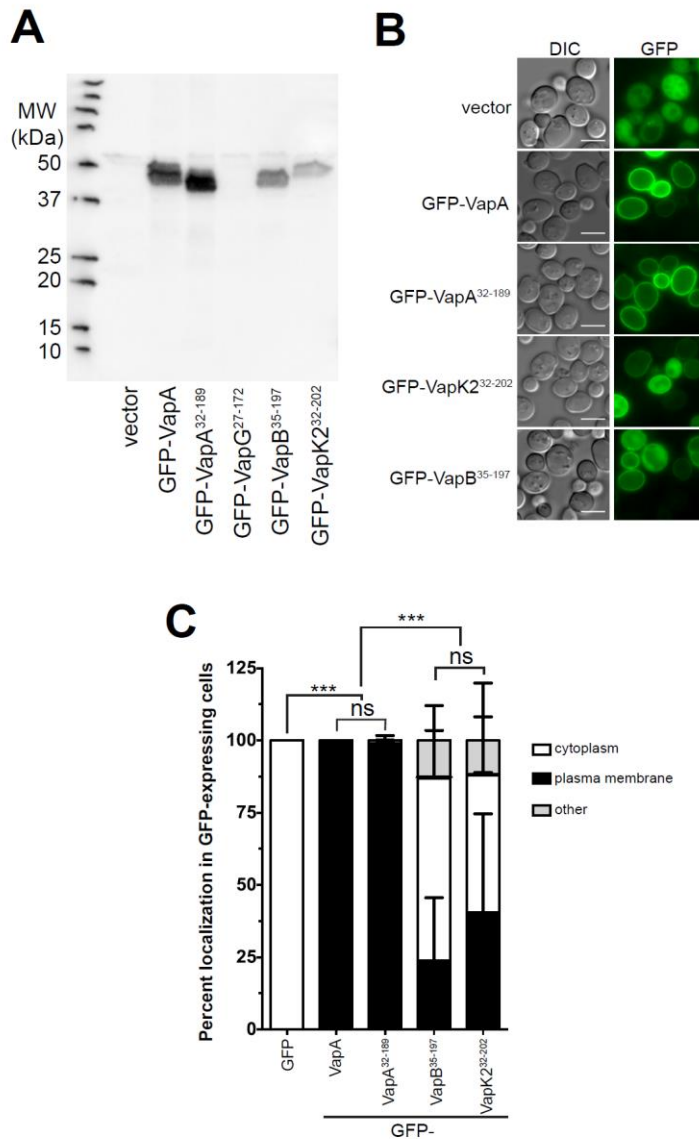


**Figure AII.5. GFP-VapA binds to the yeast plasma membrane upon expression *in vivo*.** (A) *Saccharomyces cerevisiae* strain BY4742 harboring either GFP (vector), GFP-VapA, GFP-VapA<sup>32-189</sup>, GFP-VapG<sup>27-172</sup>, GFP-VapB<sup>35-197</sup>, or GFP-VapK2<sup>32-202</sup> plasmid constructs were grown overnight and proteins were extracted from equal amounts of cell pellets, separated via SDS-PAGE, and probed with polyclonal anti-VapA antisera. (B) Cells from (A), with the exception of the strain harboring GFP-VapG<sup>27-172</sup>, were visualized for GFP localization via fluorescence microscopy. Bar = 5  $\mu$ . (C) Quantification of GFP localization from yeast strains imaged in (A); Cells with clear accumulation of GFP-Vap protein at the plasma membrane was counted as “plasma membrane”, diffuse GFP staining of the cytoplasm with no plasma membrane localization was counted as “cytoplasm;” all other morphologies were counted as “other.” 100 yeast cells were counted per experimental condition, bars denote the mean percent of cells displaying a particular Vap localization pattern. Error bars represent the standard deviation using a two-way analysis of variation (ANOVA) by way of the Holm-Sidak test, and significance pertaining to the difference in plasma membrane localization of GFP-Vap proteins is indicated.  $n = 3$ ; ns = not significant and (\*\*\*) =  $P \leq 0.001$ .

***rVapA binds liposomes containing phosphatidic acid.***

As VapA was seen to interact with both the yeast plasma membrane and the phagosomal membrane containing *R. equi*, we examined the possibility that rVapA<sup>32-189</sup> could interact directly with phospholipid bilayers. Therefore, liposomes of varying lipid concentrations were constructed, and the ability of rVapA<sup>32-189</sup> to bind to these membranes was investigated. We chose to explore rVapA<sup>32-189</sup>'s interaction with four major phospholipid constituents of the eukaryotic plasma membrane: phosphatidylcholine (PC), phosphatidylethanolamine (PE), phosphatidylserine (PS), and phosphatidic acid (PA). At a near-physiological pH of 7.4, interactions of rVapA<sup>32-189</sup> with liposomes containing either 100% PC or supplemented with 20% PE, PS, or PA were not detected, as measured by liposome co-floatation (Figure AII.6A). In contrast, rVapA<sup>32-189</sup> was found to bind to liposomes containing 20% PA when incubations were performed at a pH of 5.5; a minor interaction with PS-containing liposomes was also observed (Figure AII.6B). Furthermore, rVapA<sup>32-189</sup> bound PA-containing liposomes in a concentration-dependent manner (Figure AII.6C). Thus, rVapA<sup>32-189</sup> appears to bind to some negatively-charged lipids under acidic conditions, with a preference for membranes containing phosphatidic acid. Finally, we assayed each of the other closely related Vap proteins isolated in this study (VapG<sup>27-172</sup>, VapB<sup>35-197</sup>, and VapK2<sup>32-202</sup>) for their ability to interact with membranes containing phosphatidic acid. Results showed that none of these Vaps could appreciably interact with these liposomes (Figure AII.6D). Therefore, the interaction of VapA with phosphatidic acid appears to be unique among the Vap-family proteins tested.

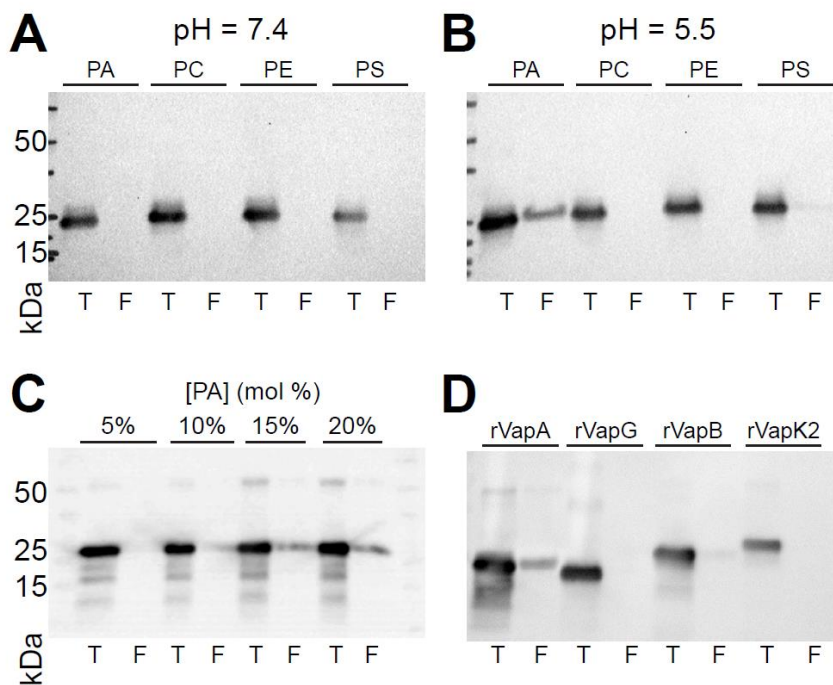


**Figure AII.6. rVapA binds phosphatidic acid containing liposomes.** Liposomes of indicated compositions (PA, 20% phosphatidic acid; PC, 100% phosphatidylcholine; PE; 20% phosphatidylethanolamine; PS, 20% phosphatidylserine) were generated as in Experimental Procedures. Liposomes were incubated with recombinant Vap protein at a pH of either (A) 7.4 or (B) 5.5, and liposomes were isolated by flotation (Experimental Procedures). Equal fractions representing 10% of the total reaction (T) and either 900 nmol (A,B) or 1  $\mu$ mol (C,D) total floated (F) liposomes were separated via SDS-PAGE and immunoblotted for VapA. (C) Liposomes containing increasing amounts of PA were assayed for VapA binding, as above in (5B). (D) Liposomes containing 20% PA were incubated with 1  $\mu$ g indicated recombinant Vap protein, and assayed for binding, as above in (5B). All recombinant Vap proteins tested cross-react with VapA antiserum.

***R. equi* resides in LAMP1-negative vesicles in the presence of VapA.**

Because the existence of VapA at the phagosomal membrane could impact host phagolysosomal trafficking, we followed the presence of the late endosomal/lysosomal marker LAMP1 (lysosomal-associated membrane protein 1) during the course of macrophage infection [523, 531]. It has been reported that RCVs associate with LAMP1 up to twenty-four hours post infection, and it has been presumed that wild type *R. equi* remain in a late endosome-like compartment by inhibiting the fusion of bacterial-containing vesicles with degradative lysosomes [50]. Using the GFP-expressing 103S and

immunofluorescence staining for LAMP1, we similarly found *R. equi*-containing vesicles to be associated with LAMP1 up to twenty-four hours post infection, and noted that the vesicular membranes were closely associated with individual bacteria (Figure AII.7, 103S, T24). We extended these observations and at 48h post infection, when bacterial loads were high, we noted that the RCV became enlarged and LAMP1 was no longer associated with *R. equi*-containing vacuoles (Figure AII.7, 103S, T48). Interestingly, LAMP1 appeared to be excluded from VapA-positive membranes (Figure AII.7 103S, insets), which continued until at least 72 h post infection (Figure AII.7B). Furthermore, there was a noticeable increase in LAMP1 staining of macrophages harboring replicating bacteria than the surrounding uninfected cells.

In contrast, RCVs containing  $\Delta vapA$  bacteria were found to be associated with LAMP1 throughout the course of infection, suggesting delivery of these mutant *R. equi* to the degradative lysosome and a lack of intracellular replication (Figure AII.7,  $\Delta vapA$ ). Contrastingly, in the presence of 100nM rVapA<sup>32-189</sup>,  $\Delta vapA$  bacteria were found to be located in both LAMP1-positive and -negative compartments at 48-72 hours post infection (Figure AII.7,  $\Delta vapA$ +rVapA, insets). Although the RCV was never found to be enlarged under these conditions, as in the wild type infections, intracellular bacterial loads increased in spite of some overlap with LAMP1-containing vesicles. Taken together, these data suggest that the presence of VapA at the RCV membrane is associated with altered phagolysosomal maturation or altered endolysosomal trafficking pathways in macrophages, and that LAMP1 displacement away from VapA-producing *R. equi* occurs beyond twenty-four hours post infection.

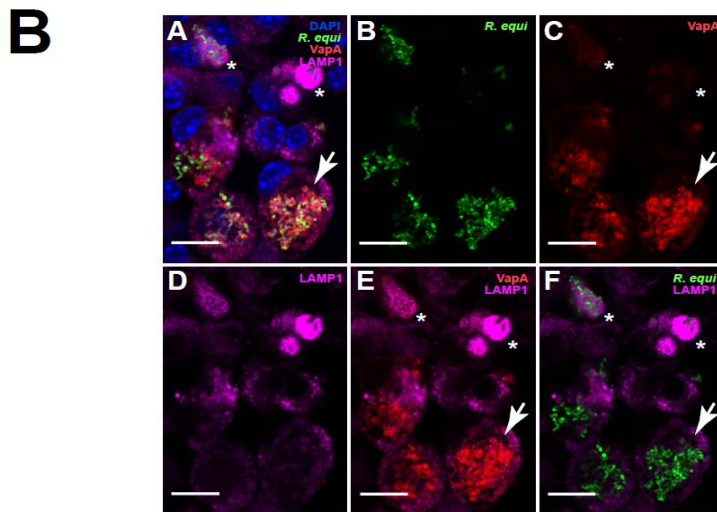
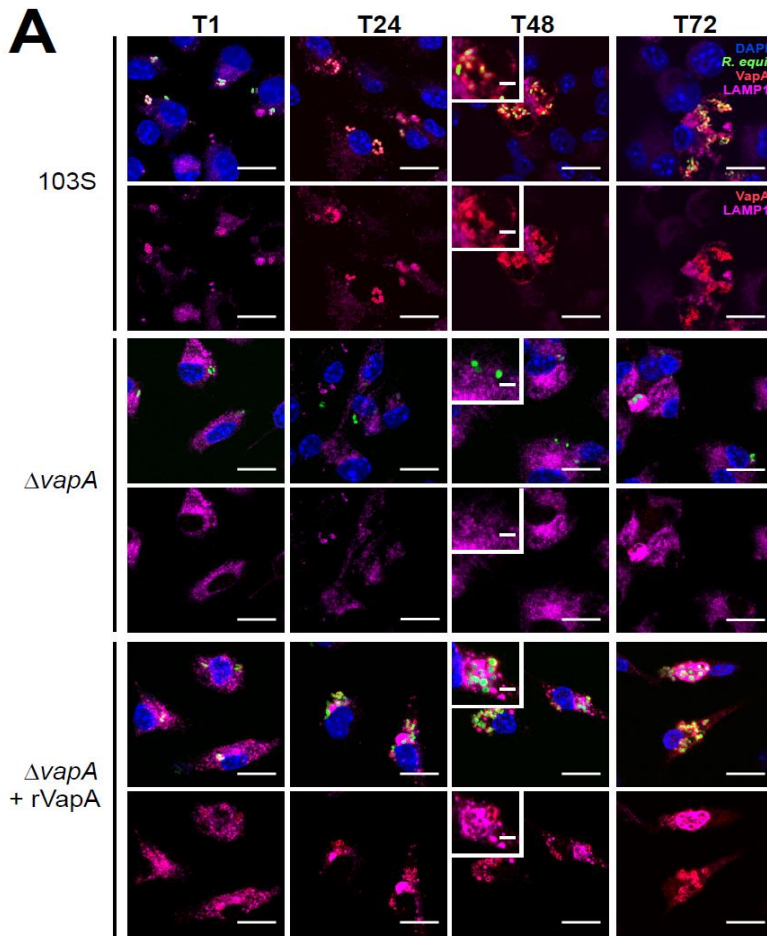


**Figure All.7. The presence of VapA prevents the accumulation of LAMP1 within the RCV 48 and 72 h post infection. (A)** BMDMs were infected with either *R. equi* 103S or  $\Delta vapA$  strains, and 100 nM rVapA<sup>32-189</sup> was added the night before the infection, where indicated. At indicated time points, cells were fixed, immunostained, and visualized via confocal microscopy. *R. equi* (GFP, green), BMDM nucleus (DAPI, blue), VapA (anti-VapA, red), and murine LAMP1 (anti-LAMP1, purple) were observed.  $n =$

3, bar = 5  $\mu$ , inset bar = 1  $\mu$ . **(B)** Representative confocal image of 103S infection of BMDMs at T72, performed and stained as in **(A)**. A large RCV containing replicating bacteria and RCV membrane-associated VapA (arrow) is shown in comparison to macrophages containing strongly LAMP1-positive compartments surrounding bacteria that lack detectable VapA at the RCV membrane (asterisks), bar = 5  $\mu$ .

## Discussion

Herein, we show that exogenous addition of rVapA<sup>32-189</sup> protein to macrophage monolayers both reversed the intracellular growth defect of *R. equi*  $\Delta$ vapA bacteria and supported the persistence of nonpathogenic *E. coli*, highlighting the ability of the major virulence determinant of *R. equi*, VapA, to broadly inhibit the killing capacity of macrophages (Figures All.1 and3). Our work determined that soluble rVapA<sup>32-189</sup> at 100 nm (1.7  $\mu$ g ml<sup>-1</sup>) was sufficient to restore intramacrophage replication of  $\Delta$ vapA to wild type levels. Our findings are supported by those of another group who very recently described the rescue of  $\Delta$ vapA growth in macrophages in the presence of 100  $\mu$ g ml<sup>-1</sup> soluble rVapA [532]. The group also reported that addition of rVapA allowed for the intracellular growth of an avirulent plasmid-cured strain of *R. equi*, 103<sup>P</sup>. The latter was a surprising result, given it is well-established that expression of wild type levels of VapA alone by virulence plasmid-free *R. equi* is not sufficient to promote intramacrophage replication [57, 524], although Sangkanjanavanich and colleagues used at least 50-fold more rVapA than we found is required to support the intracellular replication of  $\Delta$ vapA *R. equi* in this study. Interestingly, we also found that a related Vap protein encoded on the pVapB-type plasmid carried by some *R. equi* strains (e.g. 33705), rVapK2<sup>32-202</sup>, showed a similar capacity to restore the growth of  $\Delta$ vapA bacteria in macrophages, albeit to a lesser degree (Figure All.1). No other recombinant Vap protein tested shared this activity, suggesting that the ability to alter macrophage antimicrobial capabilities is specific for VapA and its functional homologs (like VapK2) across *R. equi* strains harboring different virulence plasmids.

To better understand VapA's mechanism of action, we sought to observe the localization of VapA during extended *R. equi* macrophage infection. While previous *in vitro* experimentation has

determined that VapA is located on the surface of the bacterium [71], to our knowledge, this is the first time in which this localization has been confirmed during macrophage infection. Strikingly, at 48 hours post-infection, VapA was no longer solely confined to the bacterial surface, but also appeared at the membrane of the RCV (Figure All.4A). The mechanism by which VapA is delivered to the RCV membrane is unknown, but reasoning suggests that active secretion of VapA from intracellular *R. equi*, release of VapA from shedding of the outer cell envelope from intracellularly replicating bacteria, degradation of some bacteria within the RCV, or delivery via an interaction between the bacterium and phagosomal membrane during initial phagocytic uptake are all viable possibilities. Byrne and coworkers previously described the secretion of VapC, VapD, and VapE into *R. equi* culture supernatant, but could not detect VapA via immunoblot [74]. While this demonstrates that *R. equi* does not secrete VapA across the outer lipid envelope into the supernatant during routine laboratory culture, it may be that signals within the intramacrophage environment triggers release of the protein from the bacterial surface. Some intracellular pathogens harbor type three (T3SS) and type 4 (T4SS) secretion systems allowing for bacterial effectors to be secreted into the cytoplasm of their host cell [533]. While genes encoding for a T3SS or classical T4SS are not present in *R. equi*, the *R. equi* virulence plasmid harbors genes required for the conjugal transfer of this plasmid [60]. It is unlikely that these genes are responsible for the secretion of VapA during infection, however, as this region is expendable for the proper localization of VapA on the surface of *R. equi* [70]. There is genetic evidence in *R. equi* for the presence of a type seven secretion system (T7SS; ESX) similar to *Mycobacterium tuberculosis* [66]. T7SS have been identified in a variety of Gram-positive organisms, where they participate in a wide number of functions including virulence and permitting the transport of substrates across the inner membrane and outer lipid envelope, or mycomembrane; however, these T7SS have not been shown to deliver substrates into the host cytoplasm. What role, if any, the T7SS may play in *R. equi* pathogenesis remains unknown at present.

This study provides the first experimental evidence showing VapA deposition on the membrane of the RCV during macrophage infection. VapA was not observed outside of the RCV (e.g. in the host cytosol) during macrophage infection with wild type *R. equi*. As a first step to better understand how the presence of VapA at the limiting membrane of the RCV might potentially affect phagolysosomal trafficking, we assessed the locations of both native VapA and of lysosomal-associated membrane protein 1 (LAMP1), found on late endosomes and lysosomes, over the course of macrophage infection (Figure All.7). Previously published work has established that LAMP1 associates with RCVs containing virulent *R. equi* during the 24 hours following uptake [50]. By extending this assessment further, however, we made a surprising observation: *R. equi*-containing vacuoles appear to exist in a mixed population during infection. Notably, enlarged RCVs with VapA at the limiting membrane were devoid of LAMP1, while RCVs that lacked VapA at the membrane were LAMP1 positive (Figure All.7). This finding suggests that VapA's presence at the RCV membrane is important in aiding the bacteria in avoiding destruction by the lysosomal compartment. While LAMP1 is initially gained, the RCV containing actively replicating bacteria can either displace, or avoid further accumulation of, LAMP1-containing endolysosomal vesicles (Figure All.7). Thus, there appears to be a late RCV stage that warrants further characterization, but such is beyond the scope of this work.

VapA localization to eukaryotic membranes was not restricted to macrophages, as expression of GFP-VapA in *S. cerevisiae* (VapA or VapA<sup>32-189</sup>) localized strongly to the plasma membrane (Figures All.5B and C). Likewise, GFP-VapK2<sup>32-202</sup> displayed plasma membrane localization in yeast, albeit to a lesser extent, and this reduction might account for the decreased ability of exogenous rVapK2<sup>32-202</sup> to rescue the  $\Delta vapA$  mutant and restore its replicative capacity in macrophages, at least as compared to rVapA<sup>32-189</sup> (Figures All.5B, 5C, and 1C). GFP-VapB<sup>35-197</sup> showed even less yeast plasma membrane localization than rVapK2<sup>32-202</sup> and was predominantly localized to the cytoplasm. That the two Vap proteins (rVapA<sup>32-189</sup> and rVapK2<sup>32-202</sup>) with the capacity to reverse the intramacrophage replication defect of  $\Delta vapA$

displayed localization to the yeast plasma membrane (Figure All.5B and C) prompted us to postulate that VapA might possess lipid binding properties. Thus, we found that rVapA<sup>32-189</sup> bound to synthetic liposomes containing phosphatidic acid (PA) (Figures 5B-5D), and to a much lesser extent, phosphatidylserine (PS) (Figure All.6B). Interestingly, membrane PA concentrations in yeast is highest at the outer mitochondrial and plasma membranes, wherein both of these organelles also contain a high percentage of phosphatidylethanolamine (PE). Unique to the plasma membrane, however, is a high amount of PS along with PA and PE [534]. Additionally, the more acidic environment (pH 5.5) used in these assays allowed rVapA<sup>32-189</sup> to bind PA as compared to neutral conditions (pH 7.4) (Figures All.6A and B). This increased interaction at a lower pH could be accounted for because of the lower charge PA holds in this environment [450, 535]. The fact that we found GFP-VapA able to bind the yeast plasma membrane in a near-neutral cytosolic pH may identify additional unknown lipid or protein ligands for VapA, which are required to increase the affinity of VapA for PA under these conditions.

PA is an anionic glycerophospholipid that induces the formation of negative curvature in membranes [536], and can participate in cellular signaling via both electrostatic and hydrophobic interactions with protein ligands [451]. During phagocytosis, phospholipase D actively generates PA in the phagocytic cup and post-phagocytic vesicles, which is required to properly deform the plasma membrane in order to generate the limiting membrane of the phagocytic vesicle [537]. This phagosomal pool of PA would provide VapA on the bacterial surface its host binding target upon phagocytic uptake. That we observed rVapA<sup>32-189</sup> binding to PA-containing liposomes only in an acidic environment (Figures All.6A and B) was interesting. Lack of lysosomal acidification has been well documented during *R. equi* infections using LysoTracker dye, which responds to a pH of 6.5 or lower by a shift in fluorescence intensity [50-52]. Therefore, the VapA:PA interaction may occur during an initial acidification step during infection that is later hindered by the replicating bacterium. Support of this theory comes from the ability of *R. equi* to withstand acidic conditions and the upregulation of VapA during the bacterium's acid

response [68, 73]. Previous measurements of phagosomal acidification during macrophage infections with *R. equi* have shown that while colocalization between the bacterium and LysoTracker dye is low, LysoTracker-positive vesicles are still detected early during the infection [50-52]. These acidic vesicles may fuse with the nascent *R. equi*-containing phagosome, thus providing the trigger for VapA binding. Recently, it was discerned that rVapA supplemented normal rat kidney cells had high colocalization between LysoTracker dye and lysosomes but that the lysosomes had a lower hydrolytic capacity [72]. Taken together, we can speculate that VapA is not directly altering phagosomal/lysosomal pH, but rather still-undescribed mechanisms downstream of VapA activity are required for *R. equi* to limit RCV acidification.

Signaling mediated by PA is becoming better understood as an important means for cellular communication, and is implicated in the regulation of critical cellular events including vesicular trafficking, actin polymerization, and respiratory burst [537-542]. Phosphatidic acid is able to mediate the Akt-mTOR-S6K signaling cascade at each of the pathway components and may be a way in which the bacterium promotes intramacrophage growth [538-540, 542]. Macrophages grown in PA-supplemented media activated the Akt-dependent signaling cascade, thus leading to the production of proinflammatory cytokines, nitric oxide, and prostaglandin E2. This response was abrogated in mutant Akt lines, wherein it was presumed that PA indirectly affects Akt localization, and therefore activity, through its ability to modulate phosphoinositide 3-kinase [540]. Notably, macrophages infected with either the wild type or plasmid-cured strain of *R. equi* have very similar cytokine production profiles, suggesting that Akt is likely not the primary regulatory target of VapA [543]. While PA has an indirect effect on Akt, the lipid has been found to directly interact with mTOR via the FRB domain [538, 539]. mTOR works in conjunction with the V-type ATPase on lysosomal membranes to sense available nutrients inside the phagosome [544, 545]. Thereafter, mTOR mediates downstream signaling events to alter protein synthesis and autophagic pathways [544]. Lastly, experiments studying phagocyte

chemotaxis have shown that PA stimulates S6K to promote cellular migration through a Transwell plate, and therefore likely promotes the migration of phagocytes into infected tissues [539]. Accordingly, the VapA:PA interaction could have drastic effects on a number of PA-dependent cellular physiologies, wherein modulation of the mTOR or S6K proteins later in the Akt-mTOR-S6K signaling cascade is one such example.

While we found that rVapA<sup>32-189</sup> interacted with PA-containing liposomes, neither of the pVapB encoded Vaps tested, rVapB<sup>35-197</sup> or rVapK2<sup>32-202</sup>, bound PA liposomes to levels observed with rVapA<sup>32-189</sup> (Figure All.6D). *R. equi* isolates carrying alternate virulence plasmids differ in their disease presentation and host species tropism; wherein equine isolates, carrying exclusively pVapA, present with pyogranulomatous pneumonia and swine isolates, carrying primarily pVapB, show submaxillary lymphadenitis [41, 448, 520, 546]. It has been determined, however, that *R. equi* equipped with either the pVapA or pVapB type virulence plasmids can replicate within macrophages of many species; showing that interspecies macrophage differences are not responsible for the plasmid-specific species tropism observed [547]. It has been presumed that the Vaps responsible for supporting the intramacrophage growth of differing *R. equi* isolates would employ similar molecular mechanisms during pathogenesis. Here, we have shown that while rVapK2<sup>32-202</sup> supplementation rescues the intramacrophage growth phenotype of  $\Delta vapA$  *R. equi* and that GFP-VapK2<sup>32-202</sup> to some extent localizes to the yeast plasma membrane, the protein was not detected to interact with PA (Figures All.1C, 1D, and 7D). While it is likely that the core structures of the Vap proteins are conserved [79-81], it is possible that rVapK2<sup>32-202</sup> cooperates with a different lipid in the eukaryotic membrane. Alternatively, rVapK2<sup>32-202</sup> may lack the capacity to interact with PA, but contains a shared function with VapA that has yet to be determined. Future work is required to elucidate or eliminate the possibility of lipid binding by rVapK2. It should be noted that the bulk of research on *R. equi* pathogenesis has focused on pVapA carrying isolates, as these are typical of strains derived from both diseased horses and humans. It is therefore unknown if the *R.*

*equi*-containing vacuole generated by strains harboring the pVapB-type virulence plasmid follows the same phagolysosomal maturation process as those strains harboring the pVapA-type plasmid [50-52]. This represents a gap in the knowledge regarding macrophage infection with *R. equi* and should be considered when addressing *R. equi* virulence in the future. In closing, the identification of VapA:host membrane and VapA:PA interactions define a new understanding of VapA:host molecular interactions that should provide insight into the activity of VapA during *R. equi* pathogenesis. Future work will identify the region of VapA responsible for PA binding, and may help answer the question of why the other highly homologous Vap proteins of *R. equi* are insufficient to support intramacrophage replication in the absence of the VapA protein.

**Table A1.1. Bacterial and yeast strains.**

Bacteria	Description	Source
<i>R. equi</i>		
103S	Wild type strain isolated from pneumonic foal (~80kb pVapA type virulence plasmid)	[57]
103 <sup>P-</sup>	Plasmid cured 103+ <i>R. equi</i> variant	[69]
$\Delta vapA$	103S <i>R. equi</i> variant with <i>vapA</i> deletion; Apr <sup>R</sup>	[69]
103S/pGFPmut2	103S harboring pGFPmut2; Hyg <sup>R</sup>	[548]
$\Delta vapA$ /pGFPmut2	$\Delta vapA$ harboring pGFPmut2; Hyg <sup>R</sup> and Apr <sup>R</sup>	This Study
33705	Wild type strain isolated from pig lymph node (~80kb pVapB type virulence plasmid)	[549]
<i>E. coli</i>		
pTRC His-GFP	Common lab strain of <i>E. coli</i> carrying GFP expression vector	A. Medlock (UGA)
<i>S. cerevisiae</i>		
BY4742	MAT $\alpha$ his3 $\Delta$ 1 leu2 $\Delta$ 0 lys2 $\Delta$ 0 ura3 $\Delta$ 0	GE Dharmacon

## Experimental Procedures

### Bacterial and yeast cells.

Bacterial and yeast strains used in these studies are listed in Table All.1. *Escherichia coli* was grown in Luria-Bertani (LB) broth at 37°C with antibiotics where appropriate. Selective antibiotics used for *E. coli* were carbenicillin or hygromycin at 50 µg ml<sup>-1</sup> or 180 µg ml<sup>-1</sup>, respectively. *R. equi* was grown in Brain Heart Infusion (BHI) broth at 37°C or 30°C and supplemented with either 80 µg ml<sup>-1</sup> apramycin or 180 µg ml<sup>-1</sup> hygromycin, when appropriate.

*Saccharomyces cerevisiae* strain BY4742 cells were grown on yeast extract peptone dextrose (YPD) agar or broth at 30°C. BY4742 cells transformed with a plasmid that conferred auxotrophic selection through uracil were grown at 30° C and either plated on or in complete supplemental mixture (CSM) lacking uracil.

### Recombinant Vap purification.

Plasmids utilized and constructed in this study are shown in Table S1. Vap proteins were cloned into the pHis-Parallel1 overexpression plasmid [550] as follows: Vap open reading frames were amplified from the respective virulence plasmid templates (103S plasmid for *vapA* and *vapG*; 33705 plasmid for *vapB* and *vapK2*) using the primers listed in Table S2. These primers only amplify the part of the *vap* gene that is responsible for the disordered and conserved domains of the proteins, and lack the putative N-terminal signal sequences; accession numbers for proteins are CAQ30407 (VapA), CAQ30394.1 (VapG), CAQ30336.1 (VapK2), and CAQ30339.1 (VapB) [64]. Amplicons were digested using the appropriate restriction enzymes underlined in Table S2 and cloned into pHis-Parallel1, which had been digested with the same enzymes. Resultant plasmids, pVapALMW, pVapGLMW, pVapBLMW, and pVapK2LMW, were confirmed by sequencing at the Georgia Genomics Facility (University of Georgia).

Plasmids expressing N-terminal hexahistidine fusions to Vap proteins were electroporated into the *E. coli* Tuner™ strain (EMD Millipore). Acquired transformants were grown to an OD<sub>600</sub> = 0.8-1.0 at

37 °C in LB supplemented with carbenicillin. His-Vap expression was induced with 1 mM isopropyl  $\beta$ -D-1-thiogalactopyranoside and cells were grown for another 4 hr at 37 °C with shaking. Cells were harvested and suspended in lysis buffer (1 ml 0.5 g<sup>-1</sup> wet weight pellet; 50 mM sodium phosphate pH 7.0, 300 mM NaCl, 10 mM imidazole, 1 mg ml<sup>-1</sup> lysozyme, 1 mM  $\beta$ -mercaptoethanol, and EDTA-free protease inhibitor cocktail (Thermo Scientific)). Cell mixture was incubated for 1 hr at room temperature with gentle agitation, and sonicated to disrupt cells (6 x 30 s).

Lysed cells were clarified via centrifugation (19000 x *g*, 15 min, 4 °C), and passed over Ni-NTA resin, which had been pre-equilibrated with lysis buffer lacking protease inhibitors, lysozyme, and  $\beta$ -mercaptoethanol. The resin was washed once each with 10 column volumes wash buffer (50 mM sodium phosphate pH 7.0 and 300 mM NaCl) containing increasing amounts of imidazole (20 mM, 40 mM, 60 mM). Protein was eluted with wash buffer containing 500 mM imidazole. Eluted protein was dialyzed into 50 mM potassium phosphate pH 7.4, 150 mM KCl, and 10% (v/v) glycerol, and stored at -80 °C.

#### **Proteinase K digestion of recombinant Vap proteins.**

Vap proteins were digested by Proteinase K (Novagen) in a 500:1 (protein:enzyme) mass ratio as described by Geerds and colleagues [79]. Briefly, Proteinase K and Vap proteins were incubated either with or without 1% SDS at 37°C for 75 min. Digestion was halted by addition of 2 mM phenylmethanesulfonyl-fluoride (PMSF) and resulting products were run on an SDS-PAGE gel.

#### **Construction of yeast expressing GFP tagged Vaps.**

To generate GFP-VapA yeast expression constructs, primer pairs GFP-VapA SS F and GFP-VapA R or GFP-VapA NSS F and GFP-VapA R were used to amplify the open reading frames from 103S corresponding to VapA or VapA<sup>32-189</sup> respectively. The remaining *vap* genes were amplified using their respective GFP-Vap(X) NSS F and GFP-Vap(X) R primers from either the 103S or 33705S plasmid; wherein a region containing *vapL-M* from 33705 was initially amplified in order to PCR *vapK2*. The resultant PCR

products from these primers (Table S2) provided sequence homology to the pGO35 vector, which allows for the constitutive expression of an N-terminally GFP tagged protein of interest (a gift from Alexey Merz, UW Seattle) [302, 530]. pGO35 was digested with BglII, and co-transformed with the corresponding amplicons via standard lithium acetate methods [551]. The resultant plasmids, pGFP-VapA<sup>32-189</sup>, pGFP-VapG<sup>27-172</sup>, pGFP-VapB<sup>35-197</sup>, and pGFP-VapK2<sup>32-202</sup> express GFP-tagged Vap proteins without their N-terminal signal sequences. In contrast, pGFP-VapA will express full length GFP-VapA. Imaging of these strains was completed via fluorescence microscopy.

#### **SDS-PAGE and western blotting.**

Pure protein samples were boiled for 8 min in 1 X loading dye consisting of 50 mM Tris-Cl (pH6.8), 2 % SDS, 0.1 % (w/v) bromophenol blue, 10% glycerol, and 100 mM DTT. For extracting protein from whole yeast cells, approximately 1 X10<sup>9</sup> cells were suspended in 200 µl lysis buffer (0.1 M NaOH, 0.05 M EDTA, 2 % SDS, and 2 % β-mercaptoethanol) before boiling for 10 min. Afterwards, 5 µl of 5 M glacial acetic acid was added to the yeast lysates before vortexing for 30 s and boiling samples for an additional 10 min. Yeast samples then had loading dye added to a 1 X concentration.

Prepped samples were run on an SDS-PAGE gel in 1 X Tris-Glycine SDS running buffer (Novex®). Transfer of the samples from the SDS-PAGE gel to a nitrocellulose membrane was done in a 1.4% (w/v) glycine, 0.3% (w/v) Tris Base, and 20% methanol buffer. Thereafter, the nitrocellulose membrane was blocked using the SuperBlock® T20 (TBS) blocking buffer (Thermo Scientific) for either an hour at room temperature or overnight at 4°C with agitation. Primary polyclonal rabbit αVapA was diluted 1:1,000 in blocking buffer. Primary antibodies were then incubated with the membrane for either 1 hour at room temperature or overnight at 4°C with agitation. Afterwards, while rocking, the membrane was washed 4 X for 10 minutes each with a .05% (v/v) Tween 20 and 1X PBS solution. Thereafter, secondary goat αrabbit antibody, conjugated to horseradish peroxidase (HRP), was diluted 1:20,000 in blocking buffer and incubated with the membrane as done with the primary antibody. Next, the membrane was washed

as done previously. To expose the western blot, enhanced chemiluminescent HRP substrate and peroxide buffer, both from Thermo Scientific, were mixed and added to the membrane and allowed to incubate at room temperature for 5 minutes.

### **Electroporation of *R. equi*.**

An overnight 100 ml culture of  $\Delta vapA$  *R. equi* in BHI broth was diluted to an OD<sub>600</sub> of 0.4 with fresh medium, and grown at 30°C until it reached an OD<sub>600</sub> of 0.8-1.0. Bacteria were harvested via centrifugation (3600 x *g*, 10 min, 4°C), the pellet was washed with 50 ml of cold sterile dH<sub>2</sub>O, and centrifuged for an additional 30 min. This wash step was repeated and additional time, then cells were suspended in 4 ml cold, sterile dH<sub>2</sub>O water containing 5% glycerol. Approximately 200 ng pGFPmut2 DNA was added to 400  $\mu$ l of washed bacteria and mixed by gentle pipetting. The bacteria/DNA mixture was then placed in a pre-chilled 2 mm electroporation cuvette (Bio-Rad) and electroporated (2500 V, 25  $\mu$ F, 1000  $\Omega$ ). Immediately following electroporation, 1 ml of filter sterilized BHI supplemented with 0.5 M sucrose was added to the cuvette, collected, and incubated for one hour at 30°C. Following incubation, bacteria were harvested via centrifugation, 400 $\mu$ l of the supernatant was discarded, and the bacterial pellet was suspended in the remaining supernatant. Aliquots of the resuspension were then plated to appropriate selective media, and incubated at 30°C for two days.

### **Macrophage growth conditions and isolation.**

J774A.1 macrophages (ATCC) were grown at 37°C with 5% CO<sub>2</sub> in Dulbecco's Modified Eagle Medium (DMEM) supplemented with 10% heat inactivated Fetal Bovine Serum (FBS) and 2 mM glutamine (complete medium).

Bone marrow-derived macrophages (BMDM) were isolated from femurs and tibias of BALB/c mice (Jackson Laboratories). In order to isolate BMDM precursors, femurs and tibias were dissected from the mouse and flushed with cold cation-deficient 1X PBS containing 100 units ml<sup>-1</sup> penicillin and 10 mg ml<sup>-1</sup> streptomycin (P/S). Cells retrieved from the bone marrow were centrifuged (260 x *g*, 10 min,

4°C), washed once with complete media containing P/S, then suspended in complete media supplemented with P/S and 10% supernatant from Colony Stimulating Factor-1 (CSF-1) producing L929 cells (24 ml per mouse). These precursor cells were incubated in 6-well non-tissue culture treated plates (37°C, 5% CO<sub>2</sub>; 4ml suspended cells per well) for 3 days. After incubation, 4 ml complete media containing 10% L929 cell supernatant (no P/S) were added to each well and incubation continued. On days five and six, all of the media on the cells was removed and replaced with complete media supplemented with 10% CSF-1 containing L929 cell supernatant. Following a 2 hr incubation with the fresh media on day six, the media was removed from the wells and replaced with cold 1X PBS, incubated at 4 °C for 10 min, and macrophages were harvested. Macrophages obtained were either used immediately in assays, or suspended in 90% FBS with 10% DMSO at 5X10<sup>6</sup> cells per ml and frozen in liquid nitrogen. For assays, cells were maintained in DMEM supplemented with 10% FBS, 2 mM glutamine, and 10% L929 cell supernatant containing CSF-1.

#### **Macrophage infection assays.**

1 x 10<sup>5</sup> macrophages were placed on 13 mm-diameter glass coverslips or in 24-well tissue culture plates. When applicable, filter sterilized recombinant protein was suspended in macrophage media at a concentration of 50-150 nM and incubated with the monolayer overnight. The next morning, monolayers were washed with complete media. Bacteria, suspended in PBS, were added to the monolayer at a multiplicity of infection of 5:1 (J774A.1) or 7:1 (BMDM) during *R. equi* infections or 10:1 during *E. coli* infections. After 1 hr, the monolayer was washed three times with warm DMEM without supplementation. The monolayers were maintained in complete media supplemented with 20-40 µg ml<sup>-1</sup> amikacin in order to kill any remaining extracellular bacteria; while one plate was lysed for bacterial quantification at T1.

To quantify *R. equi* loads in macrophages, cells were lysed (37 °C, 5% CO<sub>2</sub>, 20 min) with 500µl of sterile dH<sub>2</sub>O. For *E. coli* infections, 500 µl 0.5% (v/v) Triton X-100 was added to macrophages, and the

incubation time was reduced to 5 min. The resultant lysates containing bacteria were collected, serially diluted in PBS, and plated on BHI (*R. equi*) or LB (*E. coli*) agar and incubated at 37°C for 24 to 48 hr. For later time points, the monolayer was washed three times with DMEM, as before, and the lysis procedure was performed.

#### **Immunofluorescence assays.**

Infected macrophage monolayers on 13mm diameter coverslips in 24-well plates were fixed with 4% (v/v) paraformaldehyde in PBS (22 °C, 20 min, in the dark). Coverslips were washed four times with PBS supplemented with 5% FBS, and fixed cells were permeabilized with 350 µl of PBS containing 0.1% Triton X-100 (3 min). 250µl anti-VapA polyclonal antibody (diluted 1:1600 in PBS with 5% FBS and 0.1% (v/v) Triton X-100) was incubated on the coverslips for one hour in the dark at 22 °C. Coverslips were washed four times in PBS supplemented with 5% FBS and 0.1% (v/v) Triton X-100. Afterwards, 250 µl goat anti-rabbit antibody conjugated to fluorescein isothiocyanate (FITC) (1:500 in PBS with 5% FBS and 0.1 % (v/v) Triton X-100, Thermo Scientific), was incubated with the fixed monolayer and washed, as above. 250µl of an  $\alpha$ -LAMP1 mouse monoclonal conjugated to Alexa Fluor 647 (diluted 1:500 in PBS with 5% FBS and 0.1% (v/v) Triton X-100) was used to stain monolayers for LAMP1 as described for the aforementioned primary and secondary antibodies. Washing was completed as done previously. A final wash with with PBS was immediately performed before the coverslips were mounted on microscope slides using ProLong Gold antifade reagent with 4',6-diamidino-2-phenylindole (DAPI) (ThermoFisher Scientific), and were allowed to dry for 24 hours before visualization via confocal microscopy.

#### **Liposome production.**

Stock 16:0-18:1 phospholipids (Avanti Polar Lipids) were dissolved in chloroform and mixed in glass tubes to provide a final amount of 2 µmol total lipid. For quantitation, 0.5% (mol/mol) rhodamine-phosphatidylethanolamine (Rh-PE) was added to all mixtures. Lipid mixtures were composed of 1-palmitoyl-2-oleoyl-*sn*-glycero-3-phosphocholine (POPC) and either 1-palmitoyl-2-oleoyl-*sn*-glycero-3-

phosphate (POPA), 1-palmitoyl-2-oleoyl-*sn*-glycero-3-phosphoethanolamine (POPE), or 1-palmitoyl-2-oleoyl-*sn*-glycero-3-phospho-L-serine (POPS) were added to the indicated percentage. Chloroform was removed via a stream of argon gas, and complete solvent removal was obtained under vacuum for 1 hr. Dried lipids were suspended in 1 ml buffer containing either 20 mM 4-(2-hydroxyethyl)-1-piperazineethanesulfonic acid (HEPES) pH 7.4 or 50 mM 2-ethanesulfonic (MES) and 3-(*N*-morpholino)propanesulfonic (MOPS) acid pH 5.5, depending on the pH desired, 10% (v/v) glycerol, and 150 mM NaCl. The suspended lipids were placed in a 37 °C water bath and intermittently vortexed at high speed for 60 min. After 10 freeze-thaw cycles in liquid nitrogen, suspended lipids were passaged 11 times through a Mini-Extruder (Avanti Polar Lipids) fitted with a 1 µm polycarbonate membrane, which had been previously equilibrated on a heating block set to 37 °C.

Liposome quantification was determined with the use of a Rh-PE standard curve in RB150 (20 mM HEPES pH 7.4 or 50mM MES pH 5.5, 150 mM NaCl, 10% (v/v) glycerol) containing 1% (v/v) Thesit; liposomes of interest were also serially diluted in this same buffer. Fluorescence of the suspensions was determined by loading 20 µl each suspension into a 384-well, low-volume, black microplate (Corning) and a computer-controlled multimode plate reader ( $\lambda_{\text{ex}} = 540 \text{ nm}$ ,  $\lambda_{\text{em}} = 585 \text{ nm}$ ; BioTek). Liposomes were stored at 4°C until the time of assay.

#### **Liposome floatation.**

50 µl reactions containing 500 µM total lipids and 1 µg of recombinant protein of interest were incubated for 1 hr in a 37°C water bath. Afterwards, 5 µl of the reaction was collected as a control before adding 50µl of 80% filter-sterilized Histodenz (Sigma Aldrich) in the appropriate pH RB150 buffer. This mixture was inverted to mix, and placed into a 7 X 20 mm polycarbonate centrifuge tube (Beckman Coulter). Samples were then overlaid with 75µl of filter sterilized 30% Histodenz in RB150 and 75µl of RB150 media. Samples were centrifuged (96,000  $\times g$  for 2 hours at 4°C) before collecting 40µl of the floated liposomes. To analyze the samples, the harvested liposome concentrations were determined via

Rh-PE fluorescence, equivalent amounts of liposomes were separated via SDS-PAGE, and immunoblotted for Vap proteins.

### **Confocal Microscopy.**

Fluorescence images were captured on a Nikon A1R confocal microscope system (UGA College of Veterinary Medicine Cytometry Core Facility) using a 100X 1.45NA (Nikon) objective, equipped with an S-P 50 mW multiline Ar laser for imaging GFP and Alexa 488™, a Coherent Sapphire 561nm 20 mW laser for imaging dsRed, and a Coherent Cube 640nm 40mW laser for imaging Alexa 647™. Images were captured using NIS Elements software and processed with the Fiji (ImageJ v. 1.48) software package [445, 446].

### **Statistical Analysis.**

Sigma Plot version 11.2.0.5 (Systat Software, San Jose, CA) and GraphPad Prism version 6.0b (GraphPad Software, Inc., La Jolla, CA) were used for statistical analysis. Bacterial quantification was evaluated via a two-way analysis of variation (ANOVA) using the Holm-Sidak method, where a P value of  $\leq 0.05$  was considered significant.

### **Acknowledgments**

The authors would like to thank Drs. Vihbay Tripathi and Jennifer Willingham-Lane for their input and discussions regarding this work, as well as Dr. Alexey Merz for providing pGO35. We also thank Leanna Ritson for technical expertise and Dr. Amy Medlock for providing the *E. coli* strain harboring pTRCHis-GFP. V.J.S. is supported by a grant from National Institute of Allergy and Infectious Diseases (R01-AI100913). The authors have no conflicts of interest to declare.

### **Author Contributions**

LMW has made major contributions to design of the study, data acquisition/analysis, and manuscript preparation. EMC and TLB have made key contributions to data acquisition. Both MKH and VJS have substantial contributions to study conceptualization and writing of the manuscript.

## APPENDIX III

### ANALYSIS OF THE INTERPLAY BETWEEN VOPQ AND V<sub>o</sub>-CONTAINING MEMBRANES

#### Introduction

*Vibrio parahaemolyticus* is an opportunistic marine-dwelling pathogen that remains a leading cause of seafood borne gastroenteritis globally [91, 96, 97]. *V. parahaemolyticus* encodes two type III secretion systems (T3SSs), one of which T3SS1 is found in all isolates and associated with invasion and cytotoxicity, while T3SS2 is found typically only in clinical isolates and responsible for the gastroenteric symptoms of infection [112, 121]. In macrophage infections, *V. parahaemolyticus* expressing only T3SS1 is toxic and induces autophagy, cell rounding, and eventual cell lysis in a well-orchestrated manner [123]. To date, only four secreted effector proteins encoded with T3SS1 have been identified: Vibrio Outer Protein (Vop) Q, -R, -S, and VPA0450 [121]. Of those four, only VopQ has been implicated as an effector necessary for the observed cytotoxic effects upon invasion as deletion of *VOPQ* resulted in an attenuated strain compared to wild-type *V. parahaemolyticus* [124]. VopS AMPylates Rho family GTPases to manipulate downstream signaling and induces cell rounding but upon its deletion, *V. parahaemolyticus* remains toxic to macrophages [124, 126]. VPA0450 is inositol polyphosphate-5-phosphatase that hydrolyzes phosphate from PI(4,5)P<sub>2</sub> and induces plasma membrane blebbing and cell lysis and VopR has no identifiable function [128], leaving VopQ as the primary effector necessary to orchestrate invasion and for the pathogenicity of *V. parahaemolyticus*. VopQ has therefore become the focus of studies that aim to understand the virulence determinants of *V. parahaemolyticus*.

VopQ is 54kDa pore-forming protein that alone is implicated in the induction of autophagy and resulting accumulation of autophagic vesicles in eukaryotic cells [124]. Studies both in mammalian cells and the budding yeast, *Saccharomyces cerevisiae*, show that VopQ interacts with the c subunit of the

vacuolar-type H<sup>+</sup>-ATPase (V-ATPase) V<sub>0</sub> domain present at lysosomal/vacuolar membranes [125, 137]. The V-ATPase is a large complex that consists of both a cytosolic V<sub>1</sub> domain, responsible for the hydrolysis of ATP to ADP and inorganic phosphate, and membrane embedded V<sub>0</sub> domain, responsible for the translocation of protons across the vacuole membrane and into the vacuole lumen. In yeast, the V<sub>0</sub> domain consists of a proteolipid c-ring generated by the assembly of eight c (Vma3p) subunits, one c' (Vma11p) subunit, and one c'' (Vma16p) subunit in addition to the a (Vph1p), d (Vma6p), and e (Vma9p) subunits which are important for connecting the two domains (V<sub>1</sub> and V<sub>0</sub>) and targeting to the vacuole membrane, connecting the central stalk required for pumping activity and regulation of pumping activity, and assembly of V<sub>0</sub> in the ER, respectively [307, 320].

Upon invasion, VopQ embeds itself in V<sub>0</sub> containing membranes and forms an 18Å gated pore that allows the passage of ions and small molecules out of the vacuole lumen but does not alter V-ATPase pumping activity or induce vacuolar rupture [125, 406]. The pore forming activity of VopQ results in the abrogation of the pH and electrochemical gradient in the vacuole and likely results in the stimulation of stress response due to cytosolic ion levels [125]. In vitro homotypic vacuole fusion assays determined that VopQ inhibits vacuole fusion but not on account of its pore forming activity and rather through yet undefined methods [406]. Importantly, though the function of VopQ is evident in cell invasion, the method by which VopQ induces autophagy, blocks vacuole fusion, or interacts with Vma3p remains unknown but it is possible through examination of the interaction between VopQ and its binding partner, Vma3p of the V<sub>0</sub> domain, insight can be gleaned regarding not only the activity of VopQ but also about V<sub>0</sub>, which has a long debated and yet unknown role in membrane fusion events. It is the goal of this work to demonstrate the specific requirement of V<sub>0</sub> in membranes for VopQ to maintain its cytotoxic effects in *S. cerevisiae* as a highly conserved eukaryotic organism and to demonstrate V<sub>0</sub> dependent gating induced by VopQ.

## Results

### VopQ requires specifically $V_o$ for toxicity and localization to the vacuole in yeast.

Previous studies show a genetic requirement of *VMA3* for VopQ lethality in yeast [125]. In order to determine if this was unique to *VMA3* or  $V_o$  subunits in general, toxicity assays using individual  $V_o$  deletion strains and V-ATPase assembly chaperone deletion strains expressing an inducible control vector or *VOPQ* were plated in the presence and absence of the inducer, galactose. Upon expression, *VOPQ* is lethal to all V-ATPase deletion strains except *vma3 $\Delta$*  and *vma9 $\Delta$*  strains as well as the chaperone *vma21 $\Delta$*  (Figure AIII.1). Vma3p is the most abundant subunit of the  $V_o$  ring while Vma9p is a subunit involved in the assembly of  $V_o$  but dispensable to V-ATPase pumping activity. Vma21p is an assembly chaperone that is localized to the ER and functions in the assembly of the V-ATPase. Vma9p and Vma21p form a complex in the ER during V-ATPase assembly and therefore it is likely that upon deletion of either,  $V_o$  is not assembled or trafficked to the membrane and the resistance to VopQ expression is may be an artifact of failed V-ATPase assembly in the ER.

To determine if VopQ localizes strictly to the vacuole in the presence of  $V_o$ , GFP-VopQ and GFP-VopQ<sup>S200P</sup>, a VopQ mutant generated via random mutagenesis with reducing binding affinity for  $V_o$  [406], was expressed in wild-type yeast in addition to V-ATPase subunit deletion strains. Vacuoles were stained with the vacuole specific dye, FM4-64 to observed colocalization between GFP-VopQ and the vacuole membrane. In wild-type, *vma2 $\Delta$*  ( $V_1$  subunit), and *vph1 $\Delta$* , expression of GFP-VopQ shows it localizes to vacuole structures though significantly fragmented as previously described (Figure AIII.2) [406]. In  $V_o$  deletion strains (excluding *vph1 $\Delta$*  which has an isoform from the Golgi V-ATPase that may be used to function as Vph1p), VopQ fails to localize to the vacuole and rather maintains a diffuse and cytosolic distribution (Figure AIII.2). This is also true for each of the V-ATPase chaperones (data not shown). In every background, VopQ<sup>S200P</sup> fails to localize to the vacuole due to its poor affinity for  $V_o$ . Interestingly,

regardless of VopQ toxicity seen in dilution plating, VopQ localizes to the vacuole membrane only in those strains which produce a fully functional  $V_0$  domain at the vacuole membrane.

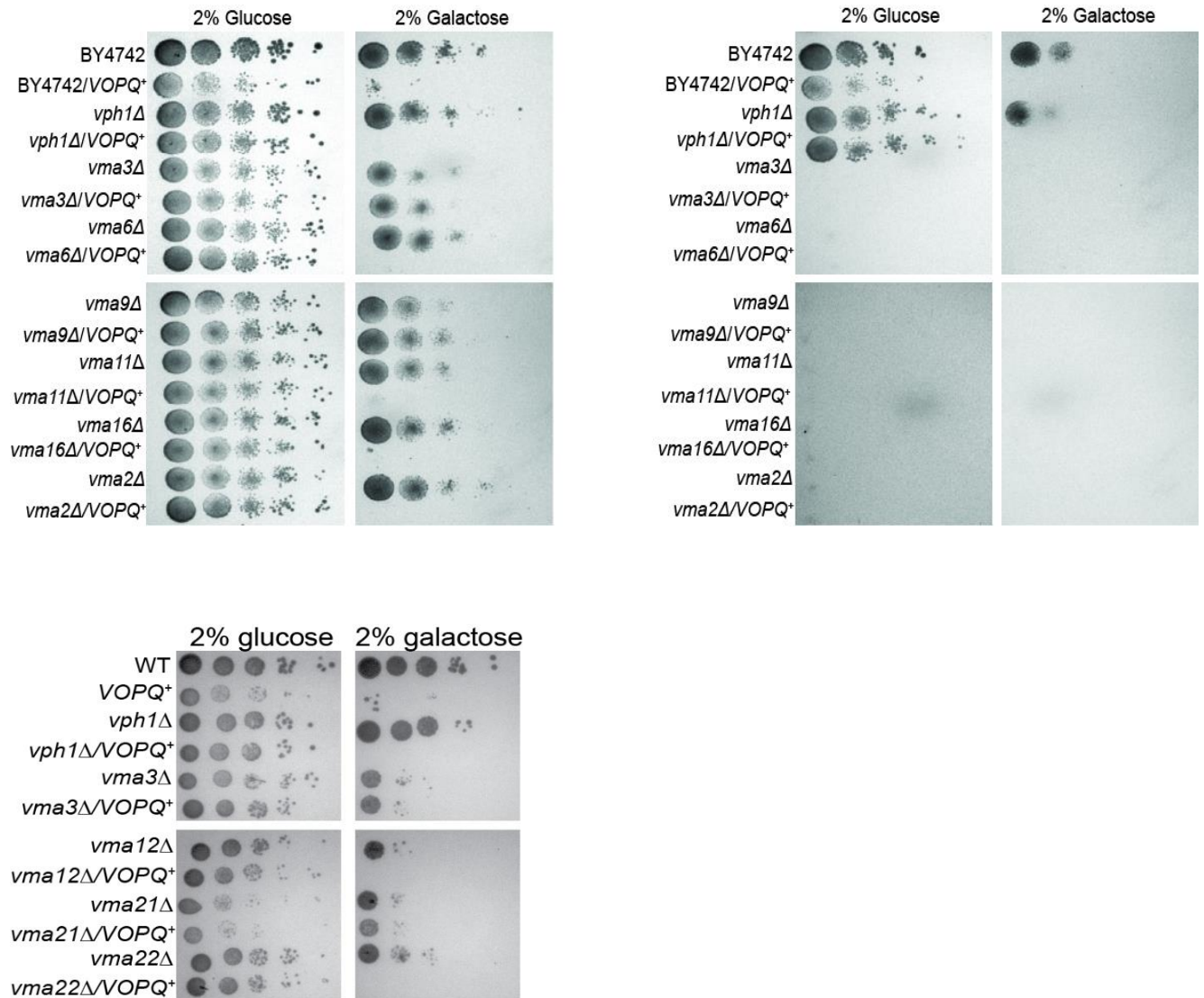


**Figure AIII.1. Yeast is resistant to VOPQ expression in the absence of VMA3, VMA9, or VMA21.**

Overnight cultures of BY4742 (*MAT $\alpha$  his3 $\Delta$ 1 leu2 $\Delta$ 0 lys2 $\Delta$ 0 ura3 $\Delta$ 0*) with noted individual deletions expressing pRS413+ or pRS413-VOPQ+ were normalized to 1 ODU and serially diluted 10-fold to 10<sup>-4</sup> in saline solution. 10 $\mu$ L of each dilution was spotted to CSM-Histidine plates with either 2% glucose or 2% galactose. Plates were incubated at 30°C for 72 hours. Top left) pH 5.5; top right) pH 7.4; bottom left) V-ATPase chaperones, pH 5.5.

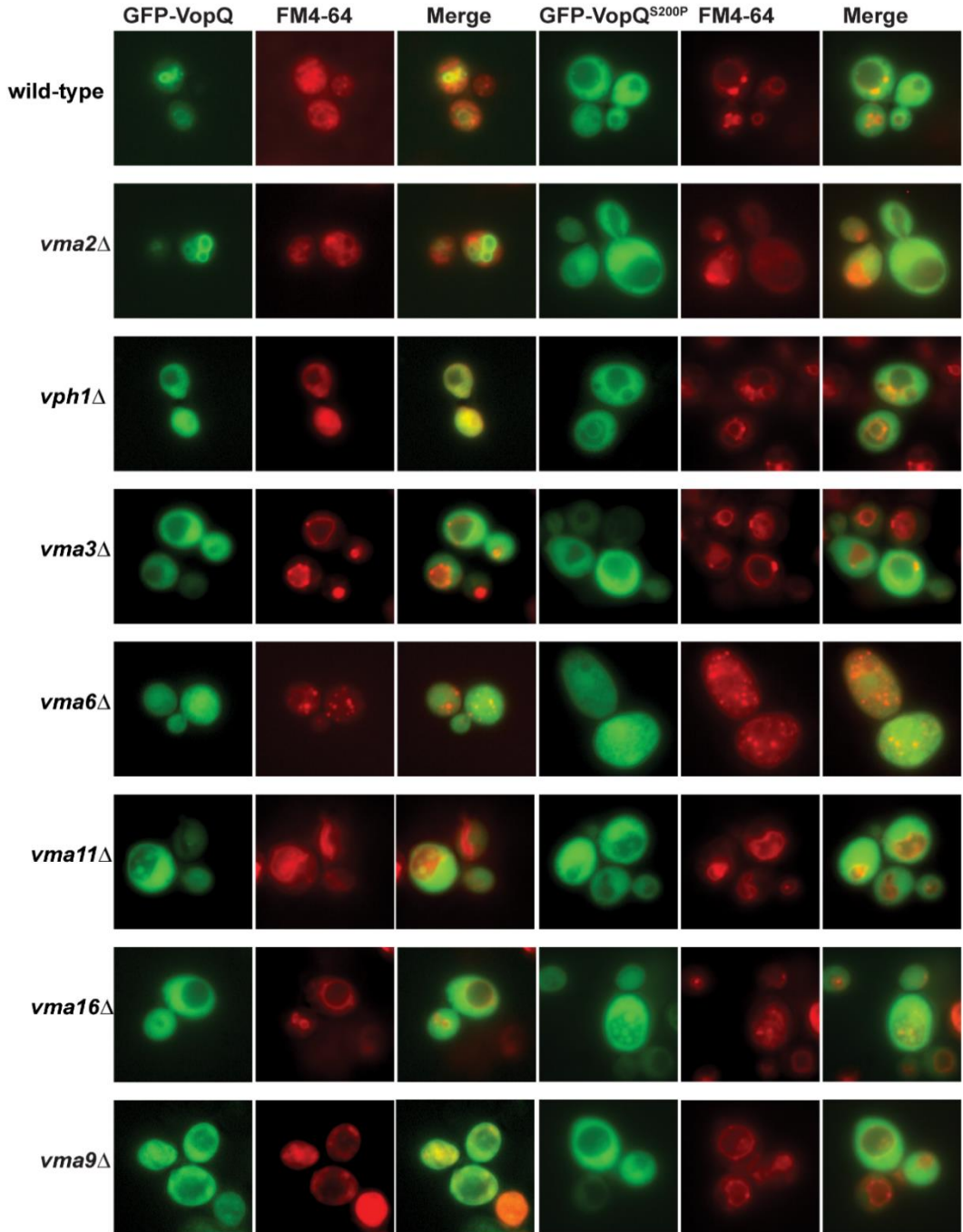


**Figure AIII.2. VopQ fails to localize to the vacuole in the absence of assembled V<sub>0</sub>.** GFP tagged VopQ and VopQ<sup>S200P</sup> were expressed in V<sub>0</sub> deletion strains and one V<sub>1</sub> deletion strain (*vma2Δ*). 1mL of overnight cultures of BY4742 *MATα his3Δ1 leu2Δ0 lys2Δ0 ura3Δ0* background with noted single deletions expressing GFP-VopQ or GFP-VopQ<sup>S200P</sup> were subcultured to fresh media containing 2% galactose for 6 hours induction prior to harvesting cell and staining the vacuole. Vacuole membranes were stained with FM4-64 dye for 30 minutes and visualized with TxRed, GFP with FITC, on Nikon Eclipse fluorescence microscope, images adjusted in ImageJ.

### Analysis of VopQ lipid binding.

VopQ with a pI of 6 was shown to bind negatively charged membranes at pH 5.5 even in the absence of  $V_o$ , however VopQ does not bind membranes of physiological pH 7.4 when VopQ is negatively charged [125]. To determine if VopQ could bind membranes regardless of pH and lipid composition in the presence of  $V_o$ , liposomes consisting of either 100% phosphatidylcholine (PC) which is neutral, or 80% PC and 20% phosphatidylserine (PS) which is negatively charged, were generated at pH 5.5 and 7.4. An additional set at each pH and lipid composition was generated with purified  $V_o$ . Liposomes were then incubated with VopQ and the binding of VopQ to each liposome composition was determined. VopQ bound membranes containing  $V_o$  in every condition including 100% PC liposomes at pH 7.4 (Figure AIII.3). Interestingly, VopQ qualitatively bound  $V_o$  containing membranes best at pH 5.5 in liposomes containing 20% PS (Figure AIII.3) which suggests that lipid content at the vacuole, the presence of  $V_o$ , and an acidic membrane enhance the binding of VopQ at its targeted membrane.

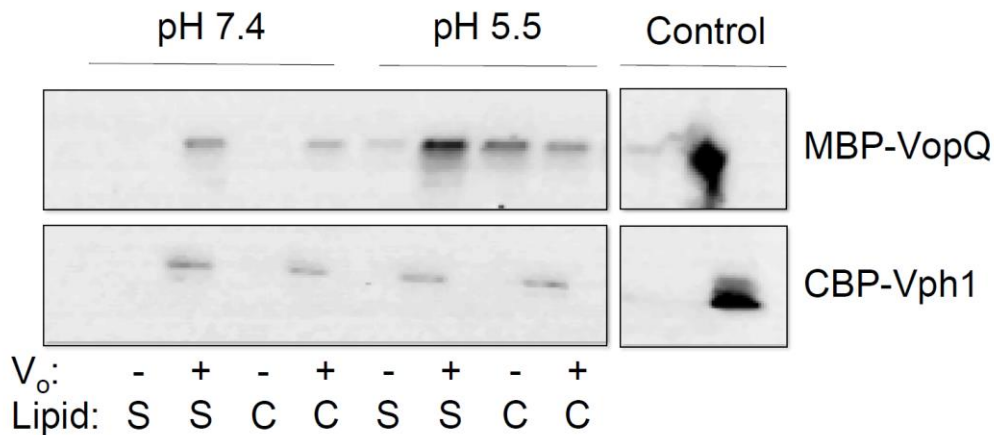
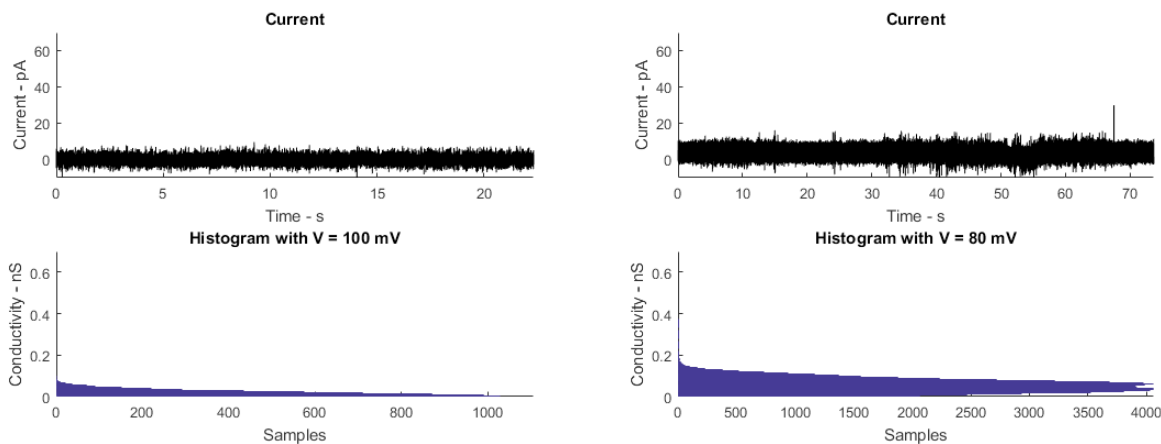


**Figure AIII.3. VopQ preferentially binds  $V_o$  containing acidic membranes.** Liposomes of specified lipid content (S= 20% phosphatidylserine, C=100% phosphatidylcholine) were generated by dialysis with or without  $V_o$  incorporated. Stock lipids of POPS and POPC or POPC alone in the presence of lipid label Rhodamine were combined to 10mM final concentration and dried out to remove chloroform under a stream of argon gas prior to resuspension in RB500/CHAPS (40mM HEPES pH7.4 or 50mM MES/MOPS pH 5.5; 500mM NaCl; 10% glycerol; 200 $\mu$ M CHAPS detergent) buffer at the appropriate pH and 25 $\mu$ g  $V_o$  or buffer control was added. Liposomes were nutated 60 min prior to dialysis into RB500 in the presence of BioBeads. Liposomes were centrifuged for 3 hours at 103,000 x g on a Histodenz gradient, harvested, and concentration was determined by Rhodamine fluorescence based on a standard curve. Liposomes at 5mM in 50 $\mu$ L reactions were incubated in the presence of 10 $\mu$ g MBP-VopQ prior to being mixed with

80% Histodenz in RB25 and layered with 30% Histodenz, and RB25 (40mM HEPES pH7.4 or 50mM MES/MOPS pH 5.5; 25mM NaCl; 10% glycerol). Reactions were centrifuged for 2 hours at 103,000 x g and floated liposomes were harvested. The concentration of liposomes was determined by measuring Rhodamine fluorescence. Equal concentrations were loaded to a gel, transferred, and immunoblotted with either  $\alpha$ VopQ or  $\alpha$ Vph1p.

### Analysis of channel gating in $V_o$ -containing membranes.

Other secreted gated pore-forming proteins have been shown to open and close a generated pore in response to cellular conditions. To determine if VopQ induced channel gating, droplet interface bilayers (DIB) were used to measure the capacitance of gating that occurred when VopQ interacted with liposomes at pH 7.4 in the presence and absence of the  $V_o$  domain. DIB allows two droplets containing liposomes of specific composition to “zipper” along the vertex at which they interact. This vertex, or interface, can be examined for changes in current to evaluate gating events resulting from the presence of different proteins at that interface. When VopQ was microinjected into lipid droplets of POPC:POPG (phosphatidylcholine:phosphoglycerol), gating occurs only in the presence of the  $V_o$  domain (Figure AIII.4), showing that VopQ maintains a very specific interaction with  $V_o$  and results in channel gating only in its presence. Gating oscillated between  $\sim 50$ pA and  $\sim 20$ pA, suggesting an open and closing of the pore generated by VopQ (Figure AIII.4, bottom right panel). Notably, the closure of the VopQ generated pore does not return the measured current to its resting stage, suggesting that it may be either a leaky pore that does not fully seal or a pore with a hemi-closed state.



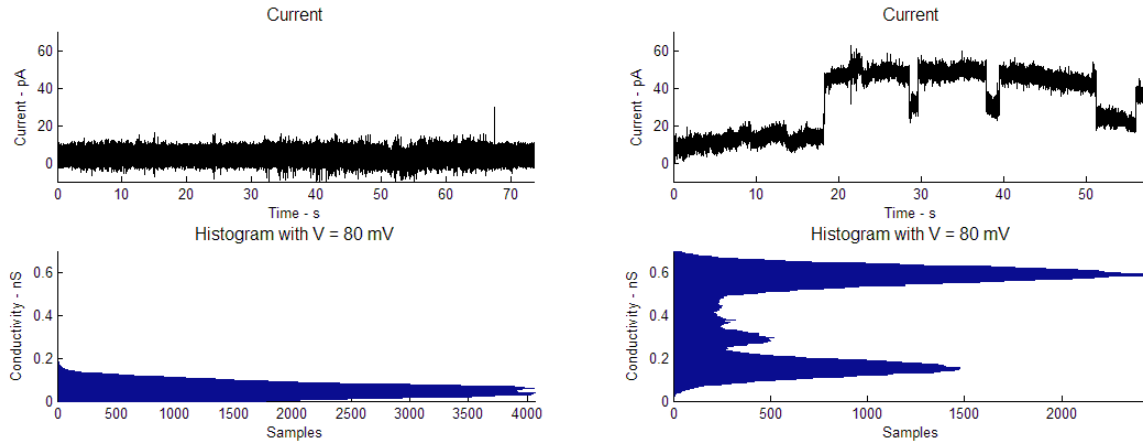


**Figure AIII.4. Conductance in nS of membrane zippering and gating events at the interface of lipid bilayers in a  $V_0$  dependent manner.** Liposomes were prepared by dialysis as previously described. Liposome droplets were suspended in RB150 buffer at pH 7.4 (40mM HEPES pH 7.4; 10% glycerol; 150mM NaCl) on a 1% agarose coated anode and brought within distance of each other. His-VopQ was injected via microinjection at 5 $\mu$ g upon successful membrane zippering as determined by physical contact and conductance. Conductance was measured until collapse of the droplets zippered interface and is shown in pA. Histograms present the number of conductivity measurements that occurred during the time span of the measured zippering events in nS. Top left: PCPG liposomes only; right: PCPG liposomes + His-VopQ injection. Bottom left: PCPG liposomes containing  $V_0$ ; right: PCPG liposomes containing  $V_0$  + His-VopQ injection.

## Discussion

VopQ requires  $V_0$  for localization to the vacuole membrane and likely relies on the negatively charged lipids at the vacuole membrane to enhance its targeted interaction with  $V_0$  and the vacuole. Importantly, there is a distinct requirement for Vma3p for toxicity in yeast though the exact nature of the interaction between Vma3p and VopQ remain unknown despite efforts to identify Vma3p mutants that could no longer bind VopQ (data not shown). Perhaps the telling data is the assembly factors which suggest that although each  $V_0$  subunit is present, without its assembly in the ER, VopQ cannot bind to  $V_0$ . This may offer explanation for the toxicity seen in other c-ring deletions because Vma3p has likely left the ER and may be present in other membranes either independently or perhaps in Vma3p ring, additionally as the most abundant subunit, *VMA3* deletion would abrogate the assembly of even a nonfunctional c-ring as only two of the ten required subunits would be present whereas with deletion of

either *VMA11* or *VMA16*, nine of the necessary ten subunits are present in the cell though nonfunctional, not assembled at the vacuole, and potentially not assembled into a c-ring form at all. Perhaps VopQ can bind a Vma3p rings and direct it to an acidified membrane through its interaction with negatively charged lipids. Studies to evaluate the toxicity of VopQ in a strain expressing *VMA3* with an ER retention signal are ongoing and may aid in deciphering why Vma3p provides resistance to VopQ though no other c-ring subunit does.

Microscopy analysis show that VopQ fails to localize in the absence of a functional  $V_o$  domain at the vacuole, showing that the toxicity of VopQ extends far beyond its ability to embed itself in the vacuole membrane and abrogate pH and electrochemical gradients as a pore-forming protein. Despite failure to localize to the vacuole, VopQ is still toxic to yeast, except in the case of a *VMA3* deletion, which suggests that its ability to induce autophagy is sufficient for toxicity independent of its pore-forming activity at the vacuole, though it may also be the case that VopQ forms pores in other acidified membranes though to a lesser extent than the vacuole membrane. VopQ may induce autophagy first chronologically and utilize an autophagy pathway for its targeted delivery to the vacuole where it can interact with  $V_o$  and embed itself in the membrane to form a pore. Analysis of both the precise autophagy genes that are required for VopQ to induce autophagy and whether *VMA* deletions alter induction of autophagy may shed light onto the type of autophagy pathway VopQ utilizes for its activity and the chronology of events induced by VopQ.

The presence of  $V_o$  in membranes enhances the targeting of VopQ to the vacuole membrane and specifically results in gating only in the presence of both  $V_o$  and VopQ. The observed gating may be evidence that VopQ oscillates between an open and closed channel conformation that allows the passage of ions and small molecules while open and in response to cellular stimuli such as ionic equilibrium, closes its channel though perhaps not completely possibly due to membrane perturbations by its embedment in the vacuolar membrane or perhaps by the very nature of the yet unclassified

channel that is generated. Either way, by doing so, VopQ would have control over cellular responses and access to molecules normally stockpiled in the vacuole, which is significant to the survival of *V.*

*parahaemolyticus*. Other pore-forming proteins have been identified that similarly modulate cellular ion concentrations and in doing so alter the induction of host defense pathways to aid in survival. Further investigation into the precise nature of the pore generated by VopQ will be necessary to understand its activity and role in the invasion and survival of *V. parahaemolyticus*.

**Materials and Methods.** See figure legends.